ORNL
MASTER COPY



OAK RIDGE NATIONAL LABORATORY
operated by
UNION CARBIDE CORPORATION
NUCLEAR DIVISION
for the
U.S. ATOMIC ENERGY COMMISSION

LOCKHEED MARTIN ENERGY RESEARCH LIBRARIES
3 4456 0513299 6

ORNL - TM - 1904

# HFIR FUEL ELEMENT STEADY STATE HEAT TRANSFER ANALYSIS REVISED VERSION

Howard A. McLain

**NOTICE** This document contains information of a preliminary nature and was prepared primarily for internal use at the Oak Ridge National Laboratory. It is subject to revision or correction and therefore does not represent a final report.

LEGAL NOTICE

This report was prepared as an account of Government sponsored work. Neither the United States, nor the Commission, nor any person acting on behalf of the Commission:

A. Makes any warranty or representation, expressed or implied, with respect to the accuracy, completeness, or usefulness of the information contained in this report, or that the use of any information, apparatus, method, or process disclosed in this report may not infringe privately owned rights; or

B. Assumes any liabilities with respect to the use of, or for damages resulting from the use of any information, apparatus, method, or process disclosed in this report.

As used in the above, "person acting on behalf of the Commission" includes any employee or contractor of the Commission, or employee of such contractor, to the extent that such employee or contractor of the Commission, or employee of such contractor prepares, disseminates, or provides access to, any information pursuant to his employment or contract with the Commission, or his employment with such contractor.

CENTRAL RESEARCH LIBRARY
JUL 28 2005

ORNL-TM-1904

Contract No. W-7405-eng-26

Reactor Division

# HFIR FUEL ELEMENT STEADY STATE HEAT TRANSFER ANALYSIS
REVISED VERSION

Howard A. McLain

DECEMBER 1967

OAK RIDGE NATIONAL LABORATORY
Oak Ridge, Tennessee
operated by
UNION CARBIDE CORPORATION
for the
U.S. ATOMIC ENERGY COMMISSION

LOCKHEED MARTIN ENERGY RESEARCH LIBRARIES

3 4456 0513299 6

CONTENTS

| | Page |
|---|---|
| Acknowledgement | v |
| Abstract | 1 |
| Introduction | 1 |
| Criteria | 3 |
| Short Outline of the Method of Analysis | 7 |
| Plant Operating Conditions | 9 |
| Power Density Distributions in the Fuel Assembly | 10 |
| Fuel Element Tolerances | 11 |
| Fluid Flow | 11 |
| Heat Transfer | 13 |
| Hot Spot Heat Transfer | 15 |
| Oxide Buildup on the Fuel Plate Surfaces | 21 |
| Deflection of the Fuel Plate Due to Differential Pressures | 23 |
| Increase of Fuel Plate Thicknesses Because of Heating | 24 |
| Fuel Plate Deflection Due to the Difference in Temperatures in Adjacent Plates | 25 |
| Fuel Plate Deflection Due to the Difference Between the Fuel Plate and the Side Plate Temperatures | 26 |
| Fuel Plate Deflection Due to Radiation Growth | 29 |
| Coolant Channel Thicknesses During Reactor Operation | 30 |
| Input Data | 38 |
| Results | 39 |
| Conclusions and Recommendations | 43 |
| Nomenclature | 45 |
| References | 53 |
| Tables | 57 |
| Figures | 83 |
| Appendix A, Detailed Procedure and Equations | 105 |
| Appendix B, Derivation of the Equations for the Overall Core Flow Rates and Pressure Drops, and Methods of Measuring These Quantities | 165 |
| Appendix C, Details of the Fuel Element Coolant Channel Flow Equations | 185 |

CONTENTS (con't)

Page

Appendix D, Estimate of the Reduction of the Longitudinal Deflection of the Fuel Plates Due to the Stretching of the Side Plates ..... 191

Appendix E, Derivation of the Side Plate Temperature Equations .. 193

## Acknowledgement

Acknowledgement is given to R. Q. Wright and J. L. Lucius for the programming of this analysis for the computer. Without their dedicated efforts, the successful completion of this program would not be possible. Many thanks to R. D. Cheverton for helpful suggestions and to L. A. Haack for deriving correlations and checking the arithmetic in many parts of the analysis.

# HFIR FUEL ELEMENT STEADY STATE HEAT TRANSFER ANALYSIS
## REVISED VERSION

Howard A. McLain


## Abstract

The steady state heat transfer analysis of the HFIR fuel elements was completely rewritten using new information regarding the thermal deflections of the fuel plates. This analysis uses an integral thermal-hydraulic model which simultaneously accounts for the nuclear, hydraulic, heat transfer, mechanical, and the corrosion history of the operating reactor. It shows that the design requirements for the HFIR fuel elements have been met. Imposing the criteria of no boiling in the fuel elements, the upper limit for the power at startup is 139 Mw and that at the end of a 25 day 100 Mw fuel cycle is 153 Mw.


---

## Introduction

The heat transfer characteristics of the HFIR fuel elements have been studied extensively by Hilvety and Chapman[1-4] to assure that the reactor can safely operate at a nominal power level of 100 Mw. Their studies considered the nuclear, hydraulic, heat transfer, mechanical, and the metal corrosion factors in a consistent manner to provide an integral thermal-hydraulic model of the reactor at the various power levels. One of the most significant assumptions in their analysis was that regarding the deflection of the fuel plates due to the operating temperatures of the fuel plates which are higher than those of the side plates. The resulting thermal deflections of the fuel plate in the radial direction generally were neglected, since the side plates of a given fuel element were designed to rotate relative to one another. But the thermal deflections of these plates in the longitudinal direction were assumed to be sine waves based on the analysis of Lyon[5] and some preliminary experiments of Chapman.[6] The magnitude of these sinusoidal deflections at the HFIR operating conditions were relatively large, reducing the minimum channel thickness from about 0.040 in. to 0.012 in. in Hilvety and Chapman's analysis.[6] Both Lyon and Chapman expressed the need for further and more precise experimental data. Subsequent experiments by Cheverton and Kelley[7] on HFIR fuel

plates have shown that they do not deflect in the manner assumed by Lyon and Chapman, but that they consistently deflect uniformly in one direction.

In addition to the error in the nature of the thermal deflections, the effect of the sinusoidal deflections on the coolant flow rate down the strip of the coolant channel in which the limiting heat flux was located (defined as the hot streak by Hilvety and Chapman) was assumed to be negligible. Results of later studies shown in Fig. 1 indicate that this was not negligible for the HFIR conditions.[8] For sinusoidal deflections of the magnitude stated above, the ratio of the pressure drop through a channel with sinusoidal walls to that through a channel with uniform walls at a given flow rate is about 6.7. This implies that for a given pressure drop, the flow rate down the hot streak would be lowered by a factor of about 2.5. The consequences resulting from this lower flow rate would be serious in Hilvety and Chapman's analysis since this would limit the reactor operating power to some value significantly below 100 Mw. Because of this, this study and the fuel plate deflections experiments by Cheverton and Kelley were initiated.

Instead of reworking the analysis of Hilvety and Chapman to incorporate the factors mentioned above, this new analysis was written. As had been mentioned by them, their study had grown much beyond its original purpose, and any further modifications to their work would be awkward and time consuming.[4] Other modifications and corrections for minor errors also were necessary. In this analysis, the power and flow distributions are considered over the entire fuel assembly instead of preselecting a "hot streak." This gives a more accurate picture of the heat transfer and reduces the magnitudes of the uncertainty factors required to assure that the results are conservative. This resulted in many more steps in the calculations, but improvements in computer technology and convergence schemes kept the running times within reasonable limits. For completeness, however, many of the assumptions and equations used and/or derived by Hilvety and Chapman are included here.

## Criteria

The upper limit for the reactor power level is defined as the maximum steady state but momentary power level at which none of the local heat fluxes in the fuel elements exceed the corresponding values of the burnout heat fluxes. In order for this limit to be meaningful, the set points of the reactor control system must be considered. At the present time, the scram set point for the HFIR safety rods is 1.3 times the normal operating power level as indicated by the neutron flux channels. This implies that the reactor should be able to operate at 130% of its normal power level for short periods of time without damage to the fuel elements. The design operating power level for the HFIR is 100 Mw. Therefore the upper limit for the reactor power level should be equal to or greater than 130 Mw in order to have confidence that the fuel elements will not be damaged during the operation of the reactor.

Burnout heat fluxes in 0.050 in. thick rectangular channels at the anticipated HFIR operating conditions have been measured and correlated by Gambill.[9,10] However the use of these data in this analysis would require a thorough examination of the data to determine if they are valid at the upper limit for the reactor power level. This is necessary since there are unknown factors regarding the stability of the coolant flow within a given flow channel and the stability of the coolant flow in parallel channels due to the formation of bubbles during the boiling process. Also there are questions regarding the applicability of these burnout data to coolant channels having thicknesses significantly less than 0.050 in., such as those that may exist in the HFIR fuel elements during the operation of the reactor because of the fuel plate deflections.

Rather than to investigate these various factors regarding the application of Gambill's burnout data, incipient boiling heat fluxes were used in place of the burnout heat fluxes to determine the upper limit for the reactor power level. Incipient boiling heat fluxes are those at which the first significant effect of the nucleate boiling bubbles on the heat transfer rate or the coolant flow rate can be observed. Flow instability problems for heat fluxes below the incipient boiling heat fluxes are then automatically eliminated. Bergles and Rohsenow[11] derived the following

relation for predicting the incipient boiling heat fluxes of water in the pressure range of 15 to 2000 psia.

$$\left(\frac{q}{A}\right)_{ib} = 15.60\ P^{1.156}\ \left(T_S - T_{sat}\right)^{2.30/P^{0.0234}} \tag{1}$$

(The various symbols used in this and the following equations are defined in the nomenclature section on page 45.) Additional studies by Davis and Anderson[12] gives support to the validity of this relation. Experimental data given in both of these papers show that the surface temperature $T_S$ predicted by Eq. (1) for incipient boiling at a given heat flux and absolute pressure tends to be low. Therefore because of these comparisons with experimental data and the way this relation is used in this analysis, an uncertainty factor of 1.00 was used for Eq. (1); that is, the use of this relation in this analysis is assumed to always give conservative results.

The subject of flow instability is a relatively new field and is yet to be thoroughly explored.[13] However some preliminary burnout studies conducted at Argonne and associated with a reactor similar to HFIR (AARR) indicate that there is a possibility that the standard burnout data can be applied to the HFIR during normal full-power operation. This is apparently not true, however, at low flow and/or low pressure conditions.[14] The influence of the channel thickness, particularly for very thin channels, on the burnout heat flux is not well known. Burnout studies at 588 psia by Kafenguaz and Bauarov[15] indicate that there were no differences in the burnout heat fluxes for water flowing in channels with thicknesses greater than 0.0315 in., but they were lower for water flowing in channels with thicknesses less than 0.0315 in. However, even for coolant channels with thicknesses as low as 0.0078 in., burnout did not occur until the channel wall temperature was at least 36°F above the water saturation temperature. This gives some support to the use of the incipient boiling heat fluxes for the burnout heat fluxes in very narrow coolant channels. Chirkin and Iukin[16] made similar burnout studies for water at atmospheric pressure. At this pressure, they found that the channel thickness had no influence on the burnout heat flux until it was below 0.098 in.

If it can be shown eventually that the possible flow instability and the narrowing of the coolant channels during the nominal full power HFIR operation do not significally decrease the burnout heat flux, the relation recommended by Gambill[17] for predicting burnout heat fluxes can be used with confidence. This relation is as follows:

$$\left(\frac{q}{A}\right)_{bo} = \left(\frac{q}{A}\right)_{bo,nb} + \left(\frac{q}{A}\right)_{bo,boil} \tag{2}$$

where

$$\left(\frac{q}{A}\right)_{bo,nb} = K' \left(\frac{k}{D_e}\right) Re^{0.8} Pr^{1/3} \left(T_{Sbo} - T\right)$$

$$\left.\frac{q}{A}\right)_{bo,boil} = KL_v\rho_v \left[\frac{\sigma g_c a\Delta\rho}{\rho_v^2}\right]^{1/4} \left[1 + \left(\frac{\rho_\ell}{\rho_v}\right)^{0.923} \frac{c_p \Delta T_{sub}}{25L_v}\right]$$

$T_{Sbo}$ is the surface temperature at burnout shown in Fig. 2. This correlation agrees with the experimental burnout data better than the Zenkevich-Subbotin relation[18] previously recommended by Gambill and used in the analysis of Hilvety and Chapman.[4] Assuming that the constants $K'$ and $K$ in Eq. (2) have the values 0.019 and 0.12 respectively, Gambill estimated that the burnout data for the normal HFIR operating conditions are correlated within a factor of 1.25 by this relation. Therefore this relation was multiplied by an uncertainty factor $U_{22}$ having a value of 1/1.25 or 0.80 when it was used in this analysis.

For water, the various physical properties in Eq. (2) can be expressed in terms of temperatures and pressures. Using the physical properties published by Gambill[19] and by Keenan and Keyes,[20] Eq. (2) was rewritten in the following form for use in the computer in the burnout option of this analysis.

$$\left(\frac{q}{A}\right)_{bo,nb} = U_{22}\Big[7.263 \times 10^3 - 2.088 \times 10T + 4.726 \times 10^{-2}T^2$$

$$-5.685 \times 10^{-5}T^3 + 2.517 \times 10^{-8}T^4\Big] \frac{w^{0.8}T^{0.9296}}{e} \left(T_{Sbo} - T\right) \tag{3a}$$

$$\left(\frac{q}{A}\right)_{bo,boil} = U_{22}\Big[2.920 \times 10^{5} + 4.739 \times 10^{3}P - 1.464 \times 10P^{2}$$

$$+ 2.498 \times 10^{-2}P^{3} - 2.119 \times 10^{-5}P^{4} + 6.887 \times 10^{-9}P^{5}\Big] \cdot$$

$$\cdot \left[1 + 0.3710P^{-0.8525}\left\{1.117 - 2.060 \times 10^{-3}\left(\frac{T_{sat} + T}{2}\right)\right.\right.$$

$$+ 1.212 \times 10^{-5}\left(\frac{T_{sat} + T}{2}\right)^{2} - 2.865 \times 10^{-8}\left(\frac{T_{sat} + T}{2}\right)^{3}$$

$$\left.\left. + 2.648 \times 10^{-11}\left(\frac{T_{sat} + T}{2}\right)^{4}\right\}\left|T_{sat} - T\right|\right] \qquad (3b)$$

The data for the surface temperature at burnout shown in Fig. 2 was correlated for the computer as

$$T_{Sbo} = T_{sat} - 6.48 \times 10^{4}\,\frac{w}{\rho e} + 80.7264 + 1.47622 \times 10^{-1}P$$

$$- 2.35910 \times 10^{-4}P^{2} + 1.08545 \times 10^{-7}P^{3}\ . \qquad (3c)$$

In the application of the above correlations for incipient boiling and burnout heat fluxes, it was assumed that the size of a hot spot and proximity of one hot spot to another have no influence on the results predicted by these relations. This is a conservative assumption since the above correlations were developed from data for uniform heat fluxes.

All of the other correlations used in this analysis are valid for the various anticipated HFIR operating conditions. However for some input parameters outside of the range of these HFIR operating conditions, it is conceivable that some of these correlations such as those for the plate deflections may not be valid. For example it was found in the calculations for power levels above 150 Mw that the fuel plate temperatures exceeded those for which the correlation for the modulus of elasticity is valid. Therefore for these situations, the calculated maximum power levels are misleading.

## Short Outline of the Method of Analysis

In order to define an integral thermal-hydraulic model of the operating reactor, the following factors must be considered simultaneously.

1. Plant operating conditions
2. Power density distributions during the fuel cycle
3. Oxide film buildup on the fuel plates
4. Fuel plate deflections induced by differential pressures and temperatures
5. Coolant flow distribution within the fuel elements
6. Fuel segregation and cladding-fuel nonbonds
7. Heat transfer and burnout characteristics

The simultaneous use of these various factors results in a rather lengthy procedure with several iterative schemes. This procedure is described in detail in Appendix A.

The basic approach used in this analysis is to calculate the thermal-hydraulic history of the fuel elements at some specified power level for all time increments prior to the time at which the reactor power level is raised to the maximum value. This accounts for the burnup of the fuel and for the buildup of the oxide on the fuel plates. Then the power level is raised to a value consistent with the incipient boiling or the burnout criteria. A brief outline of this is as follows:

1. Divide the fuel elements into several axial and radial space increments consistent with the power density data, which can be specified for as many nodal points in the reactor core as desired. Normalize the power density data for each time increment.

2. Specify a reactor power level for all time increments prior to the time at which the reactor power is raised to the maximum value.

3. For the first time increment, calculate the flow and heat transfer characteristics in the average coolant channels and for the average fuel plates in the inner and the outer fuel elements. Assume that the average coolant channels have the same initial thicknesses and that the deflections of the average fuel plates are identical.

4. Calculate the overall flow rates and pressure drops in the fuel assembly and in the core region for the first time increment.

5. Calculate the average temperature distributions in the side plates for the first time increment.

6. For the first time increment, calculate the flow and heat transfer characteristics in the narrow and the wide coolant channels adjacent to the "hot" and the "cold" fuel plates. These particular fuel plates can have abnormal "averaged" fuel distributions; the total uranium in the "hot" plate being the maximum allowed by the specifications and that in the "cold" plate being the minimum allowed by the specifications.

7. Repeat steps 3 through 6 for all time increments prior to the time at which the reactor power is raised to the maximum power level.

8. Estimate a maximum power level for the reactor.

9. Repeat steps 3 through 6 assuming a time increment of zero to determine the flow and heat transfer characteristics at the maximum power level.

10. Calculate the hot streak flow rates, the hot spot heat fluxes and/or the hot spot surface temperatures, and the incipient boiling temperatures or the burnout heat fluxes at every point in the fuel assembly.

11. Compare the hot spot surface temperatures and the incipient boiling temperatures or the hot spot heat fluxes and the burnout heat fluxes.

For the incipient boiling option

(1) If one or more of the hot spot surface temperatures is higher than the corresponding values of the incipient boiling temperature, lower the maximum power level and repeat steps 8 through 11.

(2) If all of the hot spot surface temperatures are lower than the corresponding values of the incipient boiling temperatures, raise the maximum power level and repeat steps 8 through 11.

For the burnout option

(1) If one or more of the hot spot heat fluxes is higher than the corresponding value of the burnout heat flux, lower the maximum power level and repeat steps 8 through 11.

(2) If all of the hot spot heat fluxes are lower than the corresponding values of the burnout heat fluxes, raise the maximum power level and repeat steps 8 through 11.

12. Iterate steps 8 through 11 until the hot spot surface temperatures are equal to the corresponding value of the incipient boiling temperatures or the hot spot heat fluxes are equal to the corresponding values of the burnout heat fluxes at one or more locations in the fuel assembly. At the rest of the locations, the hot spot surface temperatures must be lower than the corresponding values of the incipient boiling temperatures or the hot spot heat fluxes must be lower than the corresponding values of the burnout heat fluxes. The reactor power level at these conditions is defined as the maximum power level.

## Plant Operating Conditions

A number of the plant operating parameters, which can be measured during the operation of the reactor, are specified as input data for this analysis.

First is the operating power level of the reactor, which is determined from the primary coolant flow rate and the temperatures of the coolant entering and leaving the reactor vessel. The value of this power level, designated as Q, is accurate within 2%, and therefore an uncertainty factor of 1.02 has been assigned to it. The fraction of the reactor heat removed from the fuel element surfaces, f, is estimated to be 0.975. The temperature of the coolant entering the reactor vessel $T_{in}$ can be measured to an accuracy of about 1%, and therefore it has an uncertainty factor of 1.01.

The operating or the reference pressure of the reactor, designated as P psia, is the static pressure in the upper plenum of the reactor vessel between the reactor vessel inlet and the core shroud region inlet. This pressure can be measured during reactor operation with a special pressure tap designated as RP-4. Since this is a reference quantity, no uncertainty factor has been assigned to it.

The pressure drop across the fuel element itself, $\Delta P_F$ psi, is specified as an input variable. This quantity is defined as the difference between the static pressure just above the fuel plates and that just below the fuel plates. It is different from the core pressure drop used by Hilvety and Chapman,[1-4] which is the difference between the static pressure in

the upper plenum region of the reactor vessel and that just below the fuel plates. Both of these pressure drops may be determined during the operation of the reactor by measuring the difference between the static pressure at tap RP-4 and the impact pressure at the N-16 probes. Details of converting the data obtained from these measurements into the core pressure drop $\Delta P_{core}$ and the fuel element pressure drop $\Delta P_F$ are shown in Appendix B. Since $\Delta P_F$ is also a reference quantity it does not have an uncertainty factor.

## Power Density Distributions in the Fuel Assembly

The power density distributions in the HFIR fuel elements have been estimated by Cheverton and Sims[22] and they are listed in Table 1. These distributions are for a fuel assembly having a life of 2500 Mw-days at times of 0 days, 1.01 days, 11.57 days, 22.72 days, and 25.00 days when the reactor is operated at 100 Mw. For cores having different lifetimes or for the reactor operating at different power levels, the times at which these distributions occur are proportional to the core life and inversely proportional to the reactor power level. An uncertainty factor having a value of 1.10 has been factored into these power densities for this heat transfer analysis to account for the uncertainties in the flux distributions and fuel burnup during the fuel cycle.

The power density distribution during each entire time increment was assumed to be equal to that at the beginning of that particular time increment. In most cases, this will make the results conservative, but one must be aware of this when inspecting the results for the location of the limiting heat flux. If smaller time increments are required, additional power distribution data can be obtained.

Except for the determination of the side plate temperatures, the power densities in the nonfueled regions of the fuel plates were assumed to be negligible. As shown in Figs. 3 and 4, these nonfueled regions are located between the fuel bearing material in the fuel plates and the side plates and at the upper and lower ends of the fuel plates.

## Fuel Element Tolerances

The HFIR fuel elements shown in Figs. 3 and 4 contain involute fuel plates having nominal thicknesses of 0.050 in. which form the coolant channels having nominal thicknesses of 0.050 in. The nominal total area for the transfer of heat from the fuel bearing portion of these plates is 428.8 $ft^2$. Of course these dimensions can vary from these nominal values,[23,24] and this will affect the heat removal characteristics. The tolerances specified for these dimensions are summarized in Table 2.

In addition to the dimensional variations, the uranium distribution in the fuel plates can vary from the specified values, and it can become segregated within local areas. Blisters or nonbonds also can form between the fuel and the clad. These factors can have adverse effects on the heat transfer characteristics and will limit the maximum power level. Because of this, the fuel plates are inspected very carefully for the maldistribution of the fuel and for the nonbonds during the fabrication of the elements. Permissible tolerances for these factors are also shown in Table 2.

## Fluid Flow

One dimensional incompressible fluid flow was assumed for this entire heat transfer analysis. As shown in Fig. 5, the coolant channels and the fuel plates were divided into increments to correspond with the given power density distributions. Mass flow rates per unit width of the coolant channel (the width direction is defined as that along the involute arc) where calculated at each value of $r_i$. It was assumed that there was no mixing of the coolant between the adjacent incremental strips in a given coolant channel. This is a conservative assumption, but dye flow tests at the HFIR normal operating conditions[24] and the ATR fluid flow and heat transfer studies[25] indicate that this assumption is realistic. The static pressures above and below the fuel plates were assumed to be uniform. This is valid since the designs of the core inlet and outlet regions are such as to minimize any possible flow maldistribution. The physical properties of the coolant water were evaluated at temperatures determined from heat balances using these flow rates, which of course results in an iterative type of solution of the flow and the heat balance equations. The total

flow rate down a given coolant channel can then be determined from the sum of the products of the flow rates per unit channel width and the appropriate incremental widths.

The upper edges of the fuel plates were rounded to minimize the pressure losses at the coolant channel inlets. A conservative estimate of the permanent pressure loss at this location is 0.04 velocity head.[26] The lower edges of these plates were not rounded since this would not materially reduce the pressure losses. The pressure loss of the coolant discharging from the coolant channel was estimated to be $(1 - A_1/A_2)^2$ velocity head; where $A_1$ corresponds to the channel thickness and $A_2$ corresponds to the channel thickness plus the fuel plate thickness. The pressure loss of the coolant flowing down the length of the channel was determined from the usual Moody relation which is

$$\Delta P = \int_0^L \rho \frac{f\, v^2}{D_e 2g_c}\, dz \ . \tag{4}$$

Details of the application of these relations and assumptions in this analysis are shown in Appendix C.

The friction factor f was assumed to be correlated by the relation

$$f = F/(Re)^{0.2} \tag{5}$$

A more accurate correlation for the friction factor is that derived by Colebrook[26] which is

$$\frac{1}{\sqrt{f}} = -2\ell n \left[ \frac{\epsilon}{3.7D_e} + \frac{2.51}{Re\sqrt{f}} \right] \tag{6}$$

This relation is considered to be too complicated to warrant its use here, but it does indicate that the surface roughness of the fuel plates is an important variable. Gambill and Bundy[9] and Griess et al.[27] measured the roughness of the oxide surfaces of specimens of heated fuel plate clad material (6061 aluminum) and found the root-mean-squared value of the surface roughness to be in the neighborhood of 60 to 75 $\mu$ in. Further flow tests by Gambill and Bundy[9] on similar aluminum specimens indicated

that the friction factors corresponded to those having absolute surface roughness to equivalent diameter ratios of $6.4 \times 10^{-4}$. Because of dimensional uncertainties, they considered their results to be accurate within 15%. Subsequent data taken during the precritical operation of the HFIR[28] indicate that the absolute surface roughness to equivalent diameter ratios varied from $7.9 \times 10^{-4}$ to $11.7 \times 10^{-4}$. For this study this ratio was assumed to be $12.0 \times 10^{-4}$ and the corresponding friction factors[29] are shown in Fig. 6. Equation (5) with the constant F having the value of 0.235 is also plotted in Fig. 6 for comparison. This value was used in the friction factor relation with an uncertainty factor of 1.05 in this heat transfer study.

Integration of Eq. (4) depends on the distribution of the local thicknesses down the length of the flow channel. If the changes in these thicknesses are gradual and large relative to the mesh spacing, an average thickness can be used for each increment of length. If they vary considerably within an incremental length, either a finer mesh spacing must be chosen or this relation must be integrated within each incremental length. Details of the latter for a flow channel with sinusoidal walls are shown in Appendix C.

## Heat Transfer

For a reactor operating at a power level of Q, the heat flux from any local surface area within the fuel element is

$$\left(\frac{q}{A}\right)_{i,j} = \frac{Qf\phi_{i,j}}{A} . \tag{7}$$

This relation assumes tacitly that the heat flux on both sides of the fuel plate are identical. Actually this is not the case because of the filler material in the fuel plates and because of the possible different water conditions on each side of the fuel plates. The effect of these items will be considered in the next section together with the effect of the fuel segregation and nonbonds on the local heat fluxes. These items have no effect on the coolant heat balances nor on the average fuel plate temperatures, however.

The coolant temperature at any location within the fuel element may be found from suitable heat balances. Such a heat balance is

$$\Delta T_{i,j} = \frac{2Qf}{Aw_i} \int_0^{z_j} \phi_{i,j} dz \approx \frac{Qf}{Aw_i} \sum_{j=2}^{j=j} \phi_{i,j-1} + \phi_{i,j} \Delta z_j \ . \qquad (8)$$

As shown in Appendix A, Eqs. (7) and (8) are modified by uncertainty factors to account for the following:

1. Uncertainty in the reactor power level
2. Uncertainty in the total heat transfer area
3. Uncertainty in the power density distribution

The magnitudes of these uncertainties are described elsewhere, and typical values of the factors describing these uncertainties are shown in Table 4.

The relation recommended by Gambill and Bundy[9] for predicting local heat transfer coefficients in the HFIR fuel elements is a modified version of the Hausen equation,

$$(Nu)_b = 0.116\ (Re)_b^{2/3} - 125\ (Pr)_b^{1/3}\ 1 + 1/3\ \frac{D_e}{z}^{2/3} \cdot \frac{\mu_b}{\mu_S}^{0.14} \qquad (9)$$

This relation was rewritten for water for use on the computer, and the rewritten form is

$$h_b = \frac{U_8}{e} \left[5.429 \times 10^2 - 1.561T + 3.533 \times 10^{-3}T^2 - 4.250 \times 10^{-6}T^3 + 1.882 \times 10^{-9}T^4\right] \cdot \left[(245.5\ w\ T^{1.162})^{0.6667} - 125\right] \cdot \left[1 + 1/3 \left(\frac{2 \times 10^{-3}e}{z}\right)^{0.6669}\right] \left(\frac{T_S}{T}\right)^{0.163} \qquad (10)$$

where $U_8$ is the uncertainty factor. Since Gambill and Bundy estimated that this relation is accurate to within 10%, the value of this factor was assumed to be 0.90.

There is some reduction in the magnitude of the local heat transfer coefficients at the corners of the fuel element coolant channels. Studies of the local heat transfer coefficients near the corners of noncircular coolant channels for fluids having Prandtl numbers of 1.0 have been made by Eckert and Low.[30] Their results should be conservative for the HFIR coolant since its Prandtl number is greater than unity. The smallest included angle between the fuel plate and the side plate in the HFIR fuel assembly is that located at the outer side plate of the inner fuel element, which is 32° 42'. This case is considered in Fig. 7, which assumes that the closest approach of the fuel bearing material to the side plate is 0.045 in.[23] The ratio to the local heat transfer coefficient at this edge of the fuel bearing material to the average heat transfer coefficient is 0.99 which is considered to be acceptable.

## Hot Spot Heat Transfer

In considering the maximum possible local heat fluxes, called "hot spots," the heat balances at different positions on the surface of the fuel plate must be modified to account for any defects in the fuel plate. These include the variations of the fuel concentrations within the specified limits or the presence of nonbonds between the fuel bearing material and the clad material. A "hot plate" is defined for the purposes of this analysis as a fuel plate which has the maximum "average" fuel concentrations permitted in the specifications.[23] They state that the "average" amount of uranium within any given area measuring 1/2 in. or more along the length of the plate and across the full width of the plate must be within 10% of the nominal design value. The total fuel loading in any given plate, however, must be within 1% of the nominal value. These fuel plates also may have pockets of segregated uranium within circular portions of the plate surface having diameters of 5/64 in., the diameter of the x-ray beam of the inspection device. The quantity of fuel within this circular area must not be greater than 30% in excess of the nominal amount. In addition to these variations, the boundary of the fuel bearing material can extend beyond the design limits. This is particularly important at the sides and the lower end of the fuel element where the fuel in an individual

plate extends beyond the nominal design boundaries and be exposed to higher than nominal thermal neutron fluxes.

Calculations by Hilvety and Chapman[4] show that fuel plates with other sets of tolerances for the amount of uranium within local areas of the fuel plates are acceptable for the HFIR operating conditions. At the present time, fuel plates having "average" concentrations of uranium within 27% of the design values are being accepted for use in the HFIR.

The coolant channels adjacent to the hot plate are defined as the hot and cold channels depending on which side of the fuel plate the heat flux is the greatest. Because of the nature of the thermal deflections of the fuel plates during reactor operation, the most pessimistic situation may exist when a "cold plate" is adjacent to a "hot plate." The "cold plate" is defined as a fuel plate which has the minimum "average" fuel concentrations permitted in the specifications.

To calculate the bulk water temperatures in the hot and cold channels, the heat balance relation, Eq. (8), is modified by additional hot plate and cold plate uncertainty factors called $U_4$ and $U_5$ respectively in this study. Numerical values of these factors are a function of their location on the fuel plate surface, and they must be consistent with the specifications mentioned above. For the results reported below, the values of $U_4$ were assumed to be 0.92 for the upper half of the plate and 1.10 for the lower half of the plate. The values of $U_5$ were assumed to be 1.08 for the upper half of the plate and 0.90 for the lower half of the plate. This results in the minimum coolant channel thicknesses for the lower half of the hot channels. For the "hot streak," which is the strip of the fuel plates and the coolant channel directly above the hot spot, the "average" fuel concentrations in both fuel plates are assumed to be the maximum allowable values. In this case, the heat balance relation, for calculating the coolant temperatures, Eq. (8), is modified further by another uncertainty factor called $U_{24}$. The value of this factor for the results reported below is 1.10.

Considering the hot spots on the surface of the hot plate, it was assumed for the purpose of the incipient boiling or burnout comparisons that they could be at any location on the hot plate surface. These hot spots are due to the extension of the fuel bearing material beyond its

nominal boundaries, to local segregation of the uranium, and to nonbonds located between the fuel bearing material and the cladding. All these factors were considered simultaneously in order to calculate the maximum possible heat flux. Numerical values of these hot spot heat fluxes were determined from Eq. (7) using additional uncertainty factors to account for these three abnormalities.

The uncertainty factor to account for the extension of the fuel bearing material in the fuel plate, beyond the nominal boundaries, defined as $U_{25}$ in this analysis, is a function of the location on the fuel plate's surface. It was assumed that the value of this factor is unity at every location except at the bottom end of the fuel bearing material.* At this location, the values of this factor were assumed to be those determined by Cheverton and Sims[7] shown in Table 3. These factors are for the maximum extension of the fuel plate beyond the design boundaries permitted in the present specifications.[23]

To account for the fuel segregation and the nonbonds in the fuel plates, still another uncertainty factor, which is shown below, was used in Eq. (7). This factor considers both the maximum local fuel segregation and the nonbond, sometimes called a "blister," of the maximum possible diameter allowed by the present specifications,[23] which is 1/16 in. Values of this factor used in this analysis were those determined by Hilvety and Chapman[4] using the model shown in Fig. 8. This model assumes that the uranium within the segregated spot is a cylinder having a length equal to the thickness of the fuel bearing material and having a packing fraction of 0.74. Also, it assumes that nonbond is located between the fuel bearing material and the thick clad. The correlation derived by them is

$$U = 1.0 + (\bar{U} - 1.0)\,\frac{h}{15{,}000} \qquad (11)$$

---

*This may be a slightly optimistic assumption since this factor could have values greater than unity at the radial edges of the fuel plates. Future studies should consider these additional values for the calculation of hot streak and the hot spot temperatures.

where $\bar{U}$ is the product of a local fuel segregation factor and a local nonbond factor. The local fuel segregation factor, defined as $U_{18}$ and $U_{19}$ for the hot and cold channels respectively, is simply the ratio of the actual amount of fuel to the specified amount of fuel within the inspection spot. Since the specifications allow a maximum deviation of 30% in local fuel concentration, the value of this factor was assumed to be 1.30. The nonbond factors for the hot and cold channels, defined as $U_{20}$ and $U_{21}$ and shown in Figs. 9 and 10, have been determined by Hilvety and Chapman using the Astra HEATING code.[37] These factors consider all of the other effects at the hot spot such as the nonbond, fuel bearing material thickness, and the clad thickness. They are, therefore, functions of their location along the width of the fuel plate; and the results shown in Figs. 9 and 10 were correlated by Haack[32] as functions of this variable. For the inner fuel element this correlation is

$$U_{20} = 1.33687 - 0.35423s + 0.14503s^2 - 0.01669s^3 \tag{12}$$

for the hot channel, and

$$U_{21} = 0.863686 - 0.016507s - 0.010950s^2 + 0.0047976s^3 \tag{13}$$

for the cold channel. For the outer element it is

$$U_{20} = 1.180171 - 0.278079s + 0.151756s^2 - 0.014261s^3 \tag{14}$$

for the hot channel, and

$$U_{21} = 0.881393 - 0.249204s + 0.181639s^2 - 0.033932s^3 \tag{15}$$

for the cold channel.

Haack has reviewed the uncertainty factors defined by Eq. (11) using more recent information regarding the material properties and inspection techniques.[32] The 0.74 packing fraction for the segregated fuel is considered valid, since this is the highest value that can be obtained for uniform spheres. Random packing of uniform spheres would result in lower values, but the presence of nonspherical particles and particles of other diameters would result in higher values. These effects therefore are considered compensating. Haack obtained the thermal conductivity values of the various fuel element materials from McElroy.[33] Thermal conductivities of $U_3O_8$ – aluminum cermets were not available, and the values for these

were assumed to be equal to those of $UO_2$ – aluminum cermets shown in Fig. 11. These and other quantitative assumptions used by Haack in his review are summarized as follows:

| | |
|---|---|
| Power density | 2 Mw/ℓ of core |
| Heat generation rate in clad and oxide ($\gamma$ heating) | 100 watts/gm |
| Packing fractions of $U_3O_8$ in cermet | |
| Segregated fuel | 0.74 |
| Nominal inner element fuel | 0.128 |
| Nominal outer element fuel | 0.193 |
| Thermal conductivities | |
| Segregated fuel | 7.51 Btu/(hr)(ft)(°F) |
| Nominal inner element fuel | 76.3 Btu/(hr)(ft)(°F) |
| Nominal outer element fuel | 63.6 Btu/(hr)(ft)(°F) |
| Clad (6061 aluminum) | 87.4 Btu/(hr)(ft)(°F) |
| Oxide | 1.3 Btu/(hr)(ft)(°F) |
| Heat transfer coefficient | 15,000 Btu/(hr)(ft)(°F) |

The heat generation rates in the nominal fuel were determined from the power density data assuming that all of the heat was generated in the fuel cermet. Those in the segregated fuel were assumed to be those in the nominal fuel multiplied by the ratio of the packing fraction of the segregated fuel to that of the nominal fuel.

Using these parameters, Haack first calculated hot spot uncertainty factors for isolated pockets of segregated fuel with nonbonds using models similar to that shown in Fig. 8. Most of the cases studied by him were at the inner edge of the inner fuel element where the fuel cermet is 0.010 in. thick. Results of the various cases at this location studied by him are summarized in Fig. 12, and the uncertainty factor calculated by Hilvety and Chapman is included for comparison. It can be seen readily that the value reported by Hilvety and Chapman is conservative. The worse heat flux peaking occurs when there is a pocket of segregated fuel with a nonbond located between the fuel and the thick cladding (filler material) and there is no oxide on the fuel element surface. A second nonbond located between the fuel and the thin cladding or the buildup of the oxide

on the fuel plate surface lowers this heat flux peaking. Also the highest heat flux peaking occurs when the segregated fuel diameter within the inspection spot is the minimum value, which is 0.01957 in. in this case. Increasing the diameter but keeping the same volume of the segregated material within this inspection spot decreases the magnitude of these uncertainty factors. Some additional calculations of these factors for isolated pockets of segregated fuel at the location of the inner fuel element where the fuel cermet is 0.025 in. thick also indicate that the values calculated by Hilvety and Chapman are conservative.

Some cases were studied to obtain hot spot factors when the pockets of the segregated fuel and the nonbonds are relatively close to each other. The first case studied was a bar of segregated material across the width of fuel plate with and without a nonbond strip superimposed on it. For the purpose of these calculations, the fuel cermet thickness was assumed to be 0.010 in. across the entire width of the plate, which is conservative. This is somewhat of an idealized model, but it is possible to have bars of segregated fuel and/or a nonbond strip across the width of the fuel plate using the present inspection techniques. Uncertainty factors calculated for these situations and shown in Fig. 12 are higher than that of Hilvety and Chapman for an isolated pocket of segregated fuel and superimposed nonbond.

Another situation studied by Haack was the effect of the proximity of the pockets of segregated fuel and nonbonds to one another. The model and the results of this calculation are shown in Fig. 13. This model is again conservative, but it indicates that if the segregated fuel pocket and the nonbond centerlines are within 0.09 in. of each other, the uncertainty factors are again greater than that of Hilvety and Chapman. Haack investigated this situation further and found that one possible arrangement of the segregated fuel pockets using the present specifications and inspection techniques is that shown in Fig. 14a. Approximating this situation with the model shown in Fig. 14b, he calculated an uncertainty factor of 1.839, which is again greater than the Hilvety and Chapman value of 1.707 for an isolated segregated fuel pocket and nonbond.

Therefore, for the assumptions made in the above study, the uncertainty factors of Hilvety and Chapman are conservative for isolated pockets

of segregated fuel and nonbonds. However, if these pockets and nonbonds are close together the uncertainty factor could be greater than the value calculated by Hilvety and Chapman. It should be noted however that the proximity models were idealized for 0.010 in. thick fuel material and 1/16 in. diameter nonbonds. Further work is required using a more sophisticated model to determine if these factors are as high as those calculated here.

## Oxide Buildup on the Fuel Plate Surfaces

The aluminum fuel plates will corrode during the operation of the HFIR building up an oxide layer on the plate surfaces. This oxide decreases the coolant channel thicknesses and increases the fuel plate metal temperatures because of its low thermal conductivity. Griess et al.[27,34-36] studied the rate of this oxide buildup extensively considering the effects of the water temperature, the water pH, the heat flux from the aluminum surface, and the history of the oxide buildup. They found that the oxide is boehmite, which is the monohydrate of aluminum oxide, and that it has a thermal conductivity of 1.3 Btu/(hr)(ft$^2$)(°F)/ft. The density of this material is reported to be 3.02 g/cm$^3$. (Ref. 37)

For a constant fuel plate surface (water-oxide interface) temperature $T_S$ °R, heat fluxes from $1.0 \times 10^6$ to $2.0 \times 10^6$ Btu/(hr)(ft$^2$), a water pH from 4.7 to 5.0, and with no oxide initially on the aluminum surface, the oxide thickness in X mils after $\theta$ hrs is

$$X = 443\theta^{0.778} \exp\left(\frac{-8290}{T_S}\right) \tag{16}$$

This is the relation used in this study for the initial time step, which is conservative providing the water pH is kept in the range of 4.7 to 5.0. Water pH's in the range of 5.7 to 7.0 result in oxide thicknesses 2.7 times those calculated in Eq. (16), and a water pH of 5.3 results in oxide film thickness nearly as large as those for a water pH of 5.7 to 7.0. Therefore, control of the primary coolant pH is very important for the successful operation of the reactor. Lower surface heat fluxes result in lower oxide film thicknesses, but data for these conditions are limited.

During the subsequent time steps where the fuel plate surface temperature may change, the rate of oxide growth depends on the amount of oxide already present on the plate surface. For the second time increment where the surface temperature is $T_{S2}$ instead of $T_{S1}$, the oxide thickness is

$$X_2 = \Delta X_2 + X_1 = 443 \left\{\psi_1 + \theta_2\right\}^{0.778} \exp \frac{-8290}{T_{S2}} \tag{17}$$

where

$$X_1 = 443\theta_1^{0.778} \exp \frac{-8290}{T_{S1}} = 443\psi_1^{0.778} \exp \frac{-8290}{T_{S2}}$$

or

$$\psi_1 = \theta_1 \exp 10{,}656 \frac{T_{S1} - T_{S2}}{T_{S1}T_{S2}}$$

Generalizing this relation for the kth time increment,

$$X_k = \Delta X_k + X_{k-1} = 443 \left\{\psi_{k-1} + \theta_k\right\}^{0.778} \exp \frac{-8290}{T_{Sk}} \tag{18}$$

where

$$\psi_{k-1} = \left\{\psi_{k-2} + \theta_{k-1}\right\} \exp 10{,}656 \frac{T_{Sk-1} - T_{Sk}}{T_{Sk-1}T_{Sk}}$$

These equations have been checked against out-of-pile and in-pile experimental data[36,38] and they were found to be in good agreement. The maximum deviation in the oxide thickness measured by experiment from that predicted by the above equations is about 25%. An uncertainty factor of 1.25 therefore was factored into these relations when they were used in this study.

After the thickness of the oxide reaches 2 to 3 mils, it begins to spall or flake off from the fuel plate surface.[36] Any thermal cycling of the fuel element enhances this spalling process, but no allowance was made

for this in this analysis. Therefore it was assumed that after the oxide thickness reached 3 mils, no more oxide would be formed on the fuel plate. This is a conservative assumption since any additional oxide forming on the plate surface would spall off from the fuel plate thus increasing the channel thickness. In the cases reported below, nowhere did the oxide thicknesses including those for the hot plate exceed 2 mils.

Although boehmite has a higher density than aluminum (3.05 vs 2.70 $g/cm^3$), it also has a higher molecular weight (119.98 vs 53.96 for the equivalent amount of aluminum). This will result in a small decrease in the coolant channel thickness due to the formation of the oxide. The ratio of the thickness of the oxide formed to that of the aluminum metal consumed was then assumed to be

$$\frac{\text{Oxide thickness}}{\text{Metal thickness}} = \left[\frac{119.98 \times 2.70}{53.96 \times 3.20}\right]^{1/3} = 1.254 \qquad (19)$$

## Deflection of the Fuel Plate Due to Differential Pressures

A fuel plate located between a "narrow" coolant channel, which has the minimum average thickness permitted by the fuel element specifications, and a "wide" coolant channel, which has the maximum average thickness permitted by the specifications, is subjected to differential pressures across the thickness of the plate. This is due to the coolant velocity in the wide channel being higher than that in the narrow channel, resulting in lower operating pressures in the wide channel. As was done by Hilvety and Chapman,[4] it was assumed that this differential pressure was uniform over the entire surface of the fuel plate. This is taken to be the average of the differential pressures at the coolant channel inlet and at the coolant channel outlet. This assumption should be conservative providing the limiting heat flux occurs below the core midplane. Details of the relation for predicting this pressure difference are shown in Appendix C.

Deflections of HFIR fuel plates having fixed edges and pinned edges due to these pressure differences have been analyzed by Chapman.[39] The deflections calculated for plates with the pinned edges were generally higher than those with the fixed edges and were in closer agreement with

the experimental deflection data obtained by Chapman. The deflections for the pinned edge plates therefore were assumed for this analysis, and Haack[40] correlated Chapman's results in the form of a power series. These are for the inner fuel element plates

$$\delta = \frac{\Delta P_{nw}}{E.R.} \; 2.8372 \times 10^{-2} s^5 - 2.0491 \times 10^{-1} s^4 + 2.7529 \times 10^{-1} s^3 + 5.7806 \times 10^{-1} s^2 - 8.9329 \times 10^{-1} s \qquad (20a)$$

and for the outer fuel element plates

$$\delta = \frac{\Delta P_{nw}}{E.R.} \; 3.0799 \times 10^{-2} s^5 - 1.9700 \times 10^{-1} s^4 + 2.3697 \times 10^{-1} s^3 + 4.2645 \times 10^{-1} s^2 - 5.9068 \times 10^{-1} s \qquad (20b)$$

where

$\delta$ = mils
$\Delta P_{nw}$ = psi
$s$ = in.

The relation for the term E.R. was derived by Chapman[41] using the data reported in the Alcoa Aluminum Handbook[42] to account for the effect of temperature on the modulus of elasticity, and it is

$$E.R. = -(1.624 \times 10^{-6})T^2 + 4.719 \times 10^{-4} T + 0.9737 \qquad (21)$$

where T = °F.

Chapman estimated that the results of his analysis are accurate to within 10%. Therefore an uncertainty factor of 1.10 has been factored into Eqs. (20a) and (20b) for this heat transfer study.

## Increase of Fuel Plate Thicknesses Because of Heating

Aluminum of course will expand upon an increase in temperature, and this will decrease slightly the coolant channel thickness. The average thermal coefficient of expansion of 6061 aluminum for the temperature

range of interest here is $13.5 \times 10^{-6}$ in./(in.)(°F).[42] Since the contribution of each surface of the fuel plate to the decrease in the coolant channel thickness is considered in this analysis, the relation describing this is then (assuming a 70°F reference temperature*)

$$\delta = \frac{\alpha t}{2} (T - 70) = (6.74 \times 10^{-6} t)(T - 70) \qquad (22)$$

where

$\delta$ = mils

$t$ = mils

$T$ = °F.

There is also some contribution to the increase in the fuel plate thickness due to the partially restrained thermal expansion along the plate width and length (Poisson's effect). This increases the fuel plate thickness further by a factor of about 1.3. This factor was included as part of the total uncertainty factor $U_{12}$, which was estimated to be 2.0.

## Fuel Plate Deflection Due to the Difference in Temperatures of Adjacent Plates

Although the fuel plates are allowed to expand radially by having one of the fuel element side plates fixed and other one free to rotate, some of these plates have higher operating temperatures than others. The deflection of these hotter plates relative to the average fuel plates therefore must also be considered. Chapman analyzed this for plates with fixed and pinned edges[39] and Haack correlated Chapman's results for plates with pinned edges in the form of power series.[40] For the inner fuel element

---

*This is a conservative assumption since no allowance has been made here of the temperature expansion of the side plate. This factor should be included in any future versions of this heat transfer analysis. The thermal expansion of the side plate increases the channel thickness $\alpha e(T_{SP} - 70)$, and the additional thermal expansion of the fuel plate decreases the channel thickness $\alpha t(T - T_{SP})$. Therefore Eq. (22) should be modified to be

$$\delta = \frac{\alpha}{2} \left[ tT - (e + t)T_{SP} + 70e \right] .$$

plates, they are

$$\delta = \frac{T_M - T_{MA}}{E.R.} \left[ -3.2084 \times 10^{-4} s^5 + 4.3177 \times 10^{-3} s^4 - 1.8077 \times 10^{-2} s^3 + 1.1087 \times 10^{-2} s^2 + 4.3908 \times 10^{-2} s \right] \quad (23a)$$

and for the outer fuel element plates, they are

$$\delta = \frac{T_M - T_{MA}}{E.R.} \left[ -1.8518 \times 10^{-4} s^5 + 4.5322 \times 10^{-3} s^4 - 2.1050 \times 10^{-2} s^3 - 6.0732 \times 10^{-4} s^2 + 8.3033 \times 10^{-2} s \right] \quad (23b)$$

where

$\delta$ = mils

$T_M - T_{MA}$ = °F

$s$ = in.

Chapman estimated that the results for his analysis here are also accurate to within 10%. Therefore, an uncertainty factor of 1.10 has been factored into these equations.

## Fuel Plate Deflection Due to the Difference Between the Fuel Plate and the Side Plate Temperatures

As was mentioned in the introduction, one of the most significant deflections of the fuel plates in the analysis of Hilvety and Chapman is the longitudinal buckling of the plates due to the differences in the operating temperatures of the plates and those of the side plates. Preliminary analysis by Lyon[5] and some very preliminary experiments by Chapman[6] indicated that the fuel plates would buckle in sinusoidal waves for the HFIR operating conditions. Lyon estimated that the wave length of these deflections is 1.9 in. and that the amplitudes of these waves are those shown in Fig. 15. For the first option of this study (see Appendix A), these amplitudes were correlated by the relation

$$\delta = 0.0063(\Delta T)^{1.312} \quad (24)$$

where

$\delta$ = deflection in mils

$\Delta T$ = temperature difference in °F.

Also in this option of this study, the wave length was assumed to be 2.0 instead of the 1.9 in. value predicted by Lyon.

As was stated by Lyon,[5] his calculations were preliminary and additional experiments were necessary to verify his results. Such experiments were run by Cheverton and Kelley,[7] and they found that the fuel plates do not buckle in a sinusoidal wave, but deflect consistently in one direction for the predicted HFIR operating conditions. Figure 16 shows typical results from one of their runs where a 6061 aluminum plate was clamped in a carbon steel frame at room temperature and then heated to 400°F. The amplitudes of these deflections were found to be nearly proportional to the differential strain for plate temperatures up to 400°F. The difference in the thermal expansion of the test plate and the carbon steel frame in the furnace at 400°F was measured to be 0.046 in. Figure 16 shows that the maximum amount of deflection at this temperature is 12 mils. Assuming that the average coefficient of thermal expansion of 6061 aluminum in this temperature range is $13.8 \times 10^{-6}$ in./(in.)(°F), the maximum amount of deflection $\delta$ mils for a temperature difference of $\Delta T$ °F between the fuel plate and the side plate is

$$\delta = \frac{(12)(24)(13.8 \times 10^{-6})(\Delta T)}{(0.046)} = 8.64 \times 10^{-2} \Delta T \ . \qquad (25)$$

The deflection across the width of the fuel plate and at the ends of the fuel plate can be approximated by sine curves, and these approximations are shown as dashed lines in Fig. 16. Therefore, the thermal deflection at any location on the fuel plate for a temperature difference of $\Delta T$ °F can be described by the following relations:

For $0 < z < 6$ in.

$$\delta = 8.64 \times 10^{-2} \Delta T \sin \frac{\pi s_i}{\sum_{i=1}^{m} \Delta s_i} \sin \frac{\pi s_j}{12} \ . \qquad (26a)$$

For $6 \leq z \leq 18$ in.

$$\delta = 8.64 \times 10^{-2} \Delta T \sin \frac{\pi s_i}{\sum_{i=1}^{m} \Delta s_i} . \tag{26b}$$

For $18 < z < 24$ in.

$$\delta = 8.64 \times 10^{-2} \Delta T \sin \frac{\pi s_i}{\sum_{i=1}^{m} \Delta s_i} \sin \frac{\pi(24 - z_j)}{12} . \tag{26c}$$

These relations were used in place of Eq. (24) for the longitudinal deflection of the fuel plates in the second option of this heat transfer study (see Appendix A). The application of these equations is conservative, however, since no allowance has been made for the stretching of the side plates by the fuel plates. A rough estimate shown in Appendix D indicates that the stretching of the side plates would lower these deflections about 38%. Since the accuracy of the experiments is considered to be much better than 38%, the uncertainty factor for these relations has been given a value of 1.00.

The temperature differences in the above relations were assumed to be the difference between the average fuel plate metal temperature and the average of the side plate temperatures at any given elevation. The usual heat transfer equation for a slab with internal heat generation was used to get the side plate temperature (axial conduction being neglected). Heat transfer coefficients on the fuel plate side of the side plates were assumed to be 1/2 of the normal fuel plate heat transfer coefficient. Those on the other side were assumed to be those predicted by the Dittus-Boelter relation. Details of these equations and the justification of these assumptions are shown in Appendix E. Heat generation rates in the side plates and in the water surrounding them were estimated from Vondy's calculations.[43] For aluminum, it is 40 watts/gm and for water, it is 80 watts/gm.

## Fuel Plate Deflections Due to Radiation Growth

There is only a small amount of experimental data regarding the growth of the fuel plates due to radiation at the HFIR operating conditions. The available data[43a] indicate that by the end of the fuel cycle (~25 days), the volume of a fuel plate in the highest burnup density region will have increased by about 2%, and for the core average conditions, this increase will be about 1/2%. These volume changes are not negligible, but because of the uncertainty and the late availability of the few available data points, these changes were not included in the calculation of the results reported below. However, provisions were made in the general model to include this factor as input data.

Radiation swelling of the fuel plates reduces the coolant channel thicknesses two ways. First it increases the thicknesses of the fuel plates. A first approximation of this assumed for this analysis is that it is a linear function of the operating time, which results in the relation

$$\delta_{VR} = B\theta \tag{27}$$

where

$\delta_{VR}$ = thickness change in mils
$B$ = a constant
$\theta$ = total operating time in hours.

The second effect of the radiation swelling of the fuel plates may increase the longitudinal deflection of these plates. In the first option of this heat transfer analysis, it was assumed that the fuel plates buckled into a sinusoidal wave form. The growth of the fuel plates due to radiation could increase the magnitude of this buckling. As a first approximation of the magnitude of this increase, the change in the fuel plate material density due to radiation was related to the thermal coefficient of linear expansion in the following way:

$$\frac{1/\rho_R - 1/\rho}{1/\rho} = \left[1 + \alpha\Delta T\right]^3 - 1 \approx 3\alpha\Delta T \tag{28}$$

Combining this relation with Eq. (24) assuming that $\alpha$ is equal to $13.5 \times 10^{-6}$ in./(in.)(°F), the magnitude of the sinusoidal buckling of the fuel plates due to radiation is then

$$\delta_{MR} = 3.651 \times 10^{3} \left[ \frac{\rho}{\rho_R} - 1 \right]^{1.312} \tag{29}$$

where $\delta_{MR}$ is deflection in mils.

In the second option of this analysis, it was assumed that the fuel plates buckled consistently in one direction. It was further assumed here that the magnitude of these deflections due to radiation growth were the same for all of the fuel plates. Therefore for this situation, the effect of this deflection on the coolant channel thickness can be neglected.

The available experimental data[43a] indicate that essentially all of the changes in the plate volume appear as changes in the plate thickness. If this is actually the case, then it would not be necessary to consider the longitudinal deflections due to the radiation swelling of the fuel plates.

## Coolant Channel Thicknesses During Reactor Operation

A number of coolant channel thicknesses have been defined in order that each step in this analysis can be handled in a conservative but consistent manner. Pertinent fuel plate deflections were considered in the calculations of all of these thicknesses, and they were summed such as to give the most conservative value in each case.

The average coolant channel, which was used to determine the average fuel plate conditions and the overall core flow conditions, was assumed prior to the reactor operation to have a uniform thickness of the average value determined for each fuel element. The walls of this coolant channel were assumed to be the average fuel plates in the fuel element. Since the deflections of these average fuel plates are identical, the thicknesses of the average coolant channel during reactor operation is then

$$e = e_A - 2\delta_A - 2\delta_{VR} - 2\delta_o \tag{30}$$

where

$e_A$ = initial coolant channel thickness,

$\delta_A$ = one half of the increase in the fuel plate thickness due to heating,

$\delta_{VR}$ = one half of the increase in the fuel plate thickness due to radiation,

$\delta_o$ = increase in the fuel plate thickness due to oxide formation.

As shown in Figs. 17 and 18, the coolant channels adjacent to the hot and cold plates in the fuel element can be either "narrow" channels or "wide" channels. The "narrow" coolant channel is defined as one in which the entire channel thickness prior to reactor operation is the minimum permitted for any given cross section of an individual coolant channel. Present fuel element specifications state that the value of this quantity is 0.044 in. (Ref. 23). Similarly the "wide" coolant channel is defined as one in which the entire channel thickness prior to the reactor operation is the maximum permitted for any given cross section of an individual coolant channel. The value for this in the present HFIR fuel element specification is 0.056 in. (Ref. 23).

As discussed above the longitudinal deflections of the fuel plates were assumed to be in the form of sinusoidal waves for option I of this analysis. The greatest amount of resistance to the coolant flow for this situation would occur when two adjacent hot plates have this type of deflection 180° out of phase. Various possible arrangements of the narrow and wide coolant channels adjacent to the hot plates must be considered and these are shown in Fig. 17. They are identical to those used by Hilvety and Chapman,[4] and they assume that all of the fuel plates adjacent to the hot plate in question are also hot plates. For this situation, the thicknesses of the narrow coolant channel during reactor operation can be described by the relation

$$D_n = D_{1n} + D_{2n} \sin \frac{2\pi z}{\lambda} \tag{31}$$

where

$$D_{1n} = e_n - (2\xi_1 + 2\xi_2 + \xi_3)\delta_{\Delta P} + \xi_3(\delta_{Tnw,TA} - \delta_{Tnn,TA})$$

$$- (\xi_3 + 2\xi_4)\delta_{nn} - (2\xi_1 + 2\xi_2 + \xi_3)\delta_{nw} - 2\delta_{on} - 2\delta_{VR} \qquad (31a)$$

and

$$D_{2n} = -(\xi_3 + 2\xi_4)\delta_{Mnn} - (2\xi_1 + 2\xi_2 + \xi_3)\delta_{Mnw} - 2\delta_{MR} \ . \qquad (31b)$$

The thicknesses of the wide coolant channel during reactor operation can be described similarly by the relation

$$D_w = D_{1w} + D_{2w} \sin \frac{2\pi z}{\lambda} \qquad (32)$$

where

$$D_{1w} = (\xi_1 + \xi_2 + \xi_3)e_w - (2\xi_1 + \xi_2 + 2\xi_3)\delta_{\Delta P}$$

$$+ \xi_2(\delta_{Tww,TA} - \delta_{Tnw,TA}) - \xi_2\delta_{ww} - (2\xi_1 + \xi_2 + 2\xi_3)\delta_{nw}$$

$$- 2(\xi_1 + \xi_2 + \xi_3)\delta_{ow} - 2(\xi_1 + \xi_2 + \xi_3)\delta_{MR} \qquad (32a)$$

and

$$D_{2w} = -(2\xi_1 + \xi_2 + 2\xi_3)\delta_{Mnw} - \xi_2\delta_{Mww} - 2(\xi_1 + \xi_2 + \xi_3)\delta_{MR} \qquad (32b)$$

where

$e$ = initial channel thickness,

$\delta_{\Delta P}$ = deflection due to the pressure difference across the fuel plate,

$\delta_{T,TA}$ = deflection due to the difference of temperatures of adjacent fuel plates,

$\delta$ = one half of the increase in the fuel plate thickness due to heating,

$\delta_o$ = decrease in the channel thickness due to the oxide buildup on the plate surface,

$\delta_M$ = deflection due to the longitudinal buckling of the fuel plate because of the difference in the temperatures of the fuel plate and the side plates,

$\delta_{VR}$ = one half of the increase in the fuel plate thickness due to radiation,

$\delta_{MR}$ = deflection due to the longitudinal buckling of the fuel plate because of radiation growth,

n = subscript for the narrow coolant channel,

w = subscript for the wide coolant channel,

$\xi_1$, $\xi_2$, $\xi_3$, and $\xi_4$ = 1 respectively for Cases 1, 2, 3, and 4 shown in Fig. 17. They are 0 otherwise.

The inlet and exit thicknesses of the narrow and the wide coolant channels during reactor operation were assumed to be equal to those prior to reactor operation. This assumption was on the basis that both ends of the fuel plates do not contain fuel and are relatively rigid.

For the second option of this analysis, all of the longitudinal deflections of the fuel plates were assumed to be in the same direction. However, it was assumed in this option that there could be sinusoidal variations in the coolant channel thicknesses along the length of the channel prior to the operation of the reactor. The amplitude of these sinusoidal waves was designated as $\Delta D$. In this option, the greatest amount of resistance to the coolant flow would occur when a cold fuel plate is adjacent to a hot fuel plate. Various coolant channel arrangements adjacent to the hot and cold plates must be considered and these are shown in Fig. 18. These cases are essentially modifications of those shown in Fig. 17. The thicknesses of the narrow coolant channel during reactor operation for this option are

$$D_n = D_{1n} - \Delta D \sin \frac{2\pi z}{\lambda} \tag{33}$$

where for Cases 1 and 2 shown in Fig. 18

$$D_{1n} = e_n + \delta_{\Delta PH} + \delta_{\Delta PC} - \delta_{Tnw,TAH} + \delta_{Tnw,TAC} - \delta_{nwH} - \delta_{nwC} - \delta_{MnwH} + \delta_{MnwC} - \delta_{Tnw,TAC} - 2\delta_{VR} \tag{33a}$$

for Case 3 shown in Fig. 18

$$D_{1n} = e_n + \delta_{\Delta PC} - \delta_{Tnn,TAH} - \delta_{Tnw,TAC} - \delta_{nnH} - \delta_{nwC} - \delta_{MnnH} + \delta_{MnwC} - \delta_{onH} - \delta_{onC} - 2\delta_{VR} \tag{33b}$$

and for Case 4 shown in Fig. 18

$$D_{1n} = e_n - \delta_{Tnn,TAH} + \delta_{Tnn,TAC} - \delta_{nnH} - \delta_{nnC} - \delta_{MnnH} + \delta_{MnnC} - \delta_{onH} - \delta_{onC} - 2\delta_{VR} \qquad (33c)$$

These thicknesses for the wide coolant channel during reactor operation are

$$D_w = D_{1w} - \Delta D \sin \frac{2\pi z}{\lambda} \qquad (34)$$

where for Case 1 shown in Fig. 18

$$D_{1w} = e_w - \delta_{\Delta PH} - \delta_{\Delta PC} + \delta_{Tnw,TAH} - \delta_{Tnw,TAC} - \delta_{nwH} - \delta_{nwC} + \delta_{MnwH} - \delta_{MnwC} - \delta_{owH} - \delta_{owC} - 2\delta_{VR} \qquad (34a)$$

for Case 2 shown in Fig. 18

$$D_{1w} = e_w - \delta_{\Delta PH} + \delta_{Tnw,TAH} - \delta_{Tww,TAC} - \delta_{nwH} - \delta_{wwC} + \delta_{MnwH} - \delta_{MwwC} - \delta_{owH} - \delta_{owC} - 2\delta_{VR} \qquad (34b)$$

and for Case 3 shwon in Fig. 18

$$D_{1w} = e_w - \delta_{\Delta PH} - \delta_{\Delta PC} - \delta_{Tnw,TAH} + \delta_{Tnw,TAC} - \delta_{nwH} - \delta_{nwC} - \delta_{MnwH} + \delta_{MnwC} - \delta_{owH} - \delta_{owC} - 2\delta_{VR} \qquad (34c)$$

and where

H = subscript for the hot plate,

C = subscript for the cold plate.

For the coolant channels with sinusoidal shape walls as shown in Fig. 19, there is some question what channel thicknesses are to be used in the calculation of the fuel plate metal temperatures. Various deflections of the fuel plates are functions of these temperatures, and therefore assumptions regarding them are significant. The metal temperatures are functions of the oxide thicknesses on the fuel plate surfaces, which are in turn functions of the oxide surface (oxide-water interface) temperatures. These surface temperatures are functions of the coolant water heat

transfer coefficients, which as can be seen from Eq. (10) are inversely proportional to the coolant channel thicknesses.

For a narrow coolant channel adjacent to a wide coolant channel, having the shapes similar to those shown in Fig. 19, three cases were selected arbitrarily to calculate the metal temperatures. These are as follows:

| | Coolant Channel Thickness | |
|---|---|---|
| Case | First Channel | Second Channel |
| 1 | $D_1 + D_2$ or $D_1 - \Delta D$ | $D_1 - D_2$ or $D_1 + \Delta D$ |
| 2 | $D_1$ | $D_1$ |
| 3 | $D_1 - D_2$ or $D_1 + \Delta D$ | $D_1 + D_2$ or $D_1 - \Delta D$ |

The metal temperature was then taken as the maximum of the averaged temperatures for each of the three cases. This should give the maximum amount of the various deflections for the fuel plate, which is a conservative assumption.

When a narrow coolant channel is adjacent to another narrow coolant channel or a wide coolant channel is adjacent to another wide coolant channel, only the first two cases were considered. This is because the first and the third cases gives identical results. For these arrangements, the metal temperature was taken as the maximum of the average temperatures for each of these two cases.

The amount of oxide buildup on the plate surface during any time step was assumed to be based on surface temperatures calculated using the heat transfer coefficient determined for the thicker part of the coolant channel, $D_1 + D_2$ or $D_1 - \Delta D$. This again is a conservative assumption.

In the second option of this analysis, the magnitude of the initial sinusoidal variations in the coolant channel thicknesses may be negligible, $\Delta D = 0$, or the wavelength $\lambda$ of these variations may be large. Because of

this a second alternate for the oxide buildup was included in this option as can be seen in Appendix A. This alternate calculates the fuel plate metal temperatures and oxide thicknesses for only one case using the coolant channel thicknesses determined by Eqs. (33) and (34). This gives more realistic results for these situations and reduces the computer running time greatly.

As had been mentioned earlier in this report, the coolant flow rates in the channels having sinusoidal walls similar to those shown in Fig. 19 are lower than those in the coolant channels having equivalent uniform thicknesses. To determine the correct flow rates in channels with the sinusoidal walls, the integral in the pressure drop relation, Eq. (4) must be integrated using the thickness distribution along the length of the channel. This results in numerical techniques with fine mesh spacing, and such amount of effort for this analysis is not considered warrented. However for a coolant channel of the length $\lambda$, which is the wavelength of the sinusoidal wall, and where the amplitude of the sine wave is constant, the integral in Eq. (4) can be integrated analytically. Details of this is shown in Appendix C. Therefore the overall HFIR fuel element coolant channel was treated as a series of short channels having the lengths $\lambda$; each short channel having a sine wave of a constant amplitude. Therefore, the thicknesses of each of these short lengths of coolant channel were assumed to be sine waves varrying from $D_1 + D_2$ to $D_1 - D_2$ or from $D_1 - \Delta D$ to $D_1 + \Delta D$, where $D_1 + D_2$ or $D_1 - \Delta D$ are the minimum values determined within any given wavelength $\lambda$ of the HFIR fuel element coolant channel. Such a procedure will give conservative values for the flow rates.

Again for the second option of this analysis where the magnitude of the initial sinusoidal variations in the coolant channel thicknesses may be negligible or the wavelength $\lambda$ of these variations may be large, a second alternate for calculating the flow rates was included. In this alternate, the integral in Eq. (4) was evaluated numerically using the actual coolant channel thicknesses determined by Eqs. (33) and (34). Again this gives more realistic results and reduces the computer running time.

For the hot streaks, where the flow rates of the water cooling the hot spots are determined, the channel thicknesses prior to the reactor operation are assumed to be the minimum allowed by the specifications. This minimum is now specified to be 0.040 in. (Ref. 23). To obtain the hot streak channel thicknesses during the reactor operation, Eqs. (31) and (33) are modified by the following relation for the narrow coolant channel*

$$D_{nhs} = D_n - e_n + e_{n,min} \tag{35}$$

where $e_{n,min}$ is the minimum thickness of the narrow coolant channel, and Eqs. (32) and (34) are modified by the following relation for the wide coolant channel*

$$D_{whs} = D_w - e_w + e_{w,min} \tag{36}$$

where $e_{w,min}$ is the minimum thickness of the wide coolant channel. The hot streak flow rates are calculated in the same manner as the flow rates for the narrow and the wide coolant channels are calculated except that the thicknesses determined by Eqs. (35) and (36) are used. For the hot channel, these are the Eq. (35) thicknesses, and for the cold channel, these are the Eq. (35) thicknesses for cases 1 and 2 shown in Figs. 17 and 18 and they are the Eq. (36) thicknesses for cases 3 and 4 shown in Figs. 17 and 18.

At the hot spots, the channel thicknesses were assumed to be the minimum possible values. For the first option of this analysis, they are defined for the hot channel and for the cold channel cases 1 and 2 (shown in Fig. 17) to be**

---

*These relations are slightly optimistic since they assume that oxide thickness and the increase in the plate thickness due to the thermal expansion of the metal in the hot streak are identical to those for the hot plate. Actually these thickness are slightly higher in the hot streak, and they should be considered in any future version of this heat transfer analysis.

**The oxide thicknesses and increase in the plate thickness due to the thermal expansion of the metal at the hot spot also were assumed to be identical to those in the hot plate. However in this case, this assumption is probably slightly pessimistic since the wider channel thickness results in a lower heat transfer coefficient at the hot spot.

$$D_{min} = D_{1n} + D_{2n} - e_n + e_{n,min} \tag{37}$$

and they are defined for the cold channel cases 3 and 4 (shown in Fig. 17) to be*

$$D_{min} = D_{1w} + D_{2w} - e_w + e_{w,min} \tag{38}$$

For the second option of this analysis, they are defined for the hot channel and for the cold channel cases 1 and 2 (shown in Fig. 18) to be*

$$D_{min} = D_{1n} - \Delta D - e_n + e_{n,min} \tag{39}$$

and they are defined for the cold channel cases 3 and 4 (shown in Fig. 18) to be*

$$D_{min} = D_{1w} - \Delta D - e_w + e_{w,min} \tag{40}$$

## Input Data

Table 4 is a summary of the input data required for this analysis along with the numerical values for the results reported below. These particular values were chosen to give a conservative representation of the HFIR fuel element parameters. As mentioned above, this analysis has two options depending on the assumption regarding the longitudinal deflections of the fuel plates, and the second one was used for the results reported below. Also the second of the two alternate methods in the second option for calculating the flow rates and the second of the two alternate methods in the second option for calculating the oxide buildup on the fuel plates were used in calculating these results. As was indicated above, the values of the constants for the various correlations used in this analysis are not input data. Any changes in these constants will require changes in the Fortran statements used in the computer program.

---

*The oxide thicknesses and increase in the plate thickness due to the thermal expansion of the metal at the hot spot also were assumed to be identical to those in the hot plate. However in this case, this assumption is probably slightly pessimistic since the wider channel thickness results in a lower heat transfer coefficient at the hot spot.

## Results

Using the data listed in Table 4, the upper limits for the reactor power levels were computed at startup and at the end of a 100 Mw fuel cycle. The results of these calculations are summarized in Table 5. Both the incipient boiling and the burnout criteria were considered, but the results based on the incipient boiling criteria are the most meaningful because of the unknowns regarding the use of the burnout relations. Using the incipient boiling criteria, the maximum permissible power level varied from 139 Mw at reactor startup to 153 Mw at the end of a 100 Mw fuel cycle. For comparison, the results using the burnout criteria varied from 162 Mw at startup to 175 Mw at the end of a 100 Mw fuel cycle. The increase in the upper limit for the reactor power level during the fuel cycle is due to the redistribution of the power densities in the fuel elements because of the fuel burnup and because of the change in the control rod positions. All of these results indicate that the HFIR fuel elements can be used at reactor powers higher than 130% of the nominal 100 Mw level for short periods of time without damage to them, thus satisfying the design requirements.

In all cases, the particular heat flux which limited the reactor power level was located at the lower edge of the fuel bearing material in the fuel elements ($j = 29$). Usually it was at the lower inside corner of the fuel bearing material in the outer fuel element. This limiting heat flux varied from $3.39 \times 10^6$ to $3.88 \times 10^6$ Btu/(hr)(ft$^2$) for the incipient boiling criteria and from $4.05 \times 10^6$ to $4.50 \times 10^6$ Btu/(hr)(ft$^2$) for the burnout criteria. As can be seen from Table 5, the location of this limiting heat flux may or may not coincide with the locations of the minimum hot streak flow rate or the maximum bulk coolant temperature in the fuel elements. Also, it can be seen that the influence of the location of the adjacent narrow and wide coolant channels as described by Fig. 18 on the results is not large.

Additional information was obtained for the Fig. 18 case 3 using the incipient boiling criteria, and these results are summarized in Table 6. At the location of the limiting heat flux at startup, the coolant channel thickness is 0.0390 in. and the coolant velocity is 48.1 fps. For comparison

the average fuel plate and the average coolant channel at the same location have values of 0.0487 in. and 52.1 fps respectively. The values of these items vary from these numbers in the hot streak above this location because of the plate deflections and because of the temperature increase of the coolant along the length of the fuel element. Step decreases in the narrow channel and the hot streak thicknesses were calculated at the midplane of the fuel element (between $j = 16$ and $j = 17$). They are due to the difference in the "average" fuel concentrations on each side of the core midplane of the hot and cold plates as described by $U_4$ and $U_5$ in this analysis. These quantities influence the metal temperatures which in turn affect the thermal deflections of the fuel plates. Since there are step changes in $U_4$ and $U_5$ at the core midplane, these reflect in step changes in the coolant channel thicknesses. Of course step changes in the coolant channel thicknesses will not occur physically, but this approximation is felt to be valid and conservative.

The buildup of the oxide on the fuel plate surfaces generally causes increases in the fuel plate deflections which result in decreases in the coolant flow rates. At the location of the limiting heat flux, the coolant channel thickness is 0.0342 in. and the coolant flow rate is 0.6744 lb/(sec)(in. channel width) at the end of a 100 Mw fuel cycle. At reactor startup, these values are 0.0364 in. and 0.6840 lb/(sec)(in. channel width) respectively. The buildup of oxide during the 100 Mw fuel cycle on the hot fuel plate at this same location is 0.0012 in. and that on the cold plate is 0.0010 in. Analogous figures for the average coolant channel at the identical location are 0.0483 in. channel thickness and 1.040 lb/(sec)(in. channel width) flow rate at the end of the 100 Mw fuel cycle, and 0.0487 in. channel thickness and 1.045 lb/(sec)(in. channel width) flow rate at reactor startup. The oxide buildup in this case is 0.0007 in.

The values of the changes in the coolant channel thicknesses and the amounts of oxide buildup along the length of the hot streak during a fuel cycle vary as can be seen in Table 6. This is due to the dependency of the oxide buildup on the local surface (oxide-water interface) temperatures. Of course step changes in the channel and the oxide thicknesses in the narrow channels and the hot streaks at the core midplane are shown because

of the reasons described above. Because of the nature of the longitudinal thermal deflections of the fuel plates, the thicknesses of the narrow coolant channels and of the hot streaks above the core midplane increase during the fuel cycle while those below the core midplane decrease in this particular case.

Because of the many factors influencing the coolant velocities and because of the difference in the upper limits for the reactor power levels at startup and at the end of the fuel cycle, simple interpretation of the changes in these velocities during the fuel cycle is not possible. In most cases, they go down, but at some local spots they go up. For example at the location of the limiting heat flux at the end of the fuel cycle, the coolant velocity is 47.0 fps at startup and it is 50.0 fps at the end of the cycle. These velocities are lower at the channel inlets than at the channel exits because of the lower coolant temperatures and the larger channel thicknesses at the channel inlets during reactor operation. This is the most noticeable in the hot streaks at the end of the cycle where they are on the order of 40 fps at the channel inlet and 50 fps at the channel exit. The velocities in the average coolant channel, in comparison, vary only from 49.6 fps at the core inlet to 52.1 fps at the core exit.

Examination of the coolant channel thicknesses in Table 6 indicate that the smallest of the channel thicknesses listed is 0.0319 in. This is for the end of fuel cycle situation, but it did not occur at the position of the limiting heat flux. This gives some indication that the channel thickness may not be the limiting factor for the burnout heat flux if the burnout criteria are used in determining the upper limit for the reactor power level.

An examination of the hot plate metal temperatures in Table 6 indicate that they are all below 400°F at startup. This implies that the deflection correlations used in this analysis are valid for all power levels up to the upper limit for the reactor power of 139 Mw. At the end of the 100 Mw fuel cycle, there are some local spots, where these temperatures exceed 400°F. But since they do occur in local areas and the upper limit for the reactor power level is high, 153 Mw, this should not be a problem. These results do indicate, however, that the assumptions used in the

deflection relations would have to be examined for their temperature limitations at power levels higher than 153 Mw. The side plate temperatures are in the range of 156 to 191°F at the upper limit for the reactor power level at startup and 159 to 198°F at the upper limit for the reactor power level at the end of the fuel cycle.

The heat fluxes in the average fuel plate at the location of the limiting heat fluxes in the hot fuel plate were included in Table 6 for comparison purposes. The ratio of the limiting heat flux to the heat flux in the average fuel plate at reactor startup is 3.41/1.54 or 2.21, and at the end of the fuel cycle it is 3.35/1.59 or 2.11. This implies that the various factors such as the variations in the coolant channel thicknesses, fuel boundaries, fuel concentrations, fuel segregation, and nonbonds can increase the heat flux at this location by a factor of greater than 2.

The thermal-hydraulic history of the fuel element during the normal 100 Mw 25 day fuel cycle in the reactor is summarized in Table 7. The first observation in this table is the decrease in the total coolant flow rate through the fuel assembly during this cycle. This decrease is due primarily to the buildup of the oxide on the fuel plate surfaces. During the life of the fuel in this analysis, it was assumed that the pressure drop through the fuel plates is constant. This is not the case in the reactor since the primary coolant pumps develop higher heads at the lower flow rates and the head losses in the primary coolant system external to the fuel element are lower for lower flow rates. This will tend to counter this decrease of the flow rate through the fuel elements in the actual reactor.

The oxide thicknesses at the end of the various time intervals are listed in Table 7, and they are plotted in Figs. 20 and 21. The thicknesses shown in Fig. 20 are at the location of the limiting heat flux in the hot fuel plate at the end of a 100 Mw fuel cycle. Since the rate of its buildup is strongly dependent on the oxide-water interface temperature, it is the greatest for the hot plate adjacent to a narrow coolant channel and the least for the average plate adjacent to an average coolant channel. Of course, the amount of oxide buildup at the other locations in the fuel element will not be as large as these values. Figure 21 shows the oxide

buildup at another location in the fuel assembly, which is more typical of the general situation. The buildup of this oxide causes decreases in the coolant channel thicknesses in two ways. First, it takes up additional space in the coolant channel. Second because of its low thermal conductivity, it increases the metal temperature of the operating fuel plate. Fuel plates at higher temperatures will have higher deflections which further decreases the coolant channel thicknesses. This is very noticeable in Figs. 20 and 21. The average coolant channel thickness decreases some because of these two factors. However in the case of the hot streak channel thicknesses, which are more significantly dependent on the plate temperatures and deflections, this decrease is quite appreciable.

The increase in the average fuel plate temperatures can be seen in Table 7. They are particularly noticeable below the core midplane ($j > 16$) since the oxide buildup is the greatest in this portion of the fuel element. The side plate temperatures, which are in the range of 151 to 172°F do not vary during the fuel cycle.

## Conclusions and Recommendations

Analytical studies using an integral thermal-hydraulic model of the operating reactor incorporating the fuel plate deflection data of Cheverton and Kelley[7] showed that the design requirements for the HFIR fuel elements have been met. These requirements state that the reactor is to operate at a 100 Mw nominal power level and that this power level can be raised to 130% of this value for short periods of time without damage to the fuel elements. If no boiling is allowed, the reactor power can be raised to 139 Mw at startup and to 153 Mw at the end of a 100 Mw fuel cycle. These power levels can be raised further if boiling at heat fluxes below burnout is permitted. A suggestion is made, therefore, to investigate the conditions such as the question of flow stability in parallel coolant channels to determine the conditions for which the burnout relations are valid.

The above results are for one set of input data, and no parametric studies have been made to determine the effect of the various input data on the final results. The input data that were selected here were felt to be a conservative representation of the fuel element and other reactor

parameters. Parametric studies are recommended, however, in order to broaden the spectrum of the fuel element tolerances that may be acceptable for HFIR operation.

After the results reported above were calculated, data regarding the radiation swelling of the fuel plates became available[43a] and a slight error was found in the relations for calculating the decrease in the coolant channel thickness due to temperature increase of the fuel plate metal. Also the relations for calculating the coolant channel thicknesses at the hot streaks and at the hot spots gave slightly erroneous results. Some of these items are slightly pessimistic while others are slightly optimistic. However it is feeling of this author that the sum of these various factors gave slightly pessimistic results, but they should be included in any future revision of this heat transfer analysis.

Segregation and nonbond factors used in this analysis were those derived by Hilvety and Chapman.[4] Preliminary studies have indicated that further work on them is desirable to gain a better understanding of these factors and to possible relax the inspection requirements for the HFIR.

It is usually desired to raise the power level of a reactor above its design value after it has been built and operated for a period of time. The mathematical tools developed in this analysis could help in determining the feasibility of this regarding the fuel elements, and the possible modifications that may be required. It should be pointed out here, however, that the other components in the reactor were designed for operation at 100 Mw reactor power level with a 120°F inlet water temperature. Also the reactor safety system is designed to allow increases in the power level up to 130% of the nominal power level for short periods of time before scram action is initiated. A thorough investigation of these other factors would have to be made before the reactor power level could be increased safely.

## Nomenclature

| Symbol | Item | Units |
|---|---|---|
| $A$ | Heat transfer area | $ft^2$ |
| $A_{SP}$ | Cross sectional area of the side plate | $in.^2$ |
| $a$ | Acceleration | $ft/hr^2$ |
| $B$ | Constant in the relation for the increase in the fuel plate thickness due to radiation swelling | mils/hr |
| $C$ | Constants in the relation for the side plate temperature | |
| $c_P$ | Specific heat | Btu/(lb)(°F) |
| $D_C$ | Cold channel thickness | mils |
| $D_e$ | Equivalent diameter | ft |
| $D_H$ | Hot channel thickness | mils |
| $D_{1n}$ | Linear component of the narrow coolant channel thickness | mils |
| $D_{1w}$ | Linear component of the wide coolant channel thickness | mils |
| $D_{2n}$ | Sinusoidal component of the narrow coolant channel thickness | mils |
| $D_{2w}$ | Sinusoidal component of the wide coolant channel thickness | mils |
| $\Delta D$ | Amplitude of the initial sinusoidal wave in the coolant channel thickness | mils |
| E.R. | Elastic modulus ratio | |
| $e$ | Coolant channel thickness | mils |
| $e_A$ | Average coolant channel thickness prior to reactor operation | mils |
| $e_{en}$ | Thickness of the inlet and the exit of the narrow coolant channel prior to reactor operation | mils |
| $e_{ew}$ | Thickness of the inlet and the exit of the wide coolant channel prior to reactor operation | mils |
| $e_n$ | Average thickness of the narrow coolant channel prior to reactor operation | mils |
| $e_{n,min}$ | Minimum thickness of the narrow coolant channel prior to reactor operation | mils |

Nomenclature (Cont)

| Symbol | Item | Units |
|---|---|---|
| $e_w$ | Average thickness of the wide coolant channel prior to reactor operation | mils |
| $e_{w,min}$ | Minimum thickness of the wide coolant channel prior to reactor operation | mils |
| F | Constant in the friction factor relationship $f = F/(Re)^{0.2}$ | |
| f | Friction factor | |
| f | Fraction of the reactor power deposited in the fuel elements | |
| $g_c$ | Conversion factor | $lb_m ft/lb_f hr^2$ |
| H | Modified heat transfer coefficient | $Btu/(hr)(ft^2)(°F)$ |
| $\Delta H$ | Head difference | ft |
| h | Heat transfer coefficient | $Btu/(hr)(ft^2)(°F)$ |
| K | Constant in the boiling portion of the burnout heat flux correlation | |
| $K'$ | Constant in the non-boiling portion of the burnout heat flux correlation | |
| k | Thermal conductivity | Btu/(hr)(ft)(°F) |
| L | Length of the coolant channel | in. |
| $L_v$ | Latent heat of vaporization | Btu/lb |
| Nu | Nusselt number | |
| P | Absolute pressure | psia |
| P | Reactor vessel pressure | psia |
| $P_F$ | Absolute pressure at the inlet of the fuel element | psia |
| Pr | Prandtl number | |
| $\Delta P_F$ | Fuel element pressure drop | psi |
| $\Delta P_{core}$ | Core pressure drop | psi |
| $\Delta P_{inlet}$ | Core inlet pressure difference | psi |
| $\Delta P_{nw}$ | Average differential pressure across a fuel plate between a narrow coolant channel and a wide coolant channel | psi |
| Q | Reactor power level | Mw |
| $Q_{H_2O}$ | Coolant heat generation rate at 100 Mw reactor operation | $Btu/(hr)(in.^3)$ |

Nomenclature (Cont)

| Symbol | Item | Units |
|---|---|---|
| $Q_{SP}$ | Side plate heat generation rate at 100 Mw reactor operation | Btu/(hr)(in.$^3$) |
| q/A | Heat flux | Btu/(hr)(ft$^2$) |
| R | Outside radius of the inner side plate | in. |
| r | Radius | in. |
| Re | Reynolds number | |
| S | Total width along involute plate | in. |
| s | Width (length along the involute arc) | in. |
| T | Water temperature | °F |
| $T_M$ | Metal temperature | °F |
| $T_S$ | Fuel plate surface (oxide-water interface) temperature | °F |
| $T_{SP}$ | Average side plate temperature | °F |
| $\overline{T}$ | Temperature of the fuel plate adjacent to the side plate | °F |
| t | Fuel plate thickness | mils |
| $\Delta T_M$ | Average difference between the fuel plate temperature and the side plate temperature | °F |
| $\Delta T_{sub}$ | Amount of subcooling | °F |
| $U_1$ | Uncertainty factor for the reactor power level | |
| $U_2$ | Uncertainty factor for the total heat transfer area | |
| $U_3$ | Uncertainty factor for the power density distribution | |
| $U_4$ | Uncertainty factor for the average fuel concentration in the hot plate | |
| $U_5$ | Uncertainty factor for the average fuel concentration in the cold plate | |
| $U_6$ | Uncertainty factor for the inlet water temperature | |
| $U_7$ | Uncertainty factor for the friction factor | |
| $U_8$ | Uncertainty factor for the heat transfer coefficient correlation | |
| $U_9$ | Uncertainty factor for the oxide film correlation | |

Nomenclature (Cont)

| Symbol | Item | Units |
|---|---|---|
| $U_{10}$ | Uncertainty factor for the deflection of a fuel plate due to the differential pressure across the fuel plate | |
| $U_{11}$ | Uncertainty factor for the deflection due to the difference of the temperature of an individual fuel plate and that of an average fuel plate | |
| $U_{12}$ | Uncertainty factor for the increase in the fuel plate thickness due to heating | |
| $U_{13}$ | Uncertainty factor for the increase in the fuel plate thickness due to radiation swelling | |
| $U_{14}$ | Uncertainty factor for fuel plate deflection due to longitudinal buckling | |
| $U_{15}$ | Uncertainty factor for the longitudinal deflection of the fuel plate due to the radiation growth of the fuel plate material | |
| $U_{16}$ | Uncertainty factor for the side plate heat generation rate | |
| $U_{17}$ | Uncertainty factor for the coolant heat generation rate | |
| $U_{18}$ | Segregation factor for the hot channel | |
| $U_{19}$ | Segregation factor for the cold channel | |
| $U_{20}$ | Nonbond factor for the hot channel | |
| $U_{21}$ | Nonbond factor for the cold channel | |
| $U_{22}$ | Uncertainty factor for additive burnout correlation | |
| $U_{23}$ | Uncertainty factor for the incipient boiling relation | |
| $U_{24}$ | Hot streak factor | |
| $U_{25}$ | Flux peaking factor for fuel extending beyond the normal boundaries | |
| $\overline{U}$ | Uncertainty factor for fuel segregation and nonbonds | |
| V | Volumetric flow rate | gpm |
| v | Coolant velocity | ft/sec |
| w | Flow rate | lb/(sec)(in. width) |

Nomenclature (Cont)

| Symbol | Item | Units |
|---|---|---|
| $X$ | Oxide film thickness | mils |
| $z$ | Length along the fuel element axis | in. |
| $\alpha$ | Thermal coefficient of linear expansion | in./(in.)(°F) |
| $\Delta$ | Increment sign | |
| $\delta$ | One half of the expansion of the fuel plate thickness due to heating | mils |
| $\delta_M$ | Deflection of the fuel plates due to the longitudinal buckling | mils |
| $\delta_{MR}$ | Longitudinal deflection of the fuel plate due to the radiation growth of the fuel plate material | mils |
| $\delta_o$ | Decrease in the coolant channel thickness due to the buildup of oxide on the fuel plate surface | mils |
| $\delta_{T,TA}$ | Deflection due to the difference in the temperature of an individual fuel plate and that of an average fuel plate | mils |
| $\delta_{VR}$ | One half of the expansion of the fuel plate due to radiation swelling | mils |
| $\delta_{\Delta P}$ | Deflection due to the differential pressure across a fuel plate | mils |
| $\epsilon$ | Surface roughness | ft |
| $\theta$ | Time increment | hr |
| $\lambda$ | Wavelength of any sinusoidal longitudinal buckling of the fuel plate or any sinusoidal deviation in the initial coolant channel thickness | in. |
| $\mu$ | Viscosity | lb/(hr)(ft) |
| $\xi_1$ | Case selection factor (Has a value of 1 for Case 1 shown in Figs. 17 and 18, a value of 0 for the other cases) | |
| $\xi_2$ | Case selection factor (Has a value of 1 for Case 2 shown in Figs. 17 and 18, a value of 0 for the other cases) | |
| $\xi_3$ | Case selection factor (Has a value of 1 for Case 3 shown in Figs. 17 and 18, a value of 0 for the other cases) | |

Nomenclature (Cont)

| Symbol | Item | Units |
|---|---|---|
| $\xi_4$ | Case selection factor (Has a value of 1 for Case 4 shown in Figs. 17 and 18, a value of 0 for the other cases) | |
| $\rho$ | Density | $lb/ft^3$ |
| $\rho/\rho_R$ | Ratio of the fuel plate densities before and after irradiation | |
| $\Delta\rho$ | Difference in densities of liquid and vapor phases | $lb/ft^3$ |
| $\sigma$ | Surface tension | lb/ft |
| $\tau$ | Side plate thickness | in. |
| $\Phi$ | Normalization factor for the power density | |
| $\phi$ | Normalized power density | |
| $\phi'$ | Non-normalized power density | |
| $\psi$ | Ficticious time defined by equations (17) and (18) | hr |

Subscripts

| | |
|---|---|
| A | Averaged value |
| A | Average fuel plate and average coolant channel |
| AS | Fuel assembly |
| ave | Average value |
| b | For bulk water conditions |
| bo | Burnout conditions |
| boil | Boiling part of burnout correlation |
| bulk | Overall coolant |
| C | Control region |
| C | Cold plate |
| ex | Exit conditions |
| F | Fuel element |
| g | Particular wavelength being considered |
| H | Hot plate |
| hs | Hot streak or hot spot |

Nomenclature (Cont)

Subscripts (Cont)

| Symbol | Item |
|---|---|
| i | Mesh point along width or radius of fuel plate |
| ib | Incipient boiling conditions |
| ii | Annulus between inner fuel element and target bundle |
| ii | Inner side plate of the inner fuel element |
| in | Inlet conditions |
| inner | Inner fuel element |
| io | Outer side plate of the inner fuel element |
| j | Mesh point along length of fuel plate |
| k | Number of time increments |
| $\ell$ | Liquid phase |
| lab | Labyrinth between fuel elements |
| m | Maximum number of increments in the radial direction |
| min | Minimum value |
| n | Maximum number of increments in the axial direction |
| n | Plate surface in the narrow coolant channel |
| nb | Nonboiling part of burnout correlation |
| nn | Between two narrow coolant channels |
| nw | Between a narrow coolant channel and a wide coolant channel |
| o | At time zero |
| oi | Inner side plate of the outer fuel element |
| oo | Outer side plate of the outer fuel element |
| outer | Outer fuel element |
| R | After irradiation |
| sat | Saturation conditions |
| v | Vapor phase |
| w | Plate surface in the wide coolant channel |
| ww | Between two wide coolant channels |
| x | Generalized subscript |

## REFERENCES


1. N. Hilvety, Preliminary Hot Spot Analysis of the HFIR, USAEC Report ORNL-CF-60-3-12, Oak Ridge National Laboratory, Mar. 1, 1960.
2. N. Hilvety, Supplement to Preliminary Hot Spot Analysis of the HFIR, USAEC Report ORNL-CF-60-3-12-Supplement, Oak Ridge National Laboratory, Sept. 18, 1961.
3. N. Hilvety and T. G. Chapman, Summary of the HFIR Hot Spot Studies, Oak Ridge National Laboratory, unpublished internal document, Jan. 30, 1962.
4. N. Hilvety and T. G. Chapman, HFIR Fuel Element Steady State Heat Transfer Analysis, USAEC Report ORNL-TM-1903, Oak Ridge National Laboratory (to be published).
5. R. N. Lyon, Remarks on Thermal Buckling of Columns, Plates, and Shells with Initial Sinusoidal Distortion (HFIR Fuel Plates), USAEC Report ORNL-TM-1482, Oak Ridge National Laboratory, Apr. 7, 1966.
6. T. G. Chapman, Oak Ridge National Laboratory, personal communication, November 11, 1965.
7. R. D. Cheverton and W. H. Kelley, Deflection Characteristics of the HFIR Fuel Plates, Oak Ridge National Laboratory (to be published).
8. Memorandum from H. A. McLain to T. E. Cole, November 11, 1965, Subject: Effect of the Sinusoidal Buckling of the HFIR Fuel Element Coolant Channels.
9. W. R. Gambill and R. D. Bundy, HFIR Heat-Transfer Studies of Turbulent Water Flow in Thin Rectangular Channels, USAEC Report ORNL-3079, Oak Ridge National Laboratory, Jan. 5, 1961.
10. W. R. Gambill, Generalized Prediction of Burnout Heat Flux for Flowing Subcooled Wetting Liquids, A.I.Ch.E. Preprint 17, Fifth National Heat Transfer Conference, A.I.Ch.E.-A.S.M.E., Houston, Texas, August 5–8, 1962.
11. A. E. Bergles and W. M. Rohsenow, The Determination of Force-Convection Surface-Boiling Heat Transfer, J. Heat Transfer, ASME, 86: 365–372 (1964).
12. E. J. D vis and G. H. Anderson, The Incipience of Nucleate Boiling in Forced Convection Flow, A.I.Ch.E. Journal, 12(4): 774–780 (July 1966).
13. L. S. Tong, Instability of Two-Phase Flow, Chapt. 7, pp. 201–216 in Boiling Heat Transfer and Two-Phase Flow, Wiley, New York, 1965.
14. Argonne National Laboratory, Argonne Advanced Research Reactor (AARR), pp. 55–75, Reactor Development Program Progr. Rept. May 1966, USAEC Report ANL-7219, June 30, 1966.
15. N. L. Kafengauz and I. D. Bauarov, the Effect of the Height of a Flat Aperture on the Transformation of Heat Flow Into Water, Teploenergetika, 3: 76–78 (1959).
16. V. S. Chirkin and V. P. Iukin, Critical Point in Heat Removal From Boiling Water Flowing Through an Annular Gap, J. Tech. Phys., 1: 1503–1515 (1956).

17. W. R. Gambill, Oak Ridge National Laboratory, personal communication, January 20, 1966.

18. B. A. Zenkovich and B. I. Subbotin, Critical Heat Fluxes in Subcooled Water with Forced Circulation, Atomnaya Energiya, 3: 149 (1957); English translation in Reactor Technol., J. Nucl. Energy, Part B, 1(2): 134–136 (1959).

19. W. R. Gambill, Physical Properties of Water, Chem. Eng., 66(10): 241 (May 18, 1959).

20. J. H. Keenan and F. G. Keyes, Thermodynamics Properties of Steam, Wiley, New York, 1936.

21. L. Bernath, A Theory of Local Boiling Burnout and Its Application to Existing Data, Chem. Eng. Progr. Symposium Series, 56(30): 95–116 (1960).

22. R. D. Cheverton and T. M. Sims, HFIR Physics Report, Oak Ridge National Laboratory (to be published).

23. G. M. Adamson, Jr. and J. R. McWherter, Specifications for High Flux Isotope Reactor Fuel Elements, HFIR-FE-1, USAEC Report ORNL-TM-902, Oak Ridge National Laboratory, August 1964.

24. R. D. Cheverton, Oak Ridge National Laboratory, personal communication, November 24, 1965.

25. E. D. Waters, Heat Transfer Experiments for the Advanced Test Reactor, USAEC Report BNWL-216, Battelle Northwest Laboratory, May 1966.

26. V. L. Streeter, Handbook of Fluid Dynamics, McGraw-Hill, New York, 1961.

27. J. C. Griess et al., Effect of Heat Flux on the Corrosion of Aluminum by Water, Part I, Equipment and Preliminary Test Results, USAEC Report ORNL-2939, Oak Ridge National Laboratory, Apr. 29, 1960.

28. G. J. Dixon, Oak Ridge National Laboratory, personal communication, March 7, 1966.

29. Crane Company Technical Paper No. 410, Flow of Fluids Through Valves, Fittings, and Pipe, Chicago, Illinois, 1957.

30. E. R. G. Eckert and G. M. Low, Temperature Distribution in Internally Heated Walls Exchanger Composed of Noncircular Flow Passages, NACA Report 1022, 1955.

31. R. R. Liguori and J. W. Stephenson, the HEATING Program (Heat Engineering and Transfer in Nine Geometries, ASTRA Report 417-50, ASTRA, Inc., Jan. 1, 1961.

32. L. A. Haack, Oak Ridge National Laboratory, personal communication, June 17, 1966.

33. D. L. McElroy, Oak Ridge National Laboratory, personal communication to L. A. Haack, Oak Ridge National Laboratory, Marcy 9, 1966.

34. J. C. Griess et al., Effect of Heat Flux on the Corrosion of Aluminum by Water, Part II, Difference of Water Temperature, Velocity, and pH

on Corrosion-Product Formation, USAEC Report ORNL-3056, Oak Ridge National Laboratory, Feb. 10, 1961.

35. J. C. Griess et al., Effect of Heat Flux on the Corrosion of Aluminum by Water, Part III, Final Report on Tests Relative to the High Flux Isotope Reactor, USAEC Report ORNL-3230, Oak Ridge National Laboratory, Dec. 5, 1961.

36. J. C. Griess, H. C. Savage, and J. L. English, Effect on the Corrosion of Aluminum by Water, Part IV, Tests Relative to the Advanced Test Reactor and Correlation with Previous Results, USAEC Report ORNL-3541, Oak Ridge National Laboratory, February 1964.

37. G. Ervin, Jr., and E. F. Osborn, The System $Al_2O_3$-$H_2O$, J. Geology, 59: 381–394 (1954).

38. Memorandum from D. R. deBoisblanc to J. F. Kaufman, March 31, 1965, Subject: Results of ATR Fuel Irradiation PAED-G-12 ETR Water Loop.

39. T. G. Chapman, Thermal Expansion and Pressure Differential Induced Stress and Deflections of HFIR Involute Contoured Fuel Plates, Oak Ridge National Laboratory (to be published).

40. L. A. Haack, Oak Ridge National Laboratory, personal communication, January 24, 1966.

41. T. G. Chapman, Oak Ridge National Laboratory, personal communication, February 4, 1966.

42. Aluminum Company of America, Alcoa Aluminum Handbook, Pittsburgh, Pennsylvania, 1959.

43. D. R. Vondy, Gamma Ray and Neutron Heat Generation in the HFIR, Oak Ridge National Laboratory, unpublished internal document, Feb. 21, 1963.

43a. V. A. Walker, M. J. Graber, and G. W. Gibson, ATR Fuel Materials Development Irradiation Results, Part II, USAEC Report IDO-17157, Phillips Petroleum Company, June 1966.

44. R. Q. Wright, HFIR Fuel Element Heat Transfer Code, K-25 Report (to be published).

45. Memorandum from R. M. Hill, Jr., to J. R. McWherter, December 3, 1963, Subject: Flow Test for Annulus Between HFIR Fuel Elements.

46. R. J. Kedl, Hydraulic Tests of the HFIR Target Region, Oak Ridge National Laboratory, unpublished internal document, July 21, 1965.

47. Alden Hydraulic Laboratory, Worcester Polytechnic Institute, Calibration of Union Carbide Nuclear Company 20" × 12.545" VTS4-A Venturi Meter Serial No. 40145, February 1963.

48. W. G. Cobb, personal communication, June 11, 1965.

49. Memorandum from R. M. Hill, Jr., to J. R. McWherter, October 24, 1963, Subject: HFIR Vertical Facility Bench Test Results.

50. T. G. Chapman, Oak Ridge National Laboratory, personal communication, September 23, 1965.

51. R. V. Churchill, Introduction to Complex Variables and Application, McGraw-Hill, New York, 1948.

52. L. A. Haack, Selection of Model for Side Plate Temperature Calculations in the Revised Hot Spot Code, Oak Ridge National Laboratory (to be published).

53. S. Glasstone, Principles of Nuclear Reactor Engineering, Van Nostrand, New York, 1955.

Table 1. Power Densities in the HFIR Fuel Elements[22]
Reactor Power Level: 100 Mw
Core Life: 2500 Mw-day
Time: 0 days = 0 hrs

| Distance From Core Midplane (cm) | Distance From Core Centerline (cm) | | | | | | | | | | | | | |
|---|---|---|---|---|---|---|---|---|---|---|---|---|---|---|
| | Inner Fuel Element | | | | | | | Outer Fuel Element | | | | | | |
| | 7.14 | 8.00 | 9.00 | 10.00 | 11.00 | 12.00 | 12.60 | 15.15 | 16.00 | 17.00 | 18.00 | 19.00 | 20.00 | 21.00 |
| 25.4 | 0.678 | 1.109 | 1.379 | 1.515 | 1.470 | 1.344 | 1.186 | 1.580 | 1.512 | 1.394 | 1.254 | 1.119 | 0.719 | 0.298 |
| 24 | 0.722 | 0.741 | 0.738 | 0.771 | 0.809 | 0.830 | 0.837 | 0.970 | 0.934 | 0.770 | 0.660 | 0.542 | 0.442 | 0.293 |
| 22 | 0.815 | 0.753 | 0.738 | 0.767 | 0.802 | 0.830 | 0.824 | 0.943 | 0.860 | 0.758 | 0.650 | 0.533 | 0.425 | 0.291 |
| 20 | 0.924 | 0.848 | 0.810 | 0.821 | 0.850 | 0.889 | 0.893 | 0.961 | 0.885 | 0.796 | 0.691 | 0.578 | 0.467 | 0.323 |
| 18 | 1.031 | 0.952 | 0.904 | 0.917 | 0.939 | 0.980 | 0.988 | 1.043 | 0.978 | 0.881 | 0.781 | 0.669 | 0.562 | 0.429 |
| 16 | 1.130 | 1.043 | 0.990 | 1.007 | 1.027 | 1.067 | 1.077 | 1.146 | 1.075 | 0.977 | 0.878 | 0.769 | 0.669 | 0.552 |
| 14 | 1.227 | 1.126 | 1.068 | 1.089 | 1.107 | 1.146 | 1.162 | 1.239 | 1.165 | 1.064 | 0.964 | 0.864 | 0.775 | 0.670 |
| 12 | 1.312 | 1.198 | 1.137 | 1.163 | 1.179 | 1.217 | 1.241 | 1.320 | 1.247 | 1.143 | 1.045 | 0.946 | 0.875 | 0.787 |
| 10 | 1.387 | 1.264 | 1.200 | 1.233 | 1.241 | 1.280 | 1.316 | 1.388 | 1.319 | 1.214 | 1.117 | 1.027 | 0.973 | 0.898 |
| 8 | 1.447 | 1.322 | 1.255 | 1.285 | 1.294 | 1.334 | 1.383 | 1.448 | 1.382 | 1.279 | 1.180 | 1.101 | 1.073 | 1.019 |
| 6 | 1.493 | 1.372 | 1.306 | 1.332 | 1.339 | 1.380 | 1.445 | 1.499 | 1.437 | 1.337 | 1.239 | 1.168 | 1.169 | 1.127 |
| 4 | 1.520 | 1.398 | 1.338 | 1.369 | 1.372 | 1.410 | 1.478 | 1.539 | 1.480 | 1.382 | 1.284 | 1.222 | 1.246 | 1.224 |
| 2 | 1.532 | 1.408 | 1.350 | 1.386 | 1.388 | 1.422 | 1.490 | 1.558 | 1.500 | 1.404 | 1.306 | 1.242 | 1.285 | 1.308 |
| 0 | 1.533 | 1.403 | 1.349 | 1.386 | 1.388 | 1.420 | 1.485 | 1.559 | 1.500 | 1.405 | 1.306 | 1.242 | 1.285 | 1.308 |
| -2 | 1.523 | 1.393 | 1.335 | 1.372 | 1.375 | 1.418 | 1.464 | 1.543 | 1.483 | 1.389 | 1.291 | 1.222 | 1.237 | 1.225 |
| -4 | 1.494 | 1.368 | 1.305 | 1.342 | 1.345 | 1.380 | 1.425 | 1.510 | 1.448 | 1.353 | 1.255 | 1.174 | 1.150 | 1.117 |
| -6 | 1.448 | 1.324 | 1.256 | 1.289 | 1.295 | 1.330 | 1.372 | 1.448 | 1.387 | 1.286 | 1.190 | 1.101 | 1.067 | 0.998 |
| -8 | 1.384 | 1.264 | 1.193 | 1.221 | 1.235 | 1.283 | 1.312 | 1.379 | 1.311 | 1.209 | 1.112 | 1.021 | 0.968 | 0.882 |
| -10 | 1.312 | 1.195 | 1.127 | 1.150 | 1.167 | 1.212 | 1.248 | 1.303 | 1.232 | 1.129 | 1.030 | 0.937 | 0.868 | 0.769 |
| -12 | 1.235 | 1.120 | 1.057 | 1.077 | 1.097 | 1.144 | 1.177 | 1.222 | 1.149 | 1.045 | 0.944 | 0.846 | 0.767 | 0.661 |
| -14 | 1.148 | 1.039 | 0.982 | 1.000 | 1.023 | 1.069 | 1.098 | 1.135 | 1.060 | 0.957 | 0.854 | 0.750 | 0.662 | 0.555 |
| -16 | 1.050 | 0.952 | 0.903 | 0.920 | 0.945 | 0.988 | 1.011 | 1.044 | 0.969 | 0.865 | 0.760 | 0.649 | 0.552 | 0.438 |
| -18 | 0.944 | 0.859 | 0.820 | 0.839 | 0.864 | 0.904 | 0.916 | 0.951 | 0.876 | 0.770 | 0.662 | 0.544 | 0.433 | 0.304 |
| -20 | 0.819 | 0.762 | 0.735 | 0.755 | 0.783 | 0.816 | 0.812 | 0.845 | 0.783 | 0.675 | 0.567 | 0.449 | 0.321 | 0.174 |
| -22 | 0.709 | 0.668 | 0.667 | 0.698 | 0.735 | 0.762 | 0.753 | 0.741 | 0.700 | 0.616 | 0.517 | 0.403 | 0.282 | 0.138 |
| -24 | 0.706 | 0.678 | 0.680 | 0.713 | 0.749 | 0.760 | 0.762 | 0.744 | 0.695 | 0.613 | 0.521 | 0.420 | 0.296 | 0.112 |
| -25.4 | 0.703 | 1.028 | 1.231 | 1.342 | 1.319 | 1.216 | 1.078 | 1.342 | 1.294 | 1.173 | 1.016 | 0.848 | 0.451 | 0.034 |

Table 1. (continued)
Time: 1.014 days = 24.33 hrs

| Distance From Core Midplane (cm) | Distance From Core Centerline (cm) | | | | | | | | | | | | | |
|---|---|---|---|---|---|---|---|---|---|---|---|---|---|---|
| | Inner Fuel Element | | | | | | | Outer Fuel Element | | | | | | |
| | 7.14 | 8.00 | 9.00 | 10.00 | 11.00 | 12.00 | 12.60 | 15.15 | 16.00 | 17.00 | 18.00 | 19.00 | 20.00 | 21.00 |
| 25.4 | 0.616 | 1.000 | 1.230 | 1.339 | 1.281 | 1.163 | 1.036 | 1.343 | 1.293 | 1.197 | 1.068 | 0.933 | 0.587 | 0.234 |
| 24 | 0.655 | 0.678 | 0.685 | 0.707 | 0.708 | 0.717 | 0.719 | 0.854 | 0.789 | 0.697 | 0.600 | 0.494 | 0.368 | 0.258 |
| 22 | 0.733 | 0.688 | 0.682 | 0.703 | 0.714 | 0.732 | 0.751 | 0.850 | 0.784 | 0.692 | 0.597 | 0.494 | 0.414 | 0.297 |
| 20 | 0.853 | 0.792 | 0.746 | 0.771 | 0.797 | 0.831 | 0.856 | 0.895 | 0.828 | 0.737 | 0.651 | 0.577 | 0.516 | 0.416 |
| 18 | 0.956 | 0.904 | 0.861 | 0.873 | 0.895 | 0.928 | 0.956 | 1.001 | 0.924 | 0.835 | 0.758 | 0.683 | 0.621 | 0.535 |
| 16 | 1.054 | 1.003 | 0.963 | 0.970 | 0.989 | 1.022 | 1.049 | 1.125 | 1.038 | 0.940 | 0.862 | 0.789 | 0.727 | 0.650 |
| 14 | 1.147 | 1.093 | 1.050 | 1.058 | 1.074 | 1.109 | 1.138 | 1.224 | 1.137 | 1.039 | 0.958 | 0.887 | 0.836 | 0.768 |
| 12 | 1.230 | 1.168 | 1.122 | 1.138 | 1.152 | 1.188 | 1.221 | 1.306 | 1.222 | 1.125 | 1.047 | 0.980 | 0.945 | 0.898 |
| 10 | 1.305 | 1.233 | 1.181 | 1.207 | 1.219 | 1.258 | 1.294 | 1.371 | 1.295 | 1.202 | 1.123 | 1.068 | 1.058 | 1.035 |
| 8 | 1.369 | 1.285 | 1.230 | 1.269 | 1.279 | 1.319 | 1.359 | 1.425 | 1.354 | 1.268 | 1.193 | 1.149 | 1.173 | 1.183 |
| 6 | 1.424 | 1.329 | 1.271 | 1.320 | 1.329 | 1.371 | 1.418 | 1.468 | 1.404 | 1.323 | 1.252 | 1.221 | 1.293 | 1.360 |
| 4 | 1.459 | 1.362 | 1.302 | 1.351 | 1.361 | 1.400 | 1.465 | 1.505 | 1.444 | 1.366 | 1.302 | 1.281 | 1.363 | 1.482 |
| 2 | 1.478 | 1.380 | 1.321 | 1.370 | 1.372 | 1.411 | 1.490 | 1.537 | 1.477 | 1.408 | 1.341 | 1.315 | 1.397 | 1.520 |
| 0 | 1.482 | 1.385 | 1.326 | 1.372 | 1.372 | 1.410 | 1.491 | 1.548 | 1.492 | 1.418 | 1.347 | 1.324 | 1.406 | 1.527 |
| -2 | 1.469 | 1.373 | 1.313 | 1.360 | 1.358 | 1.399 | 1.471 | 1.538 | 1.480 | 1.403 | 1.334 | 1.309 | 1.389 | 1.501 |
| -4 | 1.443 | 1.347 | 1.285 | 1.333 | 1.332 | 1.373 | 1.430 | 1.510 | 1.445 | 1.367 | 1.297 | 1.260 | 1.332 | 1.406 |
| -6 | 1.395 | 1.302 | 1.242 | 1.286 | 1.292 | 1.329 | 1.380 | 1.451 | 1.380 | 1.297 | 1.221 | 1.174 | 1.209 | 1.221 |
| -8 | 1.323 | 1.246 | 1.190 | 1.218 | 1.229 | 1.268 | 1.319 | 1.369 | 1.296 | 1.208 | 1.136 | 1.083 | 1.085 | 1.063 |
| -10 | 1.246 | 1.180 | 1.128 | 1.147 | 1.160 | 1.199 | 1.251 | 1.281 | 1.208 | 1.120 | 1.048 | 0.988 | 0.967 | 0.922 |
| -12 | 1.165 | 1.105 | 1.058 | 1.068 | 1.087 | 1.125 | 1.172 | 1.191 | 1.116 | 1.030 | 0.955 | 0.892 | 0.851 | 0.790 |
| -14 | 1.077 | 1.023 | 0.978 | 0.987 | 1.008 | 1.045 | 1.085 | 1.095 | 1.017 | 0.935 | 0.860 | 0.792 | 0.737 | 0.661 |
| -16 | 0.988 | 0.933 | 0.892 | 0.897 | 0.926 | 0.963 | 0.990 | 0.999 | 0.921 | 0.841 | 0.764 | 0.690 | 0.625 | 0.537 |
| -18 | 0.894 | 0.837 | 0.799 | 0.813 | 0.841 | 0.874 | 0.893 | 0.906 | 0.830 | 0.746 | 0.667 | 0.589 | 0.515 | 0.416 |
| -20 | 0.799 | 0.735 | 0.701 | 0.724 | 0.753 | 0.785 | 0.788 | 0.815 | 0.742 | 0.650 | 0.569 | 0.485 | 0.407 | 0.296 |
| -22 | 0.700 | 0.649 | 0.638 | 0.655 | 0.666 | 0.691 | 0.681 | 0.744 | 0.677 | 0.590 | 0.491 | 0.390 | 0.303 | 0.178 |
| -24 | 0.651 | 0.642 | 0.644 | 0.660 | 0.653 | 0.655 | 0.652 | 0.736 | 0.677 | 0.588 | 0.491 | 0.386 | 0.258 | 0.087 |
| -25.4 | 0.598 | 0.929 | 1.119 | 1.205 | 1.149 | 1.036 | 0.915 | 1.136 | 1.095 | 1.001 | 0.872 | 0.737 | 0.378 | 0.024 |

Table 1. (continued)
Time: 11.57 days = 277.7 hrs

| Distance From Core Midplane (cm) | Distance From Core Centerline (cm) | | | | | | | | | | | | | |
|---|---|---|---|---|---|---|---|---|---|---|---|---|---|---|
| | Inner Fuel Element | | | | | | | Outer Fuel Element | | | | | | |
| | 7.14 | 8.00 | 9.00 | 10.00 | 11.00 | 12.00 | 12.60 | 15.15 | 16.00 | 17.00 | 18.00 | 19.00 | 20.00 | 21.00 |
| 25.4 | 0.504 | 0.947 | 1.181 | 1.258 | 1.211 | 1.090 | 0.950 | 1.289 | 1.281 | 1.199 | 1.082 | 0.950 | 0.607 | 0.253 |
| 24 | 0.545 | 0.669 | 0.709 | 0.723 | 0.718 | 0.731 | 0.700 | 0.802 | 0.777 | 0.720 | 0.652 | 0.569 | 0.482 | 0.310 |
| 22 | 0.575 | 0.669 | 0.688 | 0.689 | 0.707 | 0.705 | 0.694 | 0.768 | 0.743 | 0.670 | 0.608 | 0.540 | 0.459 | 0.376 |
| 20 | 0.685 | 0.769 | 0.751 | 0.751 | 0.785 | 0.785 | 0.791 | 0.825 | 0.806 | 0.741 | 0.689 | 0.631 | 0.560 | 0.486 |
| 18 | 0.818 | 0.872 | 0.836 | 0.839 | 0.860 | 0.893 | 0.881 | 0.917 | 0.892 | 0.824 | 0.772 | 0.722 | 0.715 | 0.585 |
| 16 | 0.903 | 0.965 | 0.928 | 0.932 | 0.932 | 0.981 | 0.967 | 1.007 | 0.981 | 0.912 | 0.863 | 0.814 | 0.880 | 0.685 |
| 14 | 0.979 | 1.052 | 1.016 | 1.019 | 1.004 | 1.063 | 1.061 | 1.088 | 1.069 | 1.004 | 0.951 | 0.906 | 0.989 | 0.794 |
| 12 | 1.045 | 1.130 | 1.096 | 1.098 | 1.078 | 1.137 | 1.159 | 1.162 | 1.155 | 1.097 | 1.033 | 0.999 | 1.079 | 0.908 |
| 10 | 1.105 | 1.200 | 1.169 | 1.169 | 1.157 | 1.203 | 1.252 | 1.225 | 1.234 | 1.186 | 1.112 | 1.095 | 1.165 | 1.035 |
| 8 | 1.155 | 1.259 | 1.230 | 1.232 | 1.232 | 1.262 | 1.329 | 1.276 | 1.306 | 1.260 | 1.189 | 1.185 | 1.243 | 1.176 |
| 6 | 1.191 | 1.306 | 1.281 | 1.288 | 1.293 | 1.305 | 1.376 | 1.325 | 1.366 | 1.315 | 1.252 | 1.251 | 1.308 | 1.281 |
| 4 | 1.214 | 1.339 | 1.314 | 1.329 | 1.331 | 1.334 | 1.399 | 1.366 | 1.412 | 1.355 | 1.292 | 1.291 | 1.352 | 1.341 |
| 2 | 1.228 | 1.359 | 1.336 | 1.350 | 1.346 | 1.351 | 1.405 | 1.400 | 1.438 | 1.379 | 1.316 | 1.313 | 1.370 | 1.373 |
| 0 | 1.239 | 1.365 | 1.342 | 1.352 | 1.346 | 1.358 | 1.405 | 1.415 | 1.449 | 1.391 | 1.325 | 1.322 | 1.370 | 1.386 |
| -2 | 1.230 | 1.354 | 1.329 | 1.334 | 1.339 | 1.345 | 1.397 | 1.400 | 1.435 | 1.385 | 1.314 | 1.310 | 1.364 | 1.372 |
| -4 | 1.219 | 1.329 | 1.299 | 1.300 | 1.310 | 1.315 | 1.370 | 1.362 | 1.405 | 1.358 | 1.287 | 1.284 | 1.342 | 1.331 |
| -6 | 1.197 | 1.289 | 1.249 | 1.256 | 1.265 | 1.274 | 1.326 | 1.312 | 1.355 | 1.305 | 1.244 | 1.239 | 1.291 | 1.259 |
| -8 | 1.161 | 1.237 | 1.198 | 1.206 | 1.202 | 1.223 | 1.264 | 1.254 | 1.286 | 1.235 | 1.171 | 1.156 | 1.194 | 1.141 |
| -10 | 1.108 | 1.176 | 1.140 | 1.146 | 1.136 | 1.170 | 1.196 | 1.189 | 1.204 | 1.146 | 1.077 | 1.045 | 1.062 | 0.965 |
| -12 | 1.032 | 1.106 | 1.079 | 1.079 | 1.065 | 1.110 | 1.125 | 1.122 | 1.113 | 1.049 | 0.984 | 0.933 | 0.925 | 0.812 |
| -14 | 0.948 | 1.028 | 0.999 | 1.003 | 0.996 | 1.044 | 1.045 | 1.044 | 1.017 | 0.950 | 0.891 | 0.834 | 0.813 | 0.712 |
| -16 | 0.863 | 0.943 | 0.911 | 0.918 | 0.928 | 0.965 | 0.956 | 0.960 | 0.921 | 0.858 | 0.798 | 0.743 | 0.709 | 0.617 |
| -18 | 0.783 | 0.851 | 0.819 | 0.826 | 0.848 | 0.872 | 0.861 | 0.864 | 0.830 | 0.769 | 0.710 | 0.656 | 0.609 | 0.527 |
| -20 | 0.689 | 0.745 | 0.736 | 0.738 | 0.766 | 0.760 | 0.762 | 0.775 | 0.748 | 0.681 | 0.624 | 0.567 | 0.517 | 0.439 |
| -22 | 0.569 | 0.653 | 0.673 | 0.676 | 0.679 | 0.677 | 0.659 | 0.722 | 0.693 | 0.614 | 0.542 | 0.476 | 0.424 | 0.344 |
| -24 | 0.540 | 0.661 | 0.694 | 0.716 | 0.720 | 0.684 | 0.669 | 0.742 | 0.713 | 0.644 | 0.578 | 0.489 | 0.369 | 0.211 |
| -25.4 | 0.491 | 0.926 | 1.150 | 1.221 | 1.168 | 1.041 | 0.899 | 1.111 | 1.107 | 1.032 | 0.920 | 0.788 | 0.459 | 0.125 |

Table 1. (continued)
Time: 22.72 days = 545.3 hrs

| Distance From Core Midplane (cm) | Distance From Core Centerline (cm) | | | | | | | | | | | | | |
|---|---|---|---|---|---|---|---|---|---|---|---|---|---|---|
| | Inner Fuel Element | | | | | | | Outer Fuel Element | | | | | | |
| | 7.14 | 8.00 | 9.00 | 10.00 | 11.00 | 12.00 | 12.60 | 15.15 | 16.00 | 17.00 | 18.00 | 19.00 | 20.00 | 21.00 |
| 25.4 | 0.379 | 0.874 | 1.183 | 1.276 | 1.218 | 1.053 | 0.874 | 1.120 | 1.244 | 1.226 | 1.165 | 1.050 | 0.709 | 0.327 |
| 24 | 0.403 | 0.594 | 0.695 | 0.711 | 0.706 | 0.671 | 0.624 | 0.725 | 0.740 | 0.695 | 0.651 | 0.601 | 0.534 | 0.352 |
| 22 | 0.460 | 0.599 | 0.675 | 0.707 | 0.705 | 0.677 | 0.632 | 0.722 | 0.740 | 0.691 | 0.646 | 0.607 | 0.565 | 0.431 |
| 20 | 0.547 | 0.659 | 0.707 | 0.749 | 0.757 | 0.752 | 0.714 | 0.757 | 0.799 | 0.767 | 0.731 | 0.710 | 0.705 | 0.549 |
| 18 | 0.624 | 0.759 | 0.790 | 0.835 | 0.845 | 0.836 | 0.806 | 0.826 | 0.895 | 0.870 | 0.837 | 0.826 | 0.821 | 0.648 |
| 16 | 0.688 | 0.847 | 0.833 | 0.923 | 0.926 | 0.914 | 0.890 | 0.901 | 0.984 | 0.965 | 0.934 | 0.925 | 0.923 | 0.735 |
| 14 | 0.742 | 0.927 | 0.969 | 1.006 | 1.003 | 0.987 | 0.966 | 0.970 | 1.067 | 1.049 | 1.018 | 1.013 | 1.015 | 0.813 |
| 12 | 0.788 | 0.998 | 1.046 | 1.081 | 1.074 | 1.054 | 1.034 | 1.034 | 1.139 | 1.123 | 1.092 | 1.088 | 1.094 | 0.880 |
| 10 | 0.824 | 1.055 | 1.115 | 1.150 | 1.139 | 1.116 | 1.091 | 1.090 | 1.202 | 1.187 | 1.150 | 1.154 | 1.160 | 0.936 |
| 8 | 0.857 | 1.103 | 1.176 | 1.209 | 1.197 | 1.171 | 1.139 | 1.141 | 1.256 | 1.242 | 1.199 | 1.208 | 1.214 | 0.984 |
| 6 | 0.887 | 1.143 | 1.225 | 1.260 | 1.246 | 1.219 | 1.177 | 1.184 | 1.300 | 1.285 | 1.240 | 1.251 | 1.259 | 1.021 |
| 4 | 0.914 | 1.177 | 1.261 | 1.298 | 1.282 | 1.251 | 1.210 | 1.219 | 1.338 | 1.323 | 1.272 | 1.286 | 1.289 | 1.052 |
| 2 | 0.940 | 1.203 | 1.281 | 1.315 | 1.296 | 1.266 | 1.233 | 1.250 | 1.367 | 1.349 | 1.297 | 1.300 | 1.302 | 1.072 |
| 0 | 0.962 | 1.224 | 1.286 | 1.315 | 1.297 | 1.268 | 1.243 | 1.264 | 1.377 | 1.349 | 1.301 | 1.299 | 1.303 | 1.072 |
| -2 | 0.951 | 1.210 | 1.275 | 1.304 | 1.284 | 1.254 | 1.234 | 1.249 | 1.359 | 1.330 | 1.284 | 1.280 | 1.292 | 1.048 |
| -4 | 0.934 | 1.182 | 1.248 | 1.276 | 1.256 | 1.232 | 1.207 | 1.214 | 1.328 | 1.304 | 1.260 | 1.253 | 1.269 | 1.023 |
| -6 | 0.911 | 1.145 | 1.207 | 1.236 | 1.218 | 1.193 | 1.172 | 1.172 | 1.288 | 1.269 | 1.228 | 1.221 | 1.237 | 0.993 |
| -8 | 0.880 | 1.102 | 1.159 | 1.189 | 1.174 | 1.147 | 1.127 | 1.125 | 1.242 | 1.225 | 1.189 | 1.181 | 1.196 | 0.961 |
| -10 | 0.844 | 1.050 | 1.100 | 1.131 | 1.120 | 1.094 | 1.074 | 1.072 | 1.187 | 1.175 | 1.139 | 1.133 | 1.148 | 0.922 |
| -12 | 0.798 | 0.988 | 1.031 | 1.066 | 1.059 | 1.035 | 1.015 | 1.011 | 1.121 | 1.113 | 1.080 | 1.076 | 1.089 | 0.875 |
| -14 | 0.744 | 0.916 | 0.954 | 0.990 | 0.990 | 0.969 | 0.950 | 0.947 | 1.045 | 1.038 | 1.008 | 1.007 | 1.014 | 0.808 |
| -16 | 0.680 | 0.832 | 0.869 | 0.910 | 0.915 | 0.900 | 0.879 | 0.877 | 0.961 | 0.949 | 0.919 | 0.917 | 0.914 | 0.718 |
| -18 | 0.607 | 0.737 | 0.776 | 0.822 | 0.833 | 0.825 | 0.804 | 0.804 | 0.867 | 0.847 | 0.813 | 0.802 | 0.783 | 0.599 |
| -20 | 0.526 | 0.637 | 0.694 | 0.728 | 0.748 | 0.746 | 0.722 | 0.729 | 0.764 | 0.731 | 0.692 | 0.653 | 0.612 | 0.468 |
| -22 | 0.437 | 0.589 | 0.656 | 0.680 | 0.678 | 0.664 | 0.627 | 0.688 | 0.704 | 0.657 | 0.614 | 0.575 | 0.514 | 0.381 |
| -24 | 0.407 | 0.589 | 0.663 | 0.682 | 0.674 | 0.638 | 0.590 | 0.686 | 0.703 | 0.659 | 0.618 | 0.572 | 0.510 | 0.324 |
| -25.4 | 0.379 | 0.866 | 1.165 | 1.251 | 1.191 | 1.027 | 0.849 | 1.016 | 1.150 | 1.120 | 1.054 | 0.950 | 0.627 | 0.281 |

Table 1. (continued)
Time: 25.00 days = 600.00 hrs

| Distance From Core Midplane (cm) | Distance From Core Centerline (cm) | | | | | | | | | | | | | |
|---|---|---|---|---|---|---|---|---|---|---|---|---|---|---|
| | Inner Fuel Element | | | | | | | Outer Fuel Element | | | | | | |
| | 7.14 | 8.00 | 9.00 | 10.00 | 11.00 | 12.00 | 12.60 | 15.15 | 16.00 | 17.00 | 18.00 | 19.00 | 20.00 | 21.00 |
| 25.4 | 0.358 | 0.850 | 1.170 | 1.265 | 1.198 | 1.019 | 0.824 | 1.131 | 1.294 | 1.284 | 1.243 | 1.141 | 0.805 | 0.415 |
| 24 | 0.363 | 0.558 | 0.634 | 0.654 | 0.662 | 0.645 | 0.592 | 0.746 | 0.757 | 0.723 | 0.704 | 0.690 | 0.643 | 0.439 |
| 22 | 0.422 | 0.571 | 0.633 | 0.657 | 0.665 | 0.657 | 0.609 | 0.718 | 0.759 | 0.722 | 0.709 | 0.702 | 0.693 | 0.495 |
| 20 | 0.497 | 0.648 | 0.688 | 0.725 | 0.733 | 0.727 | 0.685 | 0.739 | 0.808 | 0.794 | 0.785 | 0.786 | 0.791 | 0.586 |
| 18 | 0.568 | 0.735 | 0.772 | 0.808 | 0.821 | 0.815 | 0.766 | 0.808 | 0.896 | 0.884 | 0.877 | 0.867 | 0.879 | 0.664 |
| 16 | 0.629 | 0.814 | 0.853 | 0.885 | 0.898 | 0.894 | 0.842 | 0.883 | 0.980 | 0.967 | 0.959 | 0.943 | 0.957 | 0.729 |
| 14 | 0.684 | 0.886 | 0.929 | 0.955 | 0.973 | 0.966 | 0.909 | 0.951 | 1.057 | 1.043 | 1.034 | 1.015 | 1.026 | 0.787 |
| 12 | 0.730 | 0.950 | 0.999 | 1.032 | 1.041 | 1.029 | 0.970 | 1.011 | 1.124 | 1.111 | 1.101 | 1.078 | 1.087 | 0.838 |
| 10 | 0.768 | 1.006 | 1.065 | 1.099 | 1.100 | 1.083 | 1.024 | 1.064 | 1.183 | 1.170 | 1.159 | 1.136 | 1.142 | 0.883 |
| 8 | 0.801 | 1.054 | 1.124 | 1.160 | 1.152 | 1.129 | 1.069 | 1.110 | 1.236 | 1.220 | 1.208 | 1.185 | 1.191 | 0.923 |
| 6 | 0.826 | 1.094 | 1.176 | 1.215 | 1.198 | 1.166 | 1.108 | 1.147 | 1.275 | 1.259 | 1.249 | 1.224 | 1.232 | 0.951 |
| 4 | 0.848 | 1.126 | 1.213 | 1.246 | 1.228 | 1.195 | 1.139 | 1.172 | 1.299 | 1.283 | 1.270 | 1.241 | 1.243 | 0.963 |
| 2 | 0.866 | 1.145 | 1.231 | 1.263 | 1.243 | 1.211 | 1.159 | 1.185 | 1.312 | 1.294 | 1.277 | 1.243 | 1.243 | 0.965 |
| 0 | 0.877 | 1.147 | 1.234 | 1.269 | 1.248 | 1.215 | 1.168 | 1.189 | 1.316 | 1.295 | 1.278 | 1.243 | 1.243 | 0.966 |
| -2 | 0.868 | 1.134 | 1.229 | 1.261 | 1.242 | 1.210 | 1.168 | 1.186 | 1.312 | 1.294 | 1.277 | 1.243 | 1.243 | 0.965 |
| -4 | 0.854 | 1.114 | 1.210 | 1.242 | 1.222 | 1.193 | 1.159 | 1.173 | 1.299 | 1.284 | 1.268 | 1.240 | 1.243 | 0.965 |
| -6 | 0.833 | 1.087 | 1.176 | 1.208 | 1.190 | 1.167 | 1.134 | 1.152 | 1.276 | 1.264 | 1.246 | 1.222 | 1.236 | 0.956 |
| -8 | 0.809 | 1.054 | 1.132 | 1.166 | 1.153 | 1.133 | 1.093 | 1.117 | 1.239 | 1.223 | 1.210 | 1.186 | 1.200 | 0.930 |
| -10 | 0.778 | 1.012 | 1.079 | 1.112 | 1.108 | 1.092 | 1.044 | 1.075 | 1.190 | 1.174 | 1.162 | 1.139 | 1.152 | 0.891 |
| -12 | 0.741 | 0.960 | 1.014 | 1.052 | 1.053 | 1.043 | 0.987 | 1.024 | 1.131 | 1.114 | 1.102 | 1.081 | 1.095 | 0.846 |
| -14 | 0.692 | 0.895 | 0.943 | 0.983 | 0.991 | 0.983 | 0.924 | 0.965 | 1.062 | 1.092 | 1.033 | 1.014 | 1.030 | 0.796 |
| -16 | 0.631 | 0.813 | 0.861 | 0.906 | 0.918 | 0.913 | 0.852 | 0.896 | 0.986 | 0.965 | 0.954 | 0.938 | 0.958 | 0.741 |
| -18 | 0.552 | 0.707 | 0.770 | 0.821 | 0.836 | 0.831 | 0.774 | 0.818 | 0.896 | 0.875 | 0.862 | 0.849 | 0.874 | 0.677 |
| -20 | 0.452 | 0.595 | 0.677 | 0.731 | 0.746 | 0.738 | 0.689 | 0.750 | 0.811 | 0.778 | 0.764 | 0.752 | 0.786 | 0.603 |
| -22 | 0.395 | 0.552 | 0.626 | 0.671 | 0.676 | 0.662 | 0.610 | 0.724 | 0.767 | 0.728 | 0.714 | 0.702 | 0.686 | 0.513 |
| -24 | 0.392 | 0.557 | 0.635 | 0.665 | 0.668 | 0.647 | 0.593 | 0.738 | 0.766 | 0.732 | 0.724 | 0.700 | 0.653 | 0.414 |
| -25.4 | 0.356 | 0.829 | 1.129 | 1.217 | 1.145 | 0.971 | 0.780 | 1.090 | 1.245 | 1.231 | 1.189 | 1.086 | 0.739 | 0.350 |

Table 2. Some Pertinent HFIR Fuel Element Dimensions and Tolerances[23,24]

| | |
|---|---|
| Length of fuel plates | 24 in. |
| Nominal fuel plate thickness | 0.050 in. |
| Maximum fuel plate thickness | 0.051 in. |
| Nominal coolant channel thickness | 0.050 in. |
| Maximum coolant channel thickness averaged across width of plate at any given elevation | 0.056 in. |
| Minimum coolant channel thickness averaged across width of plate at any given elevation | 0.044 in. |
| Maximum local coolant channel thickness | 0.060 in. |
| Minimum local coolant channel thickness | 0.040 in. |
| Nominal distance of fuel bearing portion from upper and lower edges of the fuel plate | 2 in. |
| Maximum distance of fuel bearing portion from upper and lower edges of the fuel plate | 2 1/4 in. |
| Minimum distance of fuel bearing portion from upper and lower edges of the fuel plate | 1 3/4 in. |
| Minimum radial distance of the fuel bearing portion of the fuel plate from the side plate | 0.045 in. |
| Nominal heat transfer area | 428.8 $ft^2$ |
| Minimum heat transfer area | 410.3 $ft^2$ |
| Maximum diameter of non bond between fuel and clad | 1/16 in. |
| Tolerance on total fuel loading within an individual fuel plate | ±1.0% |
| Tolerance on fuel loading within a 5/64 in. diameter spot | +30%<br>-100% |
| Average tolerance on fuel loading within a rectangular area 5/64 in. × 1/2 in. | ±10% |

Table 3. Peaking Factors for Fuel Bearing Material Extending Below the Surrounding Fuel Bearing Material in the HFIR Core[22]

| R<br>Radial Distance From Longitudinal Center-Line of Reactor | Power Density at End of Fuel-Plate-Fuel Core Extending 0.530" Past Ends of Fuel-Plate-Fuel Core of Surrounding Plates Divided by Power Density at End of Fuel-Plate-Fuel Core in Surrounding Plates. |
|---|---|
| (cm) | |
| 7.14 | < 1 |
| 8 | 1.25 |
| 9 | 1.41 |
| 10 | 1.44 |
| 11 | 1.43 |
| 12 | 1.30 |
| 12.6 | 1.20 |
| 15.15 | 1.23 |
| 16 | 1.23 |
| 17 | 1.26 |
| 18 | 1.35 |
| 19 | 1.31 |
| 20 | 1.23 |
| 21 | < 1 |

Table 4. Input Data

The following are the input data required for this analysis along with some typical values.

| | |
|---|---|
| Specify Option I or Option II. | Option II used for the results reported here. |
| Specify Alternate Method I or Alternate Method II for the flow rates. | Alternate Method II used for the results reported here. |
| Specify Alternate Method I or Alternate Method II for the oxide buildup. | Alternate Method II used for the results reported here. |

| Symbol | Definition | Typical Values and Units |
|---|---|---|
| R | Outside radius of inner side plate | 2.7215 in. for inner element<br>5.8730 in. for outer element |
| $\Delta r_i$ | Radial space increments | See below |

| Inner Element | Outer Element |
|---|---|
| $\Delta r_1$ = 0 in. | $\Delta r_1$ = 0 in. |
| $\Delta r_2$ = 0.0895 in. | $\Delta r_2$ = 0.0739 in. |
| $\Delta r_3$ = 0 in. | $\Delta r_3$ = 0 in. |
| $\Delta r_4$ = 0.3386 in. | $\Delta r_4$ = 0.3346 in. |
| $\Delta r_5$ = 0.3937 in. | $\Delta r_5$ = 0.3937 in. |
| $\Delta r_6$ = 0.3937 in. | $\Delta r_6$ = 0.3937 in. |
| $\Delta r_7$ = 0.3937 in. | $\Delta r_7$ = 0.3937 in. |
| $\Delta r_8$ = 0.3937 in. | $\Delta r_8$ = 0.3937 in. |
| $\Delta r_9$ = 0.2362 in. | $\Delta r_9$ = 0.3937 in. |
| $\Delta r_{10}$ = 0 in. | $\Delta r_{10}$ = 0 in. |
| $\Delta r_{11}$ = 0.0794 in. | $\Delta r_{11}$ = 0.0443 in. |

| | | |
|---|---|---|
| $\Delta z_i$ | Longitudinal space increments | See below |

| For Both Elements | |
|---|---|
| $\Delta z_1$ = 0 in. | $\Delta z_5$ = 0.7874 in. |
| $\Delta z_2$ = 2.0000 in. | $\Delta z_6$ = 0.7874 in. |
| $\Delta z_3$ = 0 in. | $\Delta z_7$ = 0.7874 in. |
| $\Delta z_4$ = 0.5512 in. | $\Delta z_8$ = 0.7874 in. |

Table 4. (continued)

| Symbol | Definition | Typical Values and Units |
|---|---|---|
| | $\Delta z_9$ = 0.7874 in. | $\Delta z_{21}$ = 0.7874 in. |
| | $\Delta z_{10}$ = 0.7874 in. | $\Delta z_{22}$ = 0.7874 in. |
| | $\Delta z_{11}$ = 0.7874 in. | $\Delta z_{23}$ = 0.7874 in. |
| | $\Delta z_{12}$ = 0.7874 in. | $\Delta z_{24}$ = 0.7874 in. |
| | $\Delta z_{13}$ = 0.7874 in. | $\Delta z_{25}$ = 0.7874 in. |
| | $\Delta z_{14}$ = 0.7874 in. | $\Delta z_{26}$ = 0.7874 in. |
| | $\Delta z_{15}$ = 0.7874 in. | $\Delta z_{27}$ = 0.7874 in. |
| | $\Delta z_{16}$ = 0.7874 in. | $\Delta z_{28}$ = 0.7874 in. |
| | $\Delta z_{17}$ = 0.7874 in. | $\Delta z_{29}$ = 0.5512 in. |
| | $\Delta z_{18}$ = 0.7874 in. | $\Delta z_{30}$ = 0 in. |
| | $\Delta z_{19}$ = 0.7874 in. | $\Delta z_{31}$ = 2.0000 in. |
| | $\Delta z_{20}$ = 0.7874 in. | |
| $\phi'_{i,j}$ | Unnormalized power density distribution | See below |

The following is for the inner fuel element for the first time step. Values for the outer fuel element and for other time steps can be obtained by analogy from the information listed in Table 1.

| j \ i | 1 | 2 | 3 | 4 | 5 | 6 | 7 | 8 | 9 | 10 | 11(m) |
|---|---|---|---|---|---|---|---|---|---|---|---|
| 1 | 0 | 0 | 0 | 0 | 0 | 0 | 0 | 0 | 0 | 0 | 0 |
| 2 | 0 | 0 | 0 | 0 | 0 | 0 | 0 | 0 | 0 | 0 | 0 |
| 3 | 0 | 0 | 0.678 | 1.109 | 1.379 | 1.515 | 1.470 | 1.344 | 1.186 | 0 | 0 |
| 4 | 0 | 0 | 0.722 | 0.741 | 0.738 | 0.771 | 0.809 | 0.830 | 0.837 | 0 | 0 |
| 5 | 0 | 0 | 0.815 | 0.753 | 0.738 | 0.767 | 0.802 | 0.830 | 0.824 | 0 | 0 |
| 6 | 0 | 0 | 0.924 | 0.848 | 0.810 | 0.821 | 0.850 | 0.889 | 0.893 | 0 | 0 |
| 7 | 0 | 0 | 1.031 | 0.952 | 0.904 | 0.917 | 0.939 | 0.980 | 0.988 | 0 | 0 |
| 8 | 0 | 0 | 1.130 | 1.043 | 0.990 | 1.007 | 1.027 | 1.067 | 1.077 | 0 | 0 |
| 9 | 0 | 0 | 1.227 | 1.126 | 1.068 | 1.089 | 1.107 | 1.146 | 1.162 | 0 | 0 |
| 10 | 0 | 0 | 1.312 | 1.198 | 1.137 | 1.163 | 1.179 | 1.217 | 1.241 | 0 | 0 |
| 11 | 0 | 0 | 1.387 | 1.264 | 1.200 | 1.233 | 1.241 | 1.280 | 1.316 | 0 | 0 |
| 12 | 0 | 0 | 1.447 | 1.322 | 1.255 | 1.285 | 1.294 | 1.334 | 1.383 | 0 | 0 |
| 13 | 0 | 0 | 1.493 | 1.372 | 1.306 | 1.332 | 1.339 | 1.380 | 1.445 | 0 | 0 |
| 14 | 0 | 0 | 1.520 | 1.398 | 1.338 | 1.369 | 1.372 | 1.410 | 1.478 | 0 | 0 |
| 15 | 0 | 0 | 1.532 | 1.408 | 1.350 | 1.386 | 1.388 | 1.422 | 1.490 | 0 | 0 |
| 16 | 0 | 0 | 1.533 | 1.403 | 1.349 | 1.386 | 1.388 | 1.420 | 1.485 | 0 | 0 |
| 17 | 0 | 0 | 1.523 | 1.393 | 1.335 | 1.372 | 1.375 | 1.418 | 1.464 | 0 | 0 |

Table 4. (continued)

| Symbol | Definition | Typical Values and Units |
|---|---|---|

| j \ i | 1 | 2 | 3 | 4 | 5 | 6 | 7 | 8 | 9 | 10 | 11(m) |
|---|---|---|---|---|---|---|---|---|---|---|---|
| 18 | 0 | 0 | 1.494 | 1.368 | 1.305 | 1.342 | 1.345 | 1.380 | 1.425 | 0 | 0 |
| 19 | 0 | 0 | 1.448 | 1.324 | 1.256 | 1.289 | 1.295 | 1.330 | 1.372 | 0 | 0 |
| 20 | 0 | 0 | 1.384 | 1.264 | 1.193 | 1.221 | 1.235 | 1.283 | 1.312 | 0 | 0 |
| 21 | 0 | 0 | 1.312 | 1.195 | 1.127 | 1.150 | 1.167 | 1.212 | 1.248 | 0 | 0 |
| 22 | 0 | 0 | 1.235 | 1.120 | 1.057 | 1.077 | 1.097 | 1.144 | 1.177 | 0 | 0 |
| 23 | 0 | 0 | 1.148 | 1.039 | 0.982 | 1.000 | 1.023 | 1.069 | 1.098 | 0 | 0 |
| 24 | 0 | 0 | 1.050 | 0.952 | 0.903 | 0.920 | 0.945 | 0.988 | 1.011 | 0 | 0 |
| 25 | 0 | 0 | 0.944 | 0.859 | 0.820 | 0.839 | 0.864 | 0.904 | 0.916 | 0 | 0 |
| 26 | 0 | 0 | 0.819 | 0.762 | 0.735 | 0.755 | 0.783 | 0.816 | 0.812 | 0 | 0 |
| 27 | 0 | 0 | 0.709 | 0.668 | 0.667 | 0.698 | 0.735 | 0.762 | 0.753 | 0 | 0 |
| 28 | 0 | 0 | 0.706 | 0.678 | 0 680 | 0.713 | 0.749 | 0.760 | 0.762 | 0 | 0 |
| 29 | 0 | 0 | 0.703 | 1.028 | 1.231 | 1.342 | 1.319 | 1.216 | 1.078 | 0 | 0 |
| 30 | 0 | 0 | 0 | 0 | 0 | 0 | 0 | 0 | 0 | 0 | 0 |
| 31(n) | 0 | 0 | 0 | 0 | 0 | 0 | 0 | 0 | 0 | 0 | 0 |

| | | |
|---|---|---|
| $\theta_k$ | Time increment | See below |

$\theta_1 = 24.33$ hr

$\theta_2 = 253.23$ hr

$\theta_3 = 267.68$ hr

$\theta_4 = 54.78$ hr

$\theta_5 = 0$ hr

| | | |
|---|---|---|
| Q | Specified reactor power level | 100 Mw |
| f | Fraction of heat deposited in the fuel assembly | 0.975 |
| A | Nominal fuel assembly heat transfer area | 428.8 $ft^2$ |
| t | Fuel plate thickness | 51 mils |
| $e_A$ | Average fuel element coolant channel thickness prior to reactor operation* | 49 mils for both fuel elements |
| $e_n$ | Average thickness of the narrow coolant channel prior to reactor operation* | 44 mils for both fuel elements |
| $e_w$ | Average thickness of the wide coolant channel prior to reactor operation* | 56 mils for both fuel elements |

Table 4. (continued)

| Symbol | Definition | Typical Values and Units |
|---|---|---|
| $e_{ne}$ | Thickness of the inlet and exit of the narrow coolant channel prior to reactor operation* | 44 mils for both fuel elements |
| $e_{we}$ | Thickness of the inlet and exit of the wide coolant channel prior to reactor operation* | 56 mils for both fuel elements |
| $e_{n,min}$ | Minimum thickness of the narrow coolant channel prior to reactor operation* | 40 mils for both fuel elements |
| $e_{w,min}$ | Minimum thickness of the wide coolant channel prior to reactor operation* | 40 mils for both fuel elements |
| | *Specify for both the inner and the outer fuel elements | |
| $\lambda_g$ | Wavelength of sinusoidal deflection or sinusoidal variation in the channel thickness prior to reactor operation | 2 in. |
| $\xi_1$ | Assign a value of 1 for Case 1 shown in Figs. 17 or 18; a value of 0 otherwise | |
| $\xi_2$ | Assign a value of 1 for Case 2 shown in Figs. 17 or 18; a value of 0 otherwise | |
| $\xi_3$ | Assign a value of 1 for Case 3 shown in Figs. 17 or 18; a value of 0 otherwise | |
| $\xi_4$ | Assign a value of 1 for Case 4 shown in Figs. 17 or 18; a value of 0 otherwise | |
| $T_{in}$ | Inlet coolant temperature | 120°F |
| P | Reactor vessel pressure | 600 psia |
| $\Delta P_F$ | Fuel element pressure drop | 108 psi |
| F | Constant in the friction factor relation $f = F/(Re)^{0.2}$ | 0.235 |
| $Q_{SP}$ | Side plate heat generation rate at 100 Mw reactor power | 6000 Btu/(hr)(in.$^3$) |

Table 4. (continued)

| Symbol | Definition | Typical Values and Units |
|---|---|---|
| $Q_{H_2O}$ | Coolant heat generation rate at 100 Mw reactor power | 4475 Btu/(hr)(in.$^3$) |
| B | Constant in equation for increase in fuel plate thickness due to radiation | 0 mils/hr |
| $\rho/\rho_R$ | Ratio of fuel plate density before and after radiation (Specified for the different time intervals $\theta_k$) | 1.0 |
| $U_1$ | Uncertainty in the reactor power level | 1.02 |
| $U_2$ | Uncertainty in the total heat transfer area | 1.045 |
| $U_3$ | Uncertainty in the power density distribution | 1.10 |
| $U_4$ | Uncertainty in the "average" fuel concentration in the hot plate | 0.92 for $1 \leq j \leq 16$<br>1.10 for $17 \leq j \leq 31$ |
| $U_5$ | Uncertainty in the "average" fuel concentration in the cold plate | 1.08 for $1 \leq j \leq 16$<br>0.90 for $7 \leq j \leq 31$ |
| $U_6$ | Uncertainty in the inlet coolant temperature | 1.01 |
| $U_7$ | Uncertainty in the friction factor | 1.05 |
| $U_8$ | Uncertainty in the local heat transfer correlation | 0.90 |
| $U_9$ | Uncertainty in the oxide film correlation | 1.25 |
| $U_{10}$ | Uncertainty in the relationship for deflection due to the differential pressure across the plate | 1.10 |
| $U_{11}$ | Uncertainty in the relationship for deflection of plate being considered in reference to an average plate due to temperature differences | 1.10 |
| $U_{12}$ | Uncertainty in the increase in the fuel plate thickness due to thermal expansion | 2.00 |
| $U_{13}$ | Uncertainty in the increase in the fuel plate thickness due to radiation damage | 1.00 |

Table 4. (continued)

| Symbol | Definition | Typical Values and Units |
|---|---|---|
| $U_{14}$ | Uncertainty in the longitudinal buckling of the fuel plate due to the temperature differences between the fuel plate and the side plates | 1.00 |
| $U_{15}$ | Uncertainty in the longitudinal buckling of the fuel plate due to the radiation damage | 1.00 |
| $U_{16}$ | Uncertainty in the side plate heat generation rate at 100 Mw | 1.00 |
| $U_{17}$ | Uncertainty in the coolant heat generation rate at 100 Mw | 1.00 |
| $U_{18}$ | Fuel segregation flux peaking on the hot side of the fuel plate | 1.30 |
| $U_{19}$ | Fuel segregation flux peaking on the cold side of the fuel plate | 1.30 |
| $U_{22}$ | Uncertainty in the additive method burnout correlation | 0.80 |
| $U_{23}$ | Uncertainty in the incipient boiling correlation | 1.00 |
| $U_{24}$ | Hot streak factor | 1.10 |
| $U_{25}$ | Flux peaking for fuel extending beyond normal boundaries | See below |

For j, 1 through 28, 30 and 31 1.00

For j, 29

| i | Inner Element | Outer Element |
|---|---|---|
| 1 | 1.00 | 1.00 |
| 2 | 1.00 | 1.00 |
| 3 | 1.00 | 1.23 |
| 4 | 1.25 | 1.23 |
| 5 | 1.41 | 1.26 |
| 6 | 1.44 | 1.35 |
| 7 | 1.43 | 1.31 |
| 8 | 1.30 | 1.23 |
| 9 | 1.20 | 1.00 |
| 10 | 1.00 | 1.00 |
| 11 | 1.00 | 1.00 |

Table 4. (continued)

| Symbol | Definition | Typical Values and Units |
|---|---|---|
| $\Delta D$ | Amplitude of the sinusoidal variation in the coolant channel thickness prior to reactor operation* | 0 mils |
| $\Delta P_{nw}$ | Initial guess of the average differential pressure across the fuel plate between a narrow and a wide coolant channel* | 2.0 psi |
| $T_{MAi,j}$ | Initial guess of the metal temperature distribution of the average fuel plate in the fuel element* | See following page |

*Specify for both the inner and the outer fuel elements

Table 4. (continued)

Initial Guess of $T_{MAi,j}$

| j \ i | Inner Fuel Element 1 | 2 | 3 | 4 | 5 | 6 | 7 | 8 | 9 | 10 | 11(m) | Outer Fuel Element 1 | 2 | 3 | 4 | 5 | 6 | 7 | 8 | 9 | 10 | 11(m) |
|---|---|---|---|---|---|---|---|---|---|---|---|---|---|---|---|---|---|---|---|---|---|---|
| 1 | 121.2 | 121.2 | 121.2 | 121.2 | 121.2 | 121.2 | 121.2 | 121.2 | 121.2 | 121.2 | 121.2 | 121.2 | 121.2 | 121.2 | 121.2 | 121.2 | 121.2 | 121.2 | 121.2 | 121.2 | 121.2 | 121.2 |
| 2 | 121.2 | 121.2 | 121.2 | 121.2 | 121.2 | 121.2 | 121.2 | 121.2 | 121.2 | 121.2 | 121.2 | 121.2 | 121.2 | 121.2 | 121.2 | 121.2 | 121.2 | 121.2 | 121.2 | 121.2 | 121.2 | 121.2 |
| 3 | 121.2 | 121.2 | 180 | 190 | 200 | 210 | 210 | 210 | 210 | 121.2 | 121.2 | 121.2 | 121.2 | 220 | 220 | 220 | 210 | 190 | 170 | 140 | 121.2 | 121.2 |
| 4 | 121.2 | 121.2 | 180 | 180 | 180 | 180 | 190 | 190 | 200 | 121.2 | 121.2 | 121.2 | 121.2 | 200 | 200 | 190 | 180 | 170 | 160 | 140 | 121.2 | 121.2 |
| 5 | 121.2 | 121.2 | 190 | 180 | 180 | 180 | 180 | 180 | 190 | 121.2 | 121.2 | 121.2 | 121.2 | 190 | 180 | 180 | 170 | 160 | 150 | 140 | 121.2 | 121.2 |
| 6 | 121.2 | 121.2 | 200 | 190 | 180 | 180 | 190 | 190 | 190 | 121.2 | 121.2 | 121.2 | 121.2 | 190 | 190 | 180 | 180 | 170 | 160 | 150 | 121.2 | 121.2 |
| 7 | 121.2 | 121.2 | 210 | 200 | 190 | 190 | 190 | 200 | 200 | 121.2 | 121.2 | 121.2 | 121.2 | 200 | 200 | 190 | 180 | 170 | 160 | 150 | 121.2 | 121.2 |
| 8 | 121.2 | 121.2 | 220 | 200 | 200 | 200 | 200 | 200 | 210 | 121.2 | 121.2 | 121.2 | 121.2 | 210 | 200 | 200 | 190 | 180 | 170 | 160 | 121.2 | 121.2 |
| 9 | 121.2 | 121.2 | 220 | 210 | 210 | 210 | 210 | 210 | 220 | 121.2 | 121.2 | 121.2 | 121.2 | 220 | 210 | 200 | 190 | 180 | 170 | 160 | 121.2 | 121.2 |
| 10 | 121.2 | 121.2 | 230 | 220 | 210 | 210 | 210 | 220 | 220 | 121.2 | 121.2 | 121.2 | 121.2 | 220 | 220 | 210 | 200 | 190 | 180 | 170 | 121.2 | 121.2 |
| 11 | 121.2 | 121.2 | 240 | 220 | 220 | 220 | 220 | 220 | 230 | 121.2 | 121.2 | 121.2 | 121.2 | 230 | 220 | 220 | 210 | 200 | 190 | 180 | 121.2 | 121.2 |
| 12 | 121.2 | 121.2 | 240 | 230 | 220 | 220 | 220 | 230 | 240 | 121.2 | 121.2 | 121.2 | 121.2 | 240 | 230 | 220 | 210 | 200 | 190 | 190 | 121.2 | 121.2 |
| 13 | 121.2 | 121.2 | 250 | 230 | 230 | 230 | 230 | 230 | 240 | 121.2 | 121.2 | 121.2 | 121.2 | 240 | 240 | 230 | 220 | 210 | 200 | 190 | 121.2 | 121.2 |
| 14 | 121.2 | 121.2 | 250 | 240 | 230 | 230 | 230 | 240 | 250 | 121.2 | 121.2 | 121.2 | 121.2 | 250 | 240 | 230 | 220 | 210 | 200 | 200 | 121.2 | 121.2 |
| 15 | 121.2 | 121.2 | 260 | 240 | 240 | 240 | 240 | 240 | 250 | 121.2 | 121.2 | 121.2 | 121.2 | 250 | 240 | 230 | 230 | 220 | 210 | 200 | 121.2 | 121.2 |
| 16 | 121.2 | 121.2 | 260 | 250 | 240 | 240 | 240 | 250 | 260 | 121.2 | 121.2 | 121.2 | 121.2 | 260 | 250 | 240 | 230 | 220 | 210 | 200 | 121.2 | 121.2 |
| 17 | 121.2 | 121.2 | 260 | 250 | 240 | 240 | 240 | 250 | 260 | 121.2 | 121.2 | 121.2 | 121.2 | 260 | 250 | 240 | 230 | 220 | 210 | 200 | 121.2 | 121.2 |
| 18 | 121.2 | 121.2 | 260 | 250 | 240 | 240 | 240 | 250 | 260 | 121.2 | 121.2 | 121.2 | 121.2 | 260 | 250 | 240 | 230 | 220 | 210 | 200 | 121.2 | 121.2 |
| 19 | 121.2 | 121.2 | 270 | 250 | 240 | 240 | 250 | 250 | 260 | 121.2 | 121.2 | 121.2 | 121.2 | 260 | 250 | 240 | 230 | 220 | 210 | 200 | 121.2 | 121.2 |
| 20 | 121.2 | 121.2 | 270 | 250 | 250 | 240 | 250 | 250 | 260 | 121.2 | 121.2 | 121.2 | 121.2 | 260 | 250 | 240 | 230 | 220 | 210 | 200 | 121.2 | 121.2 |
| 21 | 121.2 | 121.2 | 270 | 250 | 240 | 240 | 250 | 250 | 260 | 121.2 | 121.2 | 121.2 | 121.2 | 260 | 250 | 240 | 230 | 220 | 200 | 190 | 121.2 | 121.2 |
| 22 | 121.2 | 121.2 | 270 | 250 | 240 | 240 | 240 | 250 | 260 | 121.2 | 121.2 | 121.2 | 121.2 | 260 | 250 | 240 | 230 | 210 | 200 | 180 | 121.2 | 121.2 |
| 23 | 121.2 | 121.2 | 260 | 250 | 240 | 240 | 240 | 250 | 260 | 121.2 | 121.2 | 121.2 | 121.2 | 260 | 250 | 240 | 220 | 210 | 190 | 180 | 121.2 | 121.2 |
| 24 | 121.2 | 121.2 | 260 | 250 | 240 | 240 | 240 | 250 | 250 | 121.2 | 121.2 | 121.2 | 121.2 | 250 | 240 | 230 | 220 | 210 | 190 | 180 | 121.2 | 121.2 |
| 25 | 121.2 | 121.2 | 260 | 240 | 240 | 230 | 240 | 240 | 250 | 121.2 | 121.2 | 121.2 | 121.2 | 250 | 240 | 230 | 220 | 200 | 190 | 170 | 121.2 | 121.2 |
| 26 | 121.2 | 121.2 | 250 | 240 | 230 | 230 | 230 | 240 | 250 | 121.2 | 121.2 | 121.2 | 121.2 | 250 | 240 | 230 | 210 | 200 | 190 | 170 | 121.2 | 121.2 |
| 27 | 121.2 | 121.2 | 250 | 240 | 230 | 230 | 230 | 240 | 250 | 121.2 | 121.2 | 121.2 | 121.2 | 240 | 240 | 220 | 210 | 200 | 190 | 170 | 121.2 | 121.2 |
| 28 | 121.2 | 121.2 | 250 | 240 | 240 | 240 | 240 | 250 | 260 | 121.2 | 121.2 | 121.2 | 121.2 | 250 | 240 | 230 | 220 | 200 | 190 | 170 | 121.2 | 121.2 |
| 29 | 121.2 | 121.2 | 240 | 250 | 250 | 260 | 270 | 270 | 270 | 121.2 | 121.2 | 121.2 | 121.2 | 270 | 260 | 250 | 240 | 220 | 200 | 170 | 121.2 | 121.2 |
| 30 | 121.2 | 121.2 | 200 | 190 | 190 | 190 | 190 | 190 | 200 | 121.2 | 121.2 | 121.2 | 121.2 | 200 | 190 | 190 | 180 | 170 | 160 | 160 | 121.2 | 121.2 |
| 31(n) | 121.2 | 121.2 | 200 | 190 | 190 | 190 | 190 | 190 | 200 | 121.2 | 121.2 | 121.2 | 121.2 | 200 | 190 | 190 | 180 | 170 | 160 | 160 | 121.2 | 121.2 |

Table 5. Heat Transfer and Flow Conditions in the HFIR Fuel Elements at the Upper Limit for the Reactor Power Level

A. Upper Limit for the Reactor Level Defined by the Incipient Boiling Criteria

| | Start of Cycle | | | | End of 100 Mw Cycle (25 days) | | | |
|---|---|---|---|---|---|---|---|---|
| | Case Number (See Fig. 18) | | | | Case Number (See Fig. 18) | | | |
| | 1 | 2 | 3 | 4 | 1 | 2 | 3 | 4 |
| Limiting power level, Mw | 139 | 139 | 139 | 140 | 155 | 154 | 153 | 157 |
| Fuel element flow rate, gpm | 12,460 | 12,460 | 12,460 | 12,460 | 12,410 | 12.410 | 12,410 | 12,420 |
| Limiting heat flux | | | | | | | | |
| Location, Fuel element (i,j) | Outer (3,29) | Outer (3,29) | Outer (3,29) | Outer (3,29) | Outer (4,29) | Outer (4,29) | Outer (4,29) | Outer (6,29) |
| Heat flux, Btu/(hr)(ft$^2$) | $3.42 \times 10^6$ | $3.41 \times 10^6$ | $3.41 \times 10^6$ | $3.43 \times 10^6$ | $3.39 \times 10^6$ | $3.36 \times 10^6$ | $3.35 \times 10^6$ | $3.88 \times 10^6$ |
| Bulk water temperature, °F | 296 | 297 | 297 | 295 | 309 | 311 | 312 | 288 |
| Surface temperature, °F | 479 | 479 | 479 | 479 | 478 | 478 | 478 | 479 |
| Heat transfer coefficient, Btu/(hr)(ft$^2$)(°F) | 18,760 | 18,760 | 18,760 | 18,740 | 20,070 | 20,100 | 20,140 | 20,290 |
| Flow rate, lb/(sec)(in. width) | 0.7537 | 0.7524 | 0.7485 | 0.7624 | 0.7384 | 0.6816 | 0.6744 | 0.7466 |
| Absolute pressure, psia | 489 | 489 | 489 | 489 | 487 | 487 | 487 | 486 |
| Maximum hot streak outlet bulk water temperature | | | | | | | | |
| Location, Fuel element (i) | Outer (3) | Outer (3) | Outer (4) | Outer (3) | Outer (5) | Outer (5) | Outer (5) | Outer (4) |
| Magnitude, °F | 296 | 297 | 298 | 295 | 313 | 315 | 314 | 297 |
| Flow rate, lb/(sec)(in. width) | 0.7537 | 0.7524 | 0.7043 | 0.7624 | 0.6669 | 0.6573 | 0.6568 | 0.7466 |
| Minimum flow rate | | | | | | | | |
| Location, Fuel element (i) | Inner (5) | Inner (5) | Inner (4) | Outer (9) | Outer (5) | Outer (5) | Outer (5) | Outer (7) |
| Magnitude, lb/(sec)(in. width) | 0.7086 | 0.7017 | 0.6840 | 0.7530 | 0.6669 | 0.6573 | 0.6568 | 0.7266 |
| Bulk water temperature at outlet, °F | 282 | 283 | 294 | 221 | 313 | 315 | 314 | 293 |

Table 5. (Continued)

B. Upper Limit for the Reactor Power Level Defined by the Burnout Criteria

| | Start of Cycle | | | | End of 100 Mw Cycle (25 days) | | | |
|---|---|---|---|---|---|---|---|---|
| | Case Number (See Fig. 18) | | | | Case Number (See Fig. 18) | | | |
| | 1 | 2 | 3 | 4 | 1 | 2 | 3 | 4 |
| Limiting power level, Mw | 162 | 162 | 162 | 163 | 175 | 175 | 177 | 177 |
| Fuel element flow rate, gpm | 12,490 | 12,490 | 12,490 | 12,490 | 12,440 | 12,440 | 12,440 | 12,440 |
| Limiting heat flux | | | | | | | | |
| Location, Fuel element (i,j) | Inner (6,29) | Inner (6,29) | Outer (3,29) | Inner (6,29) | Inner (6,29) | Inner (6,29) | Inner (6,29) | Inner (6,29) |
| Heat flux, Btu/(hr)(ft$^2$) | $4.36 \times 10^6$ | $4.36 \times 10^6$ | $4.05 \times 10^6$ | $4.36 \times 10^6$ | $4.45 \times 10^6$ | $4.46 \times 10^6$ | $4.50 \times 10^6$ | $4.47 \times 10^6$ |
| Bulk water temperature, °F | 304 | 304 | 326 | 301 | 316 | 316 | 313 | 310 |
| Surface temperature, °F | 523 | 523 | 532 | 522 | 520 | 520 | 519 | 520 |
| Heat transfer coefficient, Btu/(hr)(ft$^2$)(°F) | 19,950 | 19,960 | 19,620 | 19,720 | 21,800 | 21,830 | 21,830 | 21,340 |
| Flow rate, lb/(sec)(in. width) | 0.7449 | 0.7448 | 0.7506 | 0.7617 | 0.7033 | 0.7027 | 0.7214 | 0.7322 |
| Absolute pressure, psia | 488 | 487 | 489 | 488 | 484 | 484 | 484 | 485 |
| Maximum hot streak outlet bulk water temperature | | | | | | | | |
| Location, Fuel element (i) | Outer (3) | Outer (3) | Outer (4) | Outer (3) | Outer (5) | Outer (5) | Outer (5) | Outer (6) |
| Magnitude, °F | 325 | 325 | 328 | 323 | 343 | 347 | 349 | 321 |
| Flow rate, lb/(sec)(in. width) | 0.7558 | 0.7543 | 0.7041 | 0.7651 | 0.6546 | 0.6420 | 0.6426 | 0.7216 |
| Minimum flow rate | | | | | | | | |
| Location, Fuel element (i) | Inner (5) | Inner (5) | Inner (4) | Outer (9) | Outer (5) | Outer (5) | Outer (5) | Outer (7) |
| Magnitude, lb/(sec)(in. width) | 0.7074 | 0.6994 | 0.6842 | 0.7556 | 0.6546 | 0.6420 | 0.6426 | 0.7208 |
| Bulk water temperature at outlet, °F | 309 | 311 | 322 | 237 | 343 | 347 | 349 | 317 |

Table 6. Additional Heat Transfer and Flow Conditions in the HFIR Fuel Elements at the Upper Limit for the Reactor Power Level; Incipient Boiling Criteria Case No. 3 (See Fig. 18)

A. Start of Cycle (Oxide Thickness = 0)
Limiting Power Level: 139 Mw

1. Flow Conditions in the Hot Streak Above the Location of the Limiting Heat Flux

Location: Outer fuel element, i = 3
Hot Streak Flow Rate: 0.7485 lb/(sec)(in. width)

| j | Narrow Channel Thickness (mils) | Hot Streak Thickness (mils) | Hot Streak Coolant Temperature (°F) | Hot Streak Coolant Velocity (ft/sec) |
|---|---|---|---|---|
| 1 | 43.51 | 39.51 | 121.2 | 44.23 |
| 3 | 43.41 | 39.41 | 121.2 | 44.34 |
| 16 | 43.34 | 39.34 | 212.6 | 45.81 |
| 17 | 43.02 | 39.02 | 221.4 | 46.35 |
| 28 | 43.12 | 39.12 | 293.0 | 47.88 |
| 29 | 43.01 | 39.01 | 297.1 | 48.10 |
| 31 | 43.24 | 39.24 | 297.1 | 47.82 |

Flow Conditions in an Average Coolant Channel at this Hot Streak Location

Location: Outer fuel element i = 3
Flow Rate: 1.047 lb/(sec)(in. width)

| j | Average Channel Thickness (mils) | Coolant Temperature (°F) | Coolant Velocity (ft/sec) |
|---|---|---|---|
| 1 | 48.93 | 121.2 | 49.96 |
| 3 | 48.74 | 121.2 | 50.15 |
| 16 | 48.69 | 175.2 | 51.05 |
| 17 | 48.69 | 180.4 | 51.14 |
| 28 | 48.72 | 222.6 | 51.96 |
| 29 | 48.66 | 225.1 | 52.08 |
| 31 | 48.79 | 225.1 | 51.94 |

2. Flow Conditions in the Hot Streak at the Location of the Minimum Flow Rate

Location: Inner fuel element, i = 4
Hot Streak Flow Rate: 0.6840 lb/(sec)(in. width)

| j | Narrow Channel Thickness (mils) | Hot Streak Thickness (mils) | Hot Streak Coolant Temperature (°F) | Hot Streak Coolant Velocity (ft/sec) |
|---|---|---|---|---|
| 1 | 41.54 | 37.54 | 121.2 | 42.54 |
| 3 | 41.84 | 37.84 | 121.2 | 42.20 |
| 16 | 41.65 | 37.65 | 209.9 | 43.70 |
| 17 | 40.42 | 36.42 | 218.5 | 45.33 |
| 28 | 40.62 | 36.62 | 289.9 | 46.67 |
| 29 | 40.41 | 36.41 | 293.6 | 47.03 |
| 31 | 40.97 | 36.97 | 293.6 | 46.32 |

Flow Conditions in an Average Coolant Channel at This Hot Streak Location

Location: Inner fuel element, i = 4
Flow Rate: 1.045 lb/(sec)(in.width)

| j | Average Channel Thickness (mils) | Coolant Temperature (°F) | Coolant Velocity (ft/sec) |
|---|---|---|---|
| 1 | 48.93 | 121.2 | 49.86 |
| 3 | 48.93 | 121.2 | 49.86 |
| 16 | 48.71 | 169.2 | 50.82 |
| 17 | 48.71 | 173.9 | 52.32 |
| 28 | 49.74 | 212.5 | 51.62 |
| 29 | 48.70 | 214.4 | 51.71 |
| 31 | 48.80 | 214.4 | 51.60 |

3. Typical Hot Plate Metal Temperatures (Outer Fuel Element), °F

| i | j | | | | |
|---|---|---|---|---|---|
| | 3 | 16 | 17 | 28 | 29 |
| 3 | 261.4 | 309.6 | 333.7 | 316.9 | 366.0 |
| 4 | 258.7 | 307.6 | 327.3 | 312.6 | 361.2 |
| 5 | 250.9 | 298.0 | 313.0 | 295.3 | 340.9 |
| 6 | 239.3 | 284.2 | 296.3 | 271.4 | 312.6 |
| 7 | 226.7 | 272.5 | 283.5 | 247.8 | 284.7 |
| 8 | 190.2 | 272.0 | 282.7 | 229.5 | 243.9 |
| 9 | 150.6 | 271.3 | 282.1 | 207.9 | 200.7 |
| Average | 225.4 | 287.8 | 302.6 | 268.7 | 301.4 |

4. Typical Average Side Plate Temperatures, °F

| j | Inner Fuel Element | | Outer Fuel Element | |
|---|---|---|---|---|
| | Inner Side Plate | Outer Side Plate | Inner Side Plate | Outer Side Plate |
| 3 | 162 | 177 | 174 | 156 |
| 16 | 169 | 184 | 182 | 160 |
| 29 | 175 | 191 | 190 | 163 |

5. Heat Flux in an Average Fuel Plate at the Location of the Limiting Heat Flux

Location: Outer fuel element (3,29)

Heat Flux: $1.54 \times 10^6$ Btu/(hr)(ft$^2$)

Bulk Water Temperature: 225°F

Surface Temperature: 318°F

Heat Transfer Coefficient: 16,540 Btu/(hr)(ft$^2$)(°F)

B. End of 100 Mw Cycle
Limiting Power Level: 153 Mw

1. Flow Conditions in the Hot Streak Above the Location of the Limiting Heat Flux

Location: Outer fuel element, i = 4
Hot Streak Flow Rate: 0.6744 lb/(sec)(in. width)

| j | Narrow Channel Thickness (mils) | Hot Streak Thickness (mils) | Oxide Thickness on Hot Plate in Narrow Channel (mils) | Oxide Thickness on Cold Plate in Narrow Channel (mils) | Hot Streak Coolant Temperature (°F) | Hot Streak Coolant Velocity (ft/sec) |
|---|---|---|---|---|---|---|
| 1 | 42.08 | 38.08 | 0.0513 | 0.0513 | 121.2 | 41.35 |
| 3 | 42.67 | 38.67 | 0.3374 | 0.4369 | 121.2 | 40.72 |
| 16 | 42.98 | 38.98 | 0.7805 | 0.9784 | 216.4 | 41.72 |
| 17 | 38.16 | 34.16 | 0.9528 | 0.7329 | 225.5 | 47.80 |
| 28 | 39.60 | 35.60 | 0.8024 | 0.7062 | 306.9 | 47.78 |
| 29 | 38.16 | 34.16 | 1.208 | 1.006 | 311.8 | 49.95 |
| 31 | 40.97 | 36.97 | 0.3910 | 0.3910 | 311.8 | 46.15 |

Flow Conditions in an Average Coolant Channel at this Hot Streak Location

Location: Outer fuel element, i = 4
Flow Rate: 1.040 lb/(sec)(in. width)

| j | Average Channel Thickness (mils) | Oxide Thickness (mils) | Coolant Temperature (°F) | Coolant Velocity (ft/sec) |
|---|---|---|---|---|
| 1 | 48.91 | 0.0513 | 121.2 | 49.64 |
| 3 | 48.59 | 0.3074 | 121.2 | 49.97 |
| 16 | 48.38 | 0.5962 | 172.2 | 50.97 |
| 17 | 48.36 | 0.6164 | 177.1 | 51.08 |
| 28 | 48.48 | 0.4611 | 220.7 | 51.82 |
| 29 | 48.28 | 0.6890 | 223.3 | 52.10 |
| 31 | 48.70 | 0.2300 | 223.3 | 51.65 |

2. Flow Conditions in the Hot Streak at the Location of the Minimum Flow Rate

Location: Outer fuel element, i = 5
Hot Streak Flow Rate: 0.6568 lb/(sec)(in. width)

| j | Narrow Channel Thickness (mils) | Hot Streak Thickness (mils) | Oxide Thickness on Hot Plate in Narrow Channel (mils) | Oxide Thickness on Cold Plate in Narrow Channel (mils) | Hot Streak Coolant Temperature (°F) | Hot Streak Coolant Velocity (ft/sec) |
|---|---|---|---|---|---|---|
| 1 | 42.37 | 38.37 | 0.0513 | 0.0513 | 121.2 | 39.96 |
| 3 | 43.77 | 39.77 | 0.3141 | 0.4037 | 121.2 | 38.56 |
| 16 | 44.67 | 40.67 | 0.7369 | 0.9240 | 217.3 | 38.96 |
| 17 | 35.89 | 31.89 | 0.8314 | 0.6457 | 226.6 | 49.89 |
| 28 | 38.45 | 34.45 | 0.6832 | 0.6070 | 308.8 | 48.17 |
| 29 | 36.12 | 32.12 | 1.028 | 0.8632 | 313.7 | 51.79 |
| 31 | 40.63 | 36.63 | 0.3531 | 0.3531 | 313.7 | 45.41 |

Flow Conditions in an Average Coolant Channel at this Hot Streak Location

Location: Outer fuel element, i = 5
Flow Rate: 1.040 lb/(sec)(in. width)

| j | Average Channel Thickness (mils) | Oxide Thickness (mils) | Coolant Temperature (°F) | Coolant Velocity (ft/sec) |
|---|---|---|---|---|
| 1 | 48.91 | 0.0513 | 121.2 | 49.64 |
| 3 | 48.61 | 0.2795 | 121.2 | 49.95 |
| 16 | 48.41 | 0.5465 | 171.4 | 50.93 |
| 17 | 48.39 | 0.5654 | 176.2 | 51.04 |
| 28 | 48.52 | 0.4012 | 219.1 | 51.72 |
| 29 | 48.33 | 0.6046 | 221.6 | 52.01 |
| 31 | 48.71 | 0.2115 | 221.6 | 51.60 |

3. Typical Hot Plate Metal Temperatures (Outer Fuel Element), °F

| i | j | | | | |
|---|---|---|---|---|---|
| | 3 | 16 | 17 | 28 | 29 |
| 3 | 267.0 | 358.6 | 420.9 | 369.6 | 472.2 |
| 4 | 292.3 | 395.7 | 446.4 | 393.4 | 521.1 |
| 5 | 293.7 | 394.2 | 422.9 | 379.1 | 493.4 |
| 6 | 285.9 | 382.0 | 397.4 | 358.3 | 447.9 |
| 7 | 267.3 | 365.9 | 379.7 | 335.4 | 401.5 |
| 8 | 218.3 | 362.2 | 385.1 | 321.6 | 333.2 |
| 9 | 169.5 | 310.7 | 339.9 | 267.3 | 259.3 |
| Average | 256.2 | 367.0 | 398.9 | 346.3 | 418.6 |

4. Typical Average Side Plate Temperatures, °F

| j | Inner Fuel Element | | Outer Fuel Element | |
|---|---|---|---|---|
| | Inner Side Plate | Outer Side Plate | Inner Side Plate | Outer Side Plate |
| 3 | 166 | 182 | 179 | 159 |
| 16 | 173 | 191 | 188 | 164 |
| 29 | 180 | 198 | 197 | 168 |

5. Heat Flux in an Average Fuel Plate at the Location of the Limiting Heat Flux

Location: Outer fuel element (4,29)

Heat Flux: $1.59 \times 10^6$ Btu/(hr)(ft$^2$)

Bulk Water Temperature: 223°F

Surface Temperature: 319°F

Heat Transfer Coefficient: 16,560 Btu/(hr)(ft$^2$)(°F)

Table 7. Heat Transfer and Flow Conditions in the HFIR Fuel Element During a 100 Mw Fuel Cycle; Case Number 3 (See Fig. 18)

A. Fuel Element Flow Rates

| Time (hr) | Flow Rate (gpm) |
|---|---|
| 0.0 to 24.3 | 12,380 |
| 24.3 to 277.6 | 12,360 |
| 277.6 to 545.2 | 12,330 |
| 545.2 to 600.0 | 12,330 |
| 600.0 | 12,330 |

B. Channel and Oxide Thicknesses at the Location of the Limiting Heat Flux

(See Following Page)

B. Channel and Oxide Thicknesses at the Location of the Limiting Heat Flux

Location: Outer fuel element (4,29)
Reactor Power Level: 100 Mw

| Time (hr) | Average Channel Thickness (mils) | Narrow Channel Thickness (mils) | Hot Streak Thickness (mils) | Oxide Thickness on Average Plate in Average Channel (mils) | Oxide Thickness on Hot Plate in Narrow Channel (mils) | Oxide Thickness on Cold Plate in Narrow Channel (mils) |
|---|---|---|---|---|---|---|
| 0.0 to 24.3 | 48.70 | 41.18 | 37.18 | 0.0693 | 0.1228 | 0.1001 |
| 24.3 to 277.6 | 48.57 | 40.63 | 36.63 | 0.3833 | 0.6740 | 0.5611 |
| 277.6 to 545.2 | 48.43 | 40.06 | 36.06 | 0.6380 | 1.119 | 0.9322 |
| 545.2 to 600.0 | 48.41 | 39.79 | 35.79 | 0.6890 | 1.208 | 1.006 |
| 600.0 | 48.40 | 39.62 | 35.62 | 0.6890 | 1.208 | 1.006 |

Channel and Oxide Thicknesses at another Location

Location: Inner fuel element (5,18)
Reactor Power Level: 100 Mw

| | | | | | | |
|---|---|---|---|---|---|---|
| 0.0 to 24.3 | 48.75 | 40.26 | 36.26 | 0.0456 | 0.0722 | 0.0565 |
| 24.3 to 277.6 | 48.63 | 39.28 | 35.28 | 0.2924 | 0.4541 | 0.3573 |
| 277.6 to 545.2 | 48.52 | 38.58 | 34.58 | 0.4959 | 0.7666 | 0.6035 |
| 545.2 to 600.0 | 48.51 | 38.63 | 34.63 | 0.5321 | 0.8219 | 0.6472 |
| 600.0 | 48.52 | 38.73 | 34.73 | 0.5321 | 0.8219 | 0.6472 |

C. Typical Average Temperatures of the Average Fuel Plates, °F
Reactor Power Level: 100 Mw

| Time (hr) | Inner Fuel Element, j | | | | |
|---|---|---|---|---|---|
| | 3 | 8 | 16 | 23 | 29 |
| 0.0 to 24.3 | 208 | 199 | 242 | 239 | 259 |
| 24.3 to 277.6 | 206 | 202 | 259 | 249 | 265 |
| 277.6 to 545.2 | 207 | 203 | 269 | 257 | 278 |
| 545.2 to 600.0 | 207 | 200 | 264 | 253 | 278 |
| 600.0 | 206 | 197 | 241 | 251 | 273 |
| | Outer Fuel Element, j | | | | |
| 0.0 to 24.3 | 195 | 185 | 235 | 221 | 230 |
| 24.3 to 277.6 | 190 | 190 | 259 | 232 | 234 |
| 277.6 to 545.2 | 194 | 196 | 269 | 242 | 247 |
| 545.2 to 600.0 | 200 | 201 | 267 | 254 | 259 |
| 600.0 | 205 | 203 | 262 | 256 | 269 |

D. Typical Average Side Plate Temperatures, °F
Reactor Power Level: 100 Mw

| Time (hr) | Inner Fuel Element | | | | | |
|---|---|---|---|---|---|---|
| | Inner Side Plate, j | | | Outer Side Plate, j | | |
| | 3 | 16 | 29 | 3 | 16 | 29 |
| 0.0 to 24.3 | 151 | 156 | 160 | 161 | 167 | 172 |
| 24.3 to 277.6 | 151 | 156 | 160 | 161 | 167 | 172 |
| 277.6 to 545.2 | 151 | 156 | 160 | 161 | 167 | 172 |
| 545.2 to 600.0 | 151 | 156 | 160 | 161 | 167 | 172 |
| 600.0 | 151 | 156 | 160 | 161 | 167 | 172 |
| | Outer Fuel Element | | | | | |
| 0.0 to 24.3 | 159 | 166 | 171 | 146 | 149 | 152 |
| 24.3 to 277.6 | 159 | 166 | 171 | 146 | 149 | 151 |
| 277.6 to 545.2 | 159 | 166 | 171 | 146 | 149 | 151 |
| 545.2 to 600.0 | 159 | 166 | 171 | 146 | 149 | 151 |
| 600.0 | 159 | 166 | 171 | 146 | 149 | 151 |

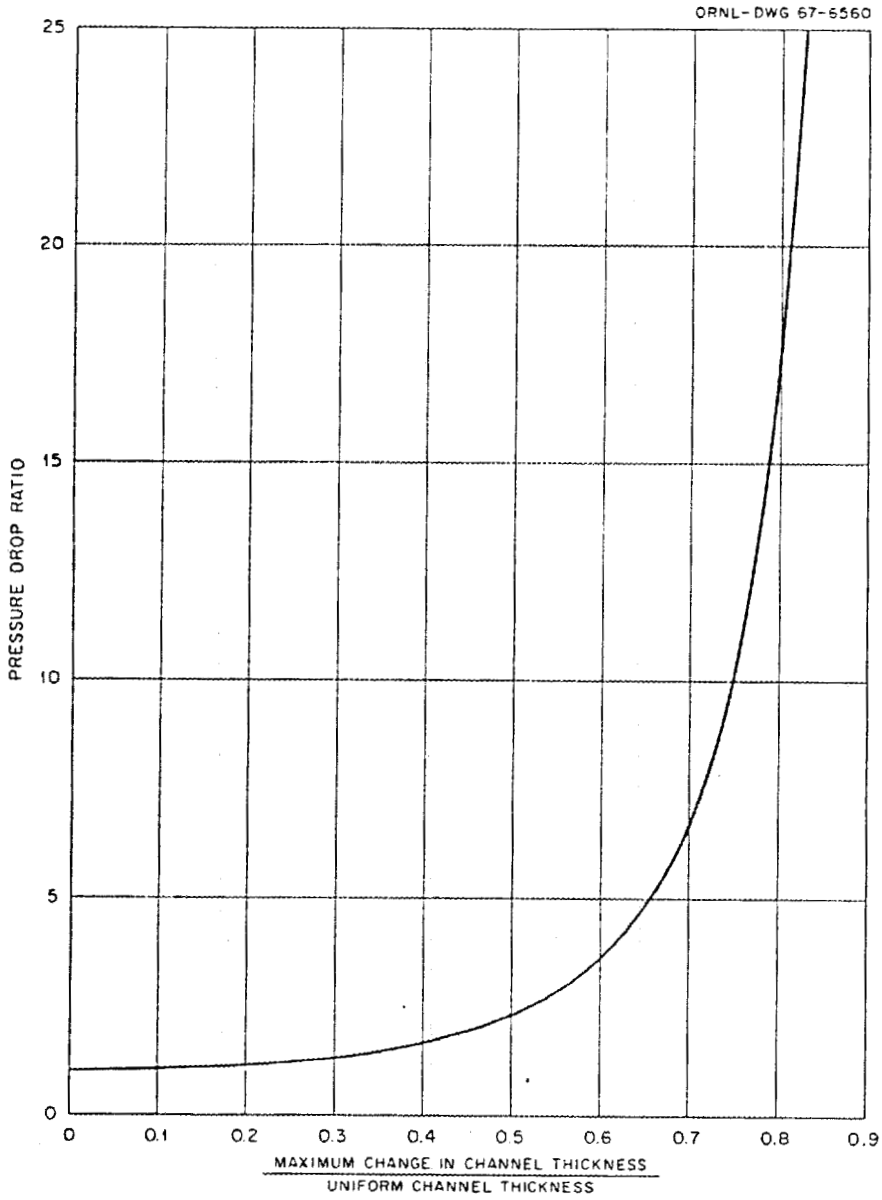


Fig. 1. Ratio of Pressure Drop in Channel with Sinusoidal Walls to that with Straight Walls.[8]

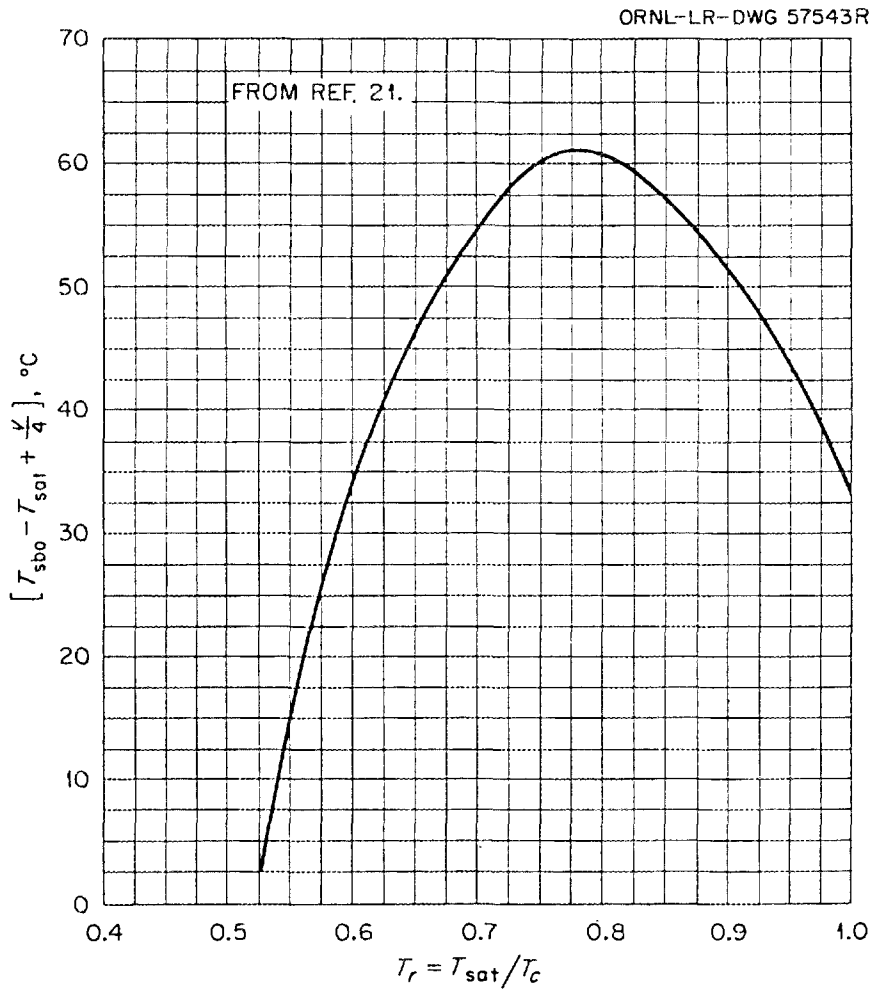


Fig. 2. Generalized Correlation of Wall Superheat at Burnout.

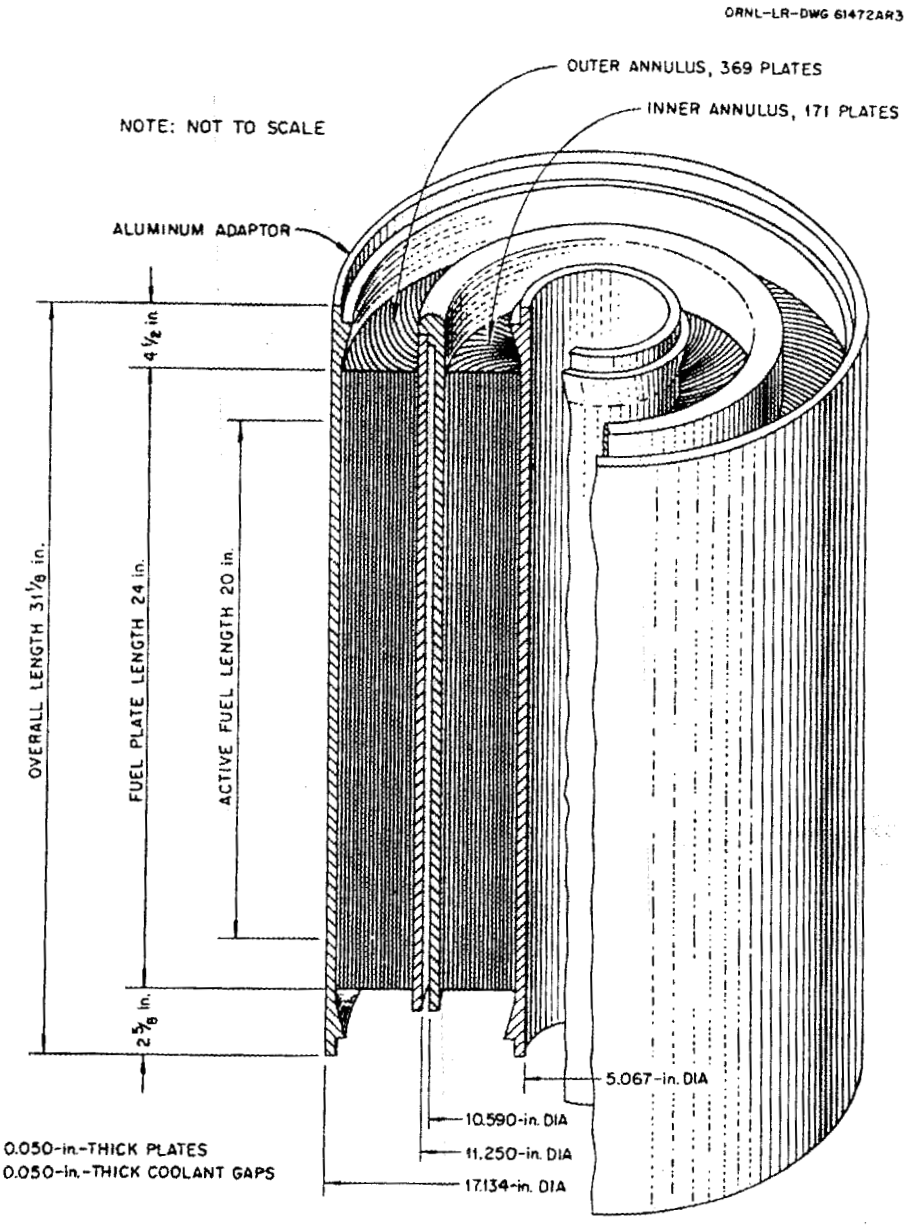


Fig. 3. HFIR Fuel Assembly.

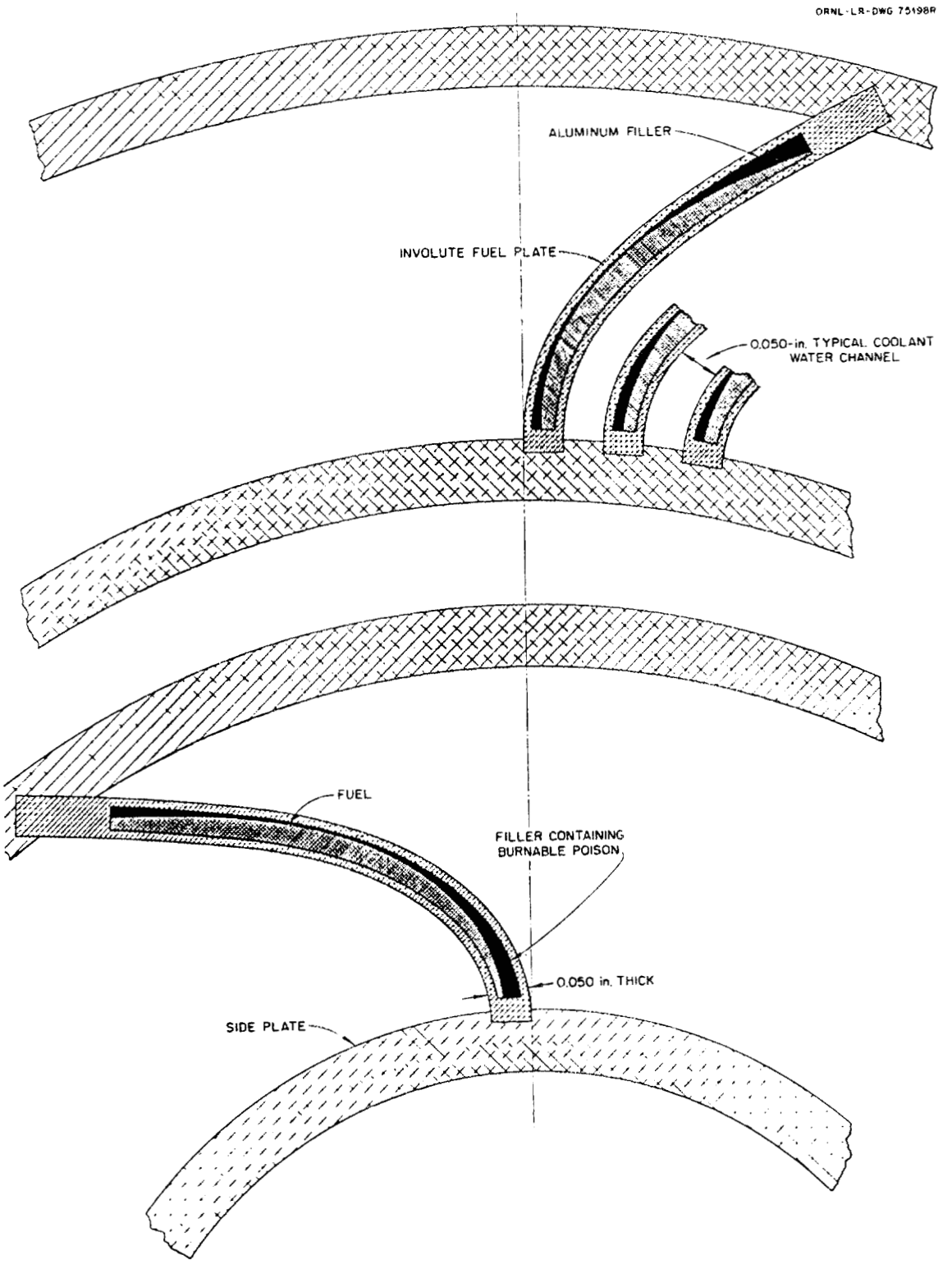


Fig. 4. Schematic Cross Section of the HFIR Fuel Assembly.

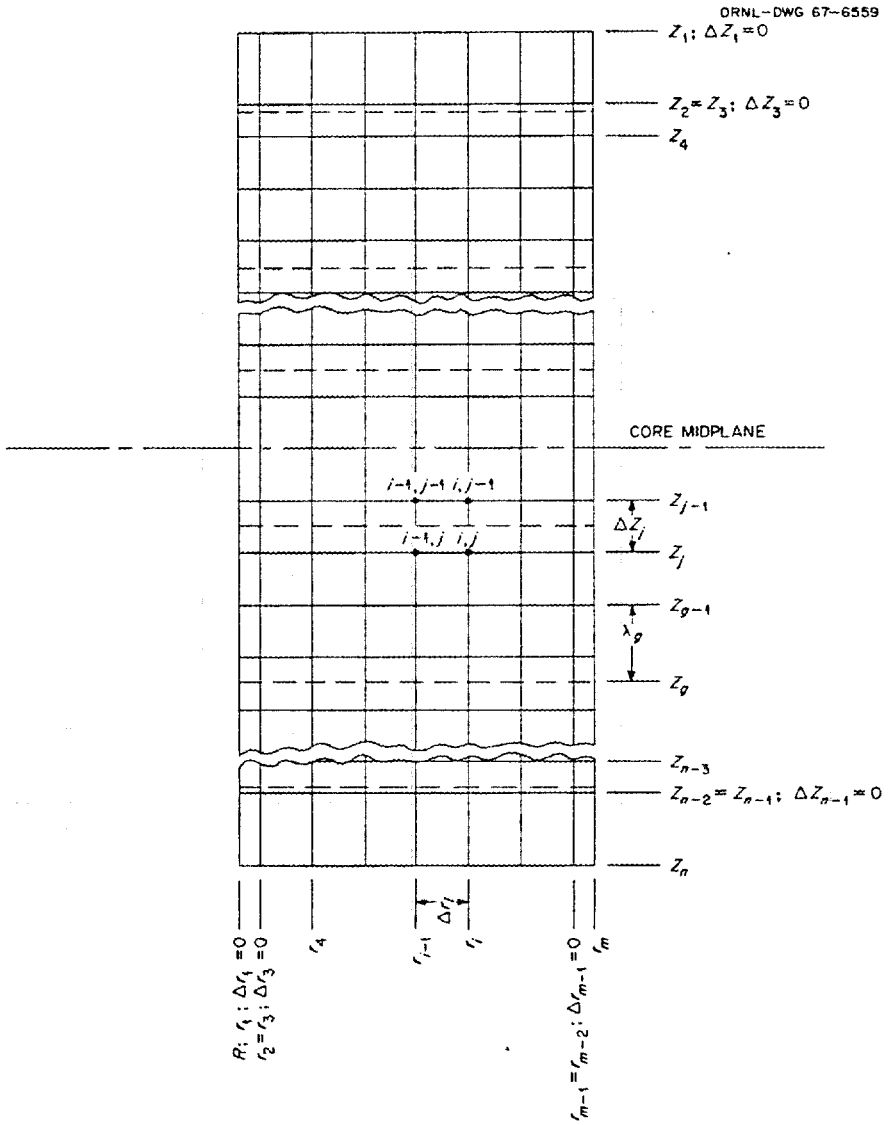


Fig. 5. Mesh System for the Heat Transfer Analysis.

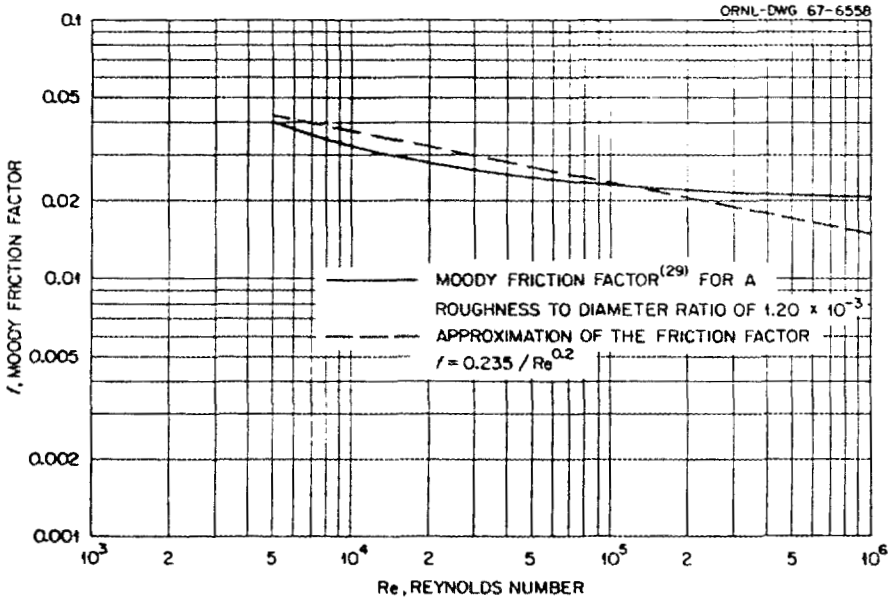


Fig. 6. Approximation of Friction Factor for HFIR Fuel Element.

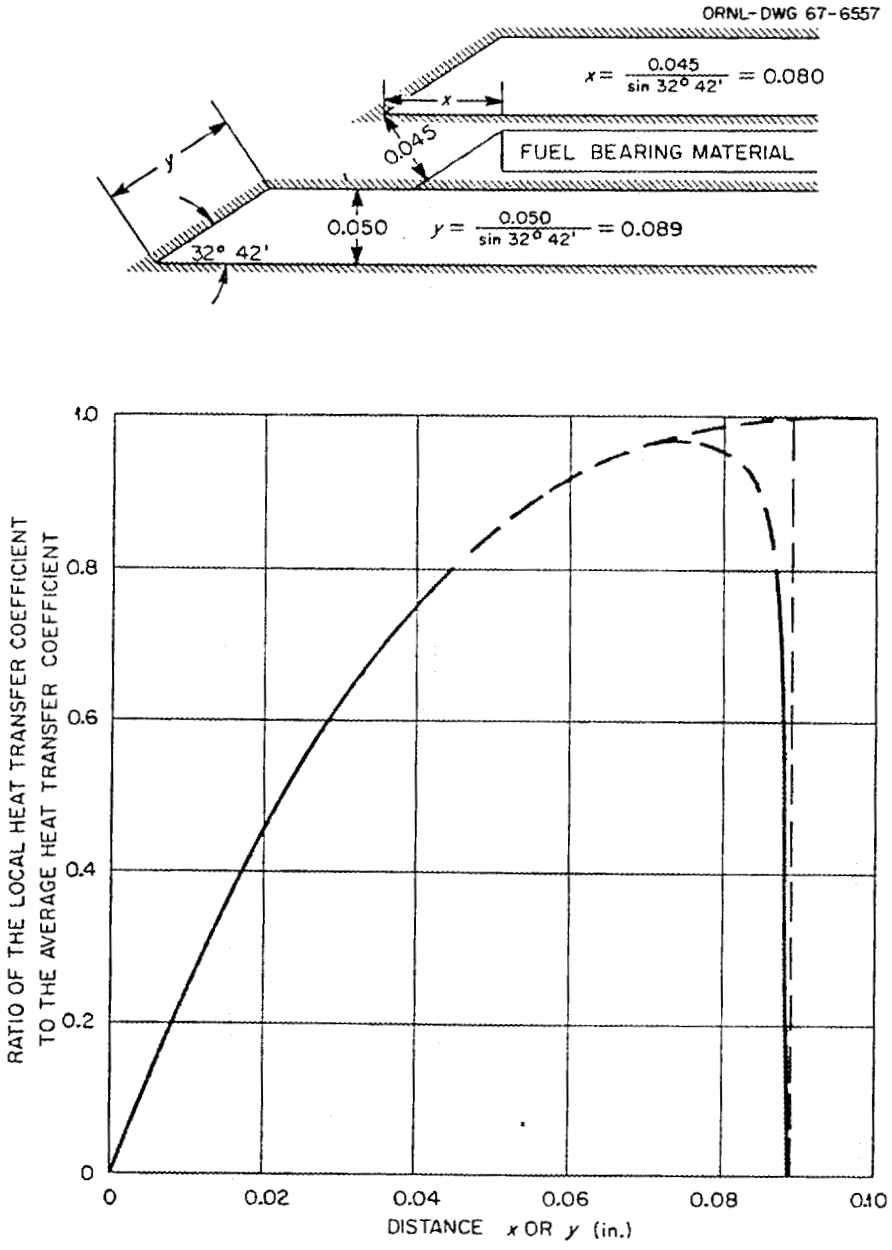


Fig. 7. Local Heat Transfer Coefficients in Corners of Coolant Channels next to the Outer Side Plates of the Inner Fuel Element. (Ref. 30)

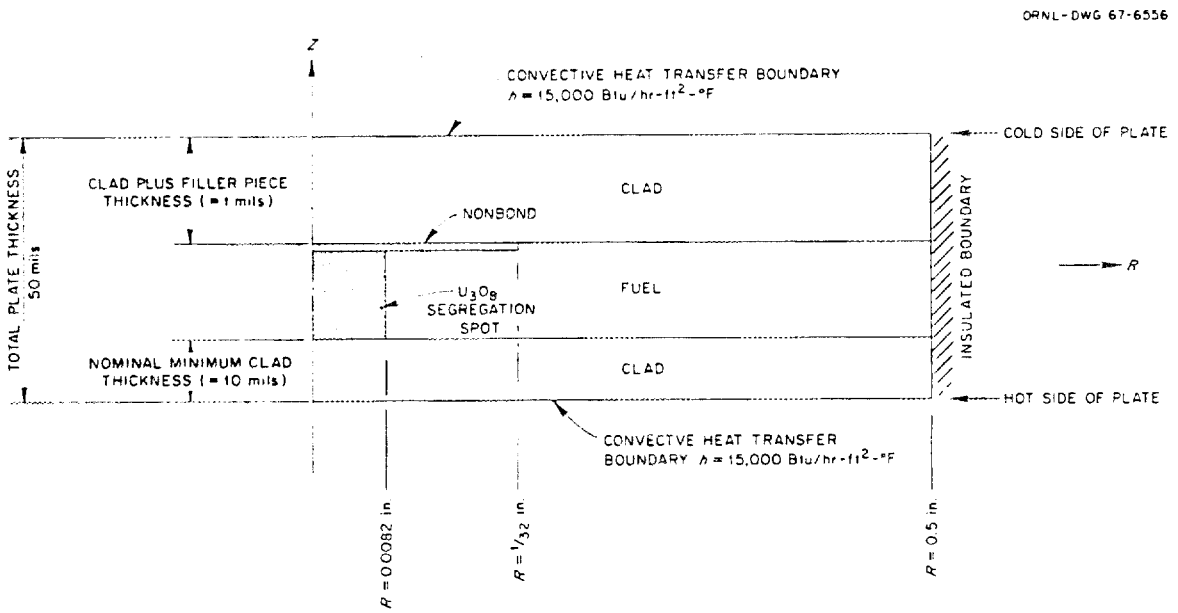


BASIC ASSUMPTIONS:

1. NO HEAT TRANSFER ACROSS NON-BOND
2. CIRCUMFERENTIAL SYMMETRY
3. PACKING FRACTION OF $U_3O_8$ PARTICLES IN SEGREGATION SPOT = 0.74

| REGION | THERMAL CONDUCTIVITY (Btu/hr-in.-°F) | (Btu/hr-ft-°F) | HEAT GENERATION RATE AT 100 MW (Btu/hr in.³) |
|---|---|---|---|
| FUEL | 8.08 | 97.0 | $1.82 \times 10^7/(50-t-10)$ |
| $U_3O_8$ SEGREGATION | 2.26 | 27.1 | $1.87 \times 10^8/(50-t-10)$ |
| CLAD | 8.08 | 97.0 | $1.51 \times 10^4$ |

Fig. 8. Model Employed by Hilvety and Chapman for Calculation of Nonbond and Fuel Segregation Heat Flux Peaking Factors. (Ref. 4)

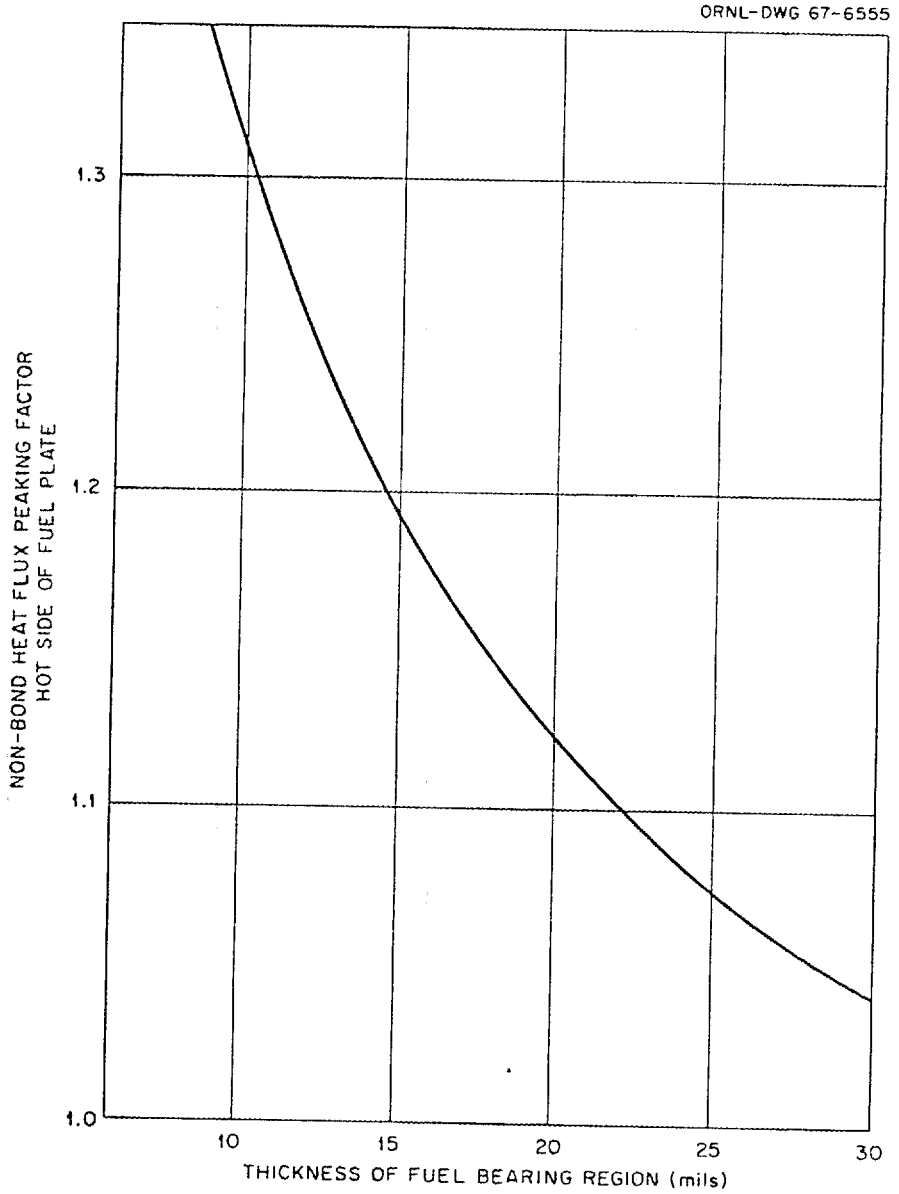


Fig. 9. Heat Flux Peaking on Hot Side of Fuel Plate Due to Nonbonds Calculated by Hilvety and Chapman. (Ref. 4)

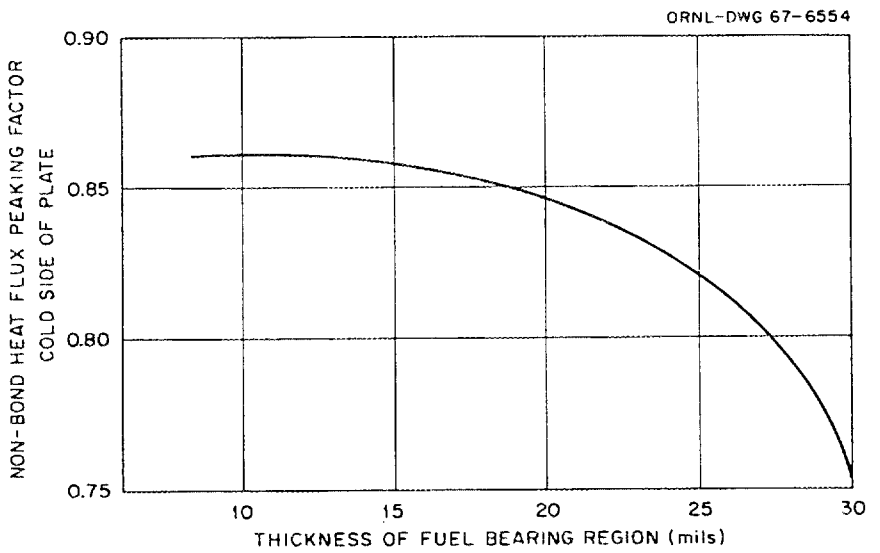


Fig. 10. Heat Flux Peaking on Cold Side of Fuel Plate Due to Nonbonds Calculated by Hilvety and Chapman. (Ref. 4)

ORNL-DWG 65-8891

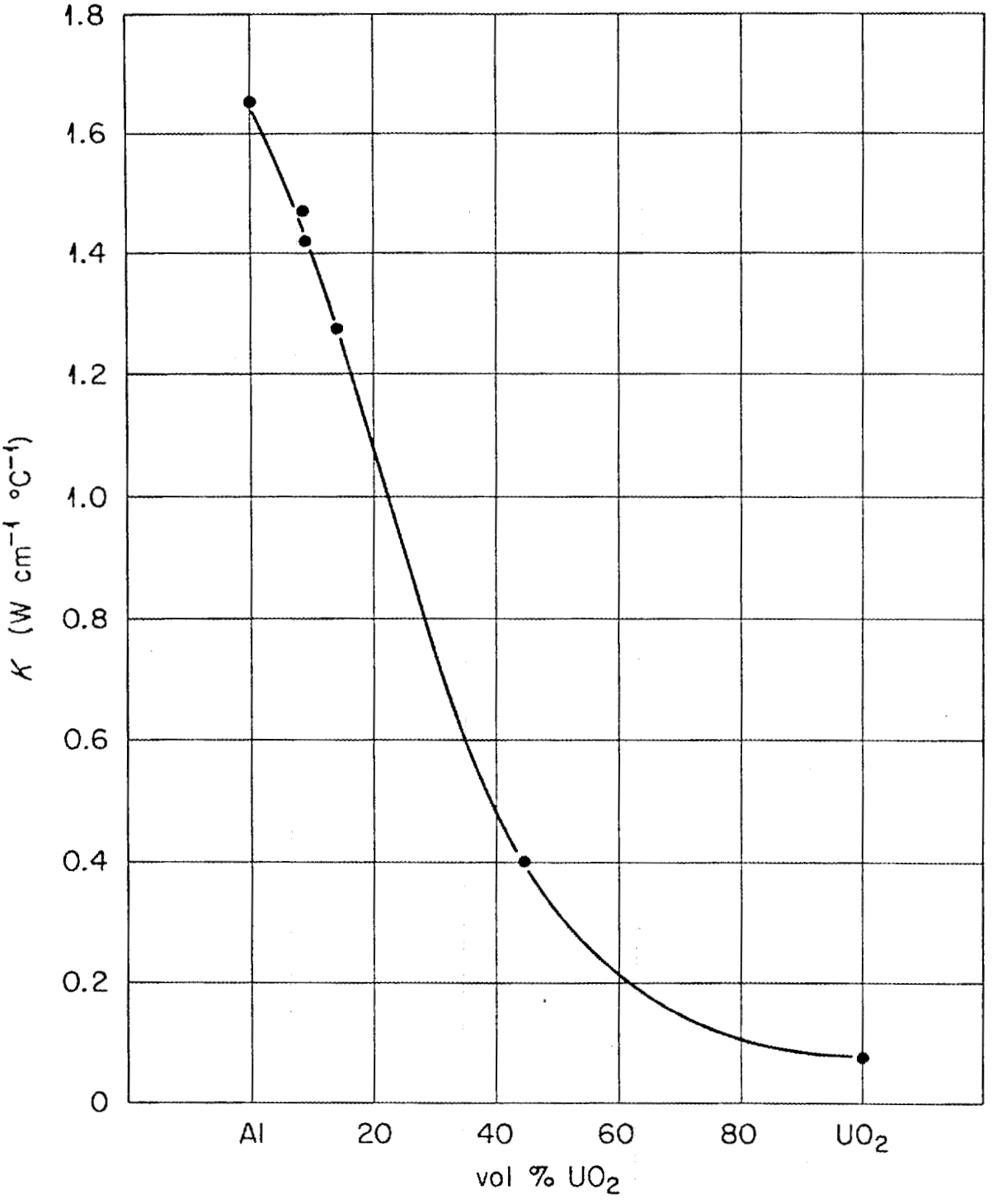


Fig. 11. Thermal Conductivity of Aluminum-$UO_2$ Compacts versus Composition at 70°C, From McElroy. (Ref. 33)

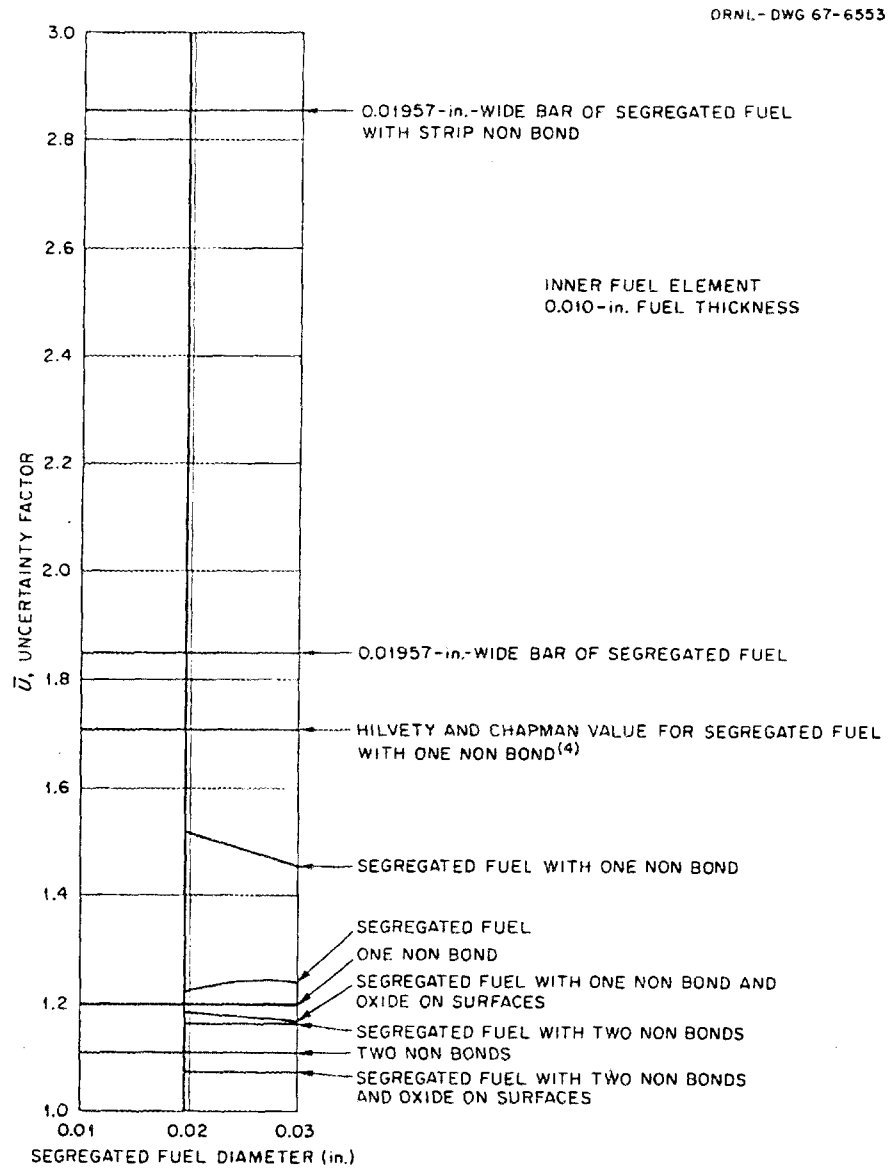


Fig. 12. Uncertainty Factors for Isolated Pockets of Segregated Fuel and Nonbonds and for Bars of Segregated Fuel and Strip Nonbonds. (Ref. 32)

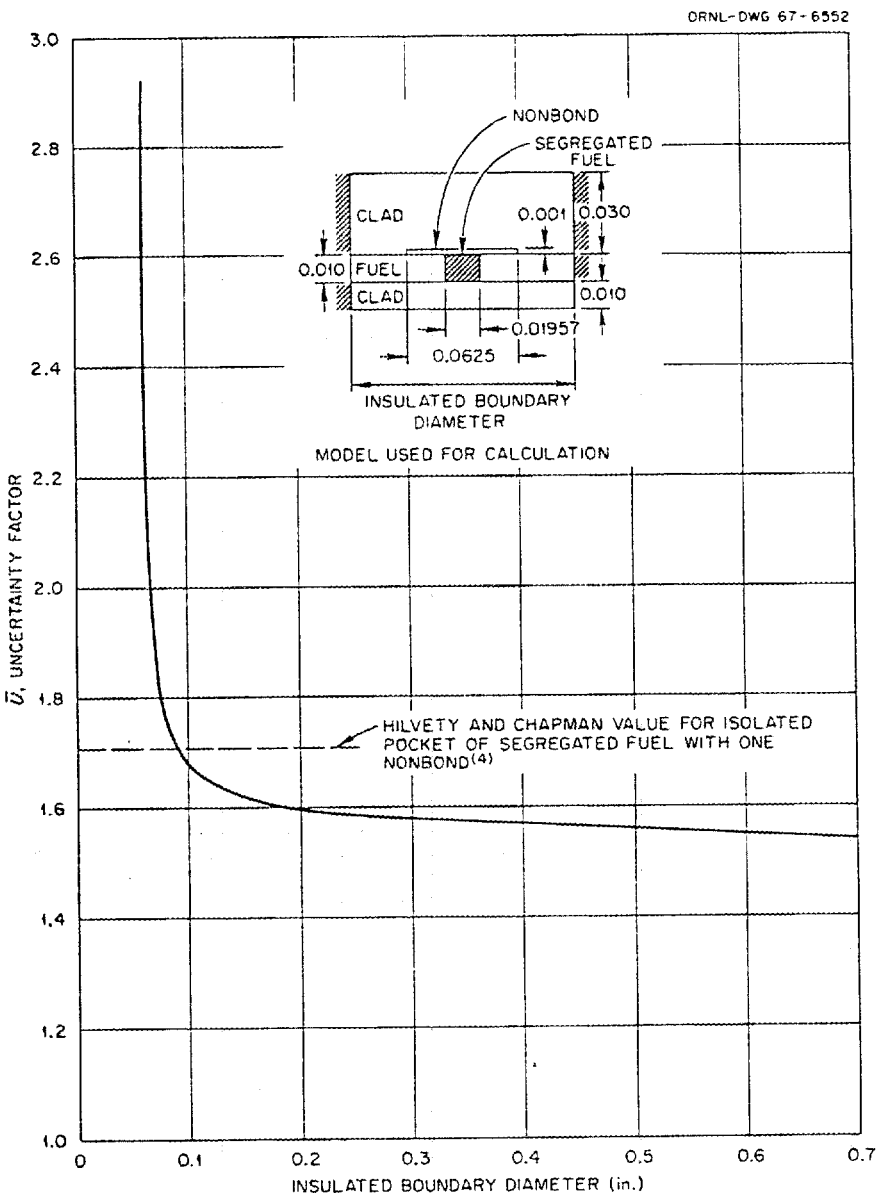


Fig. 13. Effect of Proximity of Segregated Fuel and Nonbonds on the Uncertainty Factor. (Ref. 32)

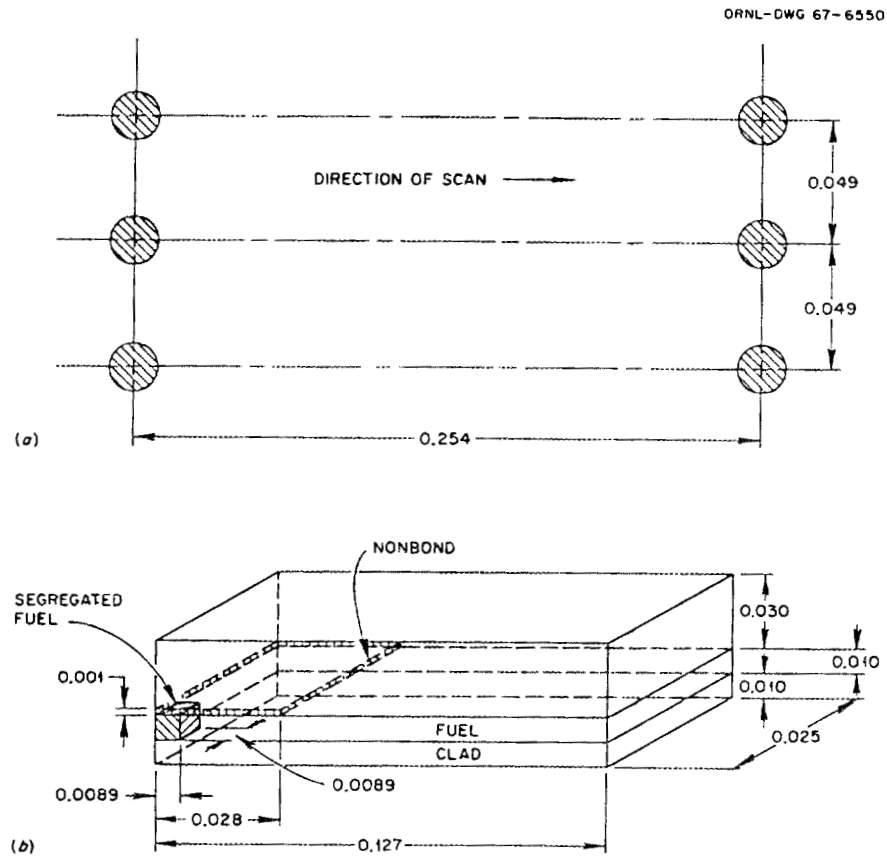


Fig. 14. (a) Possible Proximity of Segregated Fuel Pockets Using Present Specifications and Inspection Techniques. (Ref. 32), (b) Three Dimension Approximation of the Model Shown in Fig. 14(a). (Ref. 32)

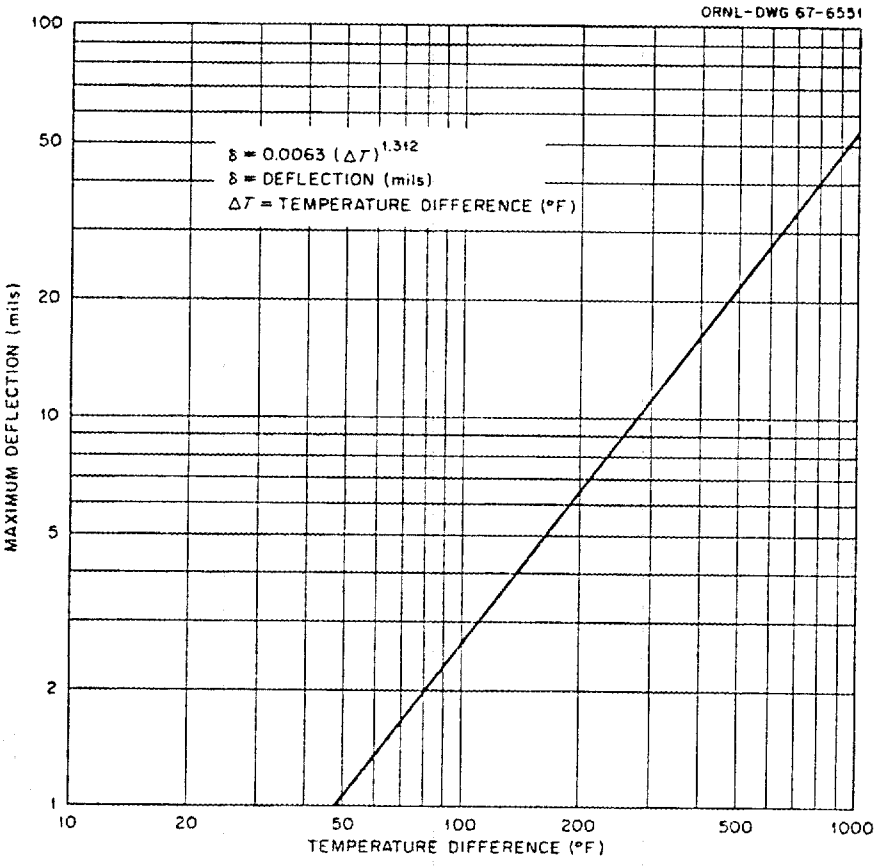


Fig. 15. Maximum Values of the Sinusoidal Deflections Predicted by Lyon. (Ref. 5)

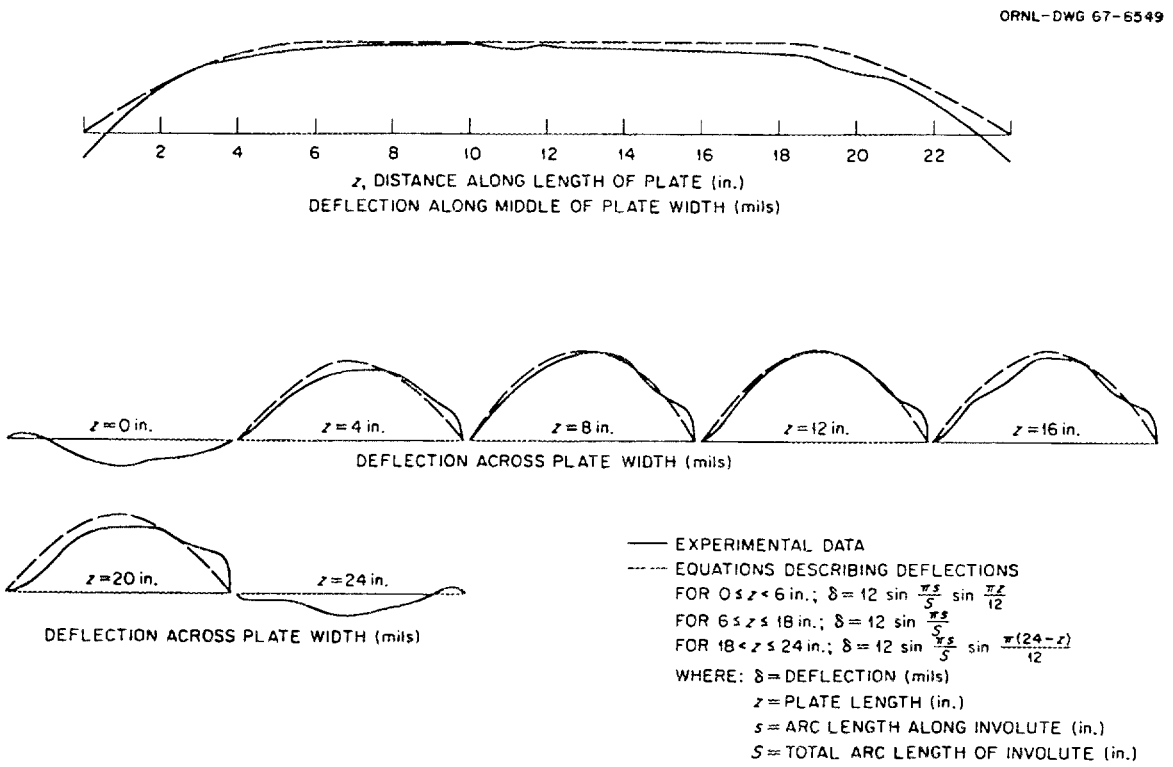


Fig. 16. Typical Fuel Plate Deflection Data Obtained by Cheverton and Kelley (Ref. 7) Oven Temperature; 400°F.

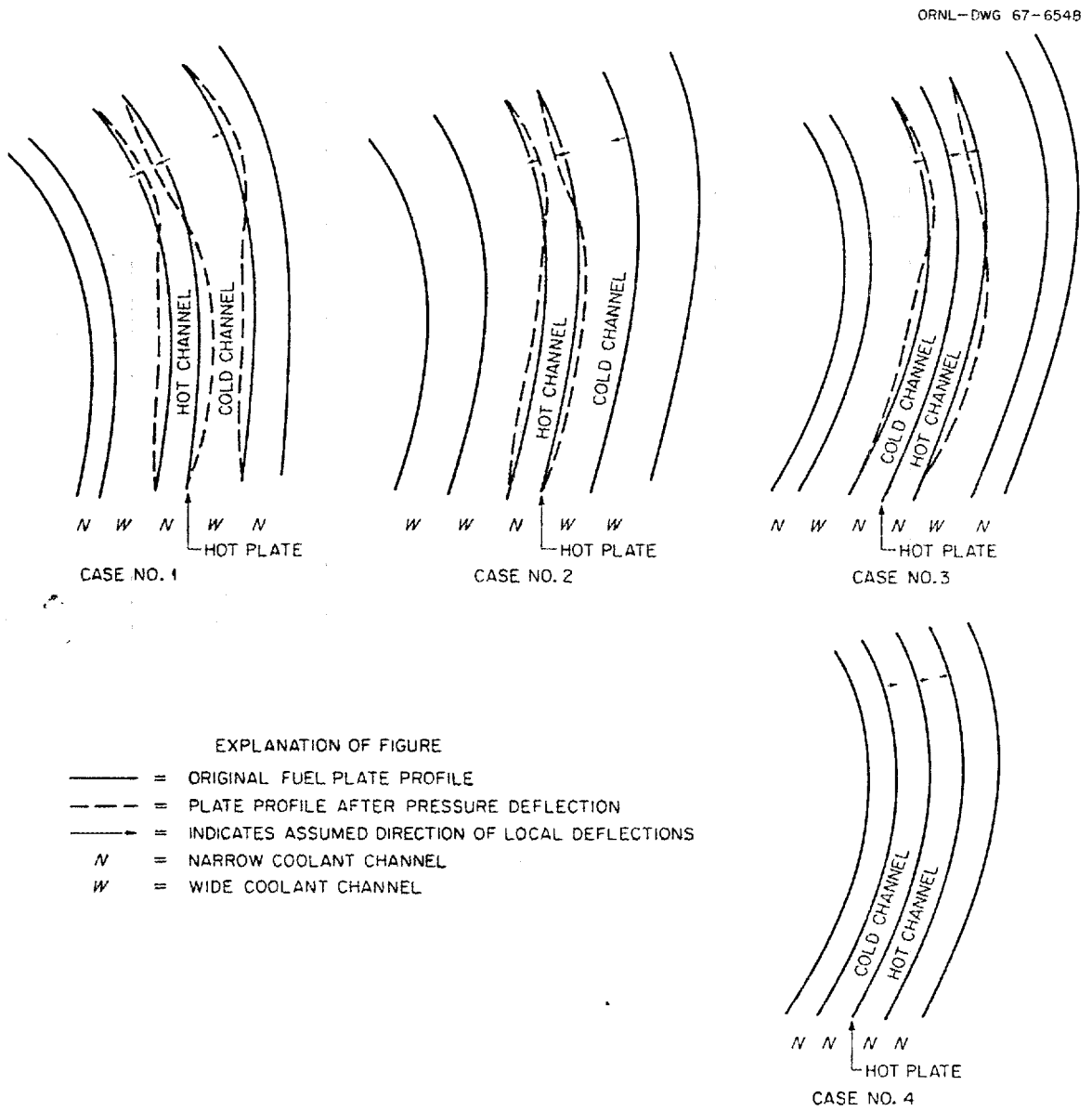


Fig. 17. Alternate Arrangements of Adjacent Coolant Channels for Option I of the Heat Transfer Analysis and for Hilvety and Chapman's Studies. (Ref. 4)

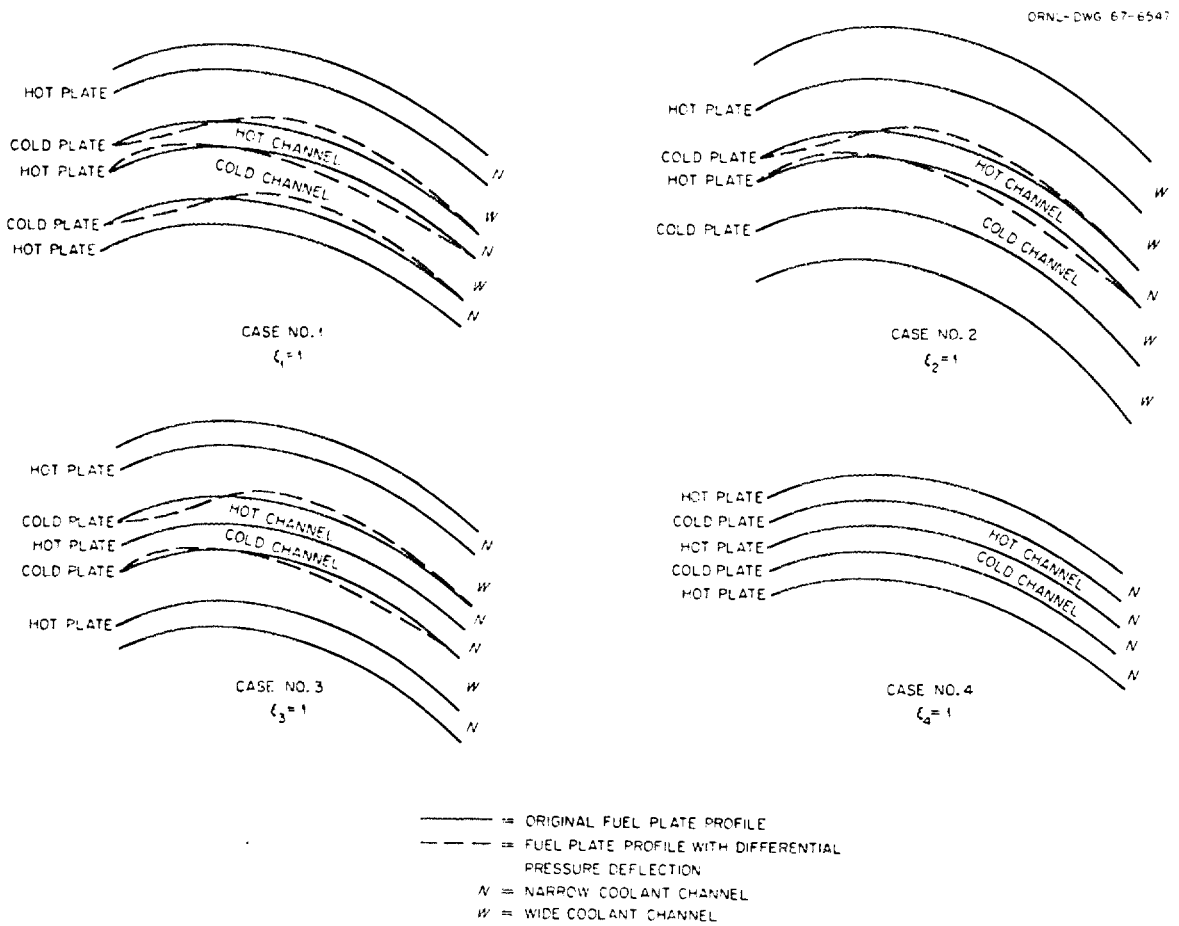


Fig. 18. Alternate Arrangements of Adjacent Coolant Channels for Option II of the Heat Transfer Analysis.

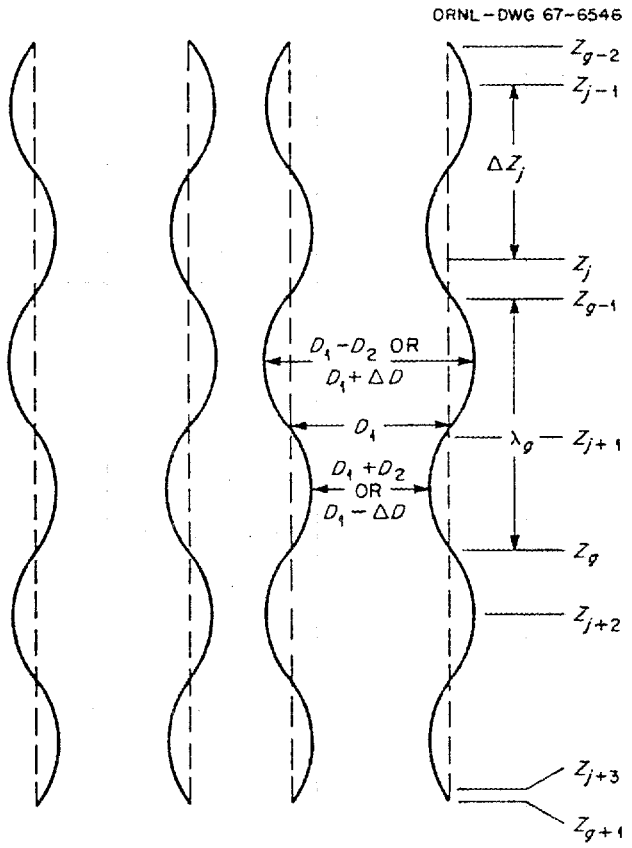


Fig. 19. Schematic of Coolant Channels with Sinusoidal Shape Walls.

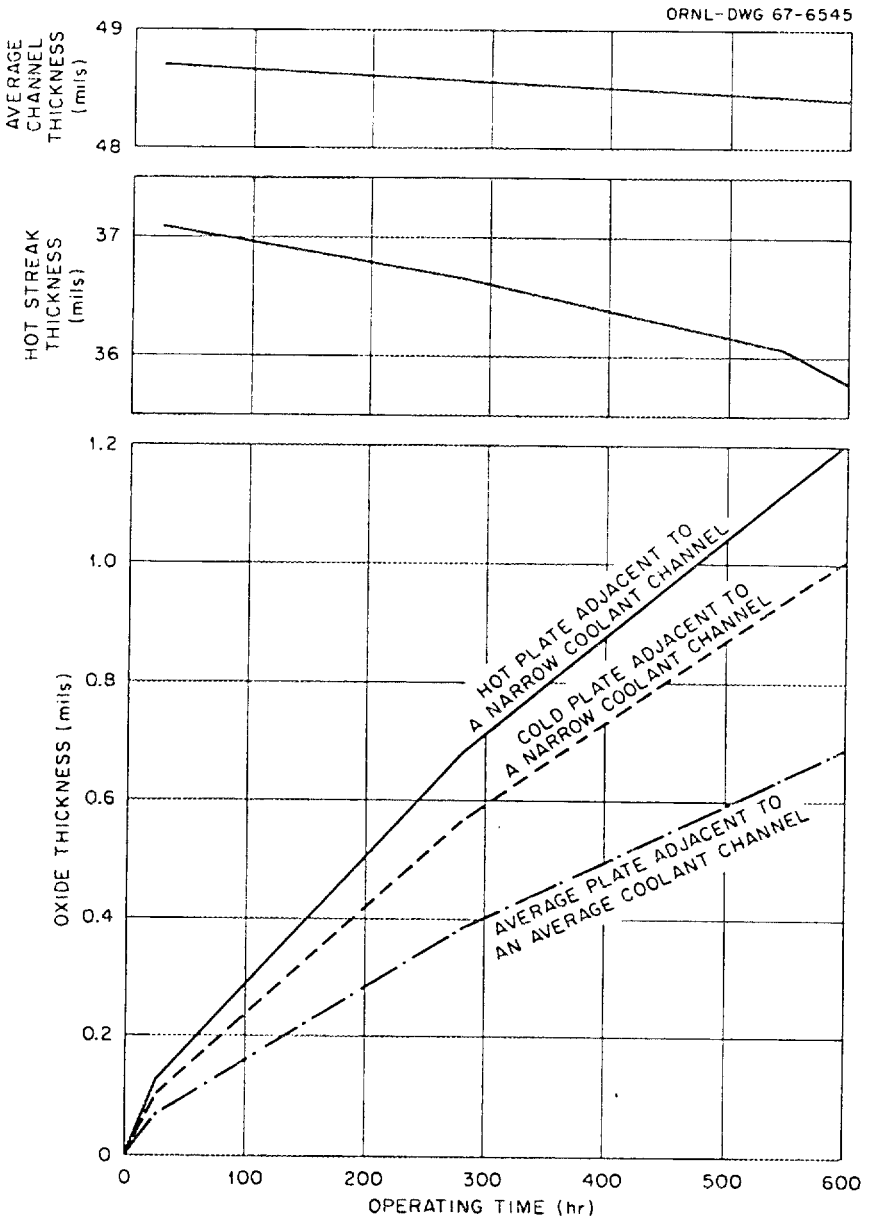


Fig. 20. Oxide and Channel Thicknesses.
Location: Outer Fuel Element 4,29.
Power Level: 100 Mw.

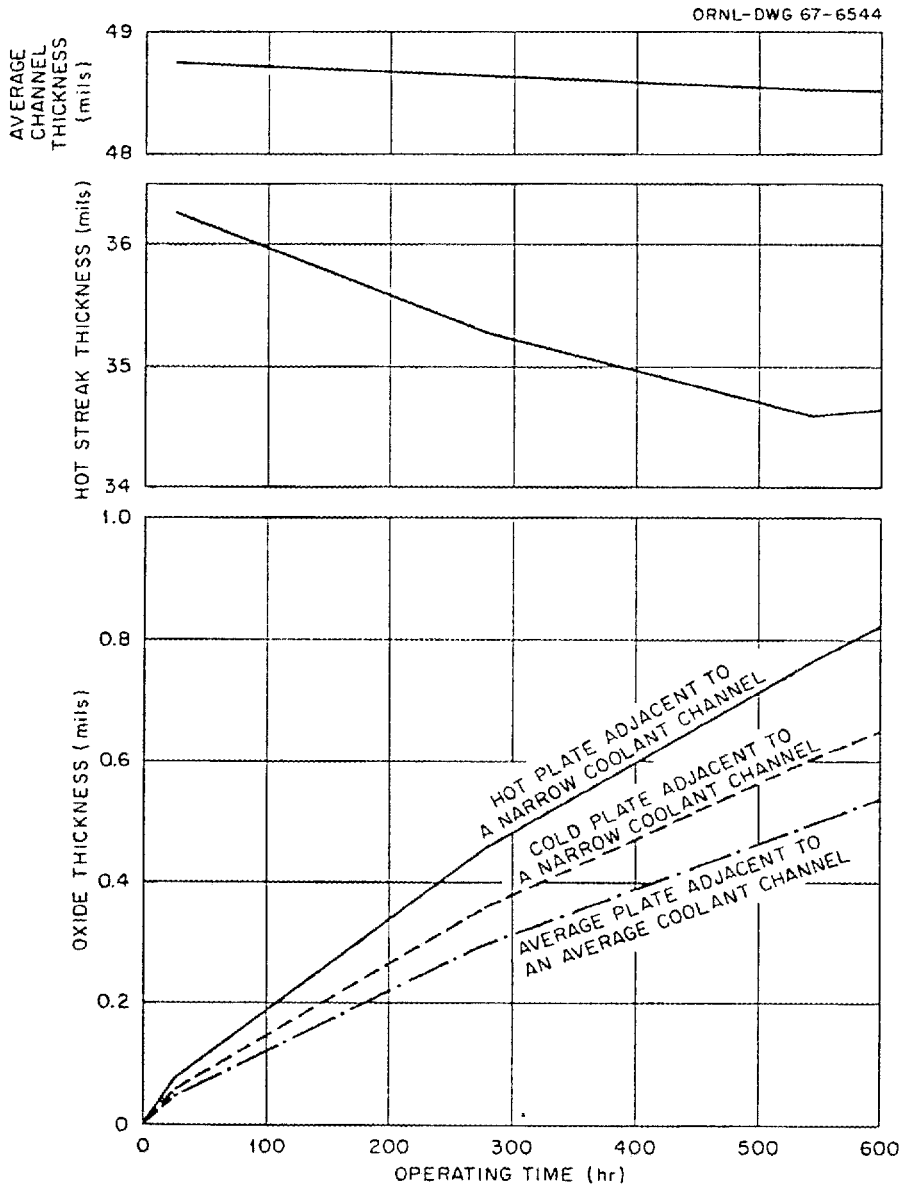


Fig. 21. Oxide and Channel Thicknesses.
Location: Inner Fuel Element 5,18.
Power Level: 100 Mw.

# Appendix A

## DETAILED PROCEDURE AND EQUATIONS

The following is the detailed procedure and associated equations used in this analysis. No information is given here regarding the Fortran statements nor the convergence criteria used in the actual code for the computer. The reader is referred to the work of Wright[44] for this. Two options of this procedure are outlined. They differ primarily in the way the fuel plates deflect due to differences in the fuel plate and side plate operating temperatures.

The first option was programmed prior to the time when Cheverton and Kelley obtained data from their fuel plate deflection experiment.[7] As was done by Hilvety and Chapman,[4] this option assumed that the fuel plates buckle in sinusoidal waves as predicted by Lyon.[5] Because of the nature of these deflections, it was assumed that the worst case regarding the coolant channel thicknesses exists when two fuel plates having the maximum permissible fuel concentrations (defined as hot plates) form the walls of the coolant channel having the minimum thickness (defined as the hot channel). A number of arrangements of coolant channel geometry adjacent to the hot channel were considered, and these are shown in Fig. 17. These arrangements are identical to those used by Hilvety and Chapman.

Since the experimental data obtained by Cheverton and Kelley showed that the fuel plates buckle in a manner different from that predicted by Lyon, a second option of this analysis was programmed. Cheverton and Kelley's data showed that the fuel plates deflect in the same direction. Therefore it was assumed in this option that the worst case regarding the coolant channel thicknesses is when a fuel plate having the maximum permissible fuel concentrations (defined as a hot plate) and a fuel plate having the minimum permissible fuel concentrations (defined as a cold plate) form the walls of the coolant channel having the minimum thickness (defined as the hot channel). The arrangements of the coolant channel geometry adjacent to the hot channel were modified to include this concept, and they are shown in Fig. 18. However, the concept of coolant channels having sinusoidal shape walls was retained in this option, but it was assumed that

these channels had this shape prior to the operation of the reactor. Since the wave lengths of these sinusoidal variations could be large or not exist at all, second alternates for the determination of the coolant flow rates and the oxide buildup on the plate surfaces were included in the second option to simplify the computer operation.

The maximum reactor power level just prior to a burnout condition within the fuel element or just prior to any incipient boiling within the fuel element can be calculated in both options. The derivations of many of the equations shown in this procedure are evident from the relations themselves. Where they are not evident, these derivations are shown elsewhere in this report. Many of the relations are identical to those used by Hilvety and Chapman.[4]

Option I

Part I

I. Specify the input data – The necessary input data along with typical values are shown in Table 4. Figure 5 shows the mesh spacing used in this analysis and Fig. 17 shows the various arrangements for the coolant channels adjacent to the hot fuel plate. The mesh spacing shown in Fig. 5 is not required to be uniform. The maximum value of i permitted in this code is 15, and the corresponding maximum value of j is 35. The increments $\Delta r_1 = 0$ and $\Delta z_1 = 0$ are included since the computer cannot accept a dimension value of zero. The maximum number of time increments permitted is 10.

II. Divide the width (length along the involute arc) into incremental widths $\Delta s_i$ to correspond with the incremental radial distances $\Delta r_i$. Do both for the inner and the outer fuel elements.

$$\Delta s_i = \frac{\Delta r_i}{2R} \left\{ \Delta r_i + 2 \left[ R + \sum_{\ell=1}^{i=1} \Delta r_\ell \right] \right\} \tag{A-1}$$

III. Normalize the power density distribution for each time increment $\theta_k$.

$$\phi_{i,j} = \frac{\phi'_{i,j}}{\phi} \tag{A-2}$$

where

$$\phi = \frac{M_{\text{Inner Element}} + M_{\text{Outer Element}}}{N_{\text{Inner Element}} + N_{\text{Outer Element}}}$$

where

$$M = \sum_{i=4}^{m-2} \sum_{j=4}^{n-2} \frac{\left[\phi'_{i-1,j-1} + \phi'_{i,j-1} + \phi'_{i-1,j} + \phi'_{i,j}\right]}{4} \cdot$$

$$\cdot \Delta z_j \left[2\left(R + \sum_{\ell=1}^{i-1} \Delta r_\ell\right) + \Delta r_i\right] \Delta r_i$$

$$N = \sum_{i=4}^{m-2} \sum_{j=4}^{n-2} \Delta z_j \left[2\left(R + \sum_{\ell=1}^{i-1} \Delta r_\ell\right) + \Delta r_i\right] \Delta r_i$$

IV. Specify a reactor power level, Q Mw.

V. For the first time increment $\theta_1$ hr, calculate the flow rate in an average coolant channel of the inner fuel element $w_A$ and a metal temperature distribution for an average fuel plate in this element $T_{MAi,j}$.

A. Assume a metal temperature distribution for the average fuel plate, $T_{MAi,j}$ (see Table 4).

B. Calculate the expansion of the fuel plate thickness due to heating.

$$\delta_{Ai,j} = U_{12} \left(6.75 \times 10^{-6} t\right)\left(T_{MAi,j} - 70\right) \qquad \text{(A-3)}$$

C. Calculate the expansion of the fuel plate thickness due to radiation swelling.

$$\delta_{VR} = U_{13}\, B \sum_{k'=1}^{k} \theta_{k'} \qquad \text{(A-4)}$$

D. Assume that the decrease in the coolant channel thickness due to the buildup of oxide on the fuel plate surface is negligible.

$$\delta_{oi,j} = 0 \tag{A-5}$$

E. Calculate the coolant channel thickness at i,j.

$$e_{i,j} = e_A - 2\delta_{Ai,j} - 2\delta_{VR} - 2\delta_{oi,j} \tag{A-6}$$

F. Calculate the inlet water conditions.

1. Assume that the inlet water temperature is $U_6T_{in}$.
2. Calculate the inlet water density at $U_6T_{in}$ using the relation

$$\rho_T = 62.99 - \left[0.5350 \times 10^{-2}\right] T - \left[0.4525 \times 10^{-4}\right] T^2 \tag{A-7}$$

3. Calculate the inlet water viscosity at $U_6T_{in}$ using the relation

$$\mu_T = 352T^{-1.162} \tag{A-8}$$

G. Calculate the mass flow rate per unit channel width $w_{Ai}$ at $s = s_i$ based on the inlet water conditions calculated in step F and the coolant channel thicknesses calculated in step E.

$$\Delta P_F = \left[\frac{8.953 \times 10^4}{\rho_{in}} + \frac{2.238 \times 10^6}{\rho_{in}} \left(1 - \frac{e_A}{e_A + t}\right)^2\right] \frac{w_{Ai}^2}{e_A^2}$$

$$+ 9.218 \times 10^8 \frac{U_7 F \mu_{in}^{0.2} w_{Ai}^{1.8}}{\rho_{in}} \sum_{j=2}^{n} \frac{\Delta z_j}{\left[e_{i,j-1} + e_{i,j}\right]^3} \tag{A-9}$$

H. Calculate the bulk coolant temperature rise at $s = s_i$ based on the flow rates calculated in step G.

$$\Delta T_{bulk,i} = 6.584 \frac{U_1 U_2 Q f}{A w_{Ai}} \sum_{j=2}^{j=n} \left[\phi_{i,j-1} + \phi_{i,j}\right] \Delta z_j \qquad \text{(A-10)}$$

I. Calculate the average coolant conditions for $s = s_i$.

1. Calculate the average coolant temperature.

$$T_{ave,i} = U_6 T_{in} + 1/2\ \Delta T_{bulk,i} \qquad \text{(A-11)}$$

2. Calculate the density at $T_{ave,i}$ using Equation (A-7).
3. Calculate the viscosity at $T_{ave,i}$ using Equation (A-8).

J. Calculate the exit coolant conditions for $s = s_i$.

1. Calculate the exit coolant temperature.

$$T_{i,n} = U_6 T_{in} + \Delta T_{bulk,i} \qquad \text{(A-12)}$$

2. Calculate the density at $T_{i,n}$ using Equation (A-7).

K. Calculate a new flow rate $w_{Ai}$ at $s = s_i$.

$$\Delta P_F = \left[\frac{8.953 \times 10^4}{\rho_{in}} + \frac{2.238 \times 10^6}{\rho_{ex}} \left(1 - \frac{e_A}{e_A + t}\right)^2\right] \frac{w_{Ai}^2}{e_A^2}$$
$$+ 9.218 \times 10^8 \frac{U_7 F \mu_{ave}^{0.2} w_{Ai}^{1.8}}{\rho_{ave}} \sum_{j=2}^{n} \frac{\Delta z_j}{\left[e_{i,j-1} + e_{i,j}\right]^3} \qquad \text{(A-13)}$$

L. Substitute this value of $w_{Ai}$ back into step H and iterate steps H through K until the value of $w_{Ai}$ converges.

M. Calculate the bulk water temperature distribution $T_{i,j}$.

$$T_{i,j} = U_6 T_{in} + 6.584 \frac{U_1 U_2 Qf}{Aw_{Ai}} \sum_{j=2}^{j=j} \left[\phi_{i,j-1} + \phi_{i,j}\right] \Delta z_j \qquad \text{(A-14)}$$

N. Calculate the oxide film thickness $X_{i,j}$ for the range $i = 3$ to $i = m - 2$.

1. Calculate the heat flux at each position i,j.

$$\left(\frac{q}{A}\right)_{i,j} = 3.413 \times 10^6 \, U_1 U_2 \frac{Qf}{A} \phi_{i,j} \qquad \text{(A-15)}$$

2. Calculate the modified heat transfer coefficient $H_{i,j}$ at each position i,j.

$$H_{i,j} = h_{i,j} \left(\frac{T_{i,j}}{T_{Si,j}}\right)^{0.163} = U_8 \left[5.429 \times 10^2 - 1.561 \, T_{i,j}\right.$$

$$\left. + 3.533 \times 10^{-3} T_{i,j}^2 - 4.250 \times 10^{-6} T_{i,j}^3 + 1.882 \times 10^{-9} T_{i,j}^4\right] \cdot$$

$$\cdot \frac{1}{e_{i,j}} \left[\left(245.5 \, w_{Ai} T_{i,j}^{1.162}\right)^{0.6667} - 125\right] \cdot \qquad \text{(A-16)}$$

$$\cdot \left[1 + \frac{1}{3}\left(\frac{2 \times 10^{-3} e_{i,j}}{z_{i,j}}\right)^{0.6667}\right]$$

3. Calculate the fuel plate surface temperature $T_{Si,j}$ at i,j.

a. For $\left(\frac{q}{A}\right)_{i,j} = 0$

$$T_{Si,j} = T_{i,j} \qquad \text{(A-17a)}$$

b. For $\left(\frac{q}{A}\right)_{i,j} \neq 0$

$$\left(\frac{T_{Si,j}}{T_{i,j}}\right)^{0.163} \left(T_{Si,j} - T_{i,j}\right) = \frac{1}{H_{i,j}} \left(\frac{q}{A}\right)_{i,j} \qquad \text{(A-17b)}$$

4. Calculate the oxide film thickness $X_{i,j}$ at i,j.

$$X_{i,j} = 443\ U_9 \theta_1^{0.778} \exp\left[\frac{-8290}{T_{Si,j} + 460}\right] \qquad \text{(A-18)}$$

O. Calculate a new value of the metal temperature $T_{MAi,j}$ for the range i = 3 to i = m − 2.

1. For $X_{i,j} \leq 3$

$$T_{MAi,j} = T_{Si,j} + \frac{\left(\frac{q}{A}\right)_{i,j} X_{i,j}}{1.56 \times 10^4} \qquad \text{(A-19a)}$$

2. For $X_{i,j} > 3$

$$T_{MAi,j} = T_{Si,j} + 1.923 \times 10^{-4} \left(\frac{q}{A}\right)_{i,j} \qquad \text{(A-19b)}$$

P. Calculate new coolant channel thicknesses using the values of $T_{MAi,j}$ and $X_{i,j}$ calculated in steps N and O.

1. Calculate the expansion of the fuel plate thickness due to heating $\delta_{Ai,j}$ using Equation (A-3).
2. Assume the value of the expansion of the fuel plate thickness due to radiation growth $\delta_{VR}$ is that calculated in step C.

3. Calculate the increase in the fuel plate thickness due to the formation of the oxide, $\delta_{oi,j}$.

a. For $X_{i,j} \leq 3$

$$\delta_{oi,j} = 0.2026\ X_{i,j} \tag{A-20a}$$

b. For $X_{i,j} > 3$

$$\delta_{oi,j} = 0.6078 \tag{A-20b}$$

4. Calculate the coolant channel thickness using Equation (A-6).

Q. Using the value of $w_{Ai}$ computed in step L as an initial value, calculate a new value of this quantity using steps H through L using the channel thicknesses calculated in step P.

R. Iterate steps H through Q until the values of $T_{MAi,j}$ converge.

S. Calculate the average metal temperature distribution of the average fuel plate along the length of fuel element.

$$T_{MA,j} = \frac{\sum_{i=4}^{m-2} \left[ \frac{T_{MAi-1,j} + T_{MA,j}}{2} \right] \Delta s_i}{\sum_{i=4}^{m-2} \Delta s_i} \tag{A-21}$$

T. Calculate the total mass flow rate through the average coolant channel using the final values of $w_{Ai}$ calculated in step R.

$$w_A = \sum_{i=1}^{m} w_{Ai} \left[ \frac{\Delta s_i + \Delta s_{i+1}}{2} \right] \tag{A-22}$$

where

$$\Delta s_{m+1} = 0$$

VI. Repeat step V for the outer fuel element.

VII. Calculate the overall flow rate for the entire fuel assembly.

A. Calculate the volumetric flow rate for the fuel elements, $V_F$.

$$V_F = \frac{448.83}{\rho_{in}} \left[171 w_{A\ inner} + 369 w_{A\ outer}\right] \qquad \text{(A-23)}$$

B. Calculate the flow rate through the labyrinth between the fuel elements.

$$V_{lab} = 124.3 \left[\Delta P_F / \rho_{in}\right]^{0.5405} \qquad \text{(A-24)}$$

C. Calculate the volumetric flow rate through the entire fuel assembly, $V_{AS}$.

$$V_{AS} = V_{lab} + V_F \qquad \text{(A-25)}$$

VIII. Calculate the core pressure drop, $\Delta P_{core}$.

$$\Delta P_{core} = \Delta P_F + 4.86 \times 10^{-10} \rho_{in} V_{AS}^2 \qquad \text{(A-26)}$$

IX. Calculate the average temperature down the length of the inner side plate of the inner fuel element, $T_{SPii,j}$.

A. Calculate the coolant flow rate in the annulus between the inner fuel element and the target bundle, $V_{ii}$.

$$5.095\ V_{ii}^{1.094} + V_{ii} = 69.20\ \Delta P_{core}^{0.5173} \qquad \text{(A-27)}$$

B. Calculate the temperature distribution of this coolant, $T_{ii,j}$.

$$T_{ii,j} = U_6 T_{in} + \left[0.001128\ U_{16} Q_{SP} + 0.009808\ U_{17} Q_{H_2O}\right] \frac{U_1 Q z_j}{V_{ii} \rho_{in}} \qquad \text{(A-28)}$$

C. Calculate the heat transfer coefficient of the coolant flowing in this annulus, $h_{ii,j}$.

$$h_{ii,j} = 13.10 \left[1 + 10^{-2}\, T_{ii,j} - 10^{-5}\, T_{ii,j}^{2}\right] V_{ii}^{0.8} \left(\frac{\rho_{in}}{\rho_{ii,j}}\right)^{0.8} \qquad \text{(A-29)}$$

where

$\rho_{in}$ is calculated by Equation (A-7) at $U_6 T_{in}$

$\rho_{ii,j}$ is calculated by Equation (A-7) at $T_{ii,j}$.

D. Calculate the temperature distribution of the fuel plate coolant next to the side plate.

$$\bar{T}_{1,j} = U_6 T_{in} + \left\{\left[\frac{0.1278\,(t + e_A)}{\Delta s_2} + t\right] U_{16} Q_{SP} + e_A U_{17} Q_{H_i}\right\} \cdot \qquad \text{(A-30)}$$

$$\cdot \frac{5.556 \times 10^{-9}\, U_1 Q z_j}{w_{A1} + w_{A2}}$$

E. Calculate the heat transfer coefficient at 1,j.

$$h_{1,j} = U_8 \left[5.429 \times 10^{2} - 1.561\, \bar{T}_{1,j} + 3.533 \times 10^{-3}\, \bar{T}_{1,j}^{2} - 4.250 \times 10^{-6}\, \bar{T}_{1,j}^{3} + 1.882 \times 10^{-9}\, \bar{T}_{1,j}^{4}\right] \cdot \qquad \text{(A-31)}$$

$$\cdot \frac{1}{e_{1,j}} \left[\left(245.5\, w_{A1} \bar{T}_{1,j}^{1.162}\right)^{0.6667} - 125\right]$$

$$\left[1 + \frac{1}{3}\left(\frac{2 \times 10^{-2} e_{1,j}}{z_j}\right)^{0.6667}\right]$$

F. Calculate the average side plate temperature down the length of the element, $T_{SPii,j}$.

$$T_{SPii,j} = -6.870 \times 10^{-6}\ U_1 U_{16} QQ_{SP} + 9.125 \times 10^{-2}\ C_1 + C_2 \qquad \text{(A-32)}$$

where

$$C_1 = \frac{0.2628\ \dfrac{U_1 U_{16} QQ_{SP}}{h_{ii,j}} + 2.061 \times 10^{-5}\ U_1 U_{16} QQ_{SP} + T_{ii,j} - \overline{T}_{1,j}}{0.1825 + \dfrac{2327}{h_{1,j}} + \dfrac{1164}{h_{ii,j}}} \qquad \text{(A-32a)}$$

$$C_2 = \frac{2327\ C_1}{h_{1,j}} + \overline{T}_{1,j} \qquad \text{(A-32b)}$$

X. Calculate the average temperature down the length of the outer side plate of the inner fuel element, $T_{SPio,j}$.

A. Calculate the temperature distribution of the coolant passing between the fuel elements, $T_{lab,j}$.

$$T_{lab,j} = U_6 T_{in} + \left[0.006342\ U_{16} Q_{SP} + 0.01369\ U_{17} Q_{H_2O}\right] \frac{U_1 Qz_j}{V_{lab} \rho_{in}} \qquad \text{(A-33)}$$

B. Calculate the heat transfer coefficient of the coolant passing between the fuel elements, $h_{lab,j}$.

$$h_{lab,j} = 11.01 \left[1 + 10^{-2}\ T_{lab,j} - 10^{-5}\ T_{lab,j}^2\right] V_{lab}^{0.8} \left(\frac{\rho_{in}}{\rho_{lab,j}}\right)^{0.8} \qquad \text{(A-34)}$$

where

$\rho_{in}$ is calculated by Equation (A-7) at $U_6 T_{in}$

$\rho_{lab,j}$ is calculated by Equation (A-7) at $T_{lab,j}$.

C. Calculate the temperature distribution of the fuel plate coolant next to the side plate.

$$\bar{T}_{m,j} = U_6 T_{in} + \left\{ \left[ \frac{0.1768 \left| t + e_A \right|}{\Delta s_m} + t \right] U_{16} Q_{SP} + e_A U_{17} Q_{H_2O} \right\} \cdot \frac{5.556 \times 10^{-9} \, U_1 Q z_j}{w_{Am-1} + w_{Am}} \tag{A-35}$$

D. Calculate the heat transfer coefficient at m,j.

$$h_{m,j} = U_8 \left[ 5.429 \times 10^2 - 1.561 \, \bar{T}_{m,j} + 3.533 \times 10^{-3} \, \bar{T}_{m,j}^{\,2} - 4.250 \times 10^{-6} \, \bar{T}_{m,j}^{\,3} + 1.882 \times 10^{-9} \, \bar{T}_{m,j}^{\,4} \right] \cdot \frac{1}{e_{m,j}} \left[ \left( 245.5 \, w_{Am} \bar{T}_{m,j}^{\,1.162} \right)^{0.6667} - 125 \right] \cdot \left[ 1 + \frac{1}{3} \left( \frac{2 \times 10^{-3} e_{m,j}}{z_j} \right)^{0.6667} \right] \tag{A-36}$$

E. Calculate the average side plate temperature down the length of the fuel element, $T_{SPio,j}$.

$$T_{SPio,j} = -1.315 \times 10^{-5} \, U_1 U_{16} Q Q_{SP} + 0.1263 \, C_1 + C_2 \tag{A-37}$$

where

$$C_1 = \frac{0.3636 \dfrac{U_1 U_{16} Q_{SP}}{h_{lab,j}} + 3.945 \times 10^{-5}\, U_1 U_{16} Q_{SP} + T_{lab,j} - \overline{T}_{m,j}}{0.2525 + \dfrac{2327}{h_{m,j}} + \dfrac{1164}{h_{lab,j}}} \tag{A-37a}$$

$$C_2 = \frac{2327\, C_1}{h_{m,j}} + \overline{T}_{m,j} \tag{A-37b}$$

XI. Calculate the average temperature along the length of the inner side plate of the outer fuel element, $T_{SPoi,j}$.

A. Calculate the temperature distribution of the fuel plate coolant next to the side plate.

$$\overline{T}_{1,j} = U_6 T_{in} + \left\{ \left[ \frac{0.1698\,(t + e_A)}{\Delta s_2} + t \right] U_{16} Q_{SP} + e_A U_{17} Q_{H_2O} \right\} \cdot \frac{5.556 \times 10^{-9}\, U_1 Q z_j}{w_{A1} + w_{A2}} \tag{A-38}$$

B. Calculate the heat transfer coefficient at 1,j.

$$h_{1,j} = U_8 \left[ 5.429 \times 10^2 - 1.561\, \overline{T}_{1,j} + 3.533 \times 10^{-3}\, \overline{T}_{1,j}^{\,2} - 4.250 \times 10^{-6}\, \overline{T}_{1,j}^{\,3} + 1.882 \times 10^{-9}\, \overline{T}_{1,j}^{\,4} \right] \cdot \frac{1}{e_{1,j}} \left[ \left( 245.5\, w_{A1} \overline{T}_{1,j}^{\,1.162} \right)^{0.6667} - 125 \right] \cdot \left[ 1 + \frac{1}{3} \left( \frac{2 \times 10^{-2} e_{1,j}}{z_j} \right)^{0.6667} \right] \tag{A-31}$$

C. Calculate the side plate temperature down the length of the element, $T_{SPoi,j}$.

$$T_{SPoi,j} = -1.213 \times 10^{-5}\ U_1 U_{16} QQ_{SP} + 0.1213\ C_1 + C_2 \qquad \text{(A-39)}$$

where

$$C_1 = \frac{0.3492\ \dfrac{U_1 U_{16} QQ_{SP}}{h_{lab,j}} + 3.639 \times 10^{-5}\ U_1 U_{16} QQ_{SP} + T_{lab,j} - \overline{T}_{1,j}}{0.2425 + \dfrac{2327}{h_{1,j}} + \dfrac{1164}{h_{lab,j}}} \qquad \text{(A-39a)}$$

$$C_2 = \frac{2327\ C_1}{h_{1,j}} + \overline{T}_{1,j} \qquad \text{(A-39b)}$$

XII. Calculate the average temperature along the length of the outer side plate of the outer fuel element, $T_{SPoo,j}$.

A. Calculate the coolant flow rate in the control region.

$$V_C = 36.6\ |\Delta P_{core}|^{0.725} \qquad \text{(A-40)}$$

B. Calculate the temperature of the control region coolant, $T_{C,j}$.

$$T_{C,j} = U_6 T_{in} + 6.25 \times 10^{-6}\ \frac{U_1 Qz_j}{V_C} \qquad \text{(A-41)}$$

C. Calculate the heat transfer coefficient in the control region.

$$h_C = 19.39\ V_C^{0.8} \qquad \text{(A-42)}$$

D. Calculate the temperature distribution of the fuel plate coolant next to the side plate.

$$\bar{T}_{m,j} = U_6 T_{in} + \left\{ \left[ \frac{0.1228 \left(t + e_A\right)}{\Delta s_m} + t \right] U_{16} Q_{SP} + e_A U_{17} Q_{H_2O} \right\} \cdot \frac{5.556 \times 10^{-9}\ U_1 Q z_j}{w_{Am-1} + w_{Am}} \qquad \text{(A-43)}$$

E. Calculate the heat transfer coefficient at m,j.

$$h_{m,j} = U_8 \left[ 5.429 \times 10^2 - 1.561\ \bar{T}_{m,j} + 3.533 \times 10^{-3}\ \bar{T}_{m,j}^{\ 2} - 4.250 \times 10^{-6}\ \bar{T}_{m,j}^{\ 3} + 1.882 \times 10^{-9}\ \bar{T}_{m,j}^{\ 4} \right] \cdot \frac{1}{e_{m,j}} \left[ \left( 245.5\ w_{Am} \bar{T}_{m,j}^{\ 1.162} \right)^{0.6667} - 125 \right] \cdot \left[ 1 + \frac{1}{3} \left( \frac{2 \times 10^{-3} e_{m,j}}{z_j} \right)^{0.6667} \right] \qquad \text{(A-36)}$$

F. Calculate the side plate temperatures down the length of the element, $T_{SPoo,j}$.

$$T_{SPoo,j} = -1.347 \times 10^{-5}\ U_1 U_{16} Q Q_{SP} + 0.1278\ C_1 + C_2 \qquad \text{(A-44)}$$

where

$$C_1 = \frac{0.3679 \dfrac{U_1 U_{16} QQ_{SP}}{h_C} + 4.040 \times 10^{-5}\, U_1 U_{16} QQ_{SP} + T_{C,j} - \overline{T}_{m,j}}{0.2555 + \dfrac{2327}{h_{m,j}} + \dfrac{1164}{h_C}} \qquad \text{(A-44a)}$$

$$C_2 = \frac{2327\, C_1}{h_{m,j}} + \overline{T}_{m,j} \qquad \text{(A-44b)}$$

Part II

Do this part of the analysis (steps XIII through XXII) for both the inner and outer elements.

XIII. For the first iteration, assume the following quantities for fuel plates between two narrow channels, between a narrow channel and a wide channel, and between two wide channels.

A. Average differential pressure across a fuel plate between a narrow channel and a wide channel $\Delta P_{nw}$ psi.

B. Average metal temperature down the length of a fuel plate between two narrow channels $T_{Mnn,j}$ equal to the value of $T_{MA,j}$ calculated in step V.

C. Average metal temperature down the length of a fuel plate between a narrow channel and a wide channel $T_{Mnw,j}$ equal to the value of $T_{MA,j}$ calculated in step V.

D. Average metal temperature down the length of a fuel plate between two wide channels $T_{Mww,j}$ equal to the value of $T_{MA,j}$ calculated in step V.

XIV. Calculate the thicknesses of the narrow and wide coolant channels at i,j.

A. Calculate the deflection of a fuel plate due to the differential pressure, $\Delta P_{nw}$.

1. Calculate the average value of $T_{Mnw,j}$.

$$T_{MnwA} = \frac{\sum_{j=4}^{n-2} \left[T_{Mnw,j-1} + T_{Mnw,j}\right] \Delta z_j}{2 \sum_{j=4}^{n-2} \Delta z_j} \qquad \text{(A-45)}$$

2. Calculate the elastic modulus ratio at $T_M = T_{MnwA}$ using the following relation.

$$\text{E.R.} = -\left(1.624 \times 10^{-6}\right) T_M^2 + \left(4.719 \times 10^{-4}\right) T_M + 0.9737 \qquad \text{(A-46)}$$

3. Calculate the deflection

a. For the inner element

$$\delta_{\Delta P} = \frac{U_{10}\Delta P_{nw}}{\text{E.R.}} \left[2.8372 \times 10^{-2} s^5 - 2.0491 \times 10^{-1} s^4 + 2.7529 \times 10^{-1} s^3 + 5.7806 \times 10^{-1} s^2 - 8.9329 \times 10^{-1} s\right] \qquad \text{(A-47a)}$$

b. For the outer element

$$\delta_{\Delta P} = \frac{U_{10}\Delta P_{nw}}{\text{E.R.}} \left[3.0799 \times 10^{-2} s^5 - 1.9700 \times 10^{-1} s^4 + 2.3697 \times 10^{-1} s^3 + 4.2645 \times 10^{-1} s^2 - 5.9068 \times 10^{-1} s\right] \qquad \text{(A-47b)}$$

B. Calculate the deflection due to the difference of the temperature of an individual fuel plate and that of an average fuel plate.

1. For the fuel plate between two narrow coolant channels
   a. Calculate E.R. at $T_{Mnn,j}$ using Equation (A-46).
   b. Calculate the deflection $\delta_{Tnn,TA}$ at $T_M = T_{Mnn,j}$
      (1) for the inner element

$$\delta_{T,TA} = \frac{U_{11}\,|T_M - T_{MA,j}|}{E.R.}\Big[-3.2084 \times 10^{-4}s^5 + 4.3177 \times 10^{-3}s^4 - 1.8077 \times 10^{-2}s^3 + 1.1087 \times 10^{-2}s^2 + 4.3908 \times 10^{-2}s\Big] \qquad \text{(A-48a)}$$

      (2) For the outer element

$$\delta_{T,TA} = \frac{U_{11}\,|T_M - T_{MA,j}|}{E.R.}\Big[-1.8518 \times 10^{-4}s^5 + 4.5322 \times 10^{-3}s^4 - 2.1050 \times 10^{-2}s^3 - 6.0732 \times 10^{-4}s^2 + 8.3033 \times 10^{-2}s\Big] \qquad \text{(A-48b)}$$

2. For a fuel plate between a narrow coolant channel and a wide coolant channel.
   a. Calculate E.R. at $T_{Mnw,j}$ using Equation (A-46).
   b. Calculate the deflection $\delta_{Tnw,TA}$ at $T_M = T_{Mnw,j}$ using Equations (A-48a) and (A-48b).
3. For a fuel plate between two wide coolant channels
   a. Calculate E.R. at $T_{Mww,j}$ using Equation (A-46).
   b. Calculate the deflection $\delta_{Tww,TA}$ at $T_M = T_{Mww,j}$ using Equations (A-48a) and (A-48b).

C. Calculate the decrease in the coolant channel thickness because of the increase in the fuel plates thickness due to heating.

1. For fuel plates between two narrow coolant channels

$$\delta_{nn} = U_{12} \left(6.75 \times 10^{-6} t\right)\left(T_{Mnni,j} - 70\right) \qquad \text{(A-49a)}$$

For the first iteration, use a value of $T_{Mnni,j} = T_{MA,j}$.

2. For fuel plates between a wide coolant channel and a narrow coolant channel

$$\delta_{nw} = U_{12} \left(6.75 \times 10^{-6} t\right)\left(T_{Mnwi,j} - 70\right) \qquad \text{(A-49b)}$$

For the first iteration, use a value of $T_{Mnwi,j} = T_{MA,j}$.

3. For fuel plates between two wide coolant channels

$$\delta_{ww} = U_{12} \left(6.75 \times 10^{-6} t\right)\left(T_{Mwwi,j} - 70\right) \qquad \text{(A-49c)}$$

For the first iteration, use a value of $T_{Mwwi,j} = T_{MA,j}$.

D. Calculate the increase in the fuel plate thickness due to the oxide formation.

1. For the first iteration, assume that $\delta_{on} = \delta_{ow} = 0$.
2. For the rest of the iterations
   a. For the narrow channel

$$\delta_{oni,j} = 0.2026\ X_{ni,j} \ ; \text{ when } X_{ni,j} \leq 3 \qquad \text{(A-20a)}$$

$$\delta_{oni,j} = 0.6078 \ ; \text{ when } X_{ni,j} > 3 \qquad \text{(A-20b)}$$

   b. For the wide channel

$$\delta_{owi,j} = 0.2026\ X_{wi,j} \ ; \text{ when } X_{wi,j} \leq 3 \qquad \text{(A-20a)}$$

$$\delta_{owi,j} = 0.6078 \ ; \text{ when } X_{wi,j} > 3 \qquad \text{(A-20b)}$$

E. Calculate the increase in the fuel plate thickness $\delta_{VR}$ due to the radiation swelling using Equation (A-4).

F. Calculate the deflection of the fuel plate due to the difference in the fuel plate and side plate temperatures.

1. Determine the average difference between the fuel plate temperature and the side plate temperatures at each elevation, $z_j$.

a. For plates between two narrow coolant channels.

(1) Inner fuel element

$$\Delta T_{Mnn,j} = T_{Mnn,j} - \frac{T_{SPii,j} + T_{SPio,j}}{2} \qquad \text{(A-50a)}$$

(2) Outer fuel element

$$\Delta T_{Mnn,j} = T_{Mnn,j} - \frac{T_{SPoi,j} + T_{SPoo,j}}{2} \qquad \text{(A-50b)}$$

b. For plates between a narrow coolant channel and a wide coolant channel.

(1) Inner fuel element

$$\Delta T_{Mnw,j} = T_{Mnw,j} - \frac{T_{SPii,j} + T_{SPio,j}}{2} \qquad \text{(A-50c)}$$

(2) Outer fuel element

$$\Delta T_{Mnw,j} = T_{Mnw,j} - \frac{T_{SPoi,j} + T_{SPoo,j}}{2} \qquad \text{(A-50d)}$$

c. For plates between two wide coolant channels.

(1) Inner fuel element

$$\Delta T_{Mww,j} = T_{Mww,j} - \frac{T_{SPii,j} + T_{SPio,j}}{2} \qquad \text{(A-50e)}$$

(2) Outer fuel element

$$\Delta T_{Mww,j} = T_{Mww,j} - \frac{T_{SPoi,j} + T_{SPoo,j}}{2} \qquad \text{(A-50f)}$$

2. Calculate the maximum deflection of the fuel plate due to buckling at $z = z_j$

$\Delta T_{M,j} = \Delta T_{Mnn,j}$ for fuel plates between two narrow coolant channels,

$\Delta T_{M,j} = \Delta T_{Mnw,j}$ for fuel plates between narrow and wide coolant channels,

$\Delta T_{M,j} = \Delta T_{Mww,j}$ for fuel plates between two wide coolant channels.

a. For $i = 1, 2, m - 1, m$

$$\delta_{M,j} = 0 \qquad \text{(A-51)}$$

b. For $i = 3$ through $m - 2$

(1) If $\Delta T_{M,j} \leq 0$

$$\delta_{M,j} = 0 \qquad \text{(A-52a)}$$

(2) If $\Delta T_{M,j} > 0$

$$\delta_{M,j} = U_{14} \left[ 0.0063 \left( \Delta T_{M,j} \right)^{1.312} \right] \qquad \text{(A-52b)}$$

Note that the actual deflection at any position is

$$\delta_{M,j} = U_{14} \left[ 0.0063 \left( \Delta T_{M,j} \right)^{1.312} \right] \sin \frac{2\pi z}{\lambda}$$

G. Calculate the maximum longitudinal deflection of the fuel plate due to the radiation growth of the fuel plate material.

$$\delta_{MR} = U_{15}\ 3.651 \times 10^3 \left| \frac{\rho}{\rho_R} - 1 \right|^{1.312} \tag{A-53}$$

Note that the actual deflection is

$$\delta_{MR} = U_{15}\ 3.651 \times 10^3 \left| \frac{\rho}{\rho_R} - 1 \right|^{1.312} \sin \frac{2\pi z}{\lambda}$$

H. Calculate the thicknesses of the coolant channels.

1. For the narrow channel

a. The linear component is

$$\begin{aligned} D_{1n,j} = {} & e_n + \left| 2\xi_1 + 2\xi_2 + \xi_3 \right| \delta_{\Delta P} \\ & + \xi_3 \left| \delta_{Tnw,TA} - \delta_{Tnn,TA} \right|_j \\ & - \left| \xi_3 + 2\xi_4 \right| \delta_{nn,j} - \left| 2\xi_1 + 2\xi_2 + \xi_3 \right| \delta_{nw,j} \\ & - 2\delta_{on,j} - 2\delta_{VR} \end{aligned} \tag{A-54a}$$

b. The sinusoidal component is

$$D_{2n,j} = -\left| \xi_3 + 2\xi_4 \right| \delta_{Mnn,j} - \left| 2\xi_1 + 2\xi_2 + \xi_3 \right| \delta_{Mnw,j} - 2\delta_{MR} \tag{A-54b}$$

2. For the wide channel

a. The linear component is

$$D_{1w,j} = \left(\xi_1 + \xi_2 + \xi_3\right) e_w - \left(2\xi_1 + \xi_2 + 2\xi_3\right) \delta_{\Delta P}$$

$$+ \xi_2 \left(\delta_{Tww,TA} - \delta_{Tnw,TA}\right)_j - \xi_2 \delta_{ww,j}$$

$$- \left(2\xi_1 + \xi_2 + 2\xi_3\right) \delta_{nw,j} - 2\left(\xi_1 + \xi_2 + \xi_3\right) \delta_{ow,j} \qquad \text{(A-55a)}$$

$$- 2\left(\xi_1 + \xi_2 + \xi_3\right) \delta_{VR}$$

b. The sinusoidal component is

$$D_{2w,j} = -\left(2\xi_1 + \xi_2 + 2\xi_3\right) \delta_{Mnw,j} - \xi_2 \delta_{Mww,j} - 2\left(\xi_1 + \xi_2 + \xi_3\right) \delta_{MR} \qquad \text{(A-55b)}$$

XV. Calculate the mass flow rate per unit width of coolant channel $w_i$ for each value of i.

A. Divide the overall length of the channel into incremental lengths $\lambda$. Designate these increments as

$\lambda_{i,g}$; where $g = 1,2,3, \ldots, \left(\frac{L}{\lambda}\right)$; where $L/\lambda$ = an integer

Do steps B through F for both the narrow and the wide channels.

B. Determine the minimum value of the channel thickness within the length $\lambda_{i,g}$, i.e. the smallest value of

$$D_{1i,j} + D_{2i,j}$$

for the range $z_{g-1} \leq z_j \leq z_g$.

Designate the values of these quantities corresponding to this minimum value as $D_{1,g}$ and $D_{2,g}$.

C. Assume that the mass flow rates down each strip are those calculated for the average coolant channel in Part I.

D. Calculate the coolant properties for each strip.

1. Assume that the inlet coolant properties are those calculated in step V.F.

2. Calculate the bulk temperature rise.

$$\Delta T_{bulk,i} = 6.584 \frac{U_1 U_2 U_3 Qf}{Aw_i} \sum_{j=2}^{n} U_4 \left[ \phi_{i,j-1} + \phi_{i,j} \right] \Delta z_j \qquad \text{(A-56)}$$

3. Calculate the average coolant properties using step V.I.
4. Calculate the exit coolant properties using step V.J.

E. Calculate new flow rates at each position i using the relation

$$\Delta P_F = \left[ \frac{8.953 \times 10^4}{\rho_{in}} + \frac{2.238 \times 10^6}{\rho_{ex,i}} \left( 1 - \frac{e_e}{e_e + t} \right)^2 \right] \frac{w_i^2}{e_e^2}$$

$$+ 1.152 \times 10^8 \frac{U_7 F \mu_{ave,i}^{0.2} w_i^{1.8}}{\rho_{ave,i}} \cdot \qquad \text{(A-57)}$$

$$\cdot \sum_{g=1}^{L/\lambda} \frac{\lambda_g}{D_{1g}^3} \frac{1 + \frac{1}{2} \left( \frac{D_{2g}}{D_{1g}} \right)^2}{\left( 1 - \left( \frac{D_{2g}}{D_{1g}} \right)^2 \right)^{5/2}}$$

F. Substitute these new values of $w_i$ back into step D, and iterate steps D and E until the values of $w_i$ converge.

XVI. Calculate the bulk water temperature distribution using the final values of $w_i$ from step XV for both the narrow and the wide coolant channels.

$$T_{i,j} = U_6 T_{in} + 6.584 \frac{U_1 U_2 U_3 Qf}{Aw_i} \sum_{j=2}^{j} U_4 \left[ \phi_{i,j-1} + \phi_{i,j} \right] \Delta z_j \qquad \text{(A-58)}$$

current version case

XVII. Calculate the fuel plate surface (oxide-water interface) temperature $T_{Si,j}$ for $i = 3$ to $i = m - 2$ for both the narrow and the wide coolant channels.

A. Calculate the heat flux at each position i,j.

$$\left(\frac{q}{A}\right)_{i,j} = 3.413 \times 10^6 \; U_1 U_2 U_3 U_4 \; \frac{Qf}{A} \; \phi_{i,j} \qquad \text{(A-59)}$$

B. Calculate the modified heat transfer coefficient $H_{i,j}$ at each position i,j for three cases.

1. Case 1. Channel thickness $= D_{1i,j} + D_{2i,j}$

$$H_{i,j} = h_{i,j} \left(\frac{T_{i,j}}{T_{Si,j}}\right)^{0.163}$$

$$= U_8 \left[5.429 \times 10^2 - 1.561 \; T_{i,j} + 3.533 \times 10^{-3} \; T_{i,j}^2 - 4.250 \times 10^{-6} \; T_{i,j}^3 + 1.882 \times 10^{-9} \; T_{i,j}^4\right] \frac{1}{\left[D_{1i,j} + D_{2i,j}\right]} \cdot \qquad \text{(A-60a)}$$

$$\cdot \left[\left(245.5 \; w_i T_{i,j}^{1.162}\right)^{0.6667} - 125\right] \cdot$$

$$\cdot \left[1 + \frac{1}{3}\left(\frac{2 \times 10^{-3} \; D_{1,j}}{z_j}\right)^{0.6667}\right]$$

2. Case 2. Channel thickness $= D_{1i,j}$

$$H_{i,j} = h_{i,j} \left(\frac{T_{i,j}}{T_{Si,j}}\right)^{0.163}$$

$$= U_8 \left[5.429 \times 10^2 - 1.561\, T_{i,j} + 3.533 \times 10^{-3}\, T_{i,j}^2 - 4.250 \times 10^{-6}\, T_{i,j}^3 + 1.882 \times 10^{-9}\, T_{i,j}^4\right] \frac{1}{D_{1i,j}} \cdot \left[245.5\, w_i T_{i,j}^{1.162}\right]^{0.6667} - 125 \cdot \left[1 + \frac{1}{3}\left(\frac{2 \times 10^{-3}\, D_{1i,j}}{z_j}\right)^{0.6667}\right] \tag{A-60b}$$

3. Case 3. Channel thickness $= D_{1i,j} - D_{2i,j}$

$$H_{i,j} = h_{i,j} \left(\frac{T_{i,j}}{T_{Si,j}}\right)^{0.163}$$

$$= U_8 \left[5.429 \times 10^2 - 1.561\, T_{i,j} + 3.533 \times 10^{-3}\, T_{i,j}^2 - 4.250 \times 10^{-6}\, T_{i,j}^3 + 1.882 \times 10^{-9}\, T_{i,j}^4\right] \frac{1}{D_{1i,j} - D_{2i,j}} \cdot$$

$$\cdot\left[\left(245.5\ w_i T_{i,j}^{1.162}\right)^{0.6667} - 125\right]\cdot \tag{A-60c}$$

$$\cdot\left[1 + \frac{1}{3}\left(\frac{2 \times 10^{-3}\ D_{1i,j}}{z_j}\right)^{0.6667}\right]$$

C. Calculate the fuel plate surface temperature for these three cases.

1. For $\left(\frac{q}{A}\right)_{i,j} = 0$

$$T_{Si,j} = T_{i,j} \tag{A-17a}$$

2. For $\left(\frac{q}{A}\right)_{i,j} \neq 0$

$$\left(\frac{T_{Si,j}}{T_{i,j}}\right)^{0.163} \left(T_{Si,j} - T_{i,j}\right) = \frac{1}{H_{i,j}} \left(\frac{q}{A}\right)_{i,j} \tag{A-17b}$$

XVIII. Calculate the oxide film thicknesses for these three cases for the range $i = 3$ to $i = m - 2$ for both the narrow and wide channels.

$$X_{i,j} = 443\ U_9 \theta^{0.778} \exp\left[\frac{-8290}{T_{Si,j} + 460}\right] \tag{A-18}$$

XIX. Calculate the average metal temperature at i,j in the range $i = 3$ to $i = m - 2$ for these three cases.

A. Calculate the temperature drop through the oxide film for all cases for both the narrow and the wide channels.

1. For $X_{i,j} \leq 3$

$$T_{Mi,j} = T_{Si,j} + \frac{\left(\frac{q}{A}\right)_{i,j} X_{i,j}}{1.56 \times 10^4} \qquad \text{(A-19a)}$$

2. For $X_{i,j} > 3$

$$T_{Mi,j} = T_{Si,j} + 1.923 \times 10^{-4} \left(\frac{q}{A}\right)_{i,j} \qquad \text{(A-19b)}$$

3. Define these results as

| | Narrow Channel | Wide Channel |
|---|---|---|
| Case 1 | $T_{Mni,j,1}$ | $T_{Mwi,j,1}$ |
| Case 2 | $T_{Mni,j,2}$ | $T_{Mwi,j,2}$ |
| Case 3 | $T_{Mni,j,3}$ | $T_{Mwi,j,3}$ |

B. Calculate the average metal temperature at i,j.

1. For plates between two narrow channels,

$T_{Mnni,j}$ = the maximum value of

$$\frac{T_{Mni,j,1} + T_{Mni,j,3}}{2} \quad \text{or} \quad T_{Mni,j,2} \qquad \text{(A-61a)}$$

2. For plates between a narrow channel and a wide channel,

$T_{Mnwi,j}$ = the maximum value of

$$\frac{T_{Mni,j,1} + T_{Mwi,j,3}}{2} \quad \text{or} \quad \frac{T_{Mni,j,2} + T_{Mwi,j,2}}{2} \qquad \text{(A-61b)}$$

$$\text{or} \quad \frac{T_{Mni,j,3} + T_{Mwi,j,1}}{2}$$

3. For plates between two wide channels,

$T_{Mwwi,j}$ = the maximum value of

$$\frac{T_{Mwi,j,1} + T_{Mwi,j,3}}{2} \quad \text{or} \quad T_{Mwi,j,2} \tag{A-61c}$$

XX. Calculate the average metal temperature down the length of the fuel plate.

A. For plates between two narrow channels.

$$T_{Mnn,j} = \frac{\sum_{i=4}^{m-2} \left[ \frac{T_{Mnn,i-1,j} + T_{Mnn,i,j}}{2} \right] \Delta s_i}{\sum_{i=4}^{m-2} \Delta s_i} \tag{A-62a}$$

B. For plates between a narrow channel and a wide channel.

$$T_{Mnw,j} = \frac{\sum_{i=4}^{m-2} \left[ \frac{T_{Mnw,i-1,j} + T_{Mnw,i,j}}{2} \right] \Delta s_i}{\sum_{i=4}^{m-2} \Delta s_i} \tag{A-62b}$$

C. For plates between two wide channels.

$$T_{Mww,j} = \frac{\sum_{i=4}^{m-2} \left[ \frac{T_{Mww,i-1,j} + T_{Mww,i,j}}{2} \right] \Delta s_i}{\sum_{i=4}^{m-2} \Delta s_i} \tag{A-62c}$$

XXI. Calculate the average differential pressure across a fuel plate between a narrow and a wide coolant channel.

A. Calculate the average differential pressure across a strip of unit width at $s = s_i$.

$$\Delta P_{nwi} = 1.119 \times 10^6 \left\{ \frac{w_{wi}^2}{e_{we}^2} \left[ \frac{1.04}{\rho_{in}} + \frac{1}{\rho_{ex,w,i}} - \frac{1}{\rho_{ex,w,i}} \cdot \left( 1 - \frac{e_{we}}{e_{we} + t} \right)^2 \right] - \frac{w_{ni}^2}{e_{ne}^2} \left[ \frac{1.04}{\rho_{in}} + \frac{1}{\rho_{ex,n,i}} - \frac{1}{\rho_{ex,n,i}} \left( 1 - \frac{e_{ne}}{e_{ne} + t} \right)^2 \right] \right\} \tag{A-63}$$

B. Calculate the average differential pressure across the entire width of the plate.

$$\Delta P_{nw} = \frac{\sum_{i=4}^{m-2} \left[ \frac{\Delta P_{nw,i-1} + \Delta P_{nw,i}}{2} \right] \Delta s_i}{\sum_{i=4}^{m-2} \Delta s_i} \tag{A-64}$$

XXII. Iterate steps XIV through XXI until convergence.

A. Substitute the following values back into step XIV.

$T_{Mnn,i,j}$ ; $T_{Mnn,j}$
$T_{Mnw,i,j}$ ; $T_{Mnw,j}$
$T_{Mww,i,j}$ ; $T_{Mww,j}$
$X_{n,i,j}$ for Case 3
$X_{w,i,j}$ for Case 3
$\Delta P_{nw}$

B. Substitute the values of $w_{ni}$ and $w_{wi}$ back into step XV.C.

C. Repeat steps XIV through XXI.

D. Iterate until the following values converge.

$T_{Mnn,j}$

$T_{Mnw,j}$

$T_{Mww,j}$

Part III

XXIII. Calculate the maximum possible heat flux in the hot and cold channels at each position i,j for the range i = 3 to i = m − 2.

A. Calculate the minimum possible channel thickness at i,j.

1. For the hot channel

$$D_{Hmin,i,j} = D_{1n,i,j} - e_n + e_{n,min} + D_{2n,i,j} \qquad \text{(A-65a)}$$

2. For the cold channel

$$D_{Cmin,i,j} = \left(\xi_1 + \xi_2\right)\left[D_{1w,i,j} - e_w + e_{w,min} + D_{2w,i,j}\right] + \left(\xi_3 + \xi_4\right)\left[D_{1ni,j} - e_n + e_{n,min} + D_{2ni,j}\right] \qquad \text{(A-65b)}$$

B. Calculate the hot streak flow rates $w_{hsi}$ for both the hot and the cold coolant channels.

1. Divide the length of each streak into increments having the length $\lambda$. Designate these increments as

$\lambda_{i,g}$; where $g = 1,2,3\ldots., \frac{L}{\lambda}$; where $\frac{L}{\lambda}$ = an integer

2. Determine the minimum value of the coolant channel thickness within the length $\lambda_{i,g}$, i.e., the smallest value of

$D_{Hmin,i,j}$ for the hot channel

$D_{Cmin,i,j}$ for the cold channel

Designate the values of $D_{1n,i,j}$; $D_{1w,i,j}$; $D_{2n,i,j}$; and

$D_{2w,i,j}$ corresponding to these minimum values of channel thickness as $D_{1n,i,g}$; $D_{1w,i,g}$; $D_{2n,i,g}$; and $D_{2w,i,g}$.

3. Assume for the initial guess of the mass flow rates the values calculated in Part II for the narrow and wide coolant channels.

   Note that the hot channel is the narrow channel for:

$$\xi_1 = 1;\ \xi_2 = 1;\ \xi_3 = 1;\ \xi_4 = 1$$

   Note that the cold channel is the wide channel for:

$$\xi_1 = 1;\ \xi_2 = 1$$

   Note that the cold channel is the narrow channel for:

$$\xi_3 = 1;\ \xi_4 = 1$$

4. Calculate the coolant properites for the hot streak using step XV.D.

5. Calculate a new hot streak flow rate $w_{hsi}$ using the relation

$$\Delta P_F = \left[\frac{8.953 \times 10^4}{\rho_{in}} + \frac{2.238 \times 10^6}{\rho_{ex,i}}\left(1 - \frac{e_e}{e_e + t}\right)^2\right] \cdot \frac{w_{hsi}^2}{e_e^2} + 1.152 \times 10^8 \frac{U_7 F \mu_{ave}^{0.2} w_{hs,i}^{1.8}}{\rho_{ave,i}} \cdot \sum_{g=1}^{L/\lambda} \frac{\lambda_g}{\left[D_{1i,g} - e + e_{min}\right]^3} \cdot \left[\frac{1 + \frac{1}{2}\left(\frac{D_{2i,g}}{D_{1i,g} - e + e_{min}}\right)^2}{\left\{1 - \left(\frac{D_{2i,g}}{D_{1i,g} - e + e_{min}}\right)^2\right\}^{5/2}}\right] \tag{A-66a}$$

where

for the hot channel

$$D_{1i,g} - e + e_{min} = D_{1n,i,g} - e_n + e_{n,min}$$

for the cold channel

$$D_{1i,g} - e + e_{min} = \left(\xi_1 + \xi_2\right)\left[D_{1w,i,g} - e_w + e_{w,min}\right] + \left(\xi_3 + \xi_4\right)\left[D_{1n,i,g} - e_n + e_{n,min}\right]$$

and for the hot channel

$$D_{2i,g} = D_{2n,i,g}$$

for the cold channel

$$D_{2i,g} = \left(\xi_1 + \xi_2\right) D_{2w,i,g} + \left(\xi_3 + \xi_4\right) D_{2n,i,g}$$

6. Substitute this new value of $w_{hsi}$ back into step 4, and iterate steps 4 and 5 until the value of $w_{hsi}$ converges.

C. Calculate the hot streak bulk water temperature distribution, $T_{hs,i,j}$.

$$T_{hs,i,j} = U_6 T_{in} + 6.584 \frac{U_1 U_2 U_3 Qf}{Aw_{hsi}} \sum_{j=2}^{j} U_4 \left[\phi_{i,j-1} + \phi_{i,j}\right] \Delta z_j \quad \text{(A-66b)}$$

D. Calculate the modified hot spot heat transfer coefficient at each position i,j.

$$H_{hsi,j} = U_8 \left[5.429 \times 10^2 - 1.561\ T_{hsi,j} + 3.533 \times 10^{-3}\ T^2_{hsi,j} - 4.250 \times 10^{-6}\ T^3_{hsi,j} + 1.882 \times 10^{-9}\ T^4_{hsi,j}\right] \frac{1}{D_{min,i,j}} \cdot \tag{A-67}$$

$$\cdot \left[\left(245.5\ w_{hsi,j} T^{1.162}_{hsi,j}\right)^{0.6667} - 125\right] \cdot$$

$$\cdot \left[1 + \frac{1}{3}\left(2 \times 10^{-3}\ \frac{\left|D_{1i,j} - e + e_{min}\right|}{z_j}\right)^{0.6667}\right]$$

where

for the hot channel,

$$D_{1i,j} - e + e_{min} = D_{1n,i,j} - e_n + e_{n,min}$$

for the cold channel,

$$D_{1i,j} - e + e_{min} = \left(\xi_1 + \xi_2\right)\left[D_{1w,i,j} - e_w + e_{w,min}\right] \cdot + \left(\xi_3 + \xi_4\right)\left[D_{1n,i,j} - e_n + e_{n,min}\right]$$

E. Calculate the hot spot surface temperature $T_{Shsi,j}$ at i,j for the hot and the cold channels.

$$H_{hsi,j} \left(\frac{T_{Shsi,j}}{T_{hsi,j}}\right)^{0.163} \left(T_{Shsi,j} - T_{hsi,j}\right)$$

$$= 3.413 \times 10^6\ U_1 U_2 U_3 U_{25}\ \frac{Qf}{A}\ \phi_{i,j} \cdot \tag{A-68}$$

$$\cdot \left[1.0 + (\bar{U} - 1.0)\ \frac{H_{hsi,j}}{15{,}000} \left(\frac{T_{Shsi,j}}{T_{hsi,j}}\right)^{0.163}\right]$$

where

$$\bar{U} = U_{18}U_{20} \text{ for the hot channel} \tag{A-68a}$$

$$\bar{U} = U_{19}U_{21} \text{ for the cold channel,} \tag{A-68b}$$

where $U_{20}$ is

$$U_{20} = 1.33687 - 0.35423s + 0.14503s^2 - 0.01669s^3 \text{ for the inner fuel element} \tag{A-68c}$$

$$U_{20} = 1.180171 - 0.278079s + 0.151756s^2 - 0.014261s^3 \text{ for the outer fuel element,} \tag{A-68d}$$

and where $U_{21}$ is

$$U_{21} = 0.863686 - 0.016507s - 0.010950s^2 + 0.0047976s^3 \text{ for the inner fuel element} \tag{A-68e}$$

$$U_{21} = 0.881393 - 0.249204s + 0.181639s^2 - 0.033932s^3 \text{ for the outer fuel element.} \tag{A-68f}$$

F. Calculate the hot spot heat flux $\left(\frac{q}{A}\right)_{boi,j}$ at each position i,j for the hot and cold channels for i = 3 to i = m − 2.

$$\left(\frac{q}{A}\right)_{hsi,j} = 3.413 \times 10^6\, U_1U_2U_3U_{25}\, \frac{Qf}{A}\, \phi_{i,j} \cdot \left[1.0 + (\bar{U} - 1.0)\, \frac{H_{hsi,j}}{15{,}000} \left(\frac{T_{Shsi,j}}{T_{hsi,j}}\right)^{0.163}\right] \tag{A-69}$$

where $\bar{U}$ is defined by Equations (68a) through (68f).

XXIV. Specify either the burnout option or the incipient boiling option for this step.

XXIV. Burnout Option

Calculate the burnout heat flux $\left(\frac{q}{A}\right)_{boi,j}$ at each position i,j for for the hot and cold channels for i = 3 to i = m − 2.

A. Calculate the pressure at the inlet of the fuel assembly.

$$P_F = P - 4.86 \times 10^{-10} \rho_{in} V_{AS}^2 \tag{A-70}$$

B. Calculate the pressure at i,j.

$$P_{i,j} = P_F + 4.077 \times 10^{-10} \rho_{in} V_F^2 - \frac{8.954 \times 10^4}{\rho_{in}} \frac{w_{hsi}^2}{e_e^2}$$

$$- \frac{2.238 \times 10^6}{\rho_{i,j}} \frac{w_{hsi}^2}{D_{min,i,j}^2} - 1.152 \times 10^8 \frac{U_7 F \mu_{ave,i}^{0.2} w_{hsi}^{1.8}}{\rho_{ave,i}} \cdot$$

$$\cdot \left\{ \sum_{\substack{g=1 \\ \text{For all } z_g < z_j}}^{g=g} \frac{\lambda_g}{\left[D_{1i,g} - e + e_{min}\right]^3} \left[ \frac{1 + \frac{1}{2}\left(\frac{D_{2i,g}}{D_{1i,g} - e + e_{min}}\right)^2}{\left\{1 - \left(\frac{D_{2i,g}}{D_{1i,g} - e + e_{min}}\right)^2\right\}^{5/2}} \right] \right. \tag{A-71}$$

$$\left. + \frac{z_j - z_g}{\left[D_{1i,j} - e + e_{min}\right]^3} \left[ \frac{1 + \frac{1}{2}\left(\frac{D_{2i,j}}{D_{1i,j} - e + e_{min}}\right)^2}{\left\{1 - \left(\frac{D_{2i,j}}{D_{1i,j} - e + e_{min}}\right)^2\right\}^{5/2}} \right] \right\}$$

where $\left[D_{1i,j} - e + e_{min}\right]$ and $D_{2i,j}$ are identical to the values defined for Equation (A-66a).

C. Calculate the saturation temperature $T_{sat,i,j}$ for each value of $P_{i,j}$.

$$T_{sat,i,j} = 118.43\ P_{i,j}^{0.221} \tag{A-72}$$

D. Calculate the burnout surface temperature for each value of i,j in the range i = 3 to i = m − 2.

$$T_{Sboi,j} = T_{sat,i,j} - 6.48 \times 10^{4} \frac{w_{hsi}}{\rho_{i,j} D_{min,i,j}}$$

$$+ 80.7264 + 1.47622 \times 10^{-1} P_{i,j} \qquad \text{(A-73a)}$$

$$- 2.35910 \times 10^{-4} P_{i,j}^{2} + 1.08545 \times 10^{-7} P_{i,j}^{3}$$

E. Calculate the nonboiling portion of the burnout heat flux.

$$\left(\frac{q}{A}\right)_{bomb} = U_{22} \left[7.263 \times 10^{3} - 2.088 \times 10\ T_{i,j}\right.$$

$$+ 4.726 \times 10^{-2} T_{i,j}^{2} - 5.685 \times 10^{-5} T_{i,j}^{3} \qquad \text{(A-73b)}$$

$$\left. + 2.517 \times 10^{-8} T_{i,j}^{4}\right] \frac{w_{hsi}^{0.8} T_{i,j}^{0.9296}}{D_{min,i,j}} \left(T_{Sboi,j} - T_{i,j}\right)$$

F. Calculate the boiling portion of the burnout heat flux.

$$\left(\frac{q}{A}\right)_{bo,boil} = U_{22} \left[2.920 \times 10^{5} + 4.739 \times 10^{3} P_{i,j}\right.$$

$$- 1.464 \times 10\ P_{i,j}^{2} + 2.498 \times 10^{-2} P_{i,j}^{3} - 2.119 \times 10^{-5} P_{i,j}^{4}$$

$$\left. + 6.887 \times 10^{-9} P_{i,j}^{5}\right] \left[1 + 0.3710\ P_{i,j}^{-0.8525} \left\{1.117 - 2.060 \times 10^{-3} \cdot\right.\right.$$

$$\cdot \left(\frac{T_{sat,i,j} + T_{i,j}}{2}\right) + 1.212 \times 10^{-5} \left(\frac{T_{sat,i,j} + T_{i,j}}{2}\right)^{2}$$

$$- 2.865 \times 10^{-8} \left(\frac{T_{sat,i,j} + T_{i,j}}{2}\right)^3 + 2.648 \times 10^{-11} \cdot \left(\frac{T_{sat,i,j} + T_{i,j}}{2}\right)^4 \Bigg\} \left(T_{sat,i,j} - T_{i,j}\right) \Bigg] \qquad \text{(A-73c)}$$

G. Calculate the burnout heat flux.

$$\left(\frac{q}{A}\right)_{bo} = \left(\frac{q}{A}\right)_{bomb} + \left(\frac{q}{A}\right)_{bo,boil} \qquad \text{(A-73d)}$$

XXIV. Incipient Boiling Option

Calculate the incipient boiling surface temperature $T_{Sib,i,j}$ at each location i,j in the range i = 3 to i = m − 2.

A. Identical to step XXIV.A in the burnout option

B. Identical to step XXIV.B in the burnout option

C. Identical to step XXIV.C in the burnout option

D. Calculate the incipient boiling surface temperature $T_{Sib,i,j}$ at i,j.

$$T_{Sib,i,j} = T_{sat,i,j} + U_{23} \left[\frac{\left(\frac{q}{A}\right)_{hsi,j}}{15.60\, P_{i,j}^{1.156}}\right]^{\frac{P_{i,j}^{0.0234}}{2.30}} \qquad \text{(A-73)}$$

XXV. Repeat steps V through XXIV for each succeeding time increment with the following exceptions.

A. Substitute the following for Equation (A-18) in steps V.N.4 and XVIII.

$$X_{i,j} = 443\, U_9 \left[\psi_{k-1} + \theta_k\right]^{0.778} \exp\left[\frac{-8290}{T_{Si,j,k} + 460}\right] \qquad \text{(A-74)}$$

where

$$\psi_{k-1} = \left[\psi_{k-2} + \theta_{k-1}\right] \exp\left[\frac{10{,}656\ (T_{Si,j,k-1} - T_{Si,j,k})}{(T_{Si,j,k-1} + 460)(T_{Si,j,k} + 460)}\right] \tag{A-74a}$$

$$\psi_o = 0 \tag{A-74b}$$

B. For the final time step, find the location where

$$\left|\left(\frac{q}{A}\right)_{boi,j} - \left(\frac{q}{A}\right)_{hsi,j}\right| \quad \text{is a minimum}$$

Select a new value of Q and iterate steps V through XXV for the final time step only until there is one or more points where

$$\left(\frac{q}{A}\right)_{boi,j} \longrightarrow \left(\frac{q}{A}\right)_{hsi,j} \tag{A-75a}$$

and for the rest of the points

$$\left(\frac{q}{A}\right)_{boi,j} - \left(\frac{q}{A}\right)_{hsi,j} > 0 \tag{A-75b}$$

C. For the incipient boiling option, change

$$\left(\frac{q}{A}\right)_{boi,j} \text{ and } \left(\frac{q}{A}\right)_{hsi,j}$$

in step B to be $T_{Sib,i,j}$ and $T_{Shs,i,j}$ respectively.

## Option II

### Part I

I through XII. Identical to Option I except the various arrangements of fuel plates and coolant channels adjacent to the hot plate shown in Fig. 17 are replaced by those shown in Fig. 18.

### Part II

Do this part of the analysis (steps XII through XXII) for both the inner and the outer fuel elements.

In this part, many of the fuel plate deflections are calculated only at the following plate metal temperatures:

| | Case | | | |
|---|---|---|---|---|
| | $\xi_1$ | $\xi_2$ | $\xi_3$ | $\xi_4$ |
| Subscript, x | | | | |
| MnnH | | | X | X |
| MnnC | | | | X |
| MnwH | X | X | X | |
| MnwC | X | X | X | |
| MwwC | | X | | |

XIII. Assume the following quantities for hot and cold plates between two narrow channels, between a narrow channel and a wide channel, and between two wide channels.

A. Average differential pressure drops across a fuel plate between a narrow channel and a wide channel.

1. For $\xi_1 = 1$, $\xi_2 = 1$, $\xi_3 = 1$; $\Delta P_{nw}$ psi
2. For $\xi_4 = 1$, delete this step.

B. Average metal temperatures down the length of the fuel plate $T_{M,j}$ for the cases shown above. For the first iteration, assume that these are equal to the values of $T_{MA,j}$ calculated in step V.S.

XIV. Calculate the thicknesses of the narrow and the wide coolant channels at i,j.

A. Calculate the deflection of the hot and cold fuel plates due to the differential pressure across these plates.

1. Calculate the average metal temperature of the hot plate $T_{MnwHA}$ or that of the cold plate $T_{MnwCA}$. Use for the hot plate the relation

$$T_{MnwHA} = \frac{\sum_{j=4}^{n-2} \left[T_{MnwH,j-1} + T_{MnwH,j}\right] \Delta z_j}{2 \sum_{j=4}^{n-2} \Delta z_j} \qquad \text{(A-45)}$$

and an analogous relation for the cold plate.

2. Calculate the elastic modulus ratios at these average metal temperatures for the hot and cold plates.

$$E.R. = -1.624 \times 10^{-6} T_M^2 + 4.719 \times 10^{-4} T_M + 0.9737 \qquad \text{(A-46)}$$

3. Calculate the deflection for the hot plate $\delta_{\Delta PH}$ and for the cold plate $\delta_{\Delta PC}$

a. For the inner element

$$\delta_{\Delta P} = \frac{U_{10} \Delta P_{nw}}{E.R.} \left[2.8372 \times 10^{-2} s^5 - 2.0491 \times 10^{-1} s^4 + 2.7529 \times 10^{-1} s^3 + 5.7806 \times 10^{-1} s^2 - 8.9329 \times 10^{-1} s\right] \qquad \text{(A-47a)}$$

b. For the outer element

$$\delta_{\Delta P} = \frac{U_{10} \Delta P_{nw}}{E.R.} \left[3.0799 \times 10^{-2} s^5 - 1.9700 \times 10^{-1} s^4 + 2.3697 \times 10^{-1} s^3 + 4.2645 \times 10^{-1} s^2 - 5.9068 \times 10^{-1} s\right] \qquad \text{(A-47b)}$$

B. Calculate the deflections due to the differences of the temperatures of the individual fuel plate $T_{Mx,j}$ from those of an average fuel plate $T_{MA,j}$ for the cases shown on page 143.

1. Calculate E.R. at $T_{M,j}$ using Equation (A-46).
2. Calculate the deflection $\delta_{T,TA}$
   a. For the inner element

$$\delta_{T,TA} = \frac{U_{11}(T_{Mx} - T_{MA})_j}{E.R.} \Big[-3.2084 \times 10^{-4}s^5 + 4.3177 \times 10^{-3}s^4 - 1.8077 \times 10^{-2}s^3 + 1.1087 \times 10^{-2}s^2 + 4.3908 \times 10^{-2}s\Big] \quad \text{(A-48a)}$$

   b. For the outer element

$$\delta_{T,TA} = \frac{U_{11}(T_{Mx} - T_{MA})_j}{E.R.} \Big[-1.8518 \times 10^{-4}s^5 + 4.5322 \times 10^{-3}s^4 - 2.1050 \times 10^{-2}s^3 - 6.0732 \times 10^{-4}s^2 + 8.3033 \times 10^{-2}s\Big] \quad \text{(A-48b)}$$

C. Calculate the decrease in the coolant channel thickness because of the expansion of the fuel plate thickness due to heating. Cases to be considered are those shown on page 143.

$$\delta_x = U_{12}\left[6.75 \times 10^{-6}t\right]\left[T_{Mxi,j} - 70\right] \quad \text{(A-49)}$$

For the first iteration, use a value of $T_{Mxi,j} = T_{Mx,j}$.

D. Calculate the increase in the fuel plate thickness due to oxide formation.

1. For the first iteration, assume that

$$\delta_{onH} = \delta_{onC} = \delta_{owH} = \delta_{owC} = 0$$

2. For the rest of the iterations

a. For the hot plate surface in the narrow channel

$$\delta_{onHi,j} = 0.2026\ X_{nHi,j}; \text{when } X_{nHi,j} \leq 3 \quad \text{(A-20a)}$$

$$\delta_{onHi,j} = 0.6078; \qquad \text{when } X_{nHi,j} > 3 \quad \text{(A-20b)}$$

b. For the cold plate surface in the narrow channel $\delta_{onCi,j}$ from $X_{nCi,j}$ using equations analogous to Equations (A-20a) and (A-20b).

c. For the hot plate surface in the wide channel (Ignore for $\xi_4 = 1$) $\delta_{owHi,j}$ from $X_{wHi,j}$ using equations analogous to Equations (A-20a) and (A-20b).

d. For the cold plate surface in the wide channel (Ignore for $\xi_4 = 1$) $\delta_{owCi,j}$ from $X_{wCi,j}$ using equations analogous to Equations (A-20a) and (A-20b).

E. Calculate the increase in the fuel plate thickness $\delta_{VR}$ due to the radiation growth using Equation (A-4).

F. Calculate the fuel plate deflection $\delta_{Mx}$ due to the differences between the fuel plate temperatures and the side plate temperatures for the cases corresponding to the fuel plate temperatures $T_{Mx,j}$ shown on page 143.

1. Determine the average difference between the fuel plate temperature and the side plate temperature at each elevation, $z_j$.

a. For the inner fuel element

$$\Delta T_{Mx,j} = T_{Mx,j} - \frac{\left[T_{SPii,j} + T_{SPio,j}\right]}{2} \qquad \text{(A-50a)}$$

b. For the outer fuel element

$$\Delta T_{Mx,j} = T_{Mx,j} - \frac{\left[T_{SPoi,j} + T_{SPoo,j}\right]}{2} \qquad \text{(A-50b)}$$

2. Calculate the deflection of the fuel plate due to buckling.

a. For $\Delta T_{Mx,j} \leq 0$

$$\delta_{Mxi,j} = 0 \tag{A-51}$$

b. For $\Delta T_{Mxi,j} > 0$

(1) For $0 \leq z < 6$

$$\delta_{Mxi,j} = U_{14}(8.64 \times 10^{-2})\Delta T_{Mx,j} \sin \frac{\pi s_i}{\sum_{i=2}^{m} \Delta s_i} \sin \frac{\pi z_j}{12} \tag{A-52a}$$

(2) For $6 \leq z \leq 18$

$$\delta_{Mxi,j} = U_{14}(8.64 \times 10^{-2})\Delta T_{Mx,j} \sin \frac{\pi s_i}{\sum_{i=2}^{m} \Delta s_i} \tag{A-52b}$$

(3) For $18 < z \leq 24$

$$\delta_{Mxi,j} = U_{14}(8.64 \times 10^{-2})\Delta T_{Mx,j} \sin \frac{\pi s_i}{\sum_{i=2}^{m} \Delta s_i} \sin \frac{\pi(24 - z_j)}{12} \tag{A-52c}$$

G. Assume that the longitudinal deflections of all of the fuel plates due to radiation growth are identical. Hence this term need not be considered further.

H. Calculate the coolant channel thicknesses.

1. Narrow coolant channel

$$D_n = D_{1n} - \Delta D \sin \frac{2\pi z}{\lambda} \tag{A-54}$$

a. $\xi_1 = 1$

$$D_{1n} = e_n + \delta_{\Delta PH} + \delta_{\Delta PC} - \delta_{Tnw,TAH} + \delta_{Tnw,TAC} - \delta_{nwH} - \delta_{nwC} - \delta_{MnwH} + \delta_{MnwC} - \delta_{onH} - \delta_{onC} - 2\delta_{VR} \tag{A-54a}$$

b. $\xi_2 = 1$; Identical to Equation (A-54a)

c. $\xi_3 = 1$

$$D_{1n} = e_n + \delta_{\Delta PC} - \delta_{Tnn,TAH} + \delta_{Tnw,TAC} - \delta_{nnH} - \delta_{nwC} - \delta_{MnnH} + \delta_{MnwC} - \delta_{onH} - \delta_{onC} - 2\delta_{VR} \tag{A-54b}$$

d. $\xi_4 = 1$

$$D_{1n} = e_n - \delta_{Tnn,TAH} + \delta_{Tnn,TAC} - \delta_{nnH} - \delta_{nnC} - \delta_{MnnH} + \delta_{MnnC} - \delta_{onH} - \delta_{onC} - 2\delta_{VR} \tag{A-54c}$$

2. Wide coolant channel

$$D_w = D_{1w} - \Delta D \sin \frac{2\pi z}{\lambda} \tag{A-55}$$

a. $\xi_1 = 1$

$$D_{1w} = e_w - \delta_{\Delta PH} - \delta_{\Delta PC} + \delta_{Tnw,TAH} - \delta_{Tnw,TAC} - \delta_{nwH} - \delta_{nwC} + \delta_{MnwH} - \delta_{MnwC} - \delta_{owH} - \delta_{owC} - 2\delta_{VR} \tag{A-55a}$$

b. $\xi_2 = 1$

$$D_{1w} = e_w - \delta_{\Delta PH} + \delta_{Tnw,TAH} - \delta_{Tww,TAC} - \delta_{nwH} - \delta_{wwC} + \delta_{MnwH} - \delta_{MwwC} - \delta_{owH} - \delta_{owC} - 2\delta_{VR} \quad \text{(A-55b)}$$

c. $\xi_3 = 1$

$$D_{1w} = e_w - \delta_{\Delta PH} - \delta_{\Delta PC} - \delta_{Tnw,TAH} + \delta_{Tnw,TAC} - \delta_{nwH} - \delta_{nwC} - \delta_{MnwH} + \delta_{MnwC} - \delta_{owH} - \delta_{owC} - 2\delta_{VR} \quad \text{(A-55c)}$$

d. $\xi_4 = 1$; delete this step.

XV. Calculate the mass flow rate per unit channel width for each position i. Provide in the input data the choice between two alternates methods.

Alternate Method I. (Very similar to the method used in Option I.)

A. Identical to this step in Option I.

Do steps B through F for both the narrow and the wide coolant channels.

B. Determine the minimum value of the channel thickness within the length $\lambda_{i,g}$, i.e. the smallest value of $D = D_1 - \Delta D$. Designate the corresponding values of $D_1$ as $D_{1i,g}$.

C. Identical to this step in Option I.

D. Calculate the coolant properties for each strip.

1. Assume that the inlet coolant properties are those calculated in step V.F.
2. Calculate the bulk temperature rise.

$$\Delta T_{bulk,i} = 3.292 \frac{U_1 U_2 U_3 Qf}{Aw_i} \sum_{j=2}^{n} \left[U_4 + U_5\right] \left[\phi_{i,j-1} + \phi_{i,j}\right] \Delta z_j \quad \text{(A-56)}$$

3. Calculate the average coolant properties using step V.I.

4. Calculate the exit coolant properties using step V.J.

E. Calculate new flow rates at each position i using the relation

$$\Delta P_F = \left[\frac{8.953 \times 10^4}{\rho_{in}} + \frac{2.238 \times 10^6}{\rho_{ex,i}}\left(1 - \frac{e_e}{e_e + t}\right)^2\right]\frac{w_i^2}{e_e^2}$$

$$+ 1.152 \times 10^8 \frac{U_7 F \mu_{ave,i}^{0.2} w_i^{1.8}}{\rho_{ave,i}} \cdot \tag{A-57}$$

$$\cdot \sum_{g=1}^{L/\lambda} \frac{\lambda_g}{D_{1i,g}^3} \left[\frac{1 + \frac{1}{2}\left(\frac{\Delta D}{D_{1i,g}}\right)^2}{\left(1 - \left(\frac{\Delta D}{D_{1i,g}}\right)^2\right)^{5/2}}\right]$$

F. Identical to this step in Option I.

<u>Alternate Method II</u>

Do for both the narrow and the wide coolant channels.

A. Identical to step XV.C in Option I.

B. Identical to step D in Alternate Method I.

C. Calculate new flow rates at each position i using the relation

$$\Delta P_F = \left[\frac{8.953 \times 10^4}{\rho_{in}} + \frac{2.238 \times 10^6}{\rho_{ex,i}}\left(1 - \frac{e_e}{e_e + t}\right)^2\right]\frac{w_i^2}{e_e^2}$$

$$+ 9.218 \times 10^8 \frac{U_7 F \mu_{ave,i}^{0.2} w_i^{1.8}}{\rho_{ave,i}} \cdot \tag{A-57}$$

$$\cdot \sum_{j=2}^{n} \left[\frac{\Delta z_j}{\left[D_{i,j-1} + D_{i,j}\right]^3}\right]$$

D. Identical to step XV.F in Option I.

XVI. Calculate the bulk water temperature distribution using the final values of $w_i$ from step XV for both the narrow and the wide coolant channels for all cases except where $\xi_4 = 1$. In the latter case, consider only the narrow channel situation.

$$T_{i,j} = U_6 T_{in} + 3.292 \frac{U_1 U_2 U_3 Qf}{A w_i} \sum_{j=2}^{j} \left[U_4 + U_5\right] \left[\phi_{i,j-1} + \phi_{i,j}\right] \Delta z_j \tag{A-58}$$

XVII. Calculate the fuel plate surface (oxide-water interface) temperature distribution $T_{Si,j}$ for the range $i = 3$ to $i = m - 2$ in both the narrow and the wide coolant channels for both the hot and cold plates.

A. Calculate the heat flux at each position i,j,

1. For the hot plate

$$\left(\frac{q}{A}\right)_{Hi,j} = 3.413 \times 10^6 \; U_1 U_2 U_3 U_4 \frac{Qf}{A} \phi_{i,j} \tag{A-59a}$$

2. For the cold plate

$$\left(\frac{q}{A}\right)_{Ci,j} = 3.413 \times 10^6 \; U_1 U_2 U_3 U_5 \frac{Qf}{A} \phi_{i,j} \tag{A-59b}$$

Provide in the input data the choice between two alternate methods for oxide buildup.

<u>Alternate Method I for Oxide Buildup</u>

B. Calculate the modified heat transfer coefficient $H_{i,j}$ at each position i,j for three cases:

1. Case 1; Channel thickness $= D_{1i,j} - \Delta D$

$$H_{i,j} = h_{i,j} \left( \frac{T_{i,j}}{T_{Si,j}} \right)^{0.163}$$

$$= U_8 \left[ 5.429 \times 10^2 - 1.561\ T_{i,j} + 3.533 \times 10^{-3}\ T_{i,j}^2 - 4.250 \times 10^{-6}\ T_{i,j}^3 + 1.882 \times 10^{-9}\ T_{i,j}^4 \right] \frac{1}{\left[ D_{1i,j} - \Delta D \right]} \cdot \left[ \left( 245.5\ w_i T_{i,j}^{1.162} \right)^{0.6667} - 125 \right] \cdot \left[ 1 + \frac{1}{3} \left( \frac{2 \times 10^{-3}\ D_{1i,j}}{z_j} \right)^{0.6667} \right] \qquad \text{(A-60)}$$

2. Case 2; Channel thickness $= D_{1i,j}$.
   Calculate $H_{i,j}$ using Equation (A-60) with $D_{1i,j}$ instead of $(D_{1i,j} - \Delta D)$ in the denominator.
3. Case 3; Chanel thickness $= (D_{1i,j} + \Delta D)$.
   Calculate $H_{i,j}$ using Equation (A-60) with $(D_{1i,j} + \Delta D)$ instead of $(D_{1i,j} - \Delta D)$ in the denominator.

C. Calculate the fuel plate surface (oxide-water interface) temperatures for the three cases.

1. When $\left( \frac{q}{A} \right)_{i,j} = 0$

$$T_{SnHi,j} = T_{SnCi,j} = T_{SwHi,j} = T_{SwCi,j} = T_{i,j} \qquad \text{(A-17a)}$$

2. When $\left( \frac{q}{A} \right)_{i,j} \neq 0$

   a. For a hot plate surface in a narrow channel.

$$\left(\frac{T_{SnHi,j}}{T_{ni,j}}\right)^{0.163} \left(T_{SnHi,j} - T_{ni,j}\right) = \frac{1}{H_{ni,j}} \left(\frac{q}{A}\right)_{Hi,j} \qquad \text{(A-17b)}$$

b. For a cold plate surface in a narrow channel. Calculate $T_{SnCi,j}$ by an equation analogous to Equation (A-17b).

c. For a hot plate surface in a wide channel. (Ignore for $\xi_4 = 1$) Calculate $T_{SwHi,j}$ by an equation analogous to Equation (A-17b).

d. For a cold plate surface in a wide channel. (Ignore for $\xi_4 = 1$) Calculate $T_{SwCi,j}$ by an equation analogous to equation (A-17b).

XVIII. Calculate the oxide film thickness in the range i = 3 to m − 2 for each value of $T_{Si,j}$ calculated in step XVII.C.

$$X_{i,j} = 443\ U_9 \theta^{0.778} \exp\left[\frac{-8290}{T_{Si,j} + 460}\right] \qquad \text{(A-18)}$$

XIX. Calculate the average metal temperature at i,j for the cases listed on page 143.

A. Calculate the metal surface (metal-oxide interface) temperature for each value of $X_{i,j}$ calculated in step XVIII.

1. When $X_{i,j} \leq 3$

$$T_{Mi,j} = T_{Si,j} + \frac{\left(\frac{q}{A}\right)_{i,j} X_{i,j}}{1.56 \times 10^4} \qquad \text{(A-19a)}$$

2. When $X_{i,j} > 3$

$$T_{Mi,j} = T_{Si,j} + 1.923 \times 10^{-4} \left(\frac{q}{A}\right)_{i,j} \qquad \text{(A-19b)}$$

B. Define these results as

| | Narrow Channel | | Wide Channel | |
|---|---|---|---|---|
| | Hot Plate | Cold Plate | Hot Plate | Cold Plate |
| Case 1 | $T_{MnHi,j,1}$ | $T_{MnCi,j,1}$ | $T_{MwHi,j,1}$ | $T_{MwCi,j,1}$ |
| Case 2 | $T_{MnHi,j,2}$ | $T_{MnCi,j,2}$ | $T_{MwHi,j,2}$ | $T_{MwCi,j,2}$ |
| Case 3 | $T_{MnHi,j,3}$ | $T_{MnCi,j,3}$ | $T_{MwHi,j,3}$ | $T_{MwCi,j,3}$ |

C. Calculate the average metal temperature at i,j for the cases listed at the top of page 143.

1. For a hot plate between two narrow channels; $T_{MnnHi,j}$ = the maximum value of

$$\frac{T_{MnHi,j,1} + T_{MnHi,j,3}}{2} \quad \text{or} \quad T_{MnHi,j,2} \tag{A-61a}$$

2. For a cold plate between two narrow channels; $T_{MnnCi,j}$ = the maximum value of

$$\frac{T_{MnCi,j,1} + T_{MnCi,j,3}}{2} \quad \text{or} \quad T_{MnCi,j,2} \tag{A-61b}$$

3. For a hot plate between a narrow channel and a wide channel; $T_{MnwHi,j}$ = the maximum value of

$$\frac{T_{MnHi,j,1} + T_{MwHi,j,3}}{2} \quad \text{or} \quad \frac{T_{MnHi,j,2} + T_{MwHi,j,2}}{2} \quad \text{or} \quad \frac{T_{MnHi,j,3} + T_{MwHi,j,1}}{2} \tag{A-61c}$$

4. For a cold plate between a narrow channel and a wide channel; $T_{MnwCi,j}$ = the maximum value of

$$\frac{T_{MnCi,j,1} + T_{MwCi,j,3}}{2} \quad \text{or} \quad \frac{T_{MnCi,j,2} + T_{MwCi,j,2}}{2}$$

$$\text{or} \quad \frac{T_{MnCi,j,3} + T_{MwCi,j,1}}{2} \tag{A-61d}$$

5. For a cold plate between two wide channels; $T_{MwwCi,j}$ = the maximum value of

$$\frac{T_{MwCi,j,1} + T_{MwCi,j,3}}{2} \quad \text{or} \quad T_{MwCi,j,2} \tag{A-61e}$$

<u>Alternate Method II for Oxide Buildup</u>

B. Calculate the modified heat transfer coefficient $H_{i,j}$ at each position i,j.

$$H_{i,j} = h_{i,j} \left(\frac{T_{i,j}}{T_{Si,j}}\right)^{0.163}$$

$$= U_8 \left[5.429 \times 10^2 - 1.561\, T_{i,j} + 3.533 \times 10^{-3}\, T_{i,j}^2 - 4.250 \times 10^{-6}\, T_{i,j}^3 + 1.882 \times 10^{-9}\, T_{i,j}^4\right] \frac{1}{D_{i,j}} \cdot \tag{A-60}$$

$$\cdot \left[\left(245.5\, w_i T_{i,j}^{1.162}\right)^{0.6667} - 125\right] \cdot$$

$$\cdot \left[1 + \frac{1}{3}\left(\frac{2 \times 10^{-3}\, D_{1i,j}}{z_j}\right)^{0.6667}\right]$$

C. Calculate the fuel plate surface (oxide-water interface) temperature at each position i,j. Method identical to step XVII.C

in alternate method I for oxide buildup except that there is only one case instead of three cases.

XVIII. Calculate the oxide film thickness in the range i = 3 to m − 2 for each value of $T_{Si,j}$ calculated in step XVII.C. Method identical to step XVII in alternate method I for oxide buildup.

XIX. Calculate the average metal temperature at i,j for the cases listed on page 143.

A. Calculate the metal surface (metal-oxide interface) temperature for each value of $X_{i,j}$ calculated in step XVIII. Method identical to step XIX.A in alternate method I for oxide buildup.

B. Define these results as

| Narrow Channel | | Wide Channel | |
|---|---|---|---|
| Hot Plate | Cold Plate | Hot Plate | Cold Plate |
| $T_{MnHi,j}$ | $T_{MnCi,j}$ | $T_{MwHi,j}$ | $T_{MwCi,j}$ |

C. Calculate the average metal temperature at i,j for the cases listed on page 143.

1. For a hot plate between two narrow channels

$$T_{MnnHi,j} = T_{MnHi,j} \tag{A-61a}$$

2. For a cold plate between two narrow channels

$$T_{MnnCi,j} = T_{MnCi,j} \tag{A-61b}$$

3. For a hot plate between a narrow channel and a wide channel

$$T_{MnwHi,j} = \frac{T_{MnHi,j} + T_{MwHi,j}}{2} \tag{A-61c}$$

4. For a cold plate between a narrow channel and a wide channel

$$T_{MnwCi,j} = \frac{T_{MnCi,j} + T_{MwCi,j}}{2} \tag{A-61d}$$

5. For a cold plate between two wide channels

$$T_{MwwCi,j} = T_{MwCi,j} \tag{A-61e}$$

XX. Calculate the average metal temperature down the length of the fuel plates for the cases listed on page 143.

$$T_{x,j} = \frac{\sum_{m=4}^{m-2} \left[ \frac{T_{x,i-1,j} + T_{x,i,j}}{2} \right] \Delta s_i}{\sum_{m=4}^{m-2} \Delta s_i} \tag{A-62}$$

XXI. Calculate the average differential pressure across a fuel plate between a narrow coolant channel and a wide coolant channel. Identical to step XXI in Option I.

XXII. Iterate steps XIV through XXI until convergence.

A. Substitute the following values back into step XIV.

$T_{x,i,j}$ and $T_{x,j}$ for the cases listed on page 143.

$X_{nHi,j}$; $X_{nCi,j}$; $X_{wHi,j}$; and $X_{wCi,j}$ (Use Case 3 values when using alternate method I for oxide buildup.)

$\Delta P_{nw}$ (Ignore for $\xi_4 = 1$)

B. Substitute the values of $w_{ni}$ and $w_{wi}$ back into step XV.C.

C. Repeat steps XIV through XXI.

D. Iterate until the following values converge.

$T_{x,j}$ for the cases listed on page 143.

Part III

XXIII. Calculate the maximum possible heat flux in the hot and cold channels at each position i,j for the range i = 3 to i = m − 2.

A. Calculate the minimum possible channel thickness at i,j.

1. For the hot channel

$$D_{H,min,i,j} = D_{1n,i,j} - e_n + e_{n,min} - \Delta D \qquad \text{(A-65a)}$$

2. For the cold channel

$$D_{C,min,i,j} = (\xi_1 + \xi_2)\left[D_{1w,i,j} - e_w + e_{w,min}\right] + (\xi_3 + \xi_4)\left[D_{1n,i,j} - e_n + e_{n,min}\right] - \Delta D \qquad \text{(A-65b)}$$

B. Calculate the hot streak flow rate $w_{hsi}$ for both the hot and the cold coolant channels.

The two alternate methods used for calculating the flow rates in step XV apply to steps XXIII.B and XXIV.B.

<u>Alternate Method I</u> (Very similar to the method used in Option I)

1. Identical to step XXIII.B.1 in Option I.
2. Identical to step XXIII.B.2 in Option I except designate values of $D_{1ni,j}$ and $D_{1wi,j}$ corresponding to these minimum values of channel thicknesses as $D_{1ni,g}$ and $D_{1wi,g}$.
3. Identical to step XXIII.B.3 in Option I.
4. Calculate the coolant properties for each strip.
   a. Assume that the inlet coolant properties are those calculated in step V.F in Option I.
   b. Calculate the bulk temperature rise,

$$\Delta T_{bulk,i} = 6.584 \frac{U_1 U_2 U_3 U_{24}}{w_{hsi} A} \sum_{j=2}^{n} \left[\phi_{i,j-1} + \phi_{i,j}\right] \Delta z_j \qquad \text{(A-56)}$$

   c. Calculate the average coolant properties using step V.I in Option I.
   d. Calculate the exit coolant properties using step V.J in Option I.

5. Calculate a new hot streak flow rate $w_{hsi}$ using the relation

$$\Delta P_F = \left[ \frac{8.953 \times 10^4}{\rho_{in}} + \frac{2.238 \times 10^6}{\rho_{ex,i}} \left( 1 - \frac{e_e}{e_e + t} \right)^2 \right] \cdot$$

$$\cdot \frac{w_{hsi}^2}{e_e^2} + 1.152 \times 10^8 \frac{U_7 F \mu_{ave}^{0.2} w_{hsi}^{1.8}}{\rho_{ave,i}} \cdot$$

$$\cdot \sum_{g=1}^{L/\lambda} \frac{\lambda_g}{\left| D_{1i,g} - e + e_{min} \right|^3} \cdot \tag{A-66a}$$

$$\cdot \left[ \frac{1 + \frac{1}{2} \left( \frac{\Delta D}{D_{1i,g} - e + e_{min}} \right)^2}{\left\{ 1 - \left( \frac{\Delta D}{D_{1i,g} - e + e_{min}} \right)^2 \right\}^{5/2}} \right]$$

where

for the hot channel,

$$D_{1i,g} - e + e_{min} = D_{1ni,g} - e + e_{n,min}$$

for the cold channel

$$D_{1i,g} - e + e_{min} = (\xi_1 + \xi_2) \left| D_{1w,i,g} - e_w + e_{w,min} \right| + (\xi_3 + \xi_4) \left| D_{1n,i,g} - e_n + e_{n,min} \right|$$

6. Substitute this new value of $w_{hsi}$ back into step 4, and iterate steps 4 and 5 until the value of $w_{hsi}$ converges.

<u>Alternate Method II</u>

1. Identical to step XXIII.B.3 in Option I.
2. Identical to step XXIII.B.4 in Alternate Method I.
3. Calculate a new hot streak flow rate $w_{hsi}$ using the relation

$$\Delta P_F = \left[\frac{8.953 \times 10^4}{\rho_{in}} + \frac{2.238 \times 10^6}{\rho_{ex,i}}\left(1 - \frac{e_e}{e_e + t}\right)^2\right]\frac{w_{hsi}^2}{e_e}$$

$$+ 9.218 \times 10^8 \frac{U_7 F \mu_{ave,i}^{0.2} w_{hsi}^{1.8}}{\rho_{ave,i}} \cdot \tag{A-66a}$$

$$\cdot \sum_{j=2}^{n} \frac{\Delta z_j}{\left[D_{i,j-1} + D_{i,j} - 2e + 2e_{min}\right]^3}$$

Use the narrow channel conditions for the hot channel for all cases; use the wide channel conditions for the cold channel for $\xi_1 = \xi_2 = 1$; use the narrow channel conditions for the cold channel for $\xi_3 = \xi_4 = 1$.

4. Substitute this new value of $w_{hsi}$ back into step 2, and iterate steps 2 and 3 until the value of $w_{hsi}$ converges.

C. Calculate the hot streak bulk water temperature distribution, $T_{hsi,j}$.

$$T_{hsi,j} = U_6 T_{in} + 6.584 \frac{U_1 U_2 U_3 U_{24} Qf}{w_{hsi} A} \sum_{j=2}^{j} \left[\phi_{i,j-1} + \phi_{i,j}\right] \Delta z_j \tag{A-66b}$$

D through F. Identical to steps XXIII.D through XXIII.F in Option I.

XXIV. Specify either the burnout option of the incipient boiling option for this step.

XXIV. Burnout Option

Calculate the burnout heat flux $\left(\frac{q}{A}\right)_{boi,j}$ at each position i,j for the hot and the cold channels for the range i = 3 to i = m − 2.

A. Identical to step XXIV.Burnout Option.A in Option I.

B. Calculate the pressure at i,j.

Alternate Method I (Similar to the method used in Option I)

$$P_{i,j} = P_F + 4.077 \times 10^{-10}\, \rho_{in} V_F^2 - \frac{8.954 \times 10^4}{\rho_{in}} \frac{w_{hsi}^2}{e_e^2}$$

$$- \frac{2.238 \times 10^6}{\rho_{i,j}} \frac{w_{hsi}^2}{D_{min,i,j}^2} - 1.152 \times 10^8 \frac{U_7 F \mu_{ave,i}^{0.2} w_{hsi}^{1.8}}{\rho_{ave,i}} \cdot$$

$$\cdot \left\{ \sum_{\substack{g=1 \\ \text{For all } z_g < z_j}}^{g} \frac{\lambda_g}{\left[D_{li,g} - e + e_{min}\right]^3} \left[ \frac{1 + \frac{1}{2}\left(\frac{\Delta D}{D_{li,g} - e + e_{min}}\right)^2}{\left\{1 - \left(\frac{\Delta D}{D_{li,g} - e + e_{min}}\right)^2\right\}^{5/2}} \right] \right.$$

$$\left. + \frac{z_j - z_g}{\left[D_{li,g} - e + e_{min}\right]^3} \left[ \frac{1 + \frac{1}{2}\left(\frac{\Delta D}{D_{li,g} - e + e_{min}}\right)^2}{\left\{1 - \left(\frac{\Delta D}{D_{li,g} - e + e_{min}}\right)^2\right\}^{5/2}} \right] \right\} \qquad \text{(A-71)}$$

Use the narrow channel conditions for the hot channel for all cases; use the wide channel conditions for the cold channel for $\xi_1 = \xi_2 = 1$; use the narrow channel conditions for the cold channel for $\xi_3 = \xi_4 = 1$.

Alternate Method II

$$P_{i,j} = P_F + 4.077 \times 10^{-10} \rho_{in} V_F^2 - \frac{8.954 \times 10^4}{\rho_{in}} \frac{w_{hsi}^2}{e_e^2}$$

$$- \frac{2.238 \times 10^6}{\rho_{i,j}} \frac{w_{hsi}^2}{D_{min,i,j}^2} - 9.218 \times 10^8 \frac{U_7 F \mu_{ave,i}^{0.2} w_{hsi}^{1.8}}{\rho_{ave,i}} \cdot \qquad \text{(A-71)}$$

$$\cdot \sum_{j=2}^{n} \frac{\Delta z_j}{\left[D_{i,j-1} + D_{i,j} - 2e + 2e_{min}\right]^3}$$

where the hot and the cold channels are defined to be identical to those defined for equation (A-71) in Alternate Method I.

C through G. Identical to steps XXIV.Burnout Option.C through G.

XXIV. Incipient Boiling Option

Calculate the incipient boiling surface temperature $T_{Sib,i,j}$ at each location i,j in the range i = 3 to i = m − 2.

A. Identical to step XXIV.A in the burnout option.

B. Identical to step XXIV.B in the burnout option.

C. Identical to step XXIV.C in the burnout option.

D. Identical to step XXIV.Incipient Boiling Option.D in Option I.

XXV. Identical to step XXV in Option I.

# Appendix B

## DERIVATION OF THE EQUATIONS FOR THE OVERALL CORE FLOW RATES AND PRESSURE DROPS, AND METHODS OF MEASURING THESE QUANTITIES

The following are the derivations of the equations for the overall core flow rates and pressure drops, and the methods of measuring these quantities. The derivation of these equations is discussed first, but the flow distribution of the coolant water within the fuel element coolant channels is not considered here. This subject is discussed in Appendix C. The methods available for measuring the overall core flow rates and pressure drops are described in the latter part of this appendix.

### Fuel Element Flow Rate

The flow rate through an average coolant channel of the inner fuel element is $w_{A\ inner}$ lb/sec and that through an average coolant channel of the outer fuel element is $w_{A\ outer}$ lb/sec. Since the inner element has 171 coolant channels and the outer element has 369 coolant channels,[23] the total volumetric flow rate through the two fuel elements is

$$V_F = \frac{448.83}{\rho_{in}} \left[171 w_{A\ inner} + 369 w_{A\ outer}\right] \tag{B-1}$$

where

$\rho_{in}$ = lb/ft$^3$,
$V_F$ = gpm.

It was assumed that the presence of the narrow and wide coolant channels in the fuel elements had no influence on this particular flow rate.

### Fuel Element Labyrinth Flow Rate

The flow rates through the labyrinth between the two fuel elements have measured experimentally,[45] and they are shown in Fig. B-1. An equation describing these results is

$$\Delta H = 0.0192\ V_{lab}^{1.85}$$

or (B-2)

$$V_{lab} = 124.3 \left[\frac{\Delta P_F}{\rho_{in}}\right]^{0.5405}$$

where

$V_{lab}$ = gpm
$\Delta P_F$ = psi
$\rho_{in}$ = lb/ft$^3$.

Fuel Assembly Flow Rate

The flow rate through the entire fuel assembly is simply the sum of the flow rates through the fuel elements and the fuel element labyrinth.

$$V_{AS} = V_{lab} + V_F \tag{B-3}$$

Core Pressure Difference

The core pressure difference is defined as the difference in the static pressure at a point in the reactor vessel just upstream of the core shroud inlet and a point just downstream of the fuel assembly. Differences in the static head just upstream of the shroud inlet and the bottom of the narrow part of the inner shroud were determined experimentally, and they are shown in Fig. B-2. An equation describing these results is

$$\Delta H = 8 \times 10^{-8} V_{AS}^2 \tag{B-4}$$

The flow area between the narrow part of the inner shroud and the target tower is 156.2 in.$^2$ and that in the fuel elements just above the fuel plates is 165.1 in.$^2$ Ignoring the friction loss between the bottom of the narrow part of the inner shroud and the top of the fuel plates and correcting for the difference in the flow areas, the core inlet pressure difference is

$$\Delta P_{inlet} = \frac{7 \times 10^{-8} \rho_{in}}{144} V_{AS}^2 = 4.86 \times 10^{-10} \rho_{in} V_{AS}^2 \tag{B-5}$$

The core pressure difference is then simply the sum of the core inlet pressure difference and the fuel element pressure drop.

$$\Delta P_{core} = \Delta P_F + \Delta P_{inlet}$$

$$= \Delta P_F + 4.86 \times 10^{-10} \rho_{in} V_{AS}^2 \qquad \text{(B-6)}$$

Flow Rate in Annulus Between Target Bundle and Inner Fuel Element

Coolant flow rates through the target holder outside of the target rod hex cans have been determined experimentally by Kedl,[46] and they are shown in Fig. B-3. These results are a function of the head difference across the target holder, and they can be correlated by the relation

$$\Delta H = 9.42 \times 10^{-3} V_{ii}^2 \qquad \text{(B-7)}$$

where

$\Delta H$ = ft $H_2O$

$V$ = gpm.

These results must be correlated with the core pressure drop in order to be useful in this analysis. Other available data regarding the target region flow rates are the target rod coolant flow rates shown in Fig. B-4 and the total target region coolant flow rates shown in Fig. B-5. Data in Fig. B-4 are correlated by

$$\Delta H = \frac{144}{61.78} \Delta p = \frac{144}{61.78} \left(2.06 \times 10^{-4}\right) V_{rods}^{1.828} = 4.802 \times 10^{-4} V_{rods}^{1.828} \qquad \text{(B-8)}$$

where

$\Delta H$ = ft $H_2O$

$\Delta p$ = psi

$V_{rods}$ = gpm

and those in Fig. B-5 are correlated by

$$\Delta H_{core} = 6.46 \times 10^{-4} V_{target}^{1.933} \qquad \text{(B-9)}$$

where

$\Delta H_{core}$ = ft $H_2O$

$V_{target}$ = gpm.

Since the head loss through the target bundle and the target rods are identical, Equations (B-7) and (B-8) can be combined to give

$$V_{rods} = 5.095\ V_{ii}^{1.094} \tag{B-10}$$

The flow rate through the target holder then can be related to the total flow rate through the target region by the relation

$$V_{target} = V_{rods} + V_{holder} = 5.095\ V_{ii}^{1.094} + V_{ii} \tag{B-11}$$

Combining Equations (B-9) and (B-11), the flow rate through the target holder as function of the core pressure difference is

$$\Delta P_{core} = \frac{61.78}{144}\ \Delta H_{core} = \frac{61.78}{144}\ \left(6.46 \times 10^{-4}\right)\left[5.095\ V_{ii}^{1.094} + V_{ii}\right]^{1.933}$$

or (B-12)

$$5.095\ V_{ii}^{1.094} + V_{ii} = 69.20\ \Delta P_{core}^{0.5173}\ .$$

Control Region Flow Rate

Pressure drop data have been obtained for the outer shroud flange, the beryllium reflector, and the control region. The data for the outer shroud flange and the beryllium reflector are shown in Figs. B-6 and B-7. For the control region, the pressure drop data can be described by the relation

$$\Delta P = 7\left(\frac{V_C}{1075}\right)^{1.75} \tag{B-13}$$

where

$\Delta P$ = psi,

$V_C$ = gpm.

Since the coolants for the control region and the beryllium reflector have common inlet and exit plenums, the pressure drops through these two regions are identical. The information in Fig. B-8 was calculated from the above data by adding the flow rates through the control and reflector regions for a given control region pressure drop and using this sum of the flow rates to get the pressure drop across the outer shroud flange from Fig. B-6. (Density of water assumed to be that at 120°F and 600 psia, which is 61.86 $lb/ft^3$.) The core pressure difference is then the sum of the control region and the outer shroud flange pressure drops. Results shown in Fig. B-8 can be correlated by the relation

$$V_C = 36.6\ \Delta P_{core}^{0.725} \qquad \text{(B-14)}$$

where

$V_C$ = gpm,

$\Delta P_{core}$ = psi.

Location of Pressure Taps in the Reactor Vessel

The HFIR reactor vessel is fitted with a number of pressure taps as shown in Fig. B-9 to permit measurement of the coolant flow distribution and the pressure drops within this vessel. The term "N-16 Pressure" in this figure is the impact pressure on the N-16 probes, and any of these four probes can be used for this purpose. These pressure taps are connected to either a differential pressure transmitter or a differential pressure gauge for the readout of these pressure drops. The specific pressure drops of interest here are:

1. Core pressure drop, RP4-RP3
2. Fuel element pressure drop, RP4-N16 Pressure
3. Pressure drop across the outer shroud flange, RP4-RP2.

In addition the coolant flows for the beam tubes and the engineering facilities are monitored by flow orifices read out on a Barton gauge.

Although not pertinent to the determination of the fuel assembly flow rates and pressure drops, the following differential pressures also can be measured:

1. Pressure difference between the reactor vessel upper plenum and the reflector upper plenum, RP4-RP1

2. Beryllium reflector pressure drop, RP1-RP3

3. Reactor vessel and the primary coolant strainer pressure drop, PdT-106

4. Primary coolant strainer pressure drop, PdT-103

The absolute pressure in the HFIR is normally measured just upstream of the primary coolant venturi, at PT-127. This is at a different location from reference absolute pressure used in this heat transfer analysis. The latter could be measured at tap RP4 if so desired, since an absolute pressure gauge could be connected to it. The total primary coolant flow is measured by a venturi located in the inlet primary coolant line, and the coolant temperatures are measured by gas-filled thermal bulbs located in the inlet and exit primary coolant lines.

## Overall Primary Coolant Flow Rate

The overall coolant flow rate is determined from the head difference measured across the primary coolant venturi, and the calibration curve for this venturi is shown in Fig. B-10. It can be seen that for a pipe Reynolds number greater than $3.8 \times 10^5$, the venturi coefficient has a constant value of 0.9823. For this situation, the venturi equation becomes

$$V_{tot} = 3.3889 \times 10^3 \sqrt{\Delta H} \qquad \text{(B-15)}$$

where

$V_{tot}$ = total primary coolant flow rate in gpm,
$\Delta H$ = venturi head difference in ft $H_2O$.

## Flow Rates Through the Beam Tubes, Engineering Facilities, and Vertical Facilities

In determining the flow rates through the fuel assembly from the total primary coolant flow rates, flow rates through the parts of the

reactor other than the fuel assembly must be known. Included are the experimental facilities which are the beam tubes, the engineering facilities, and the vertical facilities. The beam tube and the engineering facility coolant flow rates are determined from the measurements of the pressure drops across flow monitoring orifices installed for this purpose. The calibration curve for these orifices is shown in Fig. B-11. The primary coolant flow rates through the vertical facilities are determined from the core pressure drops measured between taps RP4 and RP3 using the calibration curve shown in Fig. B-12.

Determination of the Fuel Assembly Flow Rate

The fuel assembly flow rate, $V_{AS}$, is determined as follows:

1. Subtract the sum of the flow rates through the control-reflector region (determined from the pressure drop measured across the outer shroud flange, RP4-RP2, and the outer shroud flange calibration curve, Fig. B-6), beam tubes, engineering facilities, and the vertical facilities from the total flow rate. This difference is the sum of the fuel assembly and the target region flow rates, V gpm.

2. Estimate the fuel assembly flow rate, $V_{AS}$ gpm.

3. Determine the core head difference, $\Delta H_{core}$, from the differential pressure measurement (RP4-N16 Pressure) and this estimated flow rate, $V_{AS}$

$$\Delta H_{core} = (\text{RP4-N16 Pressure}) + 1.379 \times 10^{-7}\ V_{AS}^2 .$$

The quantity $1.379 \times 10^{-7}\ V_{AS}^2$ is equal to twice the velocity head at the top of the N-16 probes based on a flow area of 152.32 in.$^2$ This correction is necessary to account for the impact of the coolant on the end of the N-16 probes.

4. Determine the target region flow rate, $V_{target}$ gpm, by finding the difference of the flow rate calculated in step 1, V gpm, and the fuel assembly flow rate assumed in step 2, $V_{AS}$ gpm.

$$V_{target} = V - V_{AS}$$

5. Determine the core head difference across the target from the data in Fig. B-5. It should be noted that the quantity ($3.730 \times 10^{-6}\ V^2_{target}$), which is the velocity head in the target region at the bottom of the fuel grid assembly (flow area is 20.71 in.$^2$) is included in this head difference. It was added to the permanent head loss in the target region to get the core head difference which is used to obtain the target region flow rate.

6. Iterate steps 2 through 5 until the core head difference for the fuel assembly equals that for the target region. When they are equal, the following will have been found:

a. Fuel assembly flow rate, $V_{AS}$ gpm

b. Target region flow rate, $V_{target}$ gpm

c. Core head difference, $\Delta H_{core}$ ft.

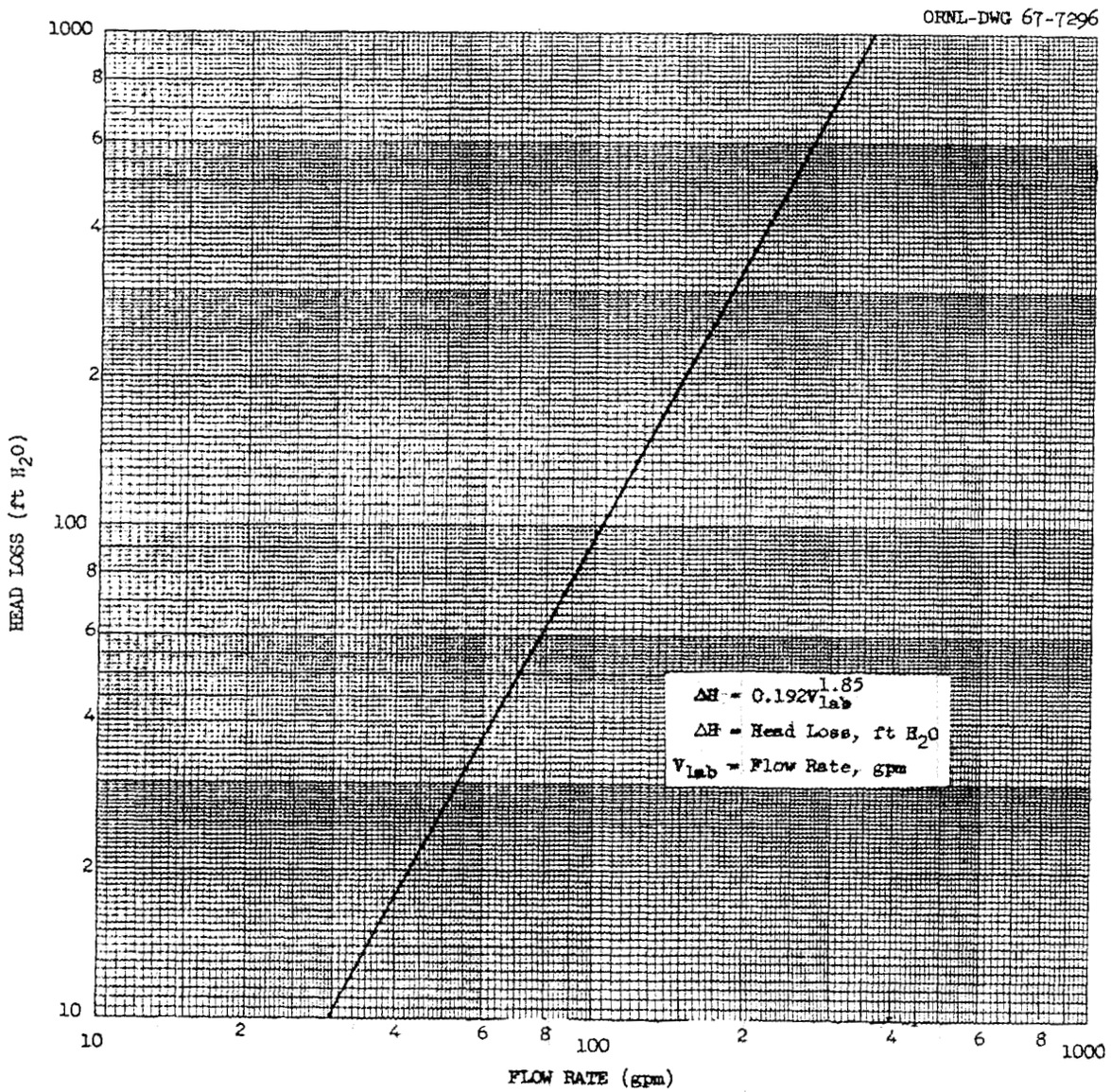


Fig. B-1. HFIR Fuel Assembly Labyrinth Flow Characteristics. (Ref. 45)

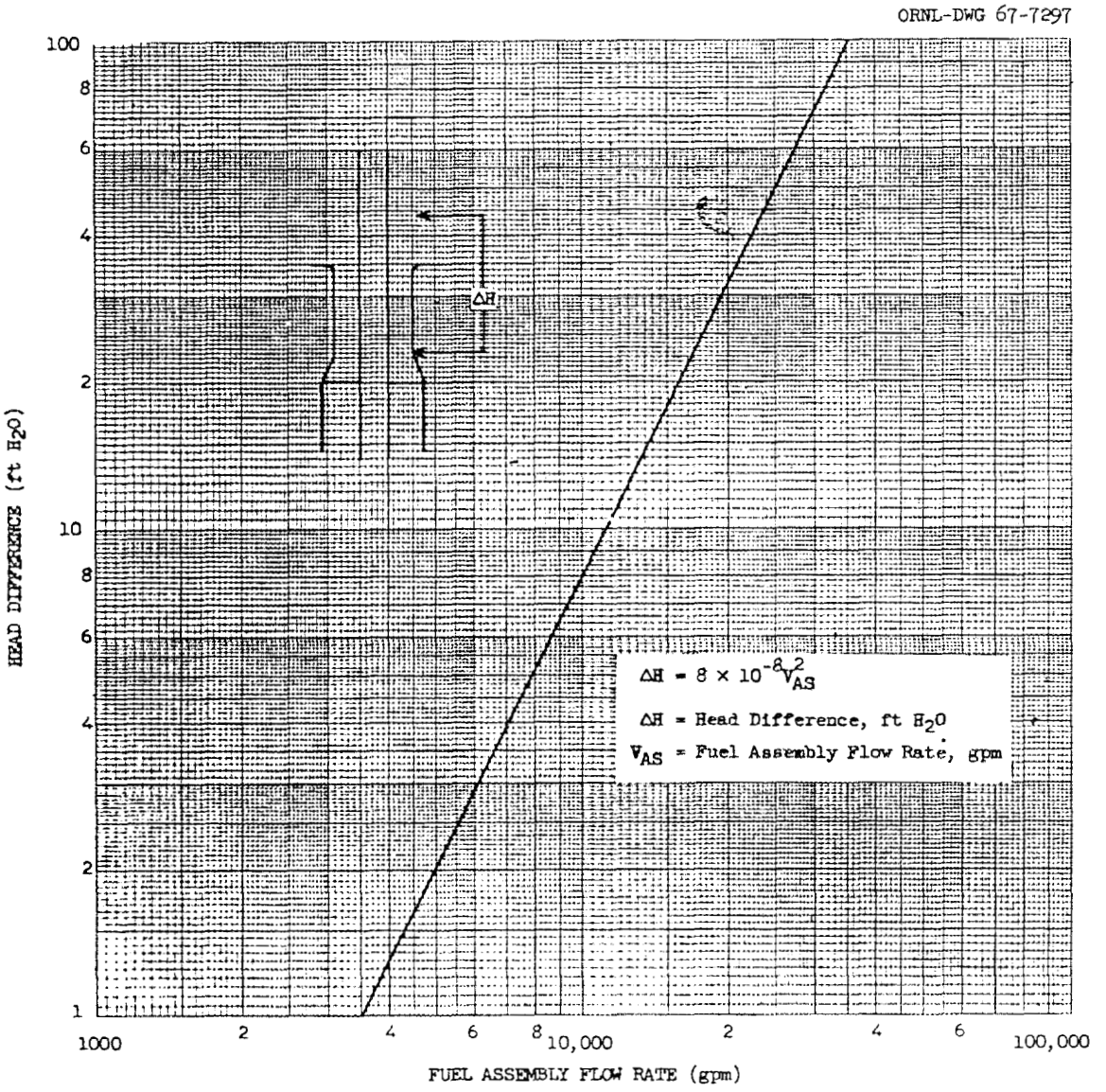


Fig. B-2. HFIR Shroud Inlet Flow Characteristics.

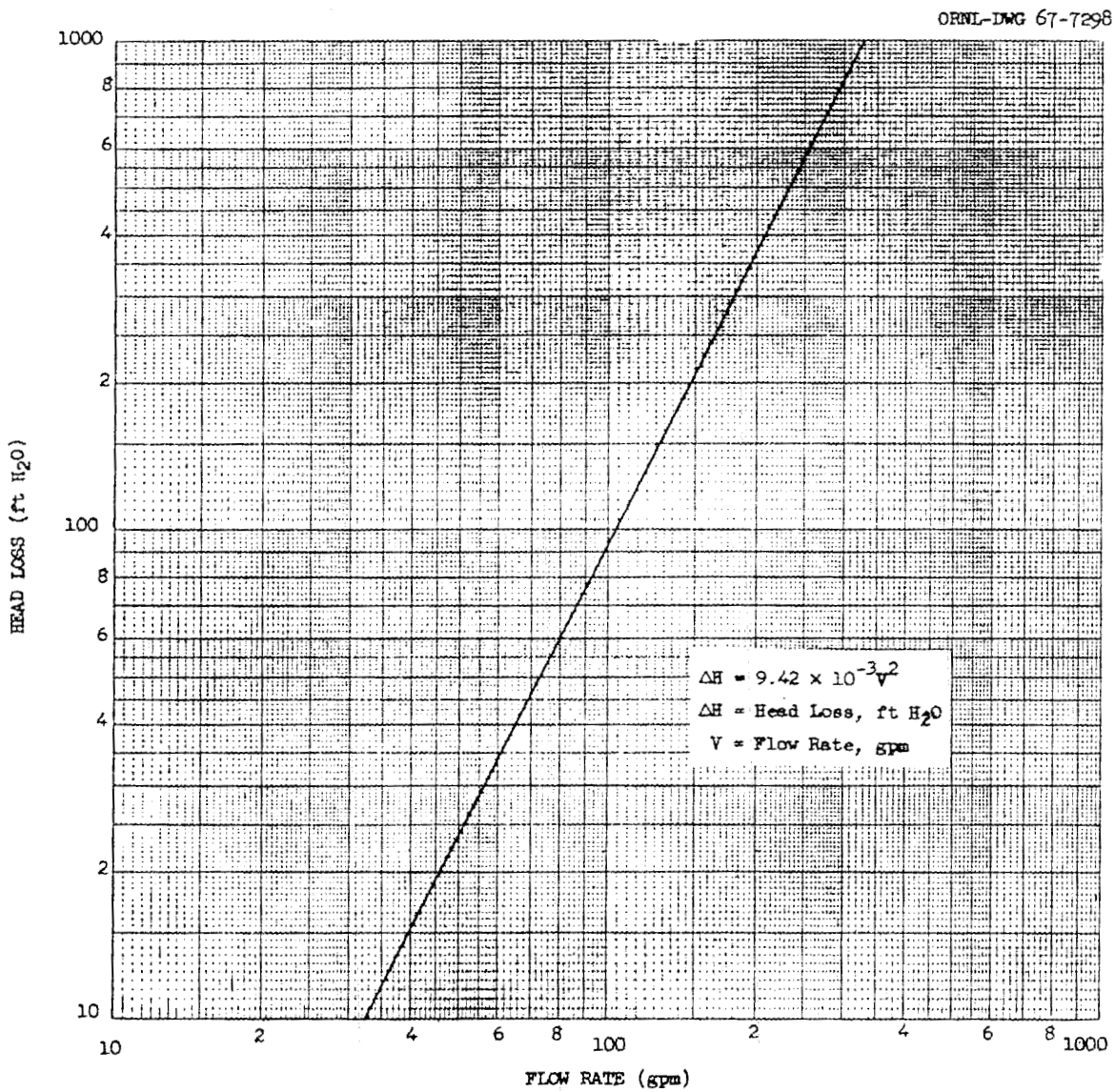


Fig. B-3. Target Holder Flow Rates (Excluding Flow Through the Target Rods). (Ref. 46)

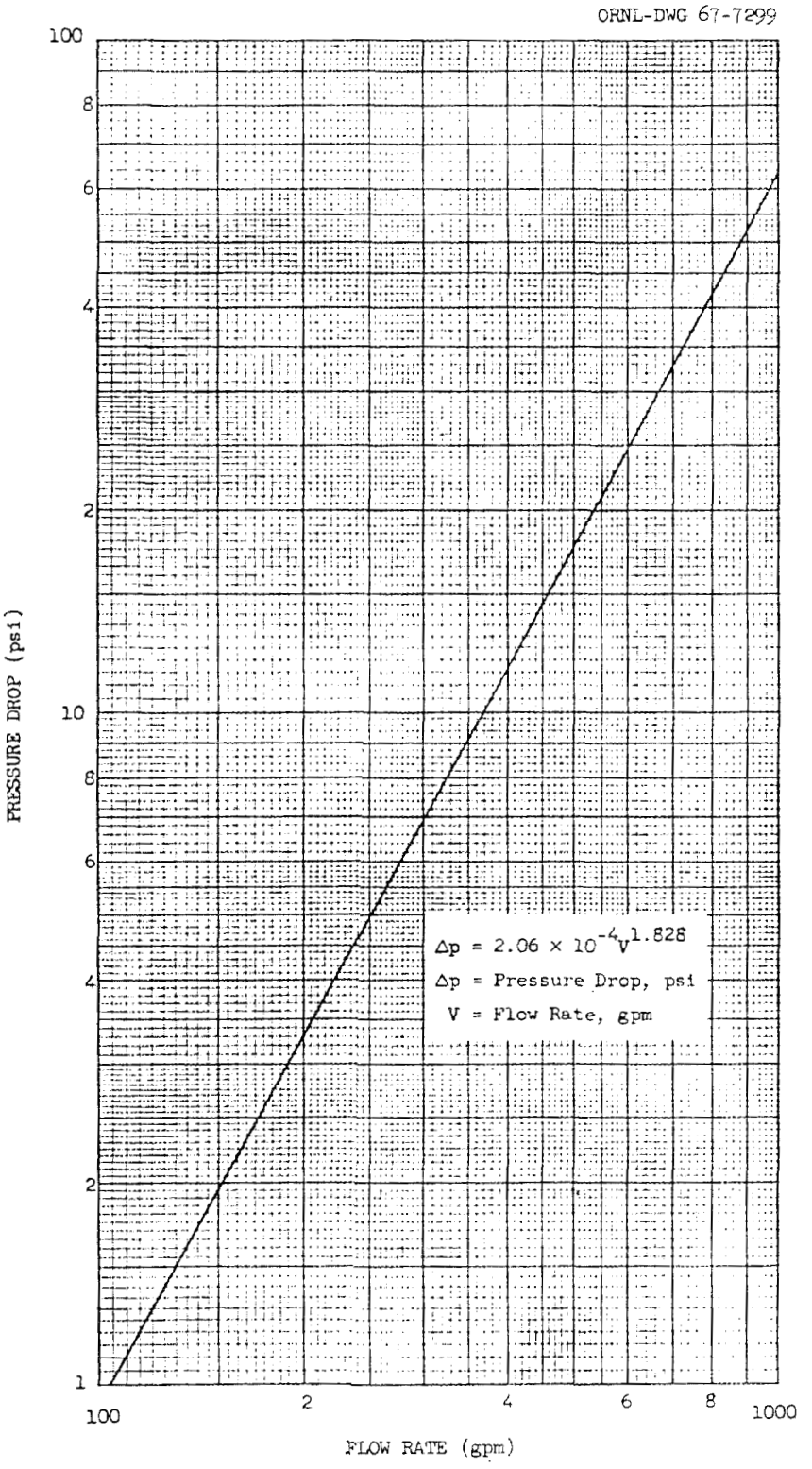


Fig. B-4. Target Rods Flow Rates at 125°F. ($\rho$ = 61.78 lb/ft$^3$)(Ref. 46)

ORNL-DWG 67-7300

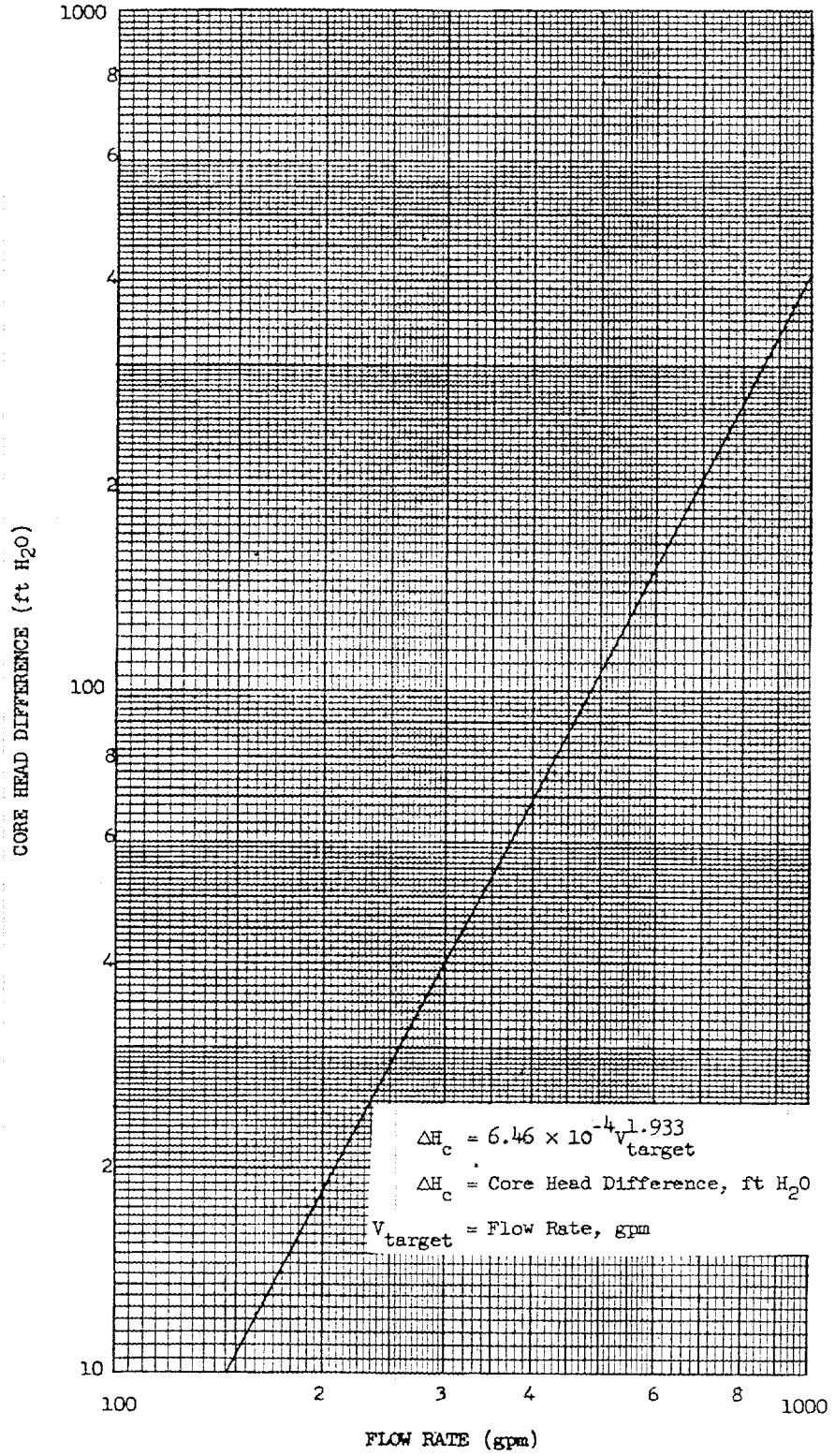


Fig. B-5. Total Target Region Flow Rates. (Ref. 46)

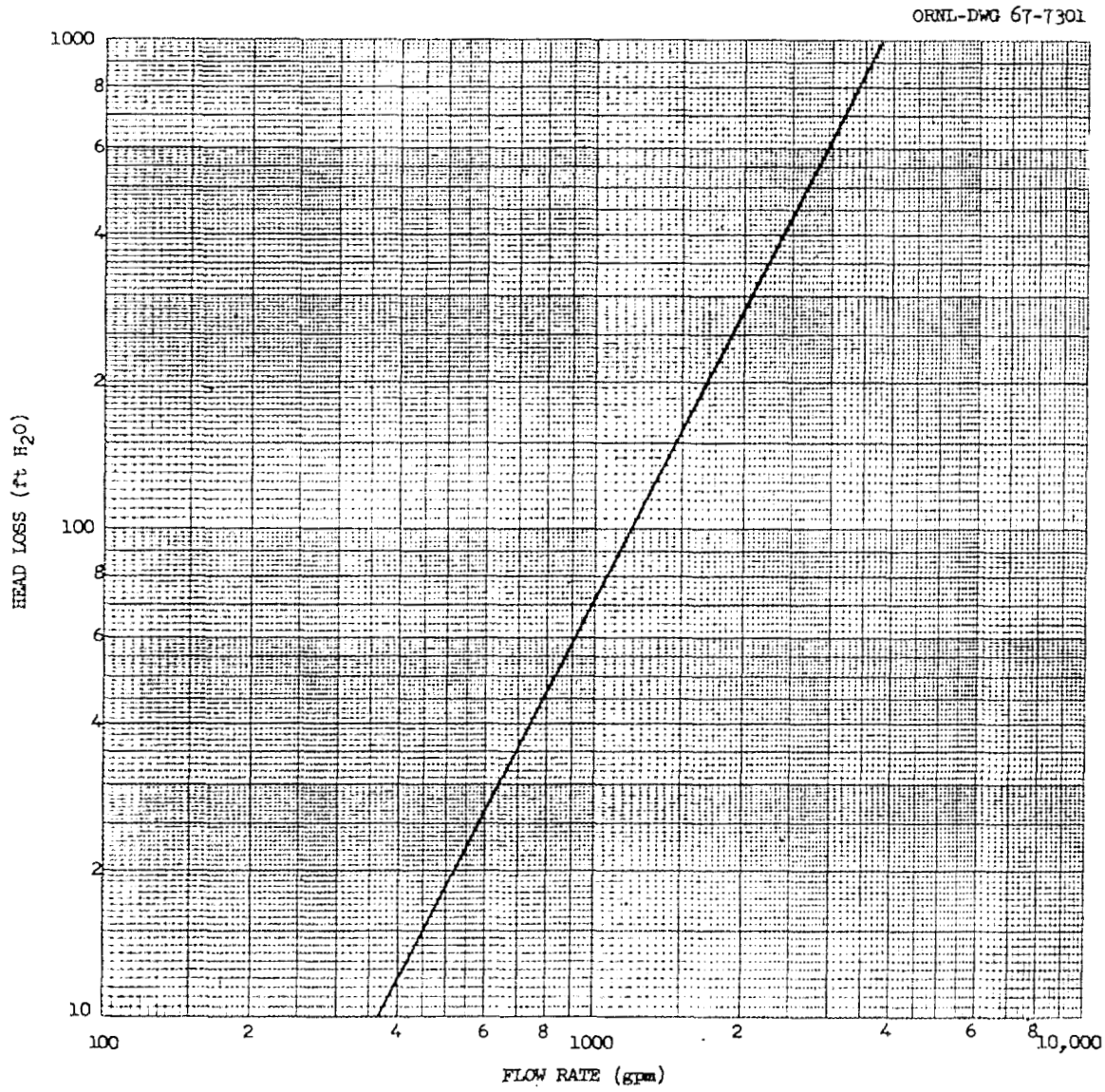


Fig. B-6. Coolant Flow Rates Through Outer Shroud Flange.

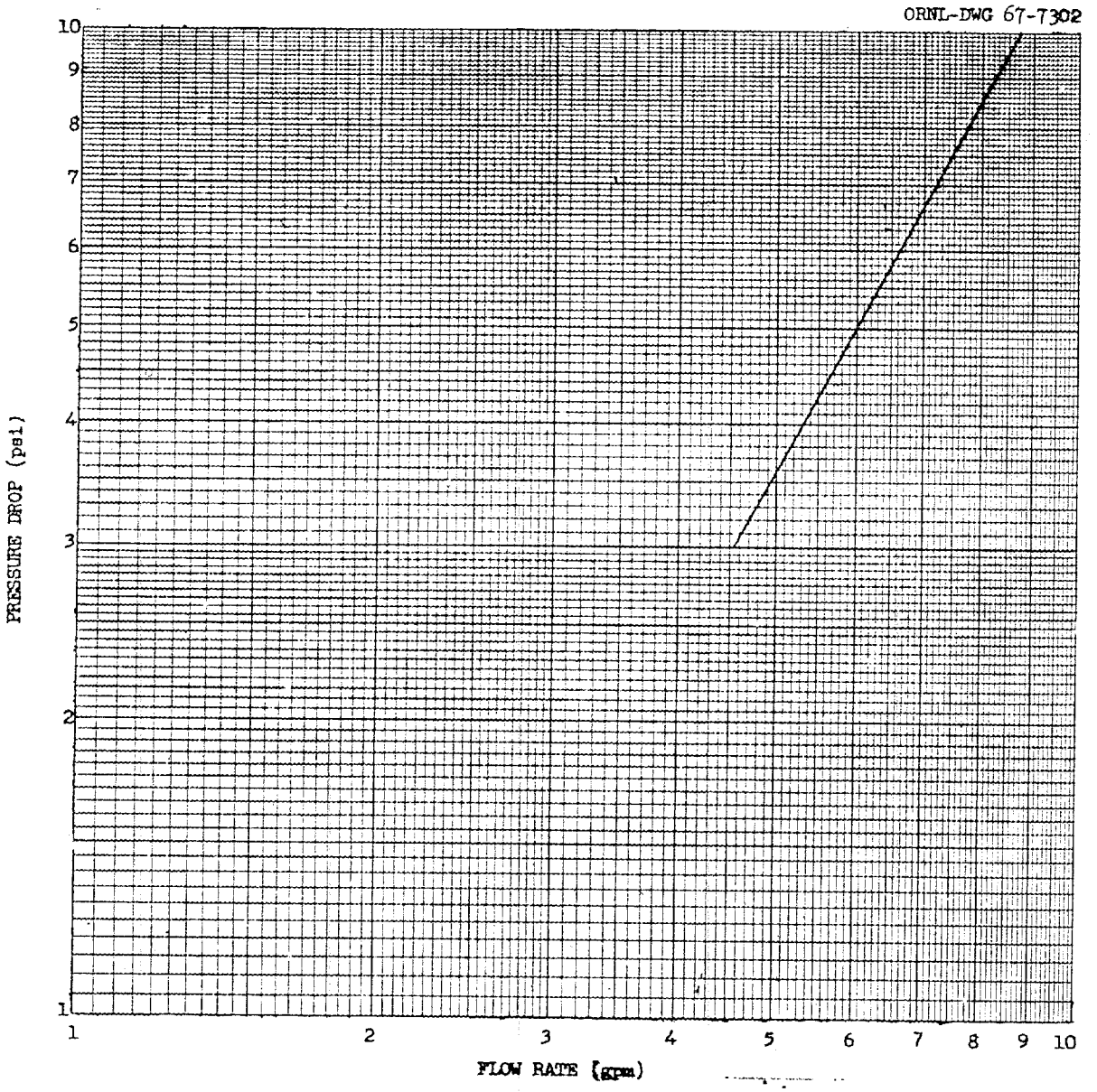


Fig. B-7. Beryllium Reflector Flow Rates.

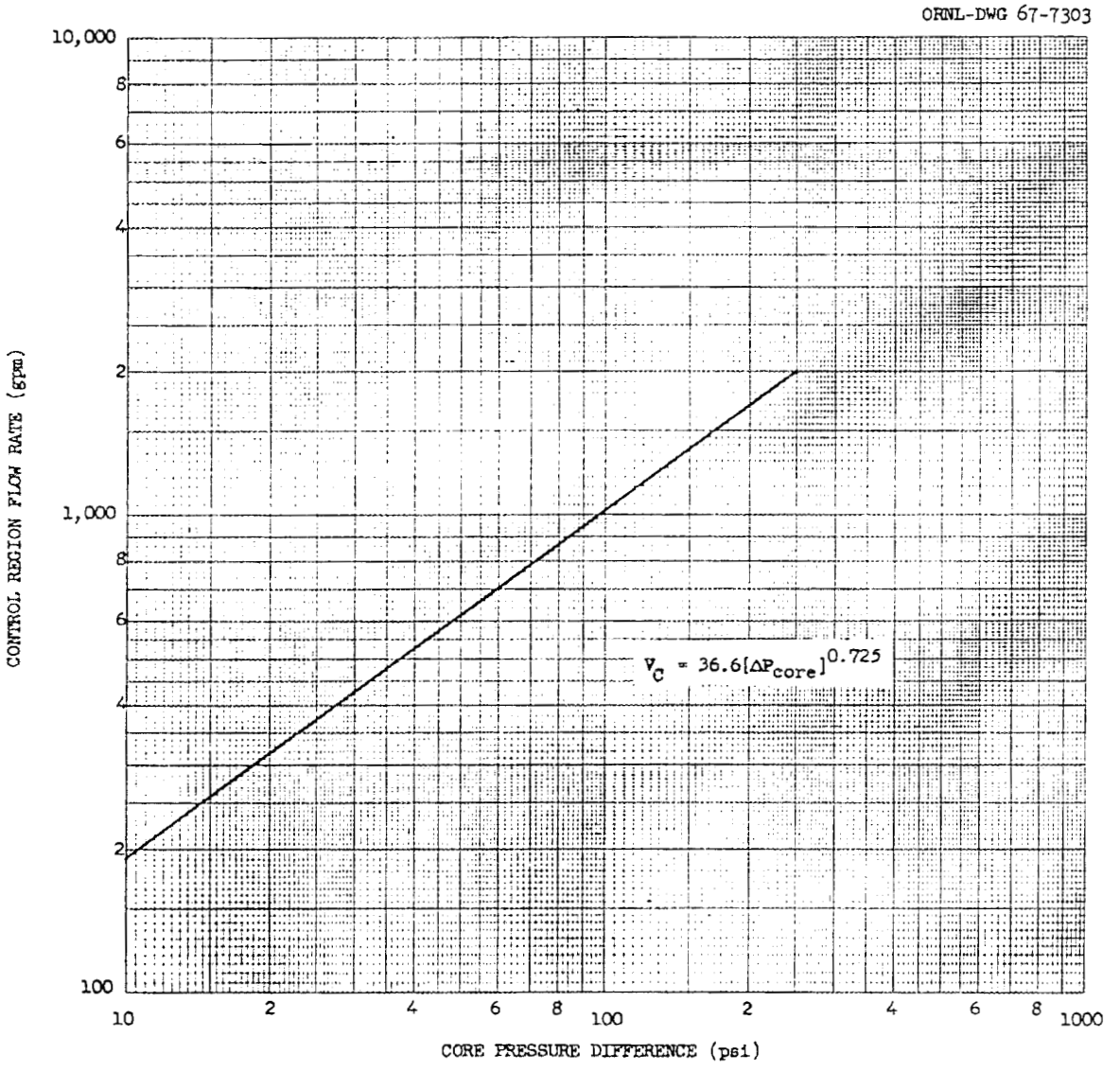


Fig. B-8. Control Region Flow Rates.

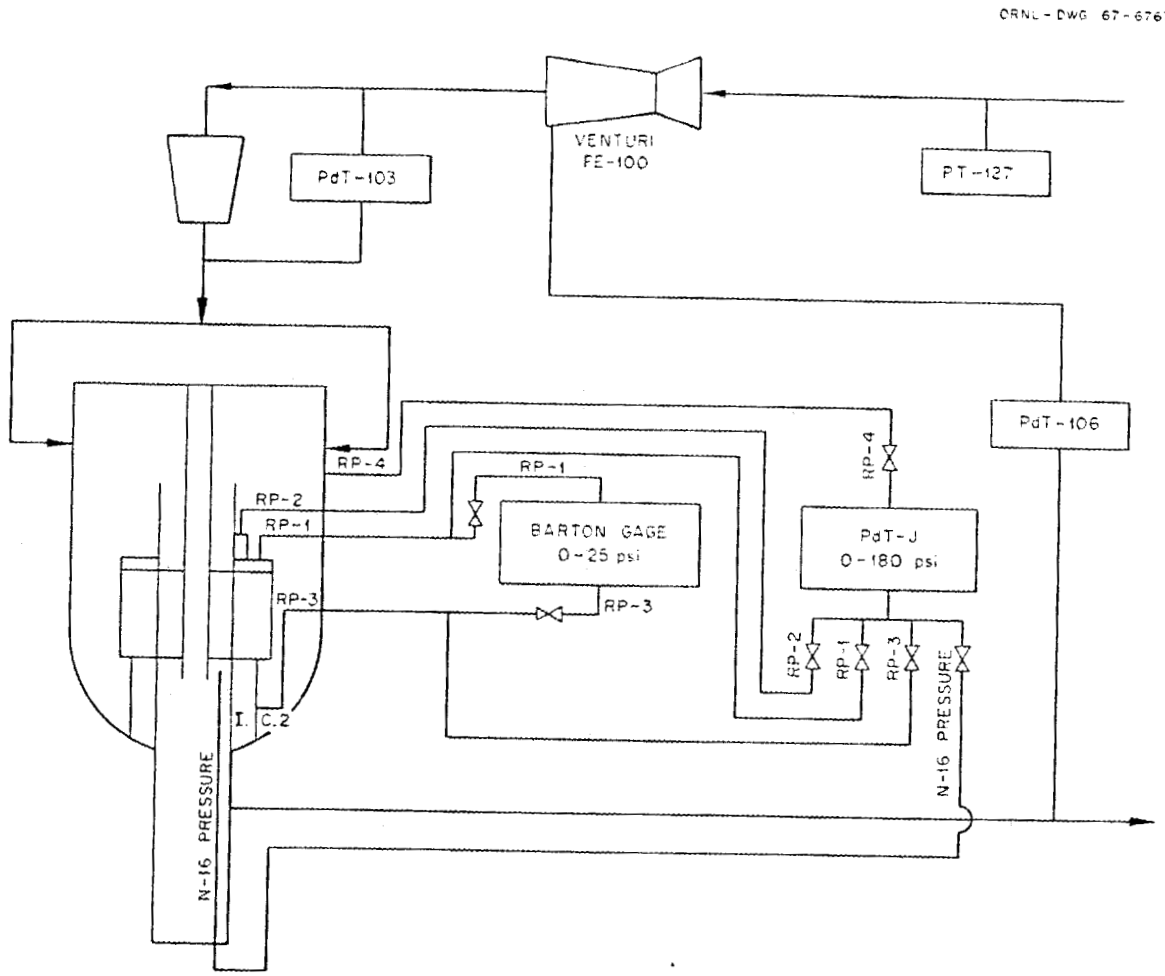


Fig. B-9. HFIR Reactor Vessel Pressure Taps and Associated Instrumentation.

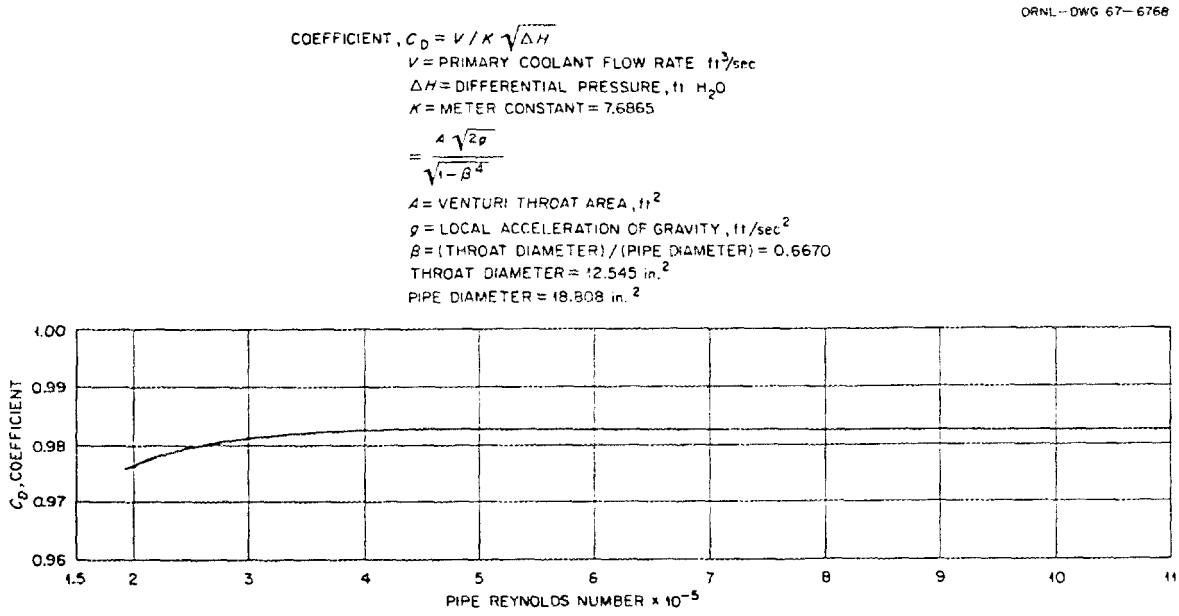


Fig. B-10. HFIR Primary Coolant Venturi Calibration. (Ref. 47)

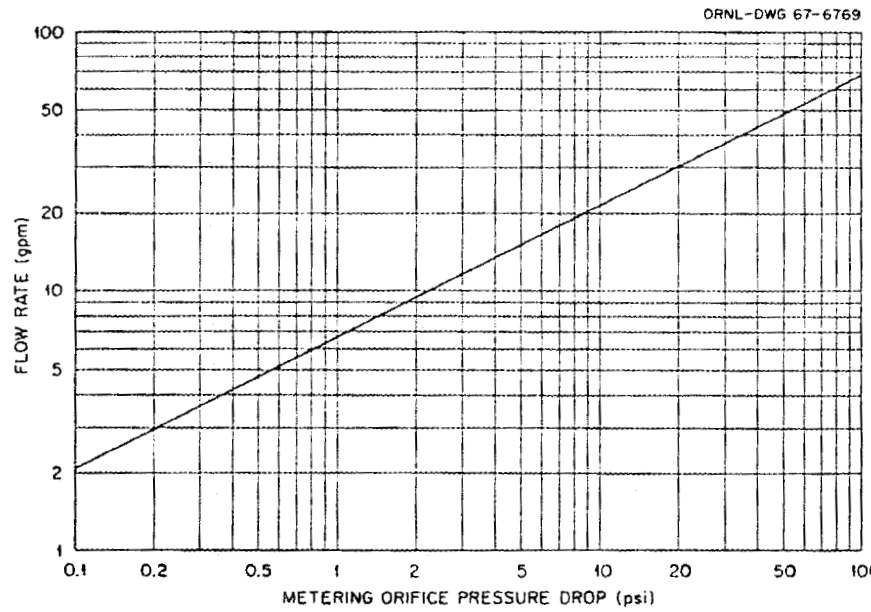


Fig. B-11. HFIR Beam Tube and Engineering Facility Metering Orifice Calibration. (Ref. 48)

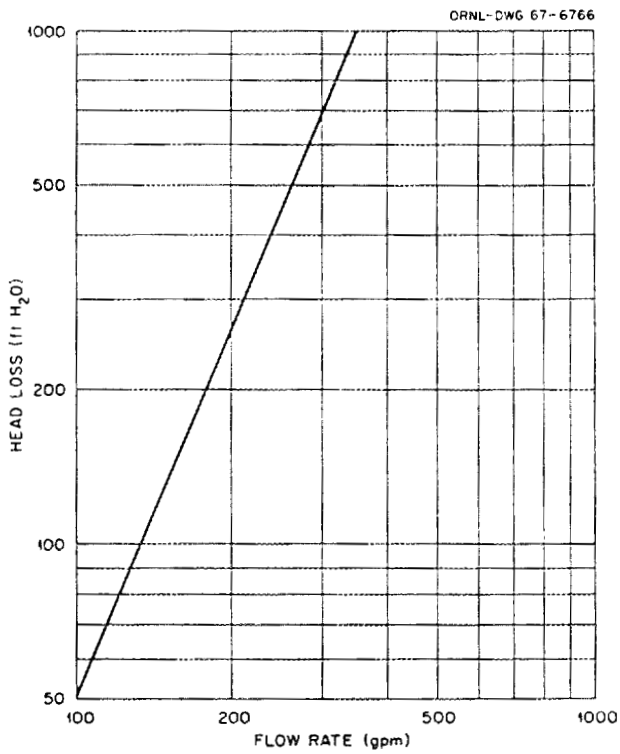


Fig. B-12. Head Loss versus Flow Rate in the HFIR Vertical Facilities.

# Appendix C

## DETAILS OF THE FUEL ELEMENT COOLANT CHANNEL FLOW EQUATIONS

### Basic Equations

One dimensional incompressible flow was assumed. Assuming that the channel inlet and exit loses are 0.04 and $(1 - A_1/A_2)^2$ velocity heads respectively,[26] and that the friction factor is $F/(Re)^{0.2}$, the pressure drop in a given coolant channel is

$$\Delta P_F = 0.04\, \rho_{in} \frac{v_{in}^2}{2g_c} + \left[1 - \frac{A_1}{A_2}\right]^2 \rho_{ex} \frac{v_{ex}^2}{2g_c} + \int_0^L \rho \frac{F}{(Re)^{0.2}} \frac{v^2}{2g_c} \frac{dz}{De} \qquad \text{(C-1)}$$

To get the absolute pressure at any point within the coolant channel, note should be made of the core inlet pressure difference derived in Appendix B.

$$\Delta P_{inlet} = 4.86 \times 10^{-10}\, \rho_{in} V_{AS}^2 \qquad \text{(B-5)}$$

and the velocity head just above the fuel plates (based on a 165.1 in.$^2$ flow area)

$$\frac{v^2}{2g_c} = 4.077 \times 10^{-10}\, \rho_{in} V_{AS}^2 \qquad \text{(C-2)}$$

If the absolute pressure in the reactor vessel plenum above the core inlet is P psia, the absolute pressure at any point within the coolant channel is

$$p = P + (4.077 - 4.86) \times 10^{-10}\, \rho_{in} V_{AS}^2 - 0.04\, \rho_{in} \frac{v_{in}^2}{2g_c} - \rho \frac{v^2}{2g_c} - \int_0^z \rho \frac{F}{(Re)^{0.2}} \frac{v^2}{2g_c} \frac{dz'}{De} \qquad \text{(C-3)}$$

For this analysis, it was assumed that the flow rate per unit width of the coolant channel is w lb/sec (in width), the local channel thickness is e mils, and the channel thickness at the inlet and outlet is $e_e$ mils. It was further assumed that the area ratio at the exit of the coolant channel is $e_e/(e_e + t)$ and that the friction factor has an uncertainty coefficient of U. Equation (C-1) for the pressure drop in the coolant channel then becomes

$$\Delta P_F = \left[\frac{8.953 \times 10^4}{\rho_{in}} + \frac{2.238 \times 10^6}{\rho_{ex}}\left(1 - \frac{e_e}{e_e + t}\right)^2\right]\frac{w^2}{e_e^2}$$

$$+ 1.152 \times 10^8 \frac{UF\mu_{ave}^{0.2} w^{1.8}}{\rho_{ave}} \int_0^L \frac{dz}{e^3} \quad \text{(C-4)}$$

and Eq. (C-2) for the absolute pressure at any point within the coolant channel becomes

$$p = P + (4.077 - 4.86) \times 10^{-10} \rho_{in} V_{AS}^2$$

$$- \frac{8.953 \times 10^4}{\rho_{in}} \frac{w^2}{e_e^2} - \frac{2.238 \times 10^6}{\rho} \frac{w^2}{e_e^2}$$

$$- 1.152 \times 10^8 \frac{UF\mu_{ave}^{0.2} w^{1.8}}{\rho_{ave}} \int_0^z \frac{dz'}{e^3} \quad \text{(C-5)}$$

Coolant Channels with Gradually Varying Thicknesses

For coolant channels whose thicknesses change gradually down the length, the integrals in Eqs. (C-4) and (C-5) are approximated by the relations

$$\int_0^L \frac{dz}{e} \approx \sum_{j=2}^{n} \frac{8\Delta z_j}{\left[e_{j-1} + e_j\right]^3} \quad \text{(C-6)}$$

and

$$\int_0^z \frac{dz'}{e} \approx \sum_{j=2}^{j} \frac{8\Delta z_j}{\left[e_{j-1} + e_j\right]^3} \tag{C-7}$$

respectively.

Coolant Channels with Sinusoidal Walls

The thicknesses of coolant channels with sinusoidal walls can be described by a relation of the form

$$e = A - B\,\frac{2\pi z}{\lambda} \tag{C-8}$$

For a given wavelength of the coolant channel $\lambda$ assuming the quantities A and B to be constant, the integral in Eqs. (C-4) and (C-5) can be evaluated analytically. This was done by Chapman[50] using the theory of residues,[51] and his result is

$$\int_0^\lambda \frac{dz}{e^3} = \int_0^\lambda \frac{dz}{\left[A - B \sin \frac{2\pi z}{\lambda}\right]^3}$$

$$= \frac{\lambda}{A^3}\left[\frac{1 + \frac{1}{2}\frac{B^2}{A^2}}{\left(1 - \frac{B^2}{A^2}\right)^{5/2}}\right] \tag{C-9}$$

Assuming that the values of A and B remain constant for each segmental length of channel $\lambda_g$, the integrals in Eqs. (C-4) and (C-5) can be approximated by the relations

$$\int_0^L \frac{dz}{e^3} \approx \sum_{g=1}^{L/\lambda} \frac{\lambda_g}{A_g^3}\left[\frac{1 + \frac{1}{2}\frac{B_g^2}{A_g^2}}{\left(1 - \frac{B_g^2}{A_g^3}\right)^{5/2}}\right]$$

and

$$\int_0^z \frac{dz'}{e^3} \approx \sum_{\substack{g'=1 \\ \text{all} \\ z_{g'}<z_j}}^{g'=g} \frac{\lambda_{g'}}{A_{g'}^3} \left[ \frac{1 + \frac{1}{2}\frac{B_{g'}^2}{A_{g'}^2}}{\left(1 - \frac{B_{g'}^2}{A_{g'}^2}\right)^{5/2}} \right] + \frac{z_j - z_g}{A_g^3} \left[ \frac{1 + \frac{1}{2}\frac{B_g^2}{A_g^2}}{\left(1 - \frac{B_g^2}{A_g^2}\right)^{5/2}} \right] \tag{C-10}$$

respectively.

Total Coolant Channel Flow Rates

The flow rates per unit width of the coolant channel $w_i$ are calculated at several positions along the width of this channel. These values are then weighted by the appropriate channel widths and summed to give the total coolant flow rate through the channel. An equation describing this is

$$w_A = \sum_{i=1}^{m} w_{Ai} \left[ \frac{\Delta s_i + \Delta s_{i+1}}{2} \right] \tag{C-11}$$

where $\Delta s_{m+1}$ is defined to be zero.

Pressure Difference Across a Fuel Plate Between a Narrow Channel and a Wide Channel

Since the flow rates in the narrow and the wide coolant channels will be different, a pressure difference will exist across a fuel plate between these channels. For this analysis, this is assumed to be the average of the pressure difference just below the coolant channel inlets and that just above the coolant channel exits. The influences of the local deflections along the length of the fuel plate have been ignored. The pressure difference just below the coolant channel inlets is

$$\Delta P_{inlet} = \frac{1.04\rho_{in}}{2g_c} \left[ v_w^2 - v_n^2 \right] \tag{C-12}$$

and that just above the exits is

$$\Delta P_{exit} = \left[1 - \left(1 - \frac{e_{we}}{e_{we} + t}\right)^2\right] \frac{\rho_{wex} v_w^2}{2g_c} - \left[1 - \left(1 - \frac{e_{ne}}{e_{ne} + t}\right)^2\right] \frac{\rho_{nex} v_n^2}{2g_c} \quad \text{(C-13)}$$

Therefore the average pressure difference at any position along the width of the fuel plate is

$$\Delta P_{nwi} = \frac{\Delta P_{inlet} + \Delta P_{exit}}{2}$$

$$= 1.119 \times 10^6 \left\{ \frac{w_{wi}^2}{e_{we}^2} \left[ \frac{1.04}{\rho_{in}} + \frac{1}{\rho_{ex,w,i}} - \frac{1}{\rho_{ex,w,i}} \left(1 - \frac{e_{we}}{e_{we} + t}\right)^2 \right] - \frac{w_{ni}^2}{e_{ne}^2} \left[ \frac{1.04}{\rho_{in}} + \frac{1}{\rho_{ex,n,i}} - \frac{1}{\rho_{ex,n,i}} \left(1 - \frac{e_{ne}}{e_{ne} + t}\right)^2 \right] \right\} \quad \text{(C-14)}$$

and the average pressure difference for the entire fuel plate is

$$\Delta P_{nw} = \frac{\sum_{i=4}^{m-2} \left[ \frac{\Delta P_{nw,i-1} + \Delta P_{nw,i}}{2} \right] \Delta s_i}{\sum_{i=4}^{m-2} \Delta s_i} \quad \text{(C-15)}$$

# Appendix D

## ESTIMATE OF THE REDUCTION OF THE LONGITUDINAL DEFLECTION OF THE FUEL PLATES DUE TO THE STRETCHING OF THE SIDE PLATES

Preliminary calculations indicate that the difference between the temperature at the lower end of the average fuel plate and that at the lower end of the side plates for 100 Mw reactor operation is about 100 °F. This difference between the lower end of the hot fuel plate and the side plate is about 170 °F.

The heat transfer analysis assumes that the longitudinal deflection of the fuel plate is based on a thermal expansion of

$$170\alpha L \tag{D-1}$$

where

$\alpha$ is the thermal coefficient of expansion of the fuel plate material

L is the length of the fuel plate.

To estimate the stretching of the side plates due to the expansion of the average fuel plates, an estimate must be made of the heated (fuel plate containing the fuel bearing material) cross section and the unheated cross section of the fuel elements. For the inner fuel element, the heated cross section is estimated to be

$$\frac{1}{2}\frac{\pi}{4}\left[(9.9152)^2 - (5.6220)^2\right] = 26.19 \text{ in}^2 \tag{D-2}$$

and the unheated cross section is estimated to be

$$\frac{\pi}{4}\left[(5.443)^2 - (5.067)^2\right] + \frac{1}{2}\frac{\pi}{4}\left[(5.622)^2 - (5.443)^2\right]$$

$$+ \frac{1}{2}\frac{\pi}{4}\left[(10.074)^2 - (9.9152)^2\right] + \frac{\pi}{4}\left[(10.590)^2 - (10.074)^2\right] \tag{D-3}$$

$$= 13.50 \text{ in}^2$$

Similarly for the outer fuel element, the heated cross section estimated to be

$$\frac{1}{2}\frac{\pi}{4}\left[(16.5334)^2 - (11.8938)^2\right] = 51.79 \text{ in}^2 \tag{D-4}$$

and the unheated cross section is estimated to be

$$\frac{\pi}{4}\left[(11.746)^2 - (11.250)^2\right] + \frac{1}{2}\frac{\pi}{4}\left[(11.8938)^2 - (11.746)^2\right]$$
$$+ \frac{1}{2}\frac{\pi}{4}\left[(16.622)^2 - (16.5334)^2\right] + \frac{\pi}{4}\left[(17.134)^2 - (16.622)^2\right] \tag{D-5}$$
$$= 25.06 \text{ in}^2$$

If simple force balances based on these areas are assumed for the inner and the outer fuel elements, the inner fuel element side plates would stretch

$$\frac{(26.19)\ \alpha L}{(26.19 + 13.50)}(100) = 66\alpha L \tag{D-6}$$

and the outer element side plates would stretch

$$\frac{(51.79)\ \alpha L}{(51.79 + 25.06)}(100) = 67\alpha L \tag{D-7}$$

Combining equations (D-1), (D-6) and (D-7), the longitudinal fuel plate deflections assumed for this heat transfer analysis probably would be lower by

$$\frac{66\alpha L}{170\alpha L}(100) = 38\% \tag{D-8}$$

# Appendix E

## DERIVATION OF THE SIDE PLATE TEMPERATURE EQUATIONS

The following are the derivations and the reasoning for the equations used for calculating the fuel element side plate temperatures. Some of the assumptions are somewhat arbitrary, but they are felt to be conservative and do not have a significant effect on the overall results.

### Basic Equations

For the purpose of heat transfer calculations, the side plates were regarded as slabs. Calculations by Hilvety and Chapman[4] and later by Haack[52] indicated that this is a good assumption provided that one half of the normal fuel element coolant channel heat transfer coefficient is used on the fuel plate side of the side plates. The effect of the lower heat transfer coefficients in the corners of the fuel element coolant channels were ignored in Haack's calculations. Therefore the slab model should yield low side plate temperatures which is a conservative assumption.

Equations for heat transfer from a slab with internal heat generation may be found in most heat transfer texts. For a slab of thickness $\tau$ with an internal heat generation rate of $Q_{SP}Q/100$ and cooled by convection on both sides, the temperature distribution is[53]

$$t = \frac{-Q_{SP}Qx^2}{200k} + C_1x + C_2 \qquad \text{(E-1)}$$

where

$$C_1 = \frac{\dfrac{Q_{SP}Q\tau}{100h} + \dfrac{Q_{SP}Q\tau^2}{200k} + T - \bar{T}}{\tau + \dfrac{k}{\bar{h}} + \dfrac{k}{h}} \qquad \text{(E-1a)}$$

$$C_2 = \frac{kC_1}{\bar{h}} + \bar{T} \qquad \text{(E-1b)}$$

where

$Q_{SP}$ = side plate heat generation rate at a reactor power level of 100 Mw

$Q$ = reactor power level

$k$ = thermal conductivity of the side plate material

$\bar{h}$ = effective heat transfer coefficient on the fuel plate side (Assumed to be one half of the normal fuel element coolant channel heat transfer coefficient)

$h$ = heat transfer coefficient on the other side of the slab

$\bar{T}$ = coolant temperature on the fuel plate side of the slab

$T$ = coolant temperature on the other side of the slab.

The side plate temperature is regarded as the average of the temperatures in this slab which is

$$T_{SP} = \frac{1}{\tau} \int_0^{\tau} t\,dx$$

$$= -\frac{Q_{SP} Q \tau^2}{600k} + \frac{C_1 \tau}{2} + C_2 \qquad \text{(E-2)}$$

The application of these equations with the appropriate values of the side plate thicknesses, thermal conductivity, and the uncertainty coefficients for the heat generation rates listed below are shown in Appendix A.

Side Plate Thicknesses

HFIR fuel element specifications[23] lists the side plate dimensions to be as follows:

Inner fuel element – Inner side plate

I. D. $5.067 \begin{smallmatrix} +0.010 \\ -0.000 \end{smallmatrix}$ in.

O. D. $5.443 \pm 0.001$ in.

Minimum thickness = 0.1825 in.

Inner fuel element – Outer side plate

I. D. 10.074 ± 0.001 in.

O. D. 10.590 ± 0.010 in.

Minimum thickness = 0.2525 in.

Outer fuel element – Inner side plate

I. D. 11.250 ± 0.010 in.

O. D. 11.746 ± 0.001 in.

Minimum thickness = 0.2425 in.

Outer fuel element – Outer side plate

I. D. 16.622 ± 0.001 in.

O. D. $17.134 \begin{smallmatrix} +0.010 \text{ in.} \\ -0.000 \text{ in.} \end{smallmatrix}$

Minimum thickness = 0.2455 in.

The values of the minimum thicknesses listed above are the values used for $\tau$ in Equations (E-1) and (E-3). This will tend to make the side plate temperatures slightly low which is conservative.

Other Related Factors

Since the side plate material is 6061 aluminum, the thermal conductivity of the slab was assumed to be 97 Btu/(hr)(ft)(°F) on the basis of the information in the Alcoa Aluminum Handbook.[42]

Uncertainty factors have been given to the reactor power level Q, the side plate heat generation rate $Q_{SP}$, and the coolant heat generation rate $Q_{H_2O}$. These are designated as $U_1$, $U_{16}$ and $U_{17}$, respectively, in the equations in Appendix A for calculating the side plate temperature.

Coolant Temperatures

The temperature of the bulk water flowing by the side plate is assumed to be dependent only on its flow rate and the heat generated in the side plate material and the coolant itself. On the fuel plate side, it is assumed that there is no mixing between the water cooling the side plate and that cooling the fuel bearing material. This of course is a conservative

assumption. The division of heat passing through each surface of the side plate must be considered in determining these coolant temperatures. From the two dimensional calculations of Haack,[49] the division of the heat flow for various coolant conditions were determined and they are shown in Table E-1. The heat transfer for the fuel plate coolant is about 15,000 Btu/(hr)(ft$^2$)(°F). That for coolant on the other side of the side plate is about 1000 Btu/(hr)(ft$^2$)(°F) for both plates of the inner fuel element and for the inner side plate of the outer fuel element. It is about 5000 Btu/(hr)(ft$^2$)(°F) for the outer side plate of the outer fuel element. From the inspection of the results shown in Table E-1, it was assumed for both side plates of the inner fuel element and for the inner side plate of the outer fuel element that 0.7 of the heat is transferred to the fuel plate coolant and 0.3 of the heat is transferred to the coolant on the other side. For the outer side plate of the outer fuel element, it was assumed that 0.5 of the heat is transferred to the fuel plate coolant and 0.5 of the heat is transferred to the coolant on the control region side.

The models used for calculating the heat balances on the coolant adjacent to the fuel plate side of the side plates are shown in Figs. E-1 and E-2. That shown in Fig. E-1 is for the inner side plates of the inner and outer fuel elements, and that shown in Fig. E-2 is for the outer side plate of the inner fuel element. The model for the outer side plate of the outer fuel element is identical to that in Fig. E-2 except that $0.7\tau$ is $0.5\tau$. Models for calculating the coolant temperatures of the coolant adjacent to the other side of the side plates are slabs having thicknesses of $0.3\tau$ for both side plates of the inner fuel element and for the inner side plate of the outer fuel element and $0.5\tau$ for the outer side plate of the outer fuel element.

A heat balance on the coolant on the fuel plate side of both side plates of the inner fuel element and on the inner side plate of the outer fuel element yields the relation

$$\Delta T = \frac{\left[0.7\tau\,(t + e_A) + t\Delta s\right]\dfrac{zQQ_{SP}}{100} + \dfrac{e_A \Delta s z Q Q_{SP}}{100}}{\left[\dfrac{w_1 + w_2}{2}\right]\Delta s} \qquad \text{(E-3)}$$

The relation for the outer side plate of the outer fuel element is identical to Equation (E-3) except that the term $0.7\tau$ is replaced by $0.5\tau$. Substituting the appropriate values for the side plate thicknesses conversion factors for the various dimensions, and the appropriate uncertainty factors, the relations for the temperatures of the fuel plate coolant next to the side plate shown as Equations (A-30), (A-38), and (A-43) in Appendix A, may be readily obtained from this equation.

To obtain the temperature of the coolant on the other side of the side plate, each case must be considered individually. The minimum flow area for the coolant passing between the inner fuel element and the target rods is estimated to be 7.867 in.$^2$ Assuming 0.3 of the heat generated in the side plate flows into this coolant, the temperature rise in this coolant is then

$$\frac{Q_{SP}Q}{100} 0.3\ A_{SP}z + \frac{Q_{H_2O}Q}{100} (7.867)\ z = V_{11}\rho_{in}\Delta T \qquad \text{(E-4)}$$

For the case of the coolant passing through the fuel element labyrinth, it was assumed that 0.3 of the heat generated in both the outer side plate of the inner fuel element and the inner side plate of the outer fuel element flows into it. From the side plate dimensions listed above, the flow area for this coolant is 10.98 in.$^2$ The temperature rise of this cooling water is then

$$\frac{Q_{SP}Q}{100} 0.3\ \left(A_{SPi} + A_{SPo}\right) z + \frac{Q_{H_2O}Q}{100} (10.98)\ z = V_{lab}\rho_{in}\Delta T \qquad \text{(E-5)}$$

The control region coolant removes some of the heat generated in the outer side plate of the outer fuel element. Calculations have shown that for 1080 gpm control region flow rate, the temperature rise of this coolant is about 30°F. This assumed that there was 4.2 Mw of heat deposited in the control region, which of course is high. Therefore it was arbitrarily decided to assume that the temperature rise of this coolant is 15°F for a 1000 gpm control region flow. The temperature increase of this cooling water therefore was defined to be

$$\Delta T = 15 \left(\frac{1000}{V_C}\right) \left(\frac{Q}{100}\right) \left(\frac{z}{24}\right)$$

$$= 6.25 \times 10^{-6} \frac{Qz}{V_C} \qquad \text{(E-6)}$$

The application of Equations (E-4), (E-5), and (E-6) using the appropriate values of the side plate cross section areas and uncertainty factors for the heat generation rates are shown in equations (A-28), (A-33), and (A-41) in Appendix A.

Heat Transfer Coefficients

Once the coolant flow rates and the coolant temperatures are known, the heat transfer coefficients may be calculated. For the coolant adjacent to the fuel plate side of the side plate, the heat transfer coefficients are assumed to be those predicted by the Hausen relation (Equation 9). This of course is the same relation for predicting the heat transfer coefficient in the rest of the fuel plate coolant channel. However, as mentioned earlier, only one half of the value of this heat transfer coefficient is actually used in Equations (E-1a) and (E-1b).

On the other side of both side plates of the inner fuel element and of the inner side plate of the outer fuel element, a modification of the Dittus-Boelter equation given in Glasstone[53] was used. This relation is

$$h = 170 \left[1 + 10^{-2}T - 10^{-5}T^2\right] \frac{v^2}{D^{0.2}} \qquad \text{(E-7)}$$

where

$h$ = Btu/(hr)(ft$^2$)(°F)
$T$ = °F
$v$ = ft/sec
$D$ = in.

In the case of the outer side plate on the other side, the heat transfer coefficient is that for the control region. In the control rod studies, this was assumed to be 4600 Btu/(hr)(ft$^2$)(°F) for a 800 gpm flow rate and

0.104 – 0.104 – 0.104 in. control rod coolant channel thicknesses. Redesign of the control region resulted in 0.104 – 0.170 – 0.095 in. control rod coolant channel thicknesses. Therefore for this analysis, this heat transfer coefficient was estimated to be

$$h_C = \frac{4600}{(800)^{0.8}} \left[\frac{0.104 + 0.104 + 0.104}{0.104 + 0.170 + 0.095}\right]^{0.8} V_C^{0.8}$$

$$= 19.39\ V_C^{0.8} \qquad \text{(E-8)}$$

Table E-1. Division of Heat Flow in the Side Plates[49]

Side Plate Thickness: 0.250 in.
Heat Generation Rate: 5280 Btu/hr in.$^3$

| Fuel Plate Side | | | Opposite Side | | |
|---|---|---|---|---|---|
| Coolant Temperature (°F) | Fuel Element Channel Heat Transfer Coefficient (Btu/hr ft$^2$ °F) | Fraction of Heat Flowing to this Side | Coolant Temperature (°F) | Heat Transfer Coefficient (Btu/hr ft$^2$ °F) | Fraction of Heat Flowing to this Side |
| 120 | 15,000 | 0.800 | 120 | 1000 | 0.200 |
| 150 | 15,000 | 0.680 | 120 | 1000 | 0.340 |
| 150 | 15,000 | 0.840 | 150 | 1000 | 0.160 |
| 150 | 15,000 | 0.520 | 120 | 2000 | 0.480 |
| 150 | 15,000 | 0.720 | 150 | 2000 | 0.280 |
| 150 | 15,000 | 0.200 | 120 | 5000 | 0.800 |
| 150 | 15,000 | 0.540 | 150 | 5000 | 0.460 |
| 150 | 10,000 | 0.760 | 150 | 1000 | 0.240 |
| 150 | 20,000 | 0.880 | 150 | 1000 | 0.120 |
| 140 | 15,000 | 0.504 | 134 | 5000 | 0.494 |

ORNL-DWG 67-6764

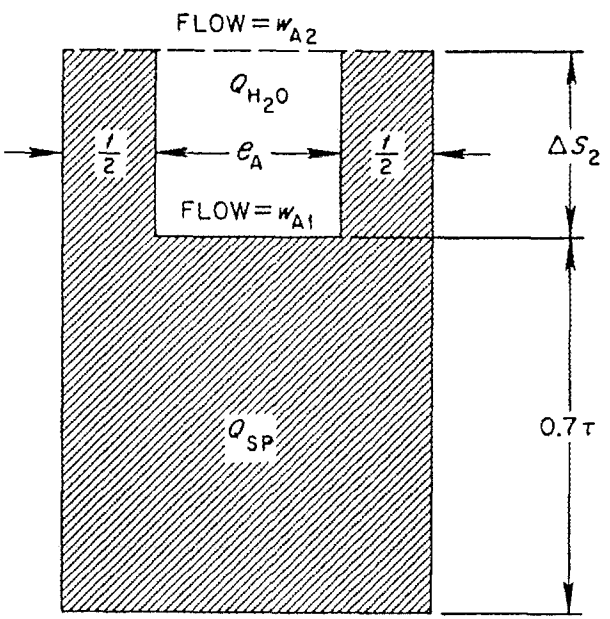


Fig. E-1. Model for Calculating Heat Balances on Coolant Adjacent to the Fuel Plate Side of the Inner Side Plates of the Inner and Outer Fuel Elements.

ORNL-DWG 67-6765

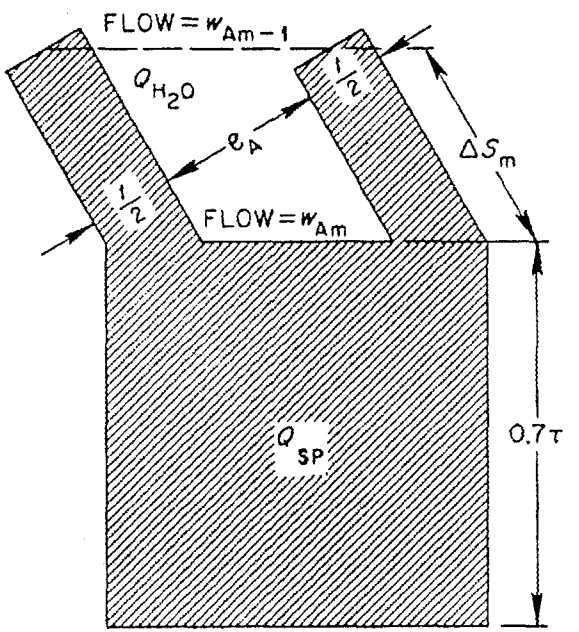


Fig. E-2. Model for Calculating Heat Balances on Coolant Adjacent to the Fuel Plate Side of the Outer Side Plate of the Inner Fuel Element.

## Internal Distribution

1. G. M. Adamson
2. S. E. Beall
3. M. Bender
4. E. S. Bettis
5. F. T. Binford
6. A. L. Boch
7. E. G. Bohlmann
8. R. B. Briggs
9. F. R. Bruce
10. C. D. Cagle
11. T. G. Chapman
12. R. D. Cheverton
13. W. G. Cobb
14. T. E. Cole
15. B. L. Corbett
16. W. B. Cottrell
17. J. A. Cox
18. E. N. Cramer
19. F. L. Culler
20. J. E. Cunningham
21. G. J. Dixon
22. B. C. Duggins
23. E. P. Epler
24. W. K. Ergen
25. D. E. Ferguson
26. A. P. Fraas
27. W. R. Gambill
28. J. C. Griess
29. L. A. Haack
30. P. N. Haubenreich
31. R. M. Hill, Jr.
32. P. R. Kasten
33. J. A. Lane
34. M. I. Lundin
35. R. N. Lyon
36. H. G. MacPherson
37–41. R. V. McCord
42. H. C. McCurdy
43–44. H. A. McLain
45. J. R. McWherter
46. A. J. Miller
47. L. C. Oakes
48. A. M. Perry
49. K. H. Poteet
50. M. W. Rosenthal
51. A. W. Savolainen
52. T. M. Sims
53. M. J. Skinner
54. I. Spiewak
55. R. S. Stone
56. D. B. Trauger
57. A. M. Weinberg
58. G. D. Whitman
59. R. Q. Wright (K-25)
60–61. Central Research Library, CRL
62–63. Y-12 Document Reference Section, DRS
64–78. Laboratory Records Department, LRD
79. Laboratory Records Department, LRD-RC
80. ORNL Patent Office

## External Distribution

81. D. F. Cope, AEC, ORNL
82. M. Shaw, Division of Reactor Development and Technology, AEC, Washington, D.C.
83. L. N. Rib, Division of Compliance, AEC, Washington, D.C.
84. T. R. Jones, Division of Research, AEC, Washington, D.C.
85–99. Division of Technical Information Extension, DTIE
100. Laboratory and University Division, ORO, AEC
101–102. Reactor Division, AEC, ORO
103. R. R. Rohde, ANL
104. D. H. Shaftman, ANL

105. M. Levenson, ANL
106. B. Kristianson, ANL
107. N. Hilvety, Union Carbide Corporation, Parma Research Center, Cleveland, Ohio
108. A. L. Babb, University of Washington, Seattle, Washington, 98105